Characterisation of Novel Drug Candidates for the Treatment of Pancreatic Ductal Adenocarcinoma via Three-Dimensional Organoid Models

A Thesis submitted for the Degree of Doctor of Philosophy

Presented by

Jan Hänsel

Heinrich Heine University Düsseldorf

Institute for Pharmaceutical Biology and Biotechnology

Faculty of Mathematics and Natural Sciences

12.06.2023

Published by permission of the Faculty of Mathematics and Natural Science at Heinrich Heine University Düsseldorf.

Supervisors:

1. Prof. Dr. Nicole Teusch

2. Prof. Dr. Thomas Kurz

Date of the oral examination: 20th October 2023

1.1 Abstract

Pancreatic Ductal Adenocarcinoma (PDAC) is the most common malignant type of pancreatic cancer, primarily characterized by a desmoplastic tumour microenvironment (TME) consisting of inflammatory cancer-associated fibroblasts (CAFs), the early metastasis into nearby organs, and an elevated resistance against chemotherapeutic intervention, resulting in a low rate of overall survival in afflicted patients. Established therapeutical options can only guarantee minor chances of successful and relapse-free curation, and more effective alternatives are urgently needed. The treatment of PDAC therefore represents an important field of scientific and pharmaceutical research.

The biological and pharmacological assays and studies depicted and elaborated in this thesis represent the examination and characterization of novel and promising substances regarding their anti-tumour properties. The following drugs, phytochemicals and synthetic substances were subjected to research and experimentation: tylophorinins, artemisinins and histone deacetylase inhibitors (HDACi). These compounds were tested in 2D and 3D co-culture models to assess and determine their cytotoxic properties. Three-dimensional organoids were created from PDAC tumour cell lines and patient-derived CAFs (pancreatic and hepatic stellate cells) to generate a more natural and appropriate model of pancreatic cancer, and organoids were stained with fluorescent antibodies and recorded via confocal and spinning disc microscopy, to examine their cellular composition and to quantify and analyse the expression of proteins of interest.

Another focus of research was the cellular process of epithelial-mesenchymal transition (EMT), which occurs during the tumour progression of PDAC and precedes invasion, dissemination in the bloodstream and liver metastasis. The expression of proteins and factors associated with EMT was examined in pancreatic cancer cell lines and organoids following treatment with efficacious HDAC inhibitors. Furthermore, protocols regarding the generation and derivation of cancer stem cells (CSCs), a chemoresistant and malignant type of tumour cells present in PDAC, were established and evaluated, and CSCs were subjected to cytotoxic drug screening.

The cytotoxic efficacy of a variety of novel substances could be verified and validated in both 2D cell culture, 3D organoids and CSC models, and PDAC tumour cells treated with potent histone deacetylase (HDAC) inhibitors partially reverted from a mesenchymal to an epithelial phenotype, both on the protein and on the mRNA level.

1.2 Table of Contents

1.3 Abbreviations

Abbreviation	Meaning
2D	two-dimensional
3D	three-dimensional
5-FU	5-fluorouracil
ABC	ATP binding cassette
ACTA2	actin, aortic smooth muscle
ADEX	aberrantly differentiated endocrine exocrine
ADM	acinar-to-ductal metaplasia
ANOVA	analysis of variance
ARS	artemisinin
ART	artesunate
BA	benzyl alcohol
BB	benzyl benzoate
BLAST	basic local alignment search tool
BP	benzophenone
BRCA1/2	breast cancer 1/2 gene
BSA	bovine serum albumine
CAA	cancer-associated adipocytes
CAF	cancer-associated fibroblasts
CD	cluster of differentiation
CD133	prominin-1
CD24	small cell lung carcinoma cluster 4 antigen
CD44	extracellular matrix receptor III
CD8	T-lymphocyte differentiation antigen T8/Leu-2
CDH1	E-cadherin
CDH2	N-cadherin
CDKN2A	cyclin-dependent kinase inhibitor 2A
CHK	checkpoint kinase
CIC	cancer-initiating cell
COX2	cyclooxygenase-2
CP	chronic pancreatitis
CSC	cancer stem cells
DAPI	4′,6-diamidino-2-phenylindole
dCK	deoxycytidine kinase
DHA	dihydroartemisinin
DMSO	dimethyl sulfoxide
ECM	extracellular matrix

EGF	epidermal growth factor
EMT	epithelial-mesenchymal transition
EpCAM	epithelial cell adhesion molecule
EthD-1	ethidium homodimer-1
FACS	fluorescence-activated cell sorting
FAK	focal adhesion kinase
FAP	fibroblast activation protein
FBS	foetal bovine serum
FGF	fibroblast growth factor
FOLFIRINOX	5-fluorouracil, leucovorin, irinotecan, and oxaliplatin
FSP-1	fibroblast-specific protein 1
GAPDH	glyceraldehyde 3-phosphate dehydrogenase
GEM	gemcitabine
GLS1	glutaminase 1
GLUT1	glucose transporter 1
GPX4	glutathione peroxidase 4
HBP	hexosamine biosynthetic pathway
HCC	hepatocellular carcinoma
HDAC(i)	histone deacetylase (inhibitor)
HIF	hypoxia-inducible factor
HNSCC	head and neck squamous carcinoma
HRP	horseradish peroxidase
HSC	hepatic stellate cell
HSP	heat shock proteins
HUVEC	human umbilical vein endothelial cells
IC	inhibitory concentration
IF	immunofluorescence
IKK2	inhibitor of nuclear factor kappa-B kinase subunit beta
IL	interleukins
IPMN	intraductal papillary mucinous neoplasms
LSM	laser scanning microscope
MAF	metastasis-associated fibroblasts
MAM	metastasis-associated macrophages
MCN	mucinous cystic neoplasms
MET	mesenchymal-epithelial transition
MMP	matrix metalloproteinases
MUC	mucins
NADPH	nicotinamide adenine dinucleotide phosphate
NF-kB	nuclear factor kappa-light-chain-enhancer of activated B cells
Nox	NADPH oxidase

ns	not significant
OSR	overall survival rate
OXCT1	oxoacid CoA-transferase 1
OXPHOS	oxidative phosphorylation
PACC	pancreatic acinar cell carcinoma
PAGE	polyacrylamide gel electrophoresis
PanIN	pancreatic intraepithelial neoplasms
PBS	phosphate-buffered saline
PC	pancreatic cancer
PCR	polymerase chain reaction
PDAC	pancreatic ductal adenocarcinoma
PDEC	pancreatic ductal epithelial cells
PDGFR	platelet derived growth factor receptor
Pen/strep	penicillin/streptomycin
PFA	paraformaldehyde
PMSF	phenylmethylsulfonyl fluoride
PNET	pancreatic neuroendocrine tumour
PsA-D	pseudopterosin A-D
PSC	pancreatic stellate cells
PFS	progression-free survival
PTM	posttranslational modification
PVP	polyvinylpirrolydone
RFU	relative fluorescence units
RLU	relative light units
ROS	radical oxygen species
RT	room temperature
RT-qPCR	real-time quantitative polymerase chain reaction
SAHA	suberoylanilide hydroxamic acid/vorinostat
SHH	sonic hedgehog
a-SMA	alpha smooth muscle actin
SDS	sodium dodecyl sulphate
SEM	standard error of the mean
SMAD4	mothers against decapentaplegic homolog 4
Smo	smoothened
TAEC	tumour-associated endothelial cells
TALM	tumour-associated lympho-monocytes
TAM	tumour-associated macrophages
TAN	tumour-associated neutrophil granulocytes
Taxol	paclitaxel
TBS	tris-buffered saline

TGF	transforming growth factor (beta)
TIL	tumour-associated/infiltrating lymphocytes
TIMP1	tissue inhibitor of matrix metalloproteases 1
TLR	toll-like receptors
TME	tumour microenvironment
TMEM	tumour microenvironment of metastasis
TNBC	triple-negative breast cancer
TNF	tumour necrosis factor
TOE	tumour organismal microenvironment
TP53	tumour protein p53
TRAIL	TNF-related apoptosis-inducing ligand
Treg	regulatory T-cells
TRIS	tris-(hydroxymethyl)-aminomethane
TSA	trichostatin A
TubaA	tubastatin A
TUM	tumorspheres
TYLO	tylophorinine
ULA	ultra-low attachment
UN	untreated
UV	ultraviolet
VEGF	vascular endothelial growth factor
VIM	vimentin
YAP	yes-associated protein 1

1.4 Tables and Figures

List of Tables

List of Figures

2 Introduction

The following section firstly presents a descriptive and comprehensive introduction and overview regarding the modern scientific research and biological understanding of pancreatic cancer, and pancreatic ductal adenocarcinoma (PDAC) specifically, focusing on the genetic process of epithelial-mesenchymal transition (EMT), the surrounding tumour microenvironment (TME), its cellular and extracellular components and their active role in tumorigenesis and tumour progression. Secondly, the theoretical and experimental background of the thesis, together with the practical applications of three-dimensional (3D) organoid models and the various pharmaceutical drugs and novel phytochemical and synthetic substances (derivatives of tylophorinines, artemisinins and histone deacetylase inhibitors), which were examined herein, will be described and illustrated.

2.1 Pancreatic Cancer and Pancreatic Ductal Adenocarcinoma

2.1.1 Pancreatic Ductal Adenocarcinoma: An Overview

Pancreatic cancer (PC) comprises a multitude of neoplasms and tumour types emerging from the pancreas, an essential organ of both the endocrine and the digestive system, responsible for the secretion of metabolic enzymes into the gastrointestinal tract of the duodenum, aiding in the digestion and absorption of food and nutrients, and the endocrine regulation of glucose metabolism via the secretion of hormones like glucagon and insulin into the bloodstream (Röder et al. 2016; Pelosi et al. 2017). Cells of the pancreatic tissues comprise acinar (exocrine), ductal (epithelial) and endocrine cells (Orth et al. 2019). The most common diseases and ailments affecting the pancreas are inflammation of the pancreas itself (pancreatitis), with chronic inflammation representing one of the highest risk factors for the development of pancreatic cancer and pancreatic ductal adenocarcinoma (PDAC), and diabetes type I and type II (Mizrahi et al. 2020; Lee et al. 2015).

Pancreatic Ductal Adenocarcinoma (PDAC) is the most prevalent type of pancreatic cancer, representing the majority of all cases, and is a highly malignant and lethal tumour type, originating from the ductal epithelial cells of the pancreas, with low patient survival and currently insufficient medical options of therapeutic intervention (Hidalgo 2010). This heterogeneous tumour entity is characterized by a desmoplastic, fibrotic and inflammatory tumour microenvironment (TME), mainly comprised of cancer-associated fibroblasts (CAFs) and tumour-associated macrophages (TAMs), and showcases chemoresistant properties and early invasion alongside metastasis into the liver and other gastrointestinal organs (Orth et al. 2019). Patients are usually around 60 to 70 years old at the time of diagnosis, and oftentimes hepatic metastasis has already occurred at this point, resulting in liver damage and jaundice, one of the first recognized clinical symptoms, which is why late medical diagnosis is one of the

main factors causing the overall low survival rate for patients, with an 5-year survival rate of 11 %, together with insufficient efficacy of chemotherapeutic treatment, as PDAC tumour cells exhibit high resistance against established forms of therapy (Siegel et al. 2022; Hruban et al. 2019; Bengtsson et al. 2020). Therefore, more efficacious and specifically targeted drugs and chemotherapeutic strategies are urgently needed to improve curation, patient survival and therapeutic outcome.

2.1.2 Pancreatic Ductal Adenocarcinoma: Types and Risk Factors

Tumours of the pancreas are characterized by their tissue of origin, and can be roughly classified in the following categories: pancreatic ductal adenocarcinoma (PDAC), pancreatic neuroendocrine tumours (PNET), pancreatic acinar cell carcinoma (PACC), pancreatoblastoma and solid-papillary neoplasms (Pelosi et al. 2017; Rawla et al. 2019). Morphological variants of pancreatic ductal adenocarcinoma (PDAC) are themselves categorized in pancreatobiliary types, adenosquamos carcinoma, colloid carcinoma, hepatoid carcinoma and medullary carcinoma, based on the expression of extracellular matrix (ECM) proteins such as mucins and different K-Ras mutations (Ingenhoff et al. 2020). Alternatively, PDAC can also be classified in the following subtypes: squamous , immunogenic, pancreatic progenitor and aberrantly differentiated endocrine exocrine (ADEX) (Bailey et al. 2016). The clinical stages of PDAC are furthermore characterized as resectable (no metastasis has occurred), borderline resectable, unresectable and metastatic (Rawla et al. 2019). Major risk factors for the initial tumorigenesis and further malignant development and progression of pancreatic cancer are the inflammation of the pancreas (pancreatitis), especially chronic pancreatitis (CP), gastrectomy, cholecystectomy, obesity, alcohol consumption and smoking (Li and Salik 2021; Becker et al. 2014; Ferdek and Jakubowska 2017). Hereditary factors (e.g. germline mutations in BRCA1/BRCA2) and other diseases affecting the pancreas like diabetes type I and II can promote the emergence of preneoplastic lesions as well (Batabyal et al. 2014; Vietri et al. 2022). Pancreatic ductal adenocarcinoma (PDAC) represents the most prevalent and lethal form of pancreatic cancer, and is usually diagnosed at a far advanced stage of the disease, with one of the earliest diagnosed symptoms being hepatic damage (mainly signified by abdominal pain, dyspepsia, diabetic-like symptoms, weight loss and jaundice) following tumour metastasis into the liver, as mobile PDAC tumour cells migrate from the main tumour body of the pancreas via the portal vein to the liver and colonize pre-metastatic niches (Mizrahi et al. 2020; Hruban et al. 2019). In the majority of all documented and recorded cases, pancreatic ductal adenocarcinoma is diagnosed after this specific process has already occurred and the patient's liver has suffered significant damage caused by the metastatic tumour cells, significantly aggravating therapeutic intervention and outcome (Hruban et al.

2019). Metastasis to the lungs does occur in advanced pancreatic ductal adenocarcinoma as well, though to a lesser degree (Vaz et al. 2016). Of all recorded pancreatic ductal adenocarcinoma (PDAC) patients, the majority succumbs to the illness six to twelve months following the initial diagnosis, with an overall survival rate ranging from 5 to 10 %, with only minimal clinical improvement of treatment and subsequent outcome, though prior to liver metastasis, the chemotherapeutic treatment of pancreatic ductal adenocarcinoma is significantly more effective and successful (Rawla et al. 2019; Bengtsson et al. 2020).

2.1.3 Pancreatic Ductal Adenocarcinoma: Tumorigenesis and Development

The tumorigenesis of pancreatic ductal adenocarcinoma (PDAC) is caused and determined by several mutations in proto-oncogenes and tumour suppressor genes and the formation of pre-neoplastic lesions in the pancreatic body. The neoplastic lesions preceding PDAC can be categorized as intraductal papillary mucinous neoplasms (IPMNs), mucinous cystic neoplasms (MCNs) and pancreatic intraepithelial neoplasms (PanIN), which are all of epithelial nature, and PanIN is further classified into the stages PanIN-1A to PanIN-3 (Pelosi et al. 2017). Tumorigenesis of pancreatic ductal epithelial cells (PDEC) is initiated by mutations in the oncogenic driver gene *KRAS*, which accelerates glycolytic metabolism via upregulation of GLUT1 expression (Bryant et al. 2014; Bernard et al. 2019). Further in PDAC tumorigenesis, *KRAS* mutations induce cell migration, invasion and metastasis (Yang et al. 2018). Following Ras activation, acinar-to-ductal metaplasia (ADM) and subsequent telomere shortening (low-grade pancreatic intraepithelial neoplasm), the tumour cells acquire mutations in the genes *TP53*, *CDKN2A* and *SMAD4* (high grade pancreatic intraepithelial neoplasm) (Orth et al. 2019; Sun et al. 2001). The cellular tumour antigen p53 is a well-researched tumour suppressor gene often mutated in PDAC and being responsible for reduced $CD8^+$ T cell infiltration, increased fibrosis and the generation of pre-metastatic niches (Barton et al. 1991; Novo et al.; Maddalena et al. 2021). *SMAD4* is a tumour suppressor gene belonging to the TGF-beta signalling pathway, being either heterozygous or homozygous deleted in PDAC (Zhao et al. 2018). *CDKN2A*, another tumour suppressor gene encoding for the protein $p16^{INK4A}$, is a negative regulator of the cell cycle and often inactivated in PDAC, leading to poor overall survival (Lin et al. 2020).

Inflammation is a crucial driver of PDAC tumorigenesis, and the canonical and non-canonical NF-κB pathways are significantly upregulated and constitutively active in pancreatic cancer cells, as mutant $K\text{-}Ras^{G12D}$ activation induces upstream NF-κB signalling, and nuclear localization of NF-κB proteins (RelA/p50) results in the expression and secretion of pro-inflammatory cytokines and interleukins (Kabacaoglu et al. 2019; Rahn et al. 2019). Further signalling pathways upregulated in pancreatic cancer cells are the sonic hedgehog (SHH), the

Hippo and the Wnt pathway (Huang et al. 2020; Taipale and Beachy 2001). Especially the activation of the Hippo pathway plays an important role in the regulation of K-Ras-mediated cell proliferation and induces the development of cancer stem cells (Xie and Chen 2020). After the formation of high-grade PanINs, the afflicted cells undergo the process of chromothripsis, resulting in loss of genetic material (Rode et al. 2016). High-grade PanIN cancer cells express pro-angiogenic enzymes like cyclooxygenase-2 (COX-2) and interleukins like IL-1 and IL-8, which induce the formation of new blood vessels in the hypovascular tumour body (Deer et al. 2010).

Another major driving factor of PDAC tumorigenesis and further progression is hypoxia in the main tumour body, caused by inflammatory effects and CAF-mediated desmoplasia, leading to increased glycolytic metabolism (Warburg effect), upregulation of pro-angiogenic factors like the vascular endothelial growth factor (VEGF), and the promotion of epithelial-mesenchymal transition (EMT) through upregulation of the stem cell transcription factors Snail and Twist-1 (Tan et al. 2020; DeBerardinis et al. 2008; Wang et al. 2020). These processes are facilitated by the tumour microenvironment (TME).

2.1.4 Pancreatic Ductal Adenocarcinoma: Metastasis and Tumour Progression

Pancreatic ductal adenocarcinoma (PDAC) is hallmarked by fibrotic desmoplasia, hypoxia and chronic inflammation. The main tumour body is surrounded by inflamed pancreatic stellate cells (PSCs), functioning as cancer-associated fibroblasts (CAFs), which can account for the majority of the tumour body mass, and are signified by an upregulation of the alpha smooth muscle actin protein (ACTA2), a histological phenomenon called desmoplasia, observed in most cases of PDAC and associated with extracellular matrix stiffness and high resistance against chemotherapeutic intervention and treatment (D'Arcangelo et al. 2020; Rice et al. 2017; Jena et al. 2020). Alongside ACTA2, these activated fibroblasts (myofibroblasts) are hallmarked by the proteins desmin, FSP-1 (fibroblast-specific protein 1), FAP (fibroblast activation protein), HIF1 (hypoxia-induced factor 1), platelet derived growth factor receptor (PDGFR), loss of retinoid droplets and secretion of collagens (D'Arcangelo et al. 2020; Calvo et al. 2013; Shi et al. 2012). Such CAFs play a major role in the tumour microenvironment (TME) and can be classified as inflammatory CAFs, myofibroblast CAFs, metastasis-associated fibroblasts (MAFs) and tumour-retarding CAFs according to their functional role in the progression and development of the particular tumour entity (Pausch et al. 2020; LeBleu and Kalluri 2018; Kobayashi et al. 2019). Inflammatory CAFs drive epithelial-mesenchymal transition (EMT) of cancer cells, remodel the extracellular matrix via secretion of matrix metalloproteinases (MMPs), induce epigenetic changes (hypomethylation of CpG isles) and stemness, and heavily contribute to chemoresistance against established anticancer agents

by forming a protective niche for the tumour cells (Mandal et al. 2018; Chen and Song 2019; Ferdek and Jakubowska 2017). Besides collagen, CAFs secrete laminins, fibronectin, hyaluronans and mucins, which lead to the fibrotic desmoplasia characteristic of PDAC (Orth et al. 2019). The mechanic stress, facilitated by the desmoplastic microenvironment, leads to increased mechanotransduction and further induces cell proliferation and migration of the pancreatic cancer cells (Jang and Beningo 2019). The tumour microenvironment (together with the tumour microenvironment of metastasis (TMEM), both summarized as the tumour organismal microenvironment (TOE)) is of significant importance in the modern biological understanding of cancer and oncological research, and especially for the progression of pancreatic cancer (Tomás-Bort et al. 2020; Laplane et al. 2019; Wang et al. 2021). It encompasses, beside cancer-associated fibroblasts (CAFs), several other types of cells: tumour-associated/infiltrating lymphocytes (TILs), tumour-associated and metastasis-associated macrophages (TAMs/MAMs), cancer-associated adipocytes (CAAs), tumour-associated lympho-monocytes (TALMs), tumour-associated neutrophil granulocytes (TANs), and tumour-associated endothelial cells (TAECs) (Egeblad et al. 2010; Ireland and Mielgo 2018; Quail and Joyce 2013; Incio et al. 2016; Choi et al. 2020). As the pancreas is connected to the digestive tract, the gastrointestinal microbiome can likewise induce pro-inflammatory circumstances via the activation of toll-like receptors (TLRs) through microbial molecules (Zambirinis et al. 2014). The TME and PDAC cells influence each other through a multitude of biochemical factors and signals (e.g. cytokines, interleukins, angiogenic growth factors, metabolic intermediates, etc.), such as the development of regulatory T-cells (T_{reg}), which modulate antitumor immunity and are controlled by the activity of the upregulated NF-κB pathway (Kabacaoglu et al. 2019). Cells of the tumour microenvironment (TME) can play both a supporting and inhibiting role and influence the enzymatic remodelling of the extracellular matrix via matrix metalloproteinases, the tumour secretome and oncosomes, angiogenesis and lymphangiogenesis, macrophage polarization and immune suppression/immune editing (Shields et al. 2012; Hou and Chen 2021; Naito et al. 2017; Murciano-Goroff et al. 2020). Due to the desmoplastic condition, and as PDAC tumours are often hypovascular, pancreatic cancer cells experience hypoxia (low intracellular oxygen concentration, impairing mitochondrial oxidative phosphorylation) and tumour acidosis, which promote the formation of new blood vessels via angiogenesis and vasculogenesis to secure nutrient supply and further tumour growth (Balamurugan 2016; Cannon et al. 2018). Malignant cancer cells will then undergo the process of epithelial-mesenchymal transition (EMT), caused by the upregulation and activation of EMT-inducing transcription factors, changing from a sessile, epithelial state to a motile, mesenchymal state (Ren et al. 2018). This change of cellular physiology is characterized by the downregulation of the epithelial marker protein E-cadherin (CDH1) and the upregulation of the mesenchymal marker proteins N-cadherin (CDH2) and vimentin,

alongside other factors such as EpCAM (Loh et al. 2019). EMT is a necessary process required for metastasis and the subsequent invasion, intravasation and colonization of further tissues and organs (Lamouille et al. 2014; Pereira and Chio 2019). Mesenchymal cancer cells secrete matrix metalloproteases (MMPs) to remodel the extracellular matrix (ECM) of the surrounding tumour microenvironment (TME) and to enter the blood stream, followed by the colonization of new pre-metastatic niches in the hepatic tissue (Ren et al. 2018; Houg and Bijlsma 2018). There is credible scientific evidence that pancreatic ductal adenocarcinoma (PDAC), and many other types of tumour entities, feature cancer stem cells (CSCs), a term denominating cancer cells exhibiting stem cell-like characteristics and features, as well as enhanced chemoresistance (Yin et al. 2011). In PDAC, CSCs could be characterized by the upregulation of CD24, CD44, CD133 and EpCAM (CD326), and they might be involved in the process of metastasis, tumour dormancy and tumour recurrence (Domenichini et al. 2019; Askan et al. 2021). When no therapeutic treatment of pancreatic cancer is possible besides palliative care, advanced metastatic PDAC progresses to cachexia, sarcopenia and subsequently ends in death in the majority of all recorded cases, due to extensive pancreatic and hepatic damage, and only best supportive care can be given when all chemotherapeutic intervention had failed (Takeda et al. 2021).

2.1.5 Pancreatic Ductal Adenocarcinoma: Therapies and Treatments

Several options of therapeutic treatments and interventions against pancreatic cancer and pancreatic ductal adenocarcinoma (PDAC) have been established and clinically evaluated. The cytostatic deoxycytidine nucleoside gemcitabine (GEM) represents the first-line regimen and most commonly applied chemotherapeutic agent, inhibiting mitosis and cellular proliferation, and is often administered alongside antibody-bound paclitaxel (Taxol/nab-paclitaxel), a microtubule stabilizer derived from the yew tree *Taxus brevifolia*, though both the gemcitabine monotherapy as well as the co-treatment (GnP) only result in poor outcome, with the majority of patients succumbing to the disease 24 months after the initial diagnosis, and an overall survival rate of ca. 5 % (Mini et al. 2006; Wilson et al. 2001; Vita et al. 2016; Goldstein et al. 2015; Burris III et al. 1997; Bianchi et al. 1994). A medical side-effect of gemcitabine/paclitaxel combination treatment can be severe neutropenia (Ito et al. 2021), and resistance against gemcitabine treatment is a common occurrence in PDAC and can be induced and caused by a multitude of cellular factors (e.g. cells of the tumour microenvironment such as cancer-associated fibroblasts and tumour-associated macrophages) and signalling pathways (e.g. the Hippo-YAP and NF-κB pathways) (Amrutkar and Gladhaug 2017; Bulle et al. 2020; Tu et al. 2019). The glycolytic metabolism in pancreatic cancer cells (Warburg effect), leading to an increased pyrimidine biosynthesis, represents one

of the main reasons behind the chemoresistance against gemcitabine (Shukla et al. 2017), though a major component regarding gemcitabine chemoresistance are the inflammatory pancreatic stellate cells (PSCs), the cancer-associated fibroblasts (CAFs) of PDAC, responsible for desmoplasia through the secretion of collagens, mucins, fibronectin, hyaluronans and other extracellular matrix components advancing tumorigenesis, the stimulation of epithelial-mesenchymal transition (EMT) and metastasis in cancer cells (Amrutkar et al. 2023; Jena et al. 2020; Skrypek et al. 2013; Wei et al. 2018; Qiao and Lu 2020).

Treatment of pancreatic cancer cells with gemcitabine also resulted in upregulation of TIMP1 (tissue inhibitor of matrix metalloproteases 1) expression, which is associated with the creation of pre-metastatic niches in the liver and immunosuppression (D'Costa et al. 2017). Gemcitabine treatment can further induce the development of cancer stem cells (CSCs) through activation of NADPH oxidase (Nox) proteins (Zhang et al. 2016). Another biological factor responsible for gemcitabine resistance is oxoacid CoA-transferase 1 (OXCT1), an enzyme of the ketone body metabolism, via the activation of the pro-inflammatory NF-κB pathway by phosphorylation of IKK2 and p65 (Ding et al. 2021). Besides the NF-κB pathway, the Hippo-YAP pathway, which is upregulated in pancreatic cancer due to matrix stiffness, induces resistance of cancer cells against gemcitabine by increasing the expression of transporter proteins, resulting in the efflux of the prodrug (Gujral and Kirschner 2017). Resistance against anti-microtubule agents (e.g. taxines) can likewise be caused by deregulation of the Hippo-YAP pathway (Nguyen and Yi 2019; Rice et al. 2017). Modulation of gemcitabine uptake and phosphorylation via the deoxycytidine kinase (dCK) by tumour-associated macrophages (TAMs), another essential cell type of the tumour microenvironment (TME), is caused by the release of pyrimidines and further restricts the chemotherapeutic efficacy of gemcitabine against pancreatic cancer (Halbrook et al. 2019). A possible solution against gemcitabine resistance might be the sensitisation of tumour cells against this cytostatic compound through pharmaceutical treatment with optimized inhibitors and agents; for example, pancreatic cancer cells were sensitized against gemcitabine via inhibition of the hexosamine biosynthetic pathway (HBP) with the novel drug FR054 (Ricciardiello et al. 2020).

New and advanced chemotherapeutic approaches against pancreatic ductal adenocarcinoma (PDAC) have been developed and evaluated, one of which is FOLFIRINOX, a multidrug regimen for the treatment of malignant metastatic pancreatic cancer, comprised of the four established anticancer agents 5-fluorouracil, leucovorin, irinotecan, and oxaliplatin, which significantly enhanced and improved the overall survival rate of pancreatic cancer patients compared to gemcitabine monotherapy in multiple clinical trials and studies, and now represents the first-line treatment option against advanced and metastatic pancreatic ductal adenocarcinoma (Conroy et al. 2018; Jesus et al. 2020). However, even with FOLFIRINOX,

progression-free survival (PFS) of patients who received treatment was usually about six to ten months, and common side effects comprise neutropenia, thrombocytopenia, anaemia, neuropathy and nausea/fatigue (Thibodeau and Voutsadakis 2018). New and future strategies for the treatment of advanced and metastatic PDAC currently researched encompass further modified versions of FOLFIRINOX, combinations of 5-fluorouracil, leucovorin, irinotecan, and oxaliplatin with gemcitabine and other novel anticancer agents (e.g. monoclonal antibodies against deregulated proteins), therapies targeting the oncogenic driver mutation K-Ras^{G12D}, disruption of the TME stroma, and photodynamic therapies (Singh and O'Reilly 2020; Sun et al. 2022; Douglas et al. 2022). Other targeted therapies currently under clinical investigation and trial involve the drugs taselisib, tegavivint and trametinib, as well as CAR-T cell application and tumour cell vaccines (Kolbeinsson et al. 2023; Turpin et al. 2022).

2.2 Subject of the Thesis

2.2.1 Overview

The scientific work presented and described below revolved around the screening of new chemotherapeutic agents for the treatment of pancreatic cancer. We examined the pharmaceutical efficacy of several novel natural and synthetic substances, and the practical applications of three-dimensional co-culture organoids. Derivatives of the natural drugs tylophorinine, artemisinin and histone deacetylase inhibitors (HDACi) were tested, screened and evaluated on pancreatic cancer cells, cancer-associated fibroblasts (CAFs) and PDAC organoid models. Special attention was given to the histone deacetylase inhibitors (HDACi) and their effect on the process of epithelial-mesenchymal transition (EMT) and the expression of the epithelial marker protein E-cadherin (CDH1) in both cancer cells and organoids. The cultivation and scientific application of tumorspheres and cancer-stem cells (CSCs) was initialized and examined as well.

2.2.2 Three-Dimensional (3D) Cell Culture and Organoids

The application of 3D cell culture for the scientific analysis and examination of biological processes in tissues and organs has several advantages over two-dimensional (2D) cell culture (Imamura et al. 2015), with diverse and promising applications for the study of tissue development, disease modelling, phenotypic profiling and tissue regeneration (Fatehullah et al. 2016; Di et al. 2014). Molecular interactions between different cell types in specialized tissues, drug responsiveness, cellular differentiation, influences of the microbiome and the constitution of the tumour microenvironment (TME) can be examined and analysed in three-

dimensional spheroids and organoids far better than in two-dimensional cultures, providing an advanced model for scientific research (Moreira et al. 2018; Shelkey et al. 2022; Sirenko et al. 2015). The creation of viable and lifelike organoids and spheroids from both normal and tumour tissue has been described and standardized for a multitude of diseases, tumour entities and organs, e.g. both the pancreas and the liver (Broutier et al. 2016; Myasnikova et al. 2019; Su et al. 2023; Tsai et al. 2018; Randriamanantsoa et al. 2022), neural tissue (Lancaster and Knoblich 2014), skin and dermal tissue (Lee and Koehler 2021; Shin et al. 2020; Hölken and Teusch 2020), colorectal cancer (Crespo et al. 2017; Li et al. 2020a), breast cancer (Kenny et al. 2007; Smolina and Goormaghtigh 2015; Reimche et al. 2022), and lung cancer (Ramamoorthy et al. 2019; Randriamanantsoa et al. 2022).

3D cell culture models can be scientifically utilized for pharmaceutical and automated drug screening and development, to improve personalized medicinal treatment and therapeutic outcome (Bengtsson et al. 2021; Breslin and O'Driscoll 2016; Edmondson et al. 2014), and to examine the biochemical, genetic and metabolic heterogeneity of tumour and non-tumour cells in the tumoral tissue and microenvironment (Bradney et al. 2020; Cavaco and Eble 2019; Di Modugno et al. 2019; Di et al. 2014; Jin and Jin 2020; Nyga et al. 2011). Organoids are suited to study the invasion and migration of tumour cells (Cheng et al. 2015) and for the evaluation of novel therapeutic methods like photodynamic activation of drugs (Obaid et al. 2019). Organoids are furthermore applied for biochip (tumour on chip/organ on chip) models as well, to study the interactions between the extracellular matrix, receptors and signalling molecules (Chernyavska et al. 2019; Lee et al. 2018b). Multiple different experimental methods and procedures for the cultivation and growth of organoids and other three-dimensional tissue models have been established: e.g. the application of scaffolds (Fischbach et al. 2007; Gong et al. 2015; Yoshii et al. 2011), purpose-built matrices and specialized hydrogels (Hughes et al. 2010; Tibbitt and Anseth 2009; Zhang et al. 2017), hanging drop assays (Foty 2011; Ware et al. 2016), and magnetic levitation systems (Jaganathan et al. 2014).

Due to the importance of the tumour microenvironment (TME) in cancer development and malignancy, as described above, represented by the cancer-associated fibroblasts (CAFs) and extracellular matrix (ECM) components and proteins in pancreatic ductal adenocarcinoma (PDAC), three-dimensional cell culture models are an essential application for the future study and research of PDAC, its tumorigenesis, progression and the efficacy of chemotherapeutic agents like gemcitabine (GEM) and paclitaxel (Dufau et al. 2012; Hwang et al. 2019; Tiriac et al. 2019; Crawford et al. 2019). In general, 3D cell culture organoids represent a better model for the screening of novel drugs and substances than their 2D counterparts (Longati et al. 2013; Schmitz et al. 2017). PDAC organoids could be generated from established tumour cell lines as well as from direct patient-derived tumour cells via xenotransplantation (Ehrenberg et al. 2019), and organoids from normal pancreatic tissues are likewise possible

(Randriamanantsoa et al. 2022). In pancreatic cancer organoids, the formation of mesenchymal cancer cells and cancer-initiating cells (CICs) exhibiting stem cell-like properties can be observed and examined (Choi et al. 2020; Shichi et al. 2019). For example, the synergistic effects of the chemotherapeutic agent gemcitabine (GEM) and checkpoint kinase (CHK) inhibitors have been evaluated and verified in Capan-2 organoids (Dufau et al. 2012). The essential importance of cancer-associated fibroblasts (CAFs), their secreted extracellular matrix (ECM) components and tumour-associated macrophages (TAMs) for the development and chemoresistance of PDAC can be replicated and examined in co-culture organoids via multiplex screening, flow cytometry, immunofluorescence staining and confocal microscopy analysis (Hwang et al. 2019; Jang et al. 2021; Kuen et al. 2017). Another method to investigate and analyse the interaction between tumour cells and cancer-associated fibroblasts (CAFs), like the upregulation of epithelial-mesenchymal transition (EMT) markers and factors, can be achieved via microfluidic biochip system, where tumour organoids are subjected to steady and controlled flow of medium and substances (Lee et al. 2018b).

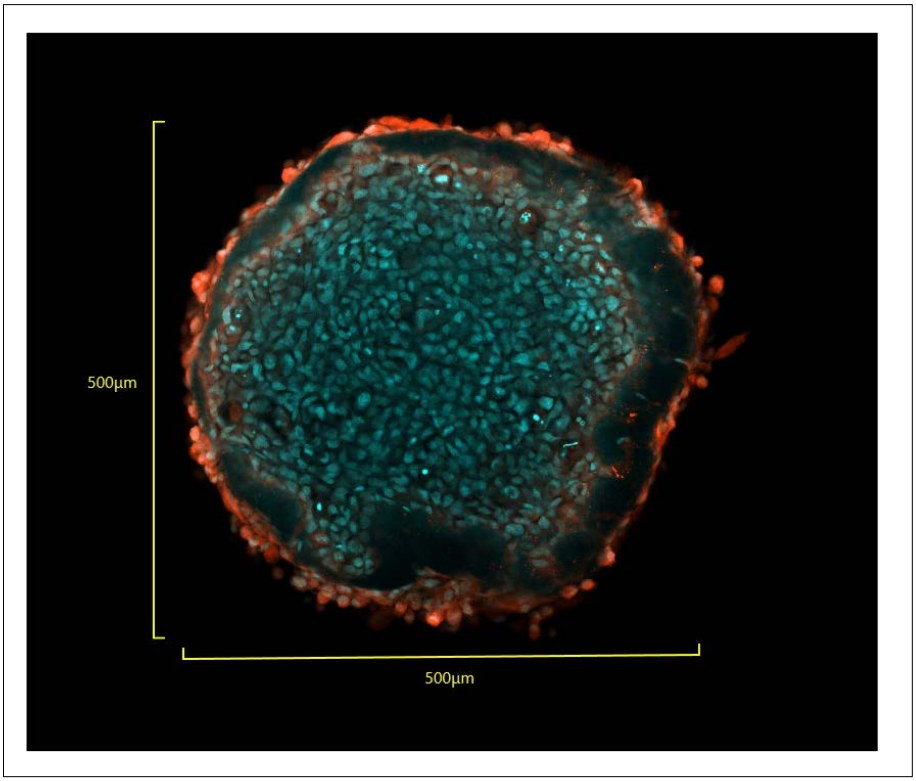

Figure 1. A PDAC organoid cultivated from Panc-1 cells and patient-derived pancreatic stellate cells (KU0020 PSC). Blue signal: DAPI-staining of nuclei (405 nm channel); red signal: IF-staining of ACTA2 (561 nm channel). Merging of both channels. Reference scales: 500 µm. Images recorded via the CQ1 Confocal Imaging Cytometer (Yokogawa Electric Corporation) and edited with the CellPathfinder software (Yokogawa).

In this thesis, we cultivated organoids from established pancreatic ductal adenocarcinoma (PDAC) cell lines and patient-derived cancer-associated fibroblasts, as previously published

by our research group and partners of the University of Bath (Xie et al. 2020), and subjected these organoids to treatment with novel substances and immunofluorescence staining with antibodies, followed by imaging via confocal microscopy and spinning disc confocal microscopy. Through machine learning-assisted analysis, we examined the protein expression of the epithelial marker E-cadherin (CDH1) in the organoid cells, to further evaluate the effect of histone deacetylase inhibitors (HDACi) on pancreatic cancer cells. We were able to cultivate organoids both on 96-well and 384-well plates, standardizing and optimizing our approach for high-throughput screening of novel substances and drugs of interests.

2.2.3 Tylophorinines

The anti-inflammatory agent tylophorinine, also known under the description pergularinine, is a natural occurring phenanthroquinolizidine alkaloid (Gao et al. 2013; Rao et al. 1997), originally isolated from the plant *Tylophora ovata* (Zhen et al. 2002), and a derivative of the cytotoxic drug tylophorine (Govindachari et al. 1961; Rao and Venkatachalam 2000), a pharmaceutical substance exhibiting anticancer activity on hepatocellular carcinoma (HCC) cells and lung cancer cells via S phase arrest, inhibition of the inflammatory NF-κB pathway and heat shock proteins (Liu et al. 2017; Lin et al. 2009; Chen et al. 2014). The pharmacological and chemotherapeutic potential of tylophorine, tylophorinine and their many derivatives and analogues (Dhiman et al. 2012; Cai et al. 2006) has been proven against various tumour entities and cells (Gao et al. 2007; Ganguly and Khar 2002), as tylophorine derivatives inhibit the function of HIF-1, the hypoxia-inducible factor-1 (Chen et al. 2016) and promote tumour apoptosis in breast cancer cells (Pratama et al. 2018). Many tylophorines showcase anti-inflammatory activities (Wang et al. 2012), and the inhibitory effect of tylophorines on heat shock proteins, especially HSP70, has been demonstrated in several studies (Wang et al. 2016; Wang et al. 2017). Tylophorines have shown anticancer effects on renal cancer cells as well (Song et al. 2015).

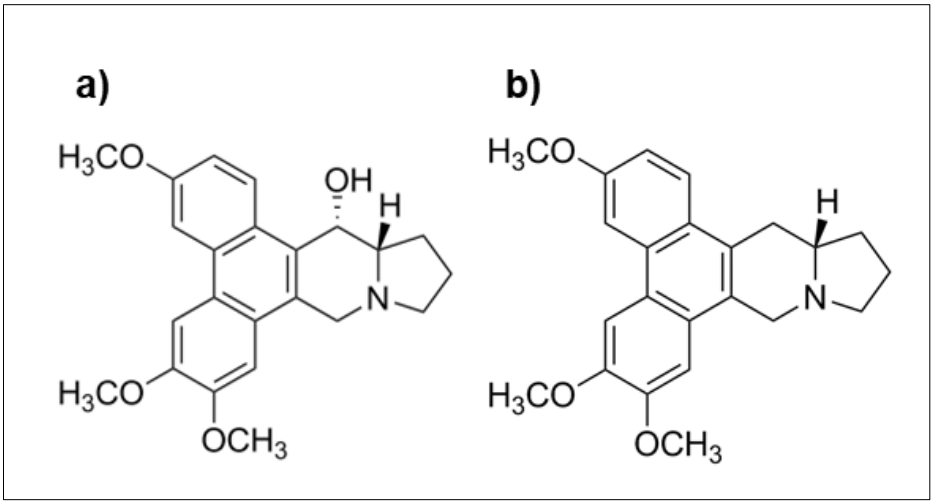

Figure 2. Chemical structure of two tylophorinine derivatives: a) *O*-methyltylophorinidine (P05C06); b) 2-demethoxytylophorine (P05C06B04). For further information, see method section 3.2.1.

Natural derivatives of tylophorinine, generously provided by the Institute of Pharmaceutical Biology and Biotechnology of the Heinrich Heine University (Düsseldorf, Germany), were screened on pancreatic cancer cells and three-dimensional co-culture organoids, as previously published (Xie et al. 2020), and exhibited high cytotoxic properties in low nanomolar concentrations. Concordant results of these substances, exhibiting anticancer efficacy on three-dimensional breast cancer organoid models, were likewise conducted in our research group and published (Reimche et al. 2022).

2.2.4 Artemisinins

Artemisinin (ARS), a sesquiterpene lactone possessing an endoperoxide bridge, essential to its cytotoxic function, is a natural substance and well-researched and established pharmacological agent, exhibiting anti-malarial and anticancer activity, originally derived from the wormwood plant *Artemisia annua* (Singh and Lai 2004; Li and Zhou 2010). The pharmaceutical and anti-malarial efficacy of artemisinin is likely caused by the cleavage of the endoperoxide bridge, leading to the production of radical oxygen species (ROS) and resulting in disruption of cellular metabolism and further cell damage (Shandilya et al. 2013; Ismail et al. 2016). The ROS-mediated anticancer effects of artemisinin and its derivatives were verified on several distinct tumour entities (Slezakova and Ruda-Kucerova 2017). Treatment with artemisinin inhibits the TGF-beta pathway and suppresses breast cancer growth and metastasis (Yao et al. 2018). In primary liver cancer cells (hepatocellular carcinoma), artemisinin promotes generation of radical oxygen species (ROS), the upregulation of E-cadherin (CDH1) and the downregulation of N-cadherin (CDH2), suppressing invasion and cell migration (Li et al. 2019b). Derivatives of artemisinin like artesunate (ART), another anti-

malarial drug, and dihydroartemisinin (DHA), have likewise demonstrated anticancer activity (Nam et al. 2007; Dai et al. 2021). Artesunate showcases pharmacological efficacy in breast cancer cells and spheroids via the promotion of apoptosis through induction of caspase activity and arrest of the cell-cycle (Greenshields et al. 2019), as well as in colon cancer cells, (Jiang et al. 2018; Kumar et al. 2019), liver cancer cells (Li et al. 2019a), thyroid cancer cells (Ma and Fei 2020) and glioma cells (Wei et al. 2020), and inhibits the expression of pro-fibrotic genes (e.g. ACTA2) in human dermal fibroblasts (Larson et al. 2019), proving its anti-inflammatory properties and its possible eligibility as a chemotherapeutic agent against pancreatic cancer. Dihydroartemisinin (DHA) exhibits similar properties on cancer cells as artemisinin and artesunate, and treatment with DHA induces apoptosis and inhibition of proteins (e.g. Smo) of the hedgehog signalling pathway, enhancing the efficacy of the cytostatic drug gemcitabine in ovarian cancer cells (Liu et al. 2018; Yang et al. 2019).

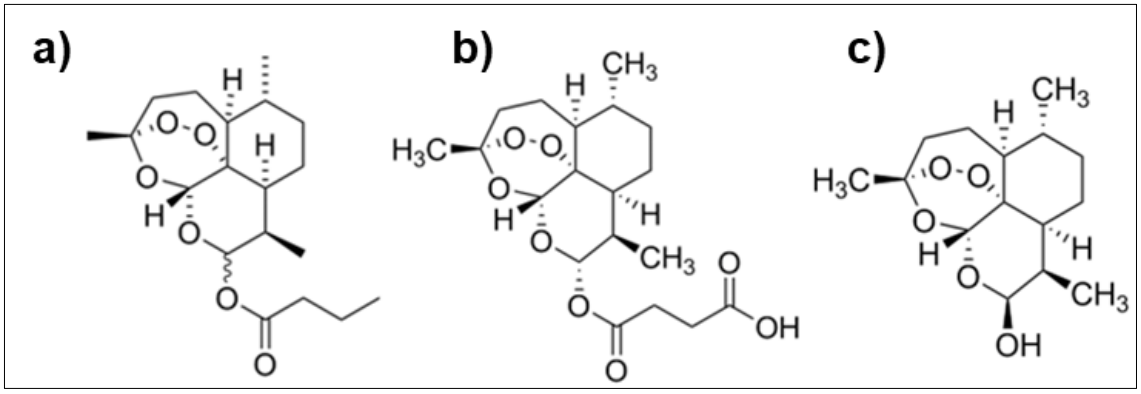

Figure 3. Artemisinin and derivatives: a) artemisinin; b) artesunate; c) dihydroartemisinin. See method section 3.2.1 for more information.

Pancreatic ductal adenocarcinoma (PDAC), a tumour type characterized by its pro-inflammatory and hypoxic tumour microenvironment (Hidalgo 2010), is a prime candidate regarding potential chemotherapy with artemisinin derivatives. Treatment of pancreatic cancer cells with dihydroartemisinin (DHA) halts cell growth, induces the downregulation of several cell cycle proteins (e.g. cyclin E and cdk2) and NF-κB, promotes apoptosis and enhances the efficacy of the established chemotherapeutic drugs gemcitabine and cisplatin (Chen et al. 2010; Wang et al. 2010; Li et al. 2016; Du et al. 2021), and similar results were achieved with artesunate (Du et al. 2010; Wang et al. 2019). The anti-proliferative effects of artemisinin and its derivatives are caused by the induction of ferroptosis, a form of regulated cell death mediated by the Fenton reaction and the accumulation of lipid peroxidation products, through generation of radical oxygen species (Chen et al. 2020; Eling et al. 2015; Ji et al. 2019; Song et al. 2019).

We tested several established and novel derivatives of artemisinin (artesunate, dihydroartemisinin, etc.) on pancreatic cancer cells, cancer-associated fibroblasts (CAFs) and

three-dimensional co-culture organoids, and evaluated the cytotoxicity of novel artemisinin hybrids activated through ultraviolet irradiation. Said substances were synthesized and generously provided by the Research Group Griesbeck of the University of Cologne (Germany). Some results discussed in this thesis were first published in the PhD thesis of Christina Bold, who synthesized several of these compounds (Bold 2022).

2.2.5 Histone Deacetylase Inhibitors (HDACi)

A promising novel class of pharmaceutical agents, suited for the medical treatment of several diseases and diverse types of cancers, are inhibitors of histone deacetylases (Eckschlager et al. 2017), of which multiple new substances were screened, examined and evaluated in this thesis (see section 4.6). The human histone deacetylase (HDAC) proteins regulate a broad field of cellular and genetic functions via diverse posttranscriptional mechanisms (e.g. deacetylation, lysine acetylation, etc.) of histone, chromatin and non-histone proteins, like gene transcription, microtubule formation, insulin secretion and mitochondrial metabolism, and are classified in Class I, Class IIa, Class IIb, Class III (sirtuins) and Class IV HDACs, mainly facilitating their enzymatic activity by catalysing the hydrolysis of the *N*-acetyl amide group (Bradner et al. 2010; Clocchiatti et al. 2011; Asfaha et al. 2019; Valenzuela-Fernandez et al. 2008; Ahuja et al. 2007; Han et al. 2019). HDAC activity via hypomethylation of DNA regions (leading to genomic instability) and hypermethylation of CpG islands (e.g. in the promoter regions of tumour-suppressor genes) plays an important role in the process of tumorigenesis, e.g. via the promotion of proliferation, expression of inflammatory proteins, angiogenesis and cell differentiation (Clocchiatti et al. 2011; Suárez-Álvarez et al. 2013; Esteller 2008; Sandoval and Esteller 2012).

In the pancreas, HDAC activity is associated with chronic inflammation and pancreatitis, cytokine secretion and activation of pancreatic stellate cells (PSC), and can thereby facilitate the development of preneoplastic lesions, leading to metaplasia and subsequently to malignant pancreatic cancer (Klieser et al. 2015). In pancreatic ductal adenocarcinoma, an upregulation of the expression of several histone deacetylases (HDAC1, HDAC2, HDAC4, HDAC6, HDAC7 and HDAC9) can be observed and linked to tumour progression, chemoresistance and metastatic processes (Schneider et al. 2010; Wang et al. 2009; Giaginis et al. 2015; Li et al. 2020b; Stojanovic et al. 2017). Overexpression of HDAC2 is associated with resistance to TRAIL-induced apoptosis (Schüler et al. 2010), and elevated enzymatic activity of HDAC1 furthermore coincides with upregulation of the mesenchymal marker vimentin (VIM) in pancreatic cancer cells (Shinke et al. 2018). Inhibition of HDAC3 and HDAC4 activity in pancreatic cancer models prevents smoking-induced invasion and metastasis (Yang et al. 2022; Edderkaoui et al. 2016), and treatment with the pan-HDAC inhibitor vorinostat (SAHA)

and the class I/class II inhibitor trichostatin A (TSA) results in the significant suppression of HDAC1, HDAC7, HDAC8 and vimentin expression, as well as in the upregulation of E-cadherin (CDH1) expression at both the mRNA and protein level (Cai et al. 2018). The downregulation of the epithelial marker protein E-cadherin in PDAC is presumably associated with the elevated activity of HDAC1 and HDAC2 (Aghdassi et al. 2012; Burstin et al. 2009), and low E-cadherin protein levels are furthermore associated with malignant tumorigenesis (Kaneta et al. 2020).

HDAC inhibitors (HDACi) can be applied for the treatment of a wide range of diseases (e.g. arrythmia, cardiac hypertrophy, etc.) and tumour entities (e.g. leukaemia, ovarian cancer and lung cancer) due to their capability to catalyse posttranslational modifications and epigenetic changes (Yoon and Eom 2016; Ververis et al. 2013), and several of these substances are candidates for clinical studies or have already been approved, such as ricolinostat, citarinostat, tefinostat, the pan-HDAC inhibitor vorinostat (SAHA; see above), trichostatin A, tinostamustine, belinostat, romidepsin, panobinostat, and many more (Ho et al. 2020). The HDACi vorinostat and romidepsin have been successfully approved for the treatment of cutaneous T-cell lymphoma, belinostat and tucidinostat for peripheral T-cell lymphoma, and panobinostat for multiple myeloma (Mann et al. 2007; Hood and Shah 2016; Grant et al. 2010; Laubach et al. 2015; Ho et al. 2020).

Based on their chemical structures, HDAC inhibitors can be classified in four distinct categories: cyclic peptides, hydroxamic acids, benzamides and short-chain fatty acids (Hull et al. 2016). In cancer therapy, the efficacy of HDAC inhibitors is caused by their ability to arrest the cell cycle, induce apoptosis, inhibit metastasis and angiogenesis (the formation of new blood vessels via endothelial cells) and reverse epithelial-mesenchymal transition (EMT), a process occurring in pancreatic cancer and pancreatic ductal adenocarcinoma, leading to resistance towards chemotherapy and liver metastasis (Li and Seto 2016; Pereira and Chio 2019; Pelosi et al. 2017). The efficacy of HDAC inhibitors on pancreatic cancer, both *in vitro* and *in vivo*, such as vorinostat (SAHA), could be validated in multiple experimental studies (Koutsounas et al. 2013).

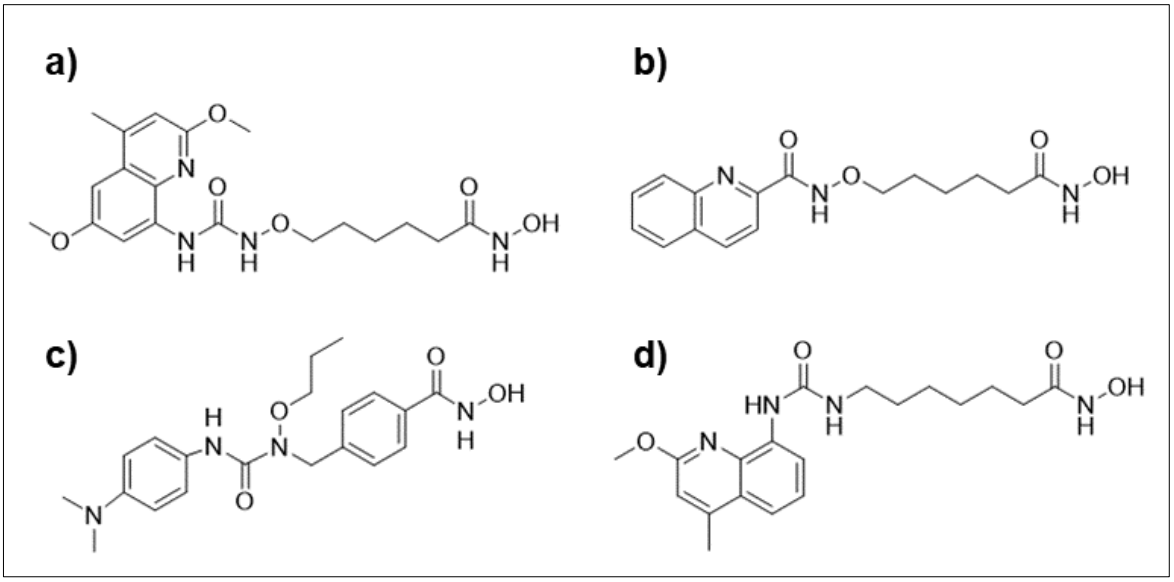

Figure 4. Four novel histone deacetylase inhibitors: a) KSK64, an HDAC1/6 inhibitor; b) LAK41, an HDAC2/6 inhibitor; c) MPK324, a nexturastat A derivative; d) MPK544, a HDAC2/6 inhibitor. See method section 3.2.1 for more information (Lee et al. 2020; Pflieger 2020; Alves Avelar et al. 2021).

In our research regarding the evaluation and screening of novel products and drug (see below), we applied the established HDAC inhibitors vorinostat (SAHA) and the three HDAC6 inhibitors ricolinostat, citarinostat and tubastatin A. Suberoylanilide hydroxamic acid (SAHA), commercially known as vorinostat, is a pan-HDAC inhibitor exhibiting efficacy against cancer such as PDAC, hepatocellular carcinoma (HCC) and triple-negative breast cancer (TNBC) (Grant et al. 2007; Kumagai et al. 2007; Looi et al. 2022; Sanaei and Kavoosi 2021). The chemotherapeutic potential of vorinostat against haematological tumours was tested in multiple clinical studies, though it only demonstrated low clinical efficacy (Kim et al. 2018; Schaefer et al. 2009). Tubastatin A is an HDAC6 inhibitor with anti-inflammatory properties and has demonstrated anticancer efficacy against colorectal and urothelial cancer, as well as against neurological diseases (Vishwakarma et al. 2013; Gupta et al. 2019; Butler et al. 2010; Shen et al. 2020). Citarinostat is an HDAC6 inhibitor capable of suppressing metastasis in head and neck squamous carcinoma (HNSCC) by inducing the degradation of matrix metalloproteinases (MMPs) and activating $CD8^+$ T-cells in multiple myeloma (Bae et al. 2018; Cho et al. 2020). Ricolinostat, another HDAC6 inhibitor with anti-inflammatory properties, exhibits anticancer efficacy on ovarian and colorectal cancer (Fukumoto et al. 2019; Lee et al. 2018a). HDAC6 has been chosen as a control drug target due to its involvement in tumour progression, inflammatory processes and T-cell regulation (Zheng et al. 2020; Youn et al. 2017; Fukumoto et al. 2019).

We screened and evaluated the cytotoxic properties of multiple substances with HDACi activity, generously provided by the research group of Professor Kurz from the Institute for Pharmaceutical and Medicinal Chemistry of the Heinrich Heine-University (Düsseldorf,

Germany) and synthesized by Marc Pflieger and Leandro Alves Avelar (Pflieger 2020; Alves Avelar et al. 2021), on pancreatic cancer cells, cancer-associated fibroblasts (CAFs), three-dimensional co-culture organoids and tumorsphere-like cells. The effects of HDAC inhibitors were examined and analysed on the cellular process of epithelial-mesenchymal transition (EMT) and the expression and transcription of EMT-associated markers and factors in pancreatic ductal adenocarcinoma (PDAC) cells and organoids. Of particular interest were the four novel HDAC inhibitors LAK41, KSK64, MPK264 and MPK544, the carba-analogue of KSK64. LAK41 is an HDAC2/6 inhibitor with an IC_{50} (HDAC2) value of 92 nM and an IC_{50} (HDAC6) value of 25 nM. The potent drug MPK544 is an HDAC2/6 inhibitor likewise, with an IC_{50} (HDAC2) value of 39.6 nM and an IC_{50} (HDAC6) value of 96.3 nM, while KSK64 is an HDAC1/6 inhibitor, with an IC_{50} (HDAC1) value of 43.2 nM and an IC_{50} (HDAC6) value of 2.80 nM. MPK264, a derivative of the established HDAC6 inhibitor nexturastat, showcases an IC_{50} (HDAC6) value of 14.0 nM (Lee et al. 2020; Pflieger 2020; Alves Avelar et al. 2021). All four pharmaceutical substances exhibited high efficacy on the tested models (see section 4.6 below). First experimental HDACi results were initially published in the master thesis of Daria Janßen (Janßen 2021).

3 Materials and Methods

3.1 Overview

In the following sections, the used materials (3.2) and applied methods (3.3) are listed, described and documented, including all chemicals (3.2.1 to 3.2.2), cell lines (3.2.4), kits (3.2.3) and devices (3.2.5), the detailed execution of experimental assays (3.3 to 3.5) and generation and handling of three-dimensional organoids (3.3.4) as well as tumorspheres (3.5).

3.2 Materials

3.2.1 Chemicals

The following tables list the specific chemicals, drugs, solutions and further substances utilized in this thesis. Table 1 details the commercially available products which were purchased. Table 2 lists the histone deacetylase inhibitors (HDACi), table 3 the artemisinins and table 4 the tylophorinine derivatives (Xie et al. 2020; Reimche et al. 2022).

Table 2. List of commercially available substances and solutions.

Chemical	Provider
Albumin Fraction V, NZ-Origin (8076.2)	Carl Roth
Ammonium peroxydisulphate (9592.2)	Carl Roth
Animal-Free Recombinant Human EGF (AF-100-15)	PeproTech
autoMACS® Running Buffer – MACS® Separation Buffer (130-091-221)	Miltenyi Biotec
B-27 Supplement (50X), serum free (17504044)	Thermo Fisher
Benzyl alcohol 99% (LO3292)	Alfa Aesar
Benzyl benzoate 99+% (LO3258)	Alfa Aesar
Blotting reagent AceGlow™ Chemiluminescence Substrate (730-1510)	VWR Peqlab
Bromophenol blue sodium salt (A512.1)	Carl Roth
Citarinostat (ACY-241)	Selleckchem
Collagen type I, rat tail (50201)	Ibidi
Collagen type I, rat tail (A1048301)	Thermo Fisher Scientific
Crystal Violet (61135)	Sigma-Aldrich
DAPI (D9542)	Sigma-Aldrich
Dimethyl sulphoxide (A994.1)	Carl Roth
Dispase II (D4693)	Sigma-Aldrich
DMEM Medium (41965-039)	Thermo Fisher Scientific
DMEM/F-12 Medium (11320-074)	Thermo Fisher Scientific
DPBS, no calcium, no magnesium (14190144)	Thermo Fisher Scientific
Erythrosin B Stain (L13002-LG)	BioCat

5-Fluoruracil (F6627)	Sigma-Aldrich
Foetal Bovine Serum (10270-106)	Thermo Fisher Scientific
Gemcitabine hydrochloride (G6423)	Sigma-Aldrich
Glycin (0079.3)	Carl Roth
Hoechst 33342 (H3570)	Thermo Fisher Scientific
Methanol (M/4000/PB17)	Thermo Fisher Scientific
Paclitaxel (T7402)	Sigma-Aldrich
PageRuler™ Prestained Protein Ladder, 10 - 180 kDa (26616)	Thermo Fisher Scientific
Paraformaldehyde, granulated (0335.2)	Carl Roth
Penicillin/Streptomycin 10.000 U/mL (15140122)	Thermo Fisher Scientific
Pierce™ Coomassie (Bradford) Protein Assay Kit (23200)	Thermo Fisher Scientific
Polyvinylpyrrolidone (P0930)	Sigma-Aldrich
Recombinant Human FGF-basic 154 a.a. (100-18B)	PeproTech
Recombinant Human Transforming Growth Factor-beta 1 (11343160)	ImmunoTools
Ricolinostat (ACY-1215)	Selleckchem
ROTIPHORESE®NF-Acrylamide/Bis-solution 30 (A124.1)	Carl Roth
RPMI 1649 Medium (21875034)	Thermo Fisher Scientific
Sodium deoxycholate (302-95-4)	Sigma-Aldrich
Sodium dihydrogen phosphate monohydrate (K300.1)	Carl Roth
Staurosporine (CAS 62996-74)	Sigma-Aldrich
TEMED (2367.3)	Carl Roth
Tubastatin A (S8049)	Selleckchem
TRIS (0188.2)	Carl Roth
Triton X 100 (3051.4)	Carl Roth
Trypan Blue Stain, 0.4% (T13001-LG)	Bio-Cat
Trypsin/EDTA (25200056)	Thermo Fisher Scientific
Tween 20 (9127.1)	Carl Roth
Vorinostat (SML0061-5MG)	Sigma-Aldrich

Table 2. List of histone deacetylase inhibitors (HDACi), alphabetically ordered. Synthesized and provided by the Institute of Pharmaceutical and Medical Chemistry of the Heinrich-Heine-University (Düsseldorf). Synthesized by Marc Pflieger and Leandro Alves Avelar (Pflieger 2020; Alves Avelar et al. 2021). Left: coded designation; right: molecular structure.

KSK64	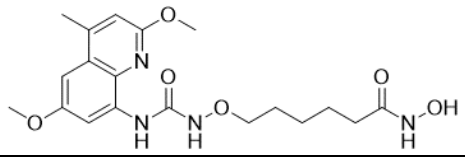
KSK75	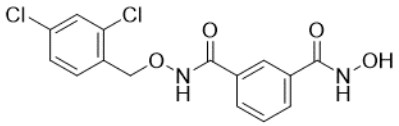
LAK41	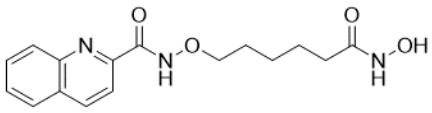
LAK53	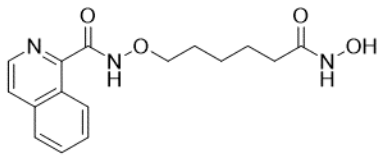
LAK61	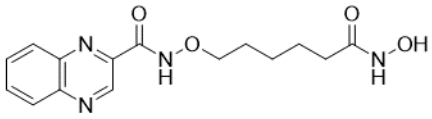
LAK67	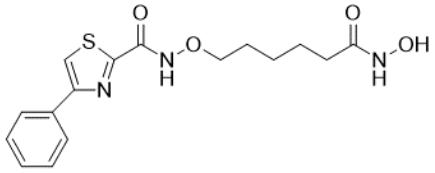
LAK92	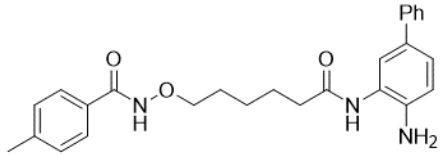
LAK107	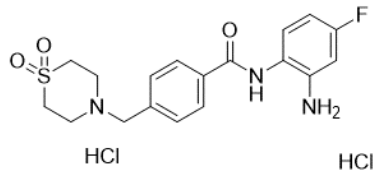
LAK110	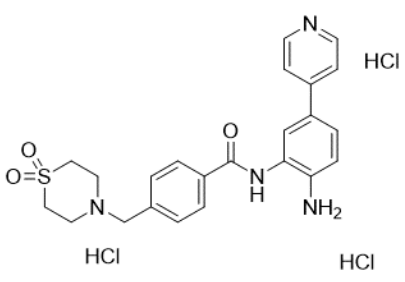

LAK121	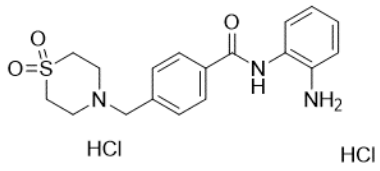
LAK127	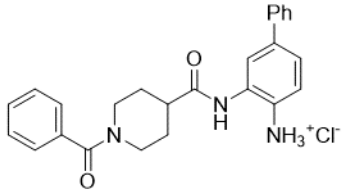
LAK-ZnFD	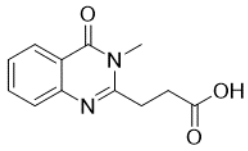
MPK264	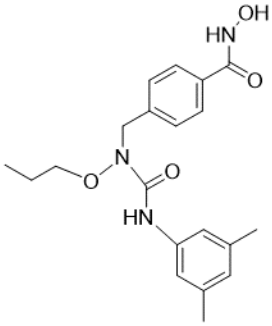
MPK265	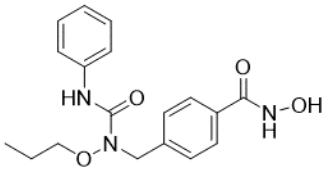
MPK324	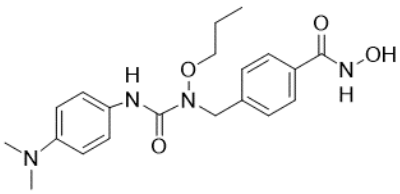
MPK544	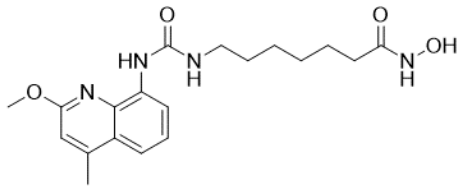

Table 3. List of artemisinin derivatives, alphabetically ordered and provided by Research Group Griesbeck, from the University of Cologne. Synthesized by Christina Bold (Bold 2022). Left: coded designation; right: molecular structure. Benzophenone included.

Artemisinin	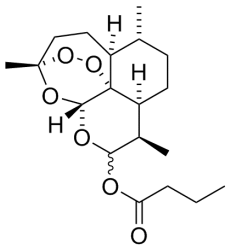
Artesunate	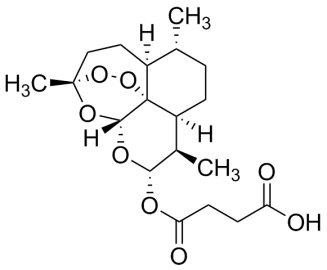
Benzophenone	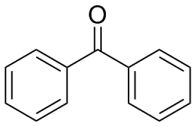
CB-108	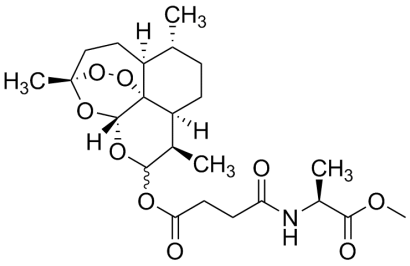
CB-110	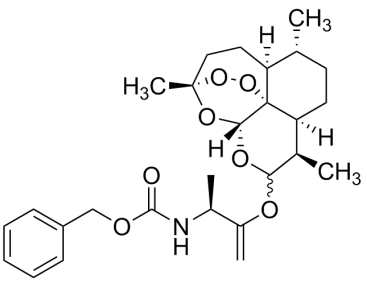

CB-66-Fr1	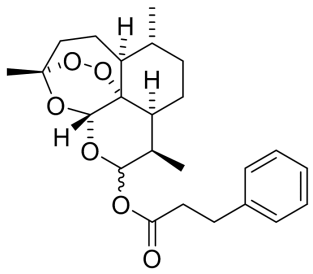
CB-84-Fr1	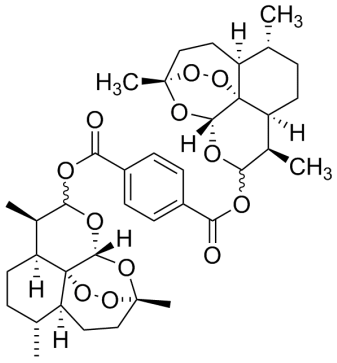
CB-AC-8	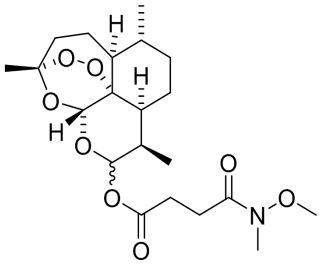
(CB)-EDV-01	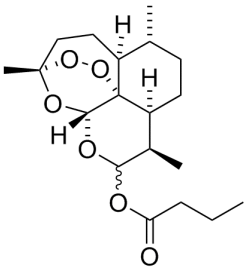
CB-Jan	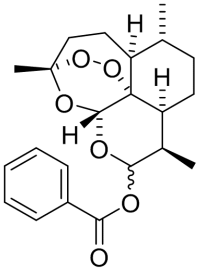

Dihydroartemisinin	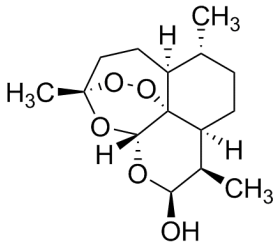
Hybrid 1	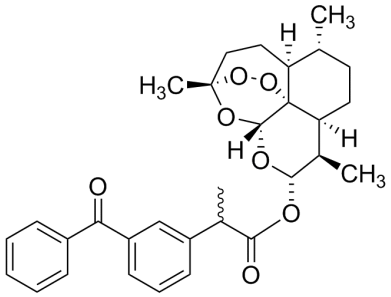

Table 4. List of tylophorinine derivatives, alphabetically ordered. Synthesized and provided by the institute of pharmaceutical biology and biotechnology of the Heinrich Heine University (Düsseldorf). Left: coded designation; right: molecular structure.

O-methyltylophorinidine (P05C06)	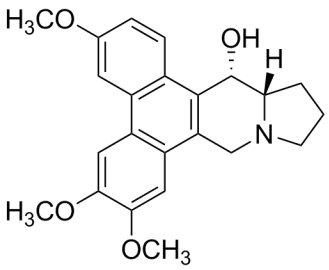
Tylophorinidine (P05C06B02)	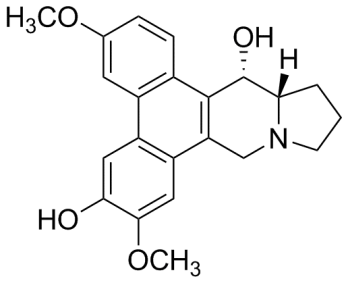

Tylophoridicine E (P05C06B03)	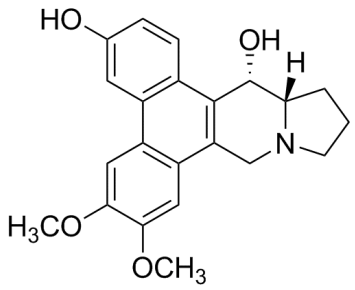
2-Demethoxytylophorine (P05C06B04)	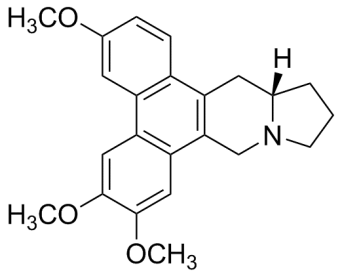
Tylophoridicine D (P05C06B05)	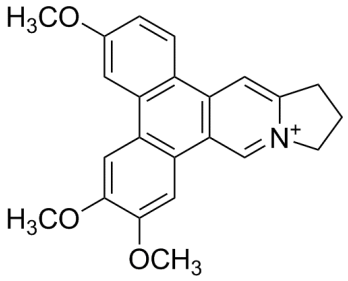
2-Demethyltylophoridicine D (P05C06B06)	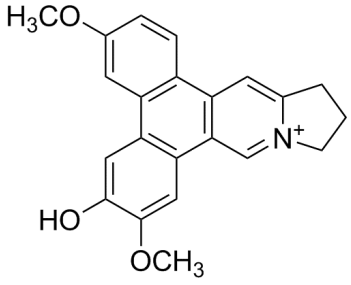

3.2.2 Antibodies

Antibodies were applied for western blotting and immunofluorescence staining of organoids.

Table 5. List of antibodies used and mentioned in this thesis.

Antibody	Provider
Actin Monoclonal Antibody (MA1-744)	Thermo Fisher Scientific
Anti-alpha smooth muscle Actin antibody (ab5694)	Abcam
Anti-Oct4 antibody [GT486] (ab184665)	Abcam
Anti-SOX2 antibody [SP76] (ab93689)	Abcam
CD163 Antibody, anti-human, PE, REAfinity (130-112-286)	Miltenyi Biotec
CD326 (EpCAM) Monoclonal Antibody (1B7) (14-9326-82)	Thermo Fisher Scientific
CD44 Antibody, anti-human, APC, REAfinity (130-113-900)	Miltenyi Biotec
Chicken anti-Mouse IgG (H+L) Cross-Adsorbed Secondary Antibody, Alexa Fluor 647 (A-21463)	Thermo Fisher Scientific
Donkey anti-Goat IgG (H+L) Cross-Adsorbed Secondary Antibody, Alexa Fluor 488 (A-11055)	Thermo Fisher Scientific
Donkey anti-Mouse IgG (H+L) Highly Cross-Adsorbed Secondary Antibody, Alexa Fluor 647 (A-31571)	Thermo Fisher Scientific
Donkey anti-Rabbit IgG (H+L) Highly Cross-Adsorbed Secondary Antibody, Alexa Fluor 546 (A10040)	Thermo Fisher Scientific
GAPDH (14C10) Rabbit mAb (#2118)	Cell Signaling Technology
Goat anti-Mouse IgG (H+L) Cross-Adsorbed Secondary Antibody HRP (31432)	Thermo Fisher Scientific
Goat anti-Rabbit IgG (H+L) Secondary Antibody, HRP (31460)	Thermo Fisher Scientific
Human/Mouse/Rat p53 Antibody (AF1355)	R&D Systems
Ki-67 (H-300) (sc-15402)	Santa Cruz Biotechnology
N-cadherin (13A9) (sc-59987)	Santa Cruz Biotechnology
Purified Mouse Anti-E-Cadherin (610182)	BD Transduction Laboratories
Vimentin Polyclonal Antibody (PA5-27231)	Thermo Fisher Scientific
YAP (63.7) (sc-101199)	Santa Cruz Biotechnology

3.2.3 Assays and Kits

Table 6. List of commercially available assays and kits.

Assay/Kit	Producer
CellTiter-Glo 3D Cell Viability Assay (G9681)	Promega
CellTiter-Glo Luminescent Cell Viability Assay (G7570)	Promega
CyQUANT NF Cell Proliferation (C35006)	Thermo Fisher Scientific
iScript cDNA Synthesis Kit (1708891)	Bio-Rad Laboratories Inc.
iTaq Universal SYBR Green Supermix (1725120)	Bio-Rad Laboratories Inc.
LIVE/DEAD™ Viability/Cytotoxicity Kit, for mammalian cells (L3224)	Thermo Fisher Scientific
Pierce™ Coomassie Bradford Protein-Assay-Kit (23200)	Thermo Fisher Scientific
PrestoBlue Cell Viability Reagent (A13262)	Thermo Fisher Scientific
ReliaPrep RNA cell Miniprep System (Z6010)	Promega
SYBR Green Master-Mix (4309155)	Thermo Fisher Scientific

3.2.4 Human Cell Lines

Different human cell lines were procured and applied for experimental research. Established and commercially available tumour cell lines are listed in the first table below (Tab.7). Patient-derived and non-immortalized cell lines are listed separately in the second table below (Tab.8). The correct cultivation and handling methods for each separate cell line are explained and detailed in Methods section 3.3.2. Table 9 lists further cell lines from which biological material was obtained.

Table 7. List of tumour cell lines, alphabetically ordered.

Cell line	Provider	Description
Capan-1	DSMZ (#ACC 244)	Liver metastasis of a pancreatic ductal adenocarcinoma
Capan-2	ATCC (#HTB-80)	Pancreatic adenocarcinoma
Panc-1	ATCC (#CRL-1469)	Pancreatic adenocarcinoma
	DMSZ (#ACC 783)	

Table 8. List of patient-derived cell lines, alphabetically ordered. These cell lines were not immortalized.

Cell line	Provider	Description
KU0020 PSC	Koç University, Center of Translational Medicine	Stellate cells isolated from pancreatic tumours
NCC06 HSC-P		Stellate cells isolated from hepatic lesions of PDAC tumours.

Table 9. List of further cell lines.

Cell line	Provider	Description
MCF-7	ATCC (#HTB-22)	Breast cancer cell lines
MCF-10A	ATCC (#CRL-10317)	
MDA-MB-231	DSMZ (#ACC 732)	

3.2.5 Devices

Table 10. List of devices and instruments.

Device	Company
Axio Vert.A1	ZEISS
CT15RE Centrifuge	VWR
CQ1 High-Content Spinning Disk System	Yokogawa Electric Corporation
CyBio Well vario	Analytik Jena
FUSION PULSE TS 6	VILBER LOURMAT DEUTSCHLAND GmbH
Heracell VIOS 160i CO2 Incubator (51030478)	Thermo Fisher Scientific
IncuCyte® Zoom	Sartorius
Mini-PROTEAN® Tetra Vertical Electrophoresis Cell for Mini Precast Gels	Bio-Rad Laboratories Inc.
LUNA-II Automated Cell Counter	Logos Biosystems
POLARstar Optima	BMG LABTECH
PowerPac Basic Power Supply	Bio-Rad Laboratories Inc.
Tecan SPARK	Tecan
Trans-Blot SD Semi-Dry Transfer Cell	Bio-Rad
UV-Lamp 022.9120	CAMAG
ZEISS LSM 880 Airy Scan	Carl Zeiss AG (ZEISS)

3.2.6 Software

Table 11. List of software and programs applied for scientific research and analysis.

Program	Usage	Company
Citavi	Literature Management	Swiss Academic Software
CellPathfinder	Imaging Software CQ1	Yokogawa Electric Corporation
CFX Maestro Software	Analysis Software for Bio-Rad CFX Real-Time PCR Systems	Bio-Rad
ChemBioDraw Ultra 13.0	Drawing Tool for Chemical Structures	PerkinElmer
CQ1 Software	Confocal Quantitative Image Cytometer CQ1	Yokogawa Electric Corporation
CyBio Composer	CyBio Well Vario Software	Analytik Jena
EvolutionCapt	Western-Blot Imaging and Analysis	VILBER LOURMAT DEUTSCHLAND GmbH
Fiji ImageJ	Imaging Software	Freeware (Github Open Source)
GraphPad PRISM 5	Statistical Analysis	GraphPad Software
GraphPad PRISM 8	Statistical Analysis	GraphPad Software
IncuCyte® Zoom	IncuCyte Software	Sartorius
Inkscape	Image editing	Inkscape
Microsoft Excel 2013	Data Management	Microsoft
Microsoft Excel 2021	Data Management	Microsoft
Microsoft Powerpoint 2013	Graphical Presentation	Microsoft
Microsoft Powerpoint 2021	Graphical Presentation	Microsoft
Microsoft Word 2013	Writing Program	Microsoft
Microsoft Word 2021	Writing Program	Microsoft
ZEISS ZEN lite	Imaging Processing Software	ZEISS

3.2.7 Miscellaneous Materials and Consumables

Table 12. List of consumables.

Consumables	Provider
384-Well-Plates F-Bottom µClear White (781098)	Greiner Bio-One
96-WELL-Plates V-Bottom Clear (651161)	Greiner Bio-One
Axygen® Multiple Well Reagent Reservoir with 4-Channel Trough (RES-MW4-HP)	Corning
Axygen® Single Well Reagent Reservoir with 96-Bottom Troughs (RES-SW96-HP-SI)	Corning
Cell Scraper 16 cm (83.1832)	Sarstedt
CELLSTAR 6-Well-Plates (657160)	Greiner Bio-One
CELLSTAR 96-Well-Plates µClear Black (655090)	Greiner Bio-One
CELLSTAR 96-Well-Plates µClear White (655098)	Greiner Bio-One
CELLSTAR 96-Well-Plates Clear (655180)	Greiner Bio-One
CELLSTAR 384-Well-Plates U-Bottom Cell-Repellent Surface (787979)	Greiner Bio-One
CELLSTAR 96-Well-Plates U-Bottom Cell-Repellent Surface (650970)	Greiner Bio-One
CELLSTAR Cell Culture Flask, 250 mL, 75 cm², PS, red filter screw cap, clear (658175)	Greiner Bio-One
CELLSTAR Cell Culture Flask, 550 mL, 175 cm², PS, red filter screw cap, clear (660175)	Greiner Bio-One
CELLSTAR Cell Culture Flask, 50 mL, 25 cm², PS, red filter screw cap, clear (690175)	Greiner Bio-One
CELLSTAR Cell-Repellent Surface Cell Culture Flask 50 mL 25 cm² clear (690985)	Greiner Bio-One
CELLSTAR Cell-Repellent Surface 6-Well-Plates (657970)	Greiner Bio-One
Corning® Primaria™ 60 mm x 15 mm Standard Cell Culture Dish (353802)	Corning
Sterican Canulae 0.60x25mm (4657667)	BRAUN
Syringes 2 mL (T135707)	Teqler
Syringes Injekt SOLO (LUER) 5 mL (4606051V)	BRAUN
Tips for CyBio Well vario pipetting head 96/250 µL (OL3800-25-559-N)	Analytik Jena
Tips for CyBio Well vario pipetting head 96/25 µL (OL3800-25-533-N)	Analytik Jena

3.3 Methods

3.3.1 Substances

All purchased and commercially available substances (growth factors, chemotherapeutics, cell media, etc.) were stored and handled as specified in their respective data sheets. Test substances were stored at -20 °C in their solid form.

All solid test substances utilized for experimental research were initially dissolved in 100 % dimethyl sulphoxide (DMSO), in a stock concentration of 100 mM (0.1 M), and the received total volume was separated into aliquots of 100 µL (0.1 mL) volume in standard 0.5 mL reaction tubes. Aliquots were marked accordingly and stored at -20 °C. Single aliquots that were removed of their storage for experimental application were transported and cooled on ice continuously to prevent molecular degradation.

Aliquots for lower concentrations (e.g. 100 µM aliquots for tylophorinine derivatives) were prepared either in DMSO or in cellular medium. In the latter case, those aliquots were only applied for single-usage and not reposited afterwards, but discarded.

3.3.2 Cultivation and Handling of Cells

The methodical cultivation and processing of adherent cell lines listed in the tables above (tables 7 to 9) are explained and described in the following sections of the thesis. Cultivation methods regarding cell lines from which material was used for singular experiments (e.g. protein lysates from MDA-MB-231 cells) are not included.

Cells were cultivated in their respective and appropriate medium at 37 °C and 5 % CO_2. Foetal bovine serum (FBS) was added to the medium in concentrations of either 10 or 20 %, depending on the cell line. The antibiotics penicillin and streptomycin (pen/strep) were always added to each medium in a concentration of 1 % to prevent bacterial contamination.

For the cryoconservation of cells, an estimated number of $1*10^6$ cells (see 3.3.2.5), dissolved in medium, was mixed with DMSO (10 % in a total volume of 1 mL) in a standard cryogenic storage vial. The cells were incubated in a -80 °C freezer for about 48 to 72 hours. Following this step, the now frozen vial of cells was stored in liquid nitrogen.

To thaw the stored cells and start the cultivation process, the selected vial was removed from the liquid nitrogen and transferred to a laminar flow cabinet. The cells were resuspended in 9 mL fresh and prewarmed cell culture medium in a 15 mL Falcon tube and centrifuged for 3 minutes at 300 g. The remaining pellet was resuspended in 5 mL medium, and the received suspension of cells was transferred to a T75 flasks and incubated at 37 °C for 24 hours, after

which the supernatant medium was replaced completely. When the cells reached a high degree of confluency, usually after 48 to 72 hours, they were trypsinized (see 3.3.2.5) and transferred to either a T75 (10 to 15 mL) or a T175 (20 to 25 mL) flask for further cultivation and experimental handling.

In this thesis, the established PDAC cell lines Panc-1, Capan-1 and Capan-2 (Blanchard II. et al. 2000; Deer et al. 2010; Friedman 2008) and the patient-derived CAF cell lines KU0020 PSC, a pancreatic stellate cell line (Farrow et al. 2009; Fan et al. 2020), and NCC06 HSC-P, a hepatic stellate cell line (Friedman 2008; Puche et al. 2013), were cultivated and utilized for experimental research.

3.3.2.1 Cultivation of Panc-1 Cells

Panc-1 (Lieber et al. 1975) cells were obtained from DSMZ (#ACC 783) and ATCC (#CRL-1469). No deviations regarding cellular profile or further characteristics regarding the two different providers were noted and documented. The majority of all experimental results shown and described in this thesis were obtained and generated with the ATCC Panc-1 cells.

Cells were cultivated in T75 flasks with 10 mL DMEM medium (10 % FBS and 1 % penicillin/streptomycin) or in T175 flasks with 25 mL medium. Cell cultures were trypsinized and split every three to four days to maintain a steady splitting rhythm. Panc-1 cells could be cultivated to high passages, but were usually discarded and thawed anew after 40 consecutive passages.

3.3.2.2 Cultivation of Capan-1 Cells

Capan-1 (Kyriazis et al. 1982) cells were obtained from DSMZ (#ACC 244). The tumour cells were cultivated in T75 flasks with 10 mL RPMI medium (20 % FBS and 1 % penicillin/streptomycin), and were trypsinized and split every three to four days. Capan-1 cells could be cultivated to high passages, but were usually discarded and thawed anew after 40 consecutive passages.

3.3.2.3 Cultivation of Capan-2 Cells

Capan-2 (Fogh 1986) cells were obtained from ATCC (#HTB-80) and cultivated in T75 flasks with 10 mL DMEM medium, (10 % FBS and 1 % penicillin/streptomycin), and were trypsinized and split every three to four days. The cells available in the laboratory were of high passage (around passage 48 to 65), and were therefore discarded after 20 cycles of splitting and cultivation.

3.3.2.4 Cultivation of Patient-Derived Cancer-associated Fibroblasts (CAF)

Two patient-derived CAF cell lines were used in this thesis: KU0020 PSC, a pancreatic stellate cell line from a PDAC tumour, and NCC06 HSC-P, a hepatic stellate cell line from a PDAC liver metastasis, generously provided from Koç University, Istanbul (Xie et al. 2020). The cells were not immortalized.

Both cell lines were cultivated in DMEM/F-12 medium (20 % FBS and 1% penicillin/streptomycin), and grown to a high degree of confluency before being split. Cells were incubated in T75 flasks with 12 mL medium and in T175 flasks with 25 mL medium. After 20 to 22 passages, both cell lines were observed to enter senescence and ceasing proliferation, so cultivation was manually stopped at 19 passages to prevent undesirable cellular changes affecting experimental outcome. Cell suspensions were never split higher than 1:4 to maintain a high cell titre and level of confluency. Cultivation medium was changed every two days, by removing and adding up to 7 mL of medium per flask.

Both CAF cell lines, KU0020 PSC and NCC06 HSC-P, secrete huge amounts of extracellular material, and one T75 flask yields about $1*10^6$ to $2.0*10^6$ cells. Cultivation of CAF cells in T175 flasks resulted in higher cell titres, but it was noted that cells entered senescence at around 16 passages when incubated in such conditions, so the approach with T75 flasks was preferred. The split rhythm was aligned with the rhythm of the tumour cells, so both cell types could be harvested on the same day for organoid generation.

3.3.2.5 Trypsinization, Counting and Seeding of Cells

For experimental application, cells had to be harvested and trypsinized. When cells reached a high degree of confluency (about 70 to 80 % for tumour cells, 80 to 90 % for CAFs) in their respective tissue culture flasks, the cultivation medium was carefully discarded. The remaining cells were washed with 2 mL PBS and dissolved with 2 mL 0.25 % Trypsin/EDTA. Trypsinization was conducted for a duration of 5 minutes for tumour cells and 8 minutes for CAFs at 37 °C. The obtained cell suspension was transferred with 4 mL fresh medium to a 15 mL Falcon tube and centrifuged for 3 minutes at 300 g. The supernatant medium was then carefully discarded without touching the cell pellet, which was resuspended in an appropriate volume of fresh medium. For tumour cell lines, a high volume (3 to 4 mL) was applied to singularize the cells. CAF cell lines were resuspended in a low volume (1 to 2 mL) to receive a high cell titre (see 3.3.2.4).

To calculate the concentration of cells, 10 µL of suspension were removed from the Falcon tubes and mixed with 10 µL of either Trypan blue (Strober 2001) or Erythrosine B (Lin and

Brusick 1986), then transferred to the LUNA-II Automated Cell Counter (Logos Biosystems). For each cell type, an optimized counting protocol was established, tested and optimized beforehand. The number of vital and singular cells was then determined and checked. At least 90 % of all counted cells should be vital, and at least 80 % of all counted cells should be present as singularized cells, to ensure reproducible experimental results. Lower values of vital cells and high values of clustered cells indicate a non-optimal cell culture, which might influence experimental outcome due to the elevated presence of dead cells and cell clusters.

Alternatively, cells could be counted with a standard haemocytometer. This was mostly done for the PSC cells, as the automated counting protocols executed by the LUNAII device turned out to be error-prone due to the intrinsic heterogeneity of the PSC cell culture.

After the cells were seeded, the remaining cell suspension was split accordingly and transferred back to either the original or a new tissue culture flask, which were changed after three to four weeks of usage to ensure sterility and operability.

3.3.3 Two-Dimensional Experimental Assays and Methods

The following section describes the different methodical approaches and assays of two-dimensional (2D) models. This will include the 2D cytotoxicity assays (3.3.3.1), the live-cell imaging with the IncuCyte® Zoom device (3.3.3.2), the western blot methods (3.3.3.3), the real-time quantitative polymerase chain reaction (RT-qPCR; 3.3.3.4), and the colony formation assay (3.3.3.5). The 3D cytotoxicity assays (3.3.4.2) and the tumorsphere methods (3.3.5) will not be discussed in this section.

3.3.3.1 Two-Dimensional Cytotoxicity Assays

2D cytotoxicity assays were performed to evaluate and examine the cytotoxic and anti-proliferative properties of novel substances and established drugs by calculating the IC_{50} values from at least three independent repeats. Pipetting steps on 96-well plates were mainly conducted manually. The CyBio Well vario (Analytik Jena) automatic pipetting device was utilized for 384-well plate methods, as manual pipetting was not feasible due to inevitable pipetting errors and subsequent high deviations in measurement. Cell seeding, substance treatment and the addition of assay solution on 96-well plates could be conducted with the CyBio Well vario device as well. After trypsinization and cell counting (see 3.3.2.5), the assays were initiated by seeding a defined number of cells (Tab. 13). On 96-well plates, 90 µL of cell suspension were pipetted in each well. On 384-well plates, 18 µL of cell suspension were pipetted in each well.

Table 13. Cell number per well, on 96- and 384-well plates, listed alphabetically. Capan-1 and Capan-2 cells were not tested on 384-well plates. NCC06 HSC-P cells were not utilized for cytotoxic assays.

Cell Line	96-Well (cells/well)	384-Well (cells/well)
Capan-1	5,000	-
Capan-2	10,000	-
KU0020 PSC	2,000	600
Panc-1	5,000	1,500

Following an incubation period of 24 hours, the plates were examined with the Axio Vert.A1 microscope to validate the adhesion of cells on the well surface and their homogenous distribution. The cells were treated with 10 µL of substance solution, obtaining a total volume of 100 µL medium on the 96-well plates. On 384-well plates, the cells were treated with 2 µL of substance solution, obtaining a total volume of 20 µL. The substances were prepared in tenfold concentrations in the respective cell medium, to receive a 1:10-dilution in the wells.

The dose-response curves (DRC) were prepared on a separate 96-V-well plate, with a minimum volume of 50 µL in each well. A standard dose-response curve (DRC) started with a concentration of 100 µM and had seven decreasing 1:3-dilution steps. The first DRC concentration was prepared by adding 7.5 µL of the stock solution (10 mM substance) to 67.5 µL medium in the first well, resulting in a volume of 75 µL with a concentration of 1 mM/1000 µM. In the following consecutive steps, 25 µL of the solution in the first well was removed and added to 50 µL medium in the next well, receiving a volume of 75 µL and a concentration of ca. 333.33 µM. This pipetting step was repeated six times further. For the tylophorinine derivatives, a lower start concentration of 1000 nM/1 µM was prepared due to the higher efficacy of these drugs.

To accurately assess the cytotoxic properties of test substances, a positive control was always added to each plate as a single concentration of an efficacious substance. A DRC of an effective substance was used as a positive control on 384-well plates. The well-established chemotherapeutic drug gemcitabine (Burris III et al. 1997; Goldstein et al. 2015) or the alkaloid staurosporine (Omura et al. 1995) were commonly applied as positive controls on 96-well plates. Gemcitabine was applied in a concentration of 100 µM, staurosporine in a concentration of 10 or 1 µM. Untreated cells were likewise needed for the correct evaluation of cytotoxicity, together with a medium control, a blank control and a solvent control of 1 % DMSO.

All substance concentrations were applied in triplicates (96-well plates) or in quadruples (384-well plates). The outer wells of the plates were never used due to medium evaporation effects. On a 96-well plate, two different dose-response curves could be tested. On a 384-well plate, up to six different dose-response curves could be tested (five test substances and one control DRC).

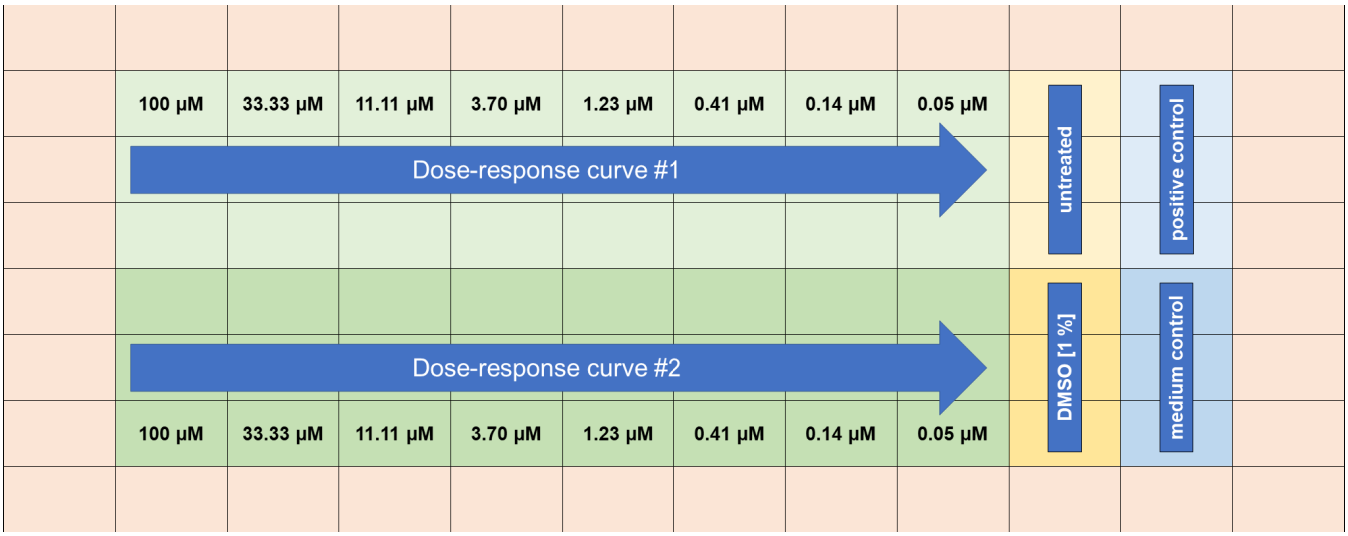

Figure 5. Standard 96-well plate preparation. The diagrammatic plan of two dose-response curves (green wells) plus a DMSO solvent control at 1 % (orange wells), a medium control (blue wells), untreated Panc-1 cells (yellow wells) and a positive control (light blue wells) is depicted here. Outer wells (red) are not utilized.

Substance treatment lasted for either 48 or 72 hours of incubation, after which the assays were conducted. Different cytotoxicity assays were applied in this thesis: the CyQUANT NF Cell Proliferation Assay (Thermo Fisher, #C35006), the CellTiter-Glo® Luminescent Cell Viability Assay (Promega, #G7570) and the PrestoBlue™ Cell Viability Reagent (Thermo Fisher, #A13262). The assays were executed as described in the respective protocols. For the CyQuant assay (Jones et al. 2001) and the PrestoBlue assay (Xu et al. 2015), who utilized fluorescence methods to measure and quantify cell viability, black plates were selected, while white plates were selected for the CellTiter-Glo® assay (Tolliday 2010), which utilized luminescence methods.

Luminescence or fluorescence signals were measured with either the Tecan SPARK (Tecan) or the POLARstar Optima device (BMG Labtech). It was observed that the CellTiter-Glo® assay would result in high luminescent values that could not be detected by the Tecan SPARK device, especially after 72 hours of incubation, so the CellTiter-Glo® assays were mainly measured with the POLARstar Optima device. Fluorescence assays were measured with the Tecan SPARK device. The IC_{50} values were calculated with the GraphPad Prism 8 software. Each experiment was repeated at least three times independently.

This protocol was slightly changed and adapted for the UV-activated artemisinin derivatives. Cells were seeded on 96-well plates as described above and subjected to substance treatment after 24 hours of incubation. Incubation under UV irradiation (366 nm), with the plate lid removed, lasted for another set of 24 hours, before the PrestoBlue assay was executed. Ultraviolet irradiation was generated by a specialized UV lamp (CAMAG). To accurately assess the effect of UV radiation, a control plate (24 hours at 37 °C only) was tested as well.

3.3.3.2 Live-Cell Imaging

Live-Cell Imaging was performed with the IncuCyte® Zoom device (Sartorius, Göttingen) to evaluate the anti-proliferative and/or cytotoxic properties of novel drugs. The proliferation assay was initiated by manually seeding 5,000 Panc-1 cells per well in a volume of 90 µL on Incucyte® Imagelock 96-well plates (Cat. #BA-04856, Sartorius).

After 24 hours of incubation, the adherent cells were treated in triplicates by adding 10 µL of substance solution ($DMEM^{+/+}$ medium) per well, obtaining a volume of 100 µL. The plate was incubated for a total duration of 96 hours. Three different concentrations were applied for each substance, and three images were recorded for each well every 60 minutes with the IncuCyte® Zoom (Sartorius) software.

All experiments were repeated three times. The quantification of tumour cell proliferation was conducted with the IncuCyte® Zoom software, and the GraphPad PRISM 8 software was used for statistical analysis. This protocol was adapted and specifically optimized for Panc-1 cells from a previous publication of our research group (Sperlich and Teusch 2018).

The scratch wound assay for cell migration analysis was conducted with the IncuCyte Zoom device and the IncuCyte® Zoom software as well. The assay was initiated by manually seeding 40,000 Panc-1 cells per well in a volume of 90 µL on Incucyte® Imagelock 96-well plates. After an incubation period of 16 hours at 37 °C, a scratch wound was produced with the IncuCyte WoundMaker tool, followed by the treatment of the adherent cells in triplicates by adding 10 µL of substance solution (in $DMEM^{+/+}$) per well, obtaining a total volume of 100 µL. The migration assay ran for 48 hours. Statistical analysis was conducted with the GraphPad PRISM 8 software.

3.3.3.3 Western Blotting

Western blotting was performed to evaluate the effect of novel substances on the expression of certain proteins of interest (Mahmood and Yang 2012). The experiment was started by seeding Panc-1 cells on 6-well plates (Greiner #657180), with 300,000 cells per well in a

volume of 1.8 mL cell culture medium. After an initial incubation period of 6 hours, the cells had successfully adhered to the well surface, and were treated with 200 µL substance solution, obtaining a total volume of 2 mL per well. For each 6-well plate, a negative control (medium only) was conducted as well.

Incubation lasted for 24 hours, and following substance treatment, the cells were washed with 1 mL PBS twice and dissolved with 100 µL RIPA-buffer (see Table 14 below) for 5 minutes while being stored on ice. The cell suspension was scraped carefully from the well surface and transferred to a standard 1.5 mL tube. The samples were centrifuged for 15 minutes at 14,000 g and 4 °C, and the liquid supernatant was saved and stored at -20 °C, while the remaining pellet of cellular debris was discarded.

Table 14. Composition of RIPA buffer. One tablet of protease inhibitor per 10 mL buffer solution. Aliquots stored at -20 °C. A volume of 10 µL 100 mM phenylmethylsulfonyl fluoride (diluted in ethanol and stored at -20 °C) was added to receive a working RIPA buffer solution.

Chemicals	Concentration
Tris/HCl (pH=7.5)	50 mM
Triton X100	1.0 %
Sodium Deoxycholate	0.5 %
Sodium Dodecyl Sulphate	0.1 %
Sodium Chloride	150 mM
EDTA	1 mM

The Pierce™ Coomassie Bradford Protein-Assay-Kit (Thermo Fisher Scientific) was used for protein determination, and samples were measured with the POLARstar Optima device. Bovine serum albumin (BSA, included in the kit) was applied to calculate the calibration curve.

The SDS-Page was started by loading 10 µg of material (20 µL cell lysate plus 5 µL sample buffer) per lane on a 12 % acrylamide gel, with 5 µL marker (Thermo Fisher Scientific) on the outer lanes. Gel electrophoresis was executed at 200 V for 1 hour at room temperature.

The proteins were transferred from the separation gel to a nitrocellulose membrane via western blotting. The filter paper, nitrocellulose membrane and gel were firstly saturated in a blocking buffer solution (192 mM glycine, 25 mM TRIS, 20 % methanol) for 15 minutes. The blotting was executed with the Trans-Blot SD Semi-Dry Transfer Cell device (Bio-Rad) at 20 V for 40 minutes.

After the blotting had concluded, the nitrocellulose membrane was washed for 5 minutes in 10 mL TBS-T buffer, blocked for 30 minutes in 10 mL TBS-T buffer with 5 % BSA, washed again

and incubated with the primary antibody in 5 mL blocking buffer (TBS-T buffer and 1 % BSA) and an antibody against a respective house-keeper gene (either GAPDH or beta-actin) on a rotator over night at 4 °C. Antibody concentrations were applied as instructed in the respective data sheets.

Following the first antibody incubation step, the blots were washed four times for 5 minutes with 5 mL TBS-T and incubated with the secondary horseradish peroxidase (HRP) antibody (see 3.2.2 for antibodies) in 5 mL blocking buffer for 1 hour at room temperature. After a second set of four washing steps, the AceGlow working solution (5 mL per blot) was applied and the luminescence signal was measured after 5 minutes of incubation, utilizing the VILBER FUSION PULSE TS 6 Imager. Signal quantification was conducted with the EvolutionCapt software (VILBER). For each experiment/substance, three independent repeats were carried out and analysed.

The statistical analysis was conducted via an ordinary one-way ANOVA with the GraphPad PRISM 8 software.

3.3.3.4 Real-Time Quantitative Polymerase Chain Reaction (RT-qPCR)

RT-qPCR was conducted to evaluate the effect of substances on the expression of proteins of interest on the mRNA and transcription level. The assay was started by seeding a total number of $1*10^6$ Panc-1 cells in a volume of 2.7 mL medium on 6 cm x 1.5 cm tissue-culture dishes. After an initial incubation period of 6 hours, the cells had successfully adhered to the well surface and were treated with 300 µL substance solution, obtaining a total volume of 3 mL. The cells were incubated for 24 hours and then washed with 2 mL PBS and dissolved via trypsinization with 1 mL 0.25 % Trypsin/EDTA for 5 minutes at 37 °C. The cell suspension was transferred to a 1.5 mL reaction tube and centrifuged at 300 g for 3 minutes.

The mRNA was isolated from the remaining cell pellet (supernatant discarded) with the ReliaPrep RNA Cell Miniprep Kit (Promega). Successful mRNA isolation was verified and evaluated via NanoDrop confirmation, and the mRNA was stored at -80 °C as quickly as possible while being kept on ice constantly in order to prevent degradation.

The cDNA synthesis was executed with up to 2 µg of isolated mRNA with the iScript cDNA Synthesis Kit (Bio-Rad). Obtained cDNA was stored at -20 °C. The RT-qPCR was conducted with the SYBR Green Master-Mix (Bio-Rad), with GAPDH as the housekeeper gene. Results were analysed with the CFX Maestro Software (Bio-Rad). The statistical analysis was executed via an ordinary one-way ANOVA with the GraphPad PRISM 8 software.

The primers for target genes were selected and taken from scientific literature and checked via BLAST (Altschul et al. 1997; Altschul et al. 1990).

Table 15. List of primers used for RT-qPCR and their respective literature sources. The primers for GAPDH and vimentin (VIM) were present in the laboratory prior to the start of the research project.

Gene Name	Forward-Primer (5'-3')	Reverse-Primer (5'-3')	Literature Source
CD24	TCCAACTAATGCCACCACCAA	GACCACGAAGAGACTGGCTGTT	Sasaki et al 2018
CD44	GATGGAGAAAGCTCTGAGCATC	TTGCTGCACAGATGGAGTTG	Hou et al 2019
CD133	TTCTTGACCGACTGAGACCCA	TCATGTTCTCCAACGCCTCTT	Chen et al 2017
E-cadherin (CDH1)	CGAGAGCTACACGTTCACGG	GGGTGTCGAGGGAAAAATAGG	Anzai et al 2017
EPCAM	CCATGTGCTGGTGTGTGTGAA	TGTGTTTTAGTTCAATGATGATCCA	Karabicici et al 2021
GAPDH	CGCTGAGTACGTCGTGGAGT	CTAGACGGCAGGTCAGGTCC	
HDAC2	ATGGCGTACAGTCAAGGAGG	TGCGGATTCTATGAGGCTTCA	Zhang et al 2019
HDAC6	CAACTGAGACCGTGGAGAG	CCTGTGCGAGACTGTAGC	Zheng et al 2020
Nanog	CCATCCTTGCAAATGTCTTCTG	CTTTGGGACTGGTGGAAGAATC	Siu et al 2019
N-Cadherin (CDH2)	CACAGCCACGGCCGTCATCA	TGGGTCGGTCTGGATGGCGA	Perrot et al 2020
Vimentin	CCAAACTTTTCCTCCCTGAACC	GTGATGCTGAGAAGTTTCGTTGA	

3.3.3.5 Colony Formation Assay

Further experimental evaluation of anti-proliferative effects on tumour cells was conducted via a colony formation assay on 6-well tissue culture plates. Panc-1 tumour cells were seeded in a low density of 1,000 cells in 2 mL medium per well. Substance treatment was conducted after an initial incubation period of 24 hours following seeding, by adding 1 mL substance solution ($DMEM^{+/+}$) to the adherent cells. For each 6-well plate, one well served as the untreated negative control. Colony formation of tumour cells lasted for 10 days (240 hours) in total before crystal violet (Cat.# 61135, Sigma Aldrich) staining was performed. Supernatant medium was discarded and cells were washed twice with 2 mL PBS before being fixated with 1 mL of ice-cold methanol (100 %, stored at -20 °C) for 10 minutes. The colonies were then stained with 1 mL 1 % crystal violet (25 % methanol) for 10 minutes and washed thrice with 2 mL sterile H_2O. All steps conducted at room temperature. Counting of colonies was conducted manually.

3.3.4 Three-Dimensional Cell Culture Methods

The following section describes the various methods and experimental procedures regarding three-dimensional organoids, their cultivation and generation (3.3.4.1), the cytotoxic evaluation of substances on organoids (3.3.4.2), the staining with antibodies and other chemicals (3.3.4.3), the microscopical imaging (3.3.4.4 to 3.3.4.5) and analysis via the CellPathfinder program (3.3.4.6).

3.3.4.1 Generation and Cultivation of Organoids

The following organoid generation protocol was taken and minimally adapted from the original research of Bailu Xie (Xie 2018) and Vanessa Mundorf (Mundorf 2018). The scientific method described below was published previously by our research team (Xie et al. 2020).

All three-dimensional organoids generated during this thesis were co-culture spheroids, consisting of 1) PDAC tumour cells, either Panc-1 or Capan-2, and 2) patient-derived CAF cells, either KU0020 PSC (pancreatic stellate cells) or NCC06 HSC-P (hepatic stellate cells). The common 3D model was the Panc-1 + PSC organoid, together with the Capan-2 + PSC organoid. Other 3D models created and utilized (Xie et al. 2020) were Panc-1 + HSC and Capan-2 + HSC organoids. An initial experiment regarding the creation of Capan-1 + HSC organoids (PDAC liver metastasis model) was executed as well, and will be explained in section 4.3.3.

Splitting, harvesting and counting of cells was performed as described above (3.3.2). The individual cell pellets were resuspended in DMEM/F-12 medium with 10 % FBS, the standard medium for all organoid suspensions. A co-culture solution with tumour cells ($1*10^4$ cells/mL), CAF cells ($2*10^4$ cells/mL) and collagen 1 (0.1 mg/mL) was then mixed together in organoid medium and kept on ice. The collagen served as the scaffolding matrix (Mundorf 2018), mimicking the tumour microenvironment (Xu et al. 2019).

Pipetting was either done manually or with the CyBio Well vario pipetting robot. All pipetting steps on 384-well plates were carried out with the CyBio Well vario robot. For both approaches, the pipetting tips were pre-cooled at -20 °C for 24 hours in advance. Manual pipetting was executed with a multi-channel pipette for faster organoid seeding. For a 96-well approach, 50 µL of volume were seeded in each well (500 Panc-1 cells + 1,000 CAF cells), and 6 mL cell suspension were prepared in advance. For a 384-well approach, 10 µL of volume were seeded in each well (100 Panc-1 cells + 200 CAF cells), and 22 mL cell suspension were prepared in advance.

After 24 hours of incubation (day 2), the newly formed organoids were controlled and checked with the Axio Vert.A1 microscope (Zeiss), and new medium was added to each well. 50 µL volume of medium were added on the 96-well plates, 8 µL on the 384-well plates. Following an incubation period of 48 hours, the organoids were treated with either 100 µL (96-well plates) or 2 µL (384-well plates) substance solution or simple medium per well, to obtain a total well volume of 200 µL on 96-well plates and 20 µL on 384-well plates. Alternatively, to avoid potential spilling of liquid on 96-well plates, only 40 µL medium could be added on day 2, followed by 10 µL medium on day 4, to obtain a total well volume of 100 µL instead of 200 µL. No change in organoid growth or viability were noted or observed regarding the different well volumes, and the lower volume approach was favoured as it simplified later procedural stages.

Organoids were stable and spherical on day 4, after 72 hours of incubation, and could be utilized for further experimental approaches, either for cytotoxicity assays or for antibody-staining. All organoids on a 96-well plate were examined and evaluated with the Axio Vert.A1 microscope beforehand, to sort out unsuitable organoids. In some cases, organoids did not grow or form correctly, taking on a lopsided shape. These misshapen organoids were not utilized any further.

Panc-1 + PSC organoids could be cultivated for at least nine days following seeding without losing their spheroidal shape and form. Different organoid variations (Panc-1 + HSC, Capan-2 + PSC, etc.) were not examined for time periods longer than 144 hours.

3.3.4.2 3D Cytotoxicity Assays

Testing and screening of substances regarding their cytotoxic efficacy on 3D organoids was performed with the CellTiter-Glo 3D Cell Viability Assay (Promega). Dose-response curves (DRC) were prepared and applied analogously to 2D methods (3.3.3.1), with eight consecutive concentration steps, either in triplicates (on 96-well plates) or quadruples (on 384-well plates). Positive, negative, medium and solvent controls were applied as well. As described in section 3.3.4.1, 96-well organoids were incubated in a volume of 90 µL and treated with 10 µL substance solution at day 4, while 384-well organoids were incubated in a volume of 18 µL and treated with 2 µL substance solution. All pipetting steps regarding 384-well plates were always conducted and executed with the CyBio Well vario pipetting robot.

Following the addition of substances, the plates were incubated for 72 hours at 37 °C and 5 % CO_2. The cytotoxicity was then evaluated with the CellTiter-Glo 3D Cell Viability Assay (Promega). After the assay solution was added (1:1 volume), the 96-well plates were put on a rotator for 5 minutes at low speed and incubated for a further period of 25 minutes, while the 384-well plates were rotated for 30 minutes in total, to ensure the successful lysis of organoids

by the assay solution. The luminescence values were recorded with the Tecan SPARK device. Statistical analysis was executed with the GraphPad PRISM 8 software to calculate the IC_{50} values.

3.3.4.3 Staining of Three-Dimensional Organoids

Organoids were stained with antibodies (3.3.4.3.1) and other chemicals (3.3.4.3.2) for visualization and imaging via confocal and spinning disc confocal microscopy (3.3.4.4 to 3.3.4.5).

3.3.4.3.1 Immunofluorescence Staining

Organoids were stained with fluorescent antibodies following fixation and permeabilization. The PDAC organoids became compact and spheroidal around four days after the initial seeding (day 1), and were harvested and fixated at day 7. Prior to day 4, organoids could not be pipetted correctly and immunofluorescence staining procedures were unable to be executed.

Treatment with different substances of interest was conducted on day 6, by selecting correctly formed and round organoids from the plate and adding substances, dissolved in organoid medium in appropriate concentrations. For each concentration, at least six replicates were done. Substance incubation usually lasted for 24 hours, but could be extended to 72 hours.

Following substance incubation, the organoids were carefully transferred to standard 1.5 mL tubes (six organoids per tube), washed with 1 mL PBS twice and fixated with 1 mL 4 % PFA/PBS for 1 hour at room temperature. The organoids could be stored at 4 °C for up to two weeks after being washed with 1 mL PVP/PBS (3 mg/mL) four times (Wong et al. 2002). Fixated organoids were not stored longer in this condition and were commonly stained on the next day or immediately afterwards.

The antibody staining was initiated by permeabilization of the organoids via incubation with 0.5 mL 0.25 % Triton X-100 (in PVP/PBS) for 1 hour at room temperature, and followed by blocking with 0.5 mL blocking solution (0.1 % BSA, 0.01 %Tween 20 in PBS) under the same conditions. The permeabilization buffer was always freshly prepared. The blocking buffer was prepared in advance and stored at -20°C. The primary antibodies were dissolved in blocking solution (1:100) and the organoids were incubated in 100 µL antibody solution for 16 to 24 hours at 4 °C on a rotator.

After being washed with blocking solution thrice for 15 minutes each, the secondary antibody solution (fluorescent Alexa Fluor antibodies, 1:200 in blocking buffer) was applied and incubated for another 16 to 24 hours at 4 °C on a rotator. DAPI was added in a concentration of 2 µg/mL for nuclear staining (Kapuscinski 1995).

After the second antibody incubation step had concluded, the organoids were washed another four times with blocking solution for 15 minutes at room temperature. To prepare the organoids for their imaging, essential clearing steps with six increasing concentrations of ethanol (30, 50, 70, 90, 96 and 100 %) were performed, with 1 mL ethanol solution per tube for 30 minutes each, followed by a last clearing step with 200 µL benzyl alcohol/benzyl benzoate (1:2) for 1 hour. All clearing steps were executed at room temperature. The organoids were, following this step, no longer visible unless viewed under fluorescent light, and were carefully transferred in a volume of 50 to 100 µL BABB to a fitting imaging plate (Cat. #89626, ibidi). A lower volume of BABB was preferred to prevent organoid movement, which complicated Z-stack imaging and microscopical analysis.

This staining protocol was adapted and optimized from Nichols et al. (2009) and the work of Bailu Xie (Xie 2018).

3.3.4.3.2 Live/Dead-Staining

The second 3D organoid staining approach was performed with the LIVE/DEAD® Viability/Cytotoxicity Kit (Invitrogen). Staining was commonly conducted with ethidium homodimer-1 (EthD-1), the respective dead stain of the kit (Gaugain et al. 1978). Calcein AM functioned as the respective live stain of the kit (Homolya et al. 1993).

Organoids were stained 144 hours after seeding (day 7). Staurosporine was applied as a substance of high toxicity (Omura et al. 1995), in a concentration of 1 and 10 µM, to validate the function of the dead stain EthD-1. To correctly assess and evaluate the staining, a negative control with only organoid cultivation medium had to be applied as well.

Following 24 hours of staurosporine incubation, the organoids were carefully transferred to a standard 1.5 mL reaction tube, and the supernatant medium was aspirated. After being washed with 1 mL PBS twice, the organoids were stained with 500 µL EthD-1 (4 µM) and/or Calcein AM (4 µM) solution (dissolved in 1xPBS). Staining with EthD-1 lasted for 1 hour at room temperature. Staining with Calcein AM lasted for six hours at 37 °C. Staining solution was discarded afterwards and the organoids were washed with 1 mL PBS twice. Fixation was executed with 300 µL PFA (4 %) for 1 hour at room temperature. The organoids were then permeabilized with 500 µL 0.25 % Triton X-100 in PVP/PBS (3 mg/mL) for 1 hour at room

temperature and further stained with 500 µL DAPI (2 µg/mL) under the same conditions. DAPI staining of organoids was impossible without prior permeabilization.

Stained organoids were protected from light and stored at 4 °C in 1 mL PVP/PBS (3 mg/mL) for up to two weeks. Clearing was conducted as described above (3.3.4.3.1). The organoids were imaged with the CQ1 Confocal Imaging Cytometer (Yokogawa).

3.3.4.4 Confocal Microscopy of Organoids

High-resolution images of three-dimensional organoids stained with fluorescent antibodies were recorded with the Zeiss confocal laser scanning microscope (LSM) 880 (Carl Zeiss, Jena, Germany) (Xie et al. 2020; Xie 2018). Fluorescence signals were recorded with the laser wavelengths at 405 (2.00 %), 488 (0.5 %), 561 (2.00 %) and 633 nm (2.40 %). For the excitation wavelength of 405 nm, an emission wavelength of 442 nm and a detection wavelength of 410 to 473 nm were applied. For the excitation wavelength of 488 nm, an emission wavelength of 522 nm and a detection wavelength of 493 to 550 nm were applied. For the excitation wavelength of 561 nm, an emission wavelength of 588 nm and a detection wavelength of 566 to 609 nm were applied. For the excitation wavelength of 633 nm, an emission wavelength of 703 nm and a detection wavelength of 648 to 758 nm were applied. Technical parameters were fixed at a line time of 30.00 µs, a binning mode of 1x1 and a digital gain of 1.0. Images were recorded with a bit depth of 16 bit, a scaling of 0.69 µm x 0.69 µm x 1.00 µm per pixel and an image size of 1024 x 1024 pixels.

Recorded images and Z-stacks were analysed and edited with the ZEISS ZEN lite and ImageJ software.

3.3.4.5 Spinning Disc Confocal Microscopy of Organoids

The CQ1 Confocal Imaging Cytometer (Yokogawa Electric Corporation, Musashino, Japan) was utilized for confocal microscopy of organoids and the quantitative analysis of fluorescence signals. The device was pre-cooled to room temperature (22 °C) prior to imaging. Microscopical images and Z-stacks of organoids were recorded with the laser wavelengths 405 nm, 488 nm, 561 nm and 640 nm. Technical parameters were fixed at 20 % power and 300 ms of exposure for all channels. Z-Stacks were recorded with 20x magnification and a bit depth of 16 bit. Recorded images and Z-stacks were analysed and edited with the CellPathfinder (Yokogawa) and ImageJ software. Further parameters and details regarding the usage of the CQ1 Confocal Imaging Cytometer are described below (3.3.4.6).

3.3.4.6 Quantitative Analysis of Organoids

The quantitative analysis of fluorescent signals from secondary antibodies in Z-stacks of three-dimensional organoids was executed to determine the effect of substances on the expression of proteins of interests. The following protocol was established to analyse the expression of E-cadherin in Panc-1 + PSC organoids after treatment with potent histone deacetylase inhibitors (HDACi). The experimental evaluation and optimization of earlier protocols and methodical approaches of organoid quantification are not included in this thesis.

Z-Stacks were recorded as described above (3.3.4.5) with the CQ1 spinning disc confocal microscope. For each organoid, a standardized recording with 100 Z-stacks (1 slice per µm) and the same parameters was conducted. The Z-Stack images were then analysed with the CellPathfinder software, by utilizing the machine learning feature.

The organoid shape was defined with the computations *MeanImage* (Mask Size: 2.0 µm), *Threshold* (1,500.0 grey level), *ClosingCircle* (Diameter: 5,0 µm) and *OpeningCircle* (diameter: 40.0 µm).

The nuclei were detected and counted with the DAPI signal channel (405 nm), with the computations *MeanImage* (Mask Size: 2.0 µm), *DynamicThreshold* (Mask Size: 20 µm, Detect Factor: 4.0, Min. Gray Offset: 200.0 (gray level)), followed by *FindMaximumImage* (Remove Size: 7.0 (µm))), *DilationCircle* (Diameter: 2.0 (µm)), *Labeling*, *ExpandRegion3D* and *SizeFilter* (Range: 0.0 - 7,515.4 (µm²)).

The signal of the CDH1 channel (640 nm) was quantified with the algorithmic computations *MeanImage* (Mask Size: 2.0 µm), *Classification by Machine-Learning*, *PickupRegion* (Value: 1 (gray level)), *Threshold* (0.0 (gray level)), *ClosingCircle* (Diameter: 0.1 µm), and *OpeningCircle* (Diameter: 0.1 µm).

For the machine learning application, an individual image library for each organoid with around 200 to 300 sample sections was assembled with three different slices of the Z-Stack file (slices at 1, 50 and 100 µm height), for the positive and the negative signal-channel each.

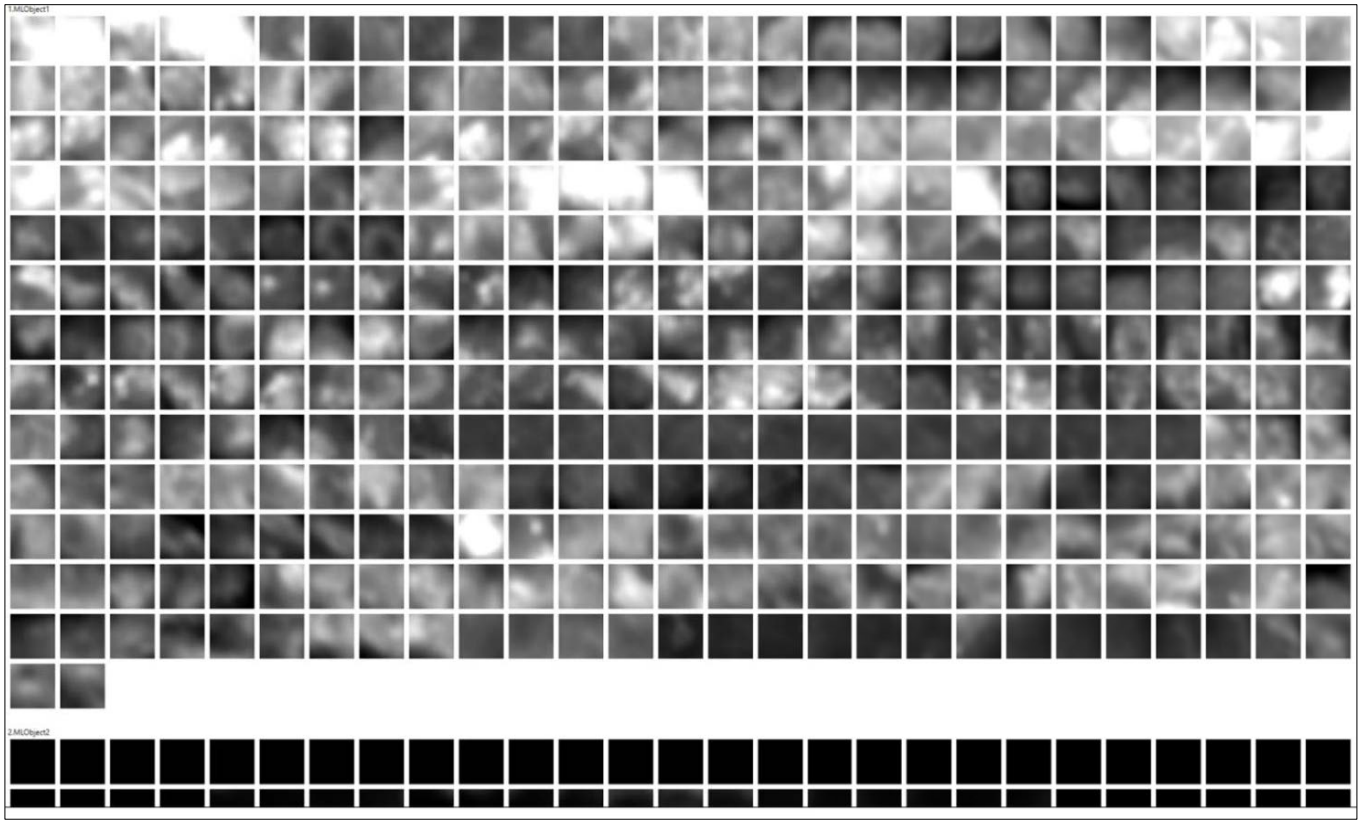

Figure 6. Exemplary image library (compiled in the CellPathfinder software) for the automated machine learning approach to identify and quantify the fluorescent signal of the secondary antibody Alexa Fluor 647, which has bound to the respective anti-CDH1 antibody. Depicted here is a cut-out of the graphical user interface for visual clarification. Upper images: positive antibody signal; lower images: negative signal/background signal. 300 images were selected and recorded for each label (either" positive signal" or "negative signal").

Figure 6 (see above) depicts the compilation of the image library, with selected images for the positive signals of the respective secondary antibody corresponding to the protein of interest, and images for the negative signal corresponding to background noise and the absence of protein expression.

In Figure 7 (below), the successful labelling of the corresponding fluorescent signals of the protein of interest is depicted. The areas marked in red were recognized by the algorithmic protocol, which the image library (see Fig. 6 above) was fed into, and therefore used for the quantification of the protein expression. Following the application of the analysis protocol generated in this process, the areas of protein expression were labelled and marked, as depicted in Figure 8 (see below). Quantitative results were calculated by the CellPathfinder software as well. The generated data was presented in an Microsoft Office Excel sheet and analysed with either the CellPathfinder or the GraphPad Prism 8 software.

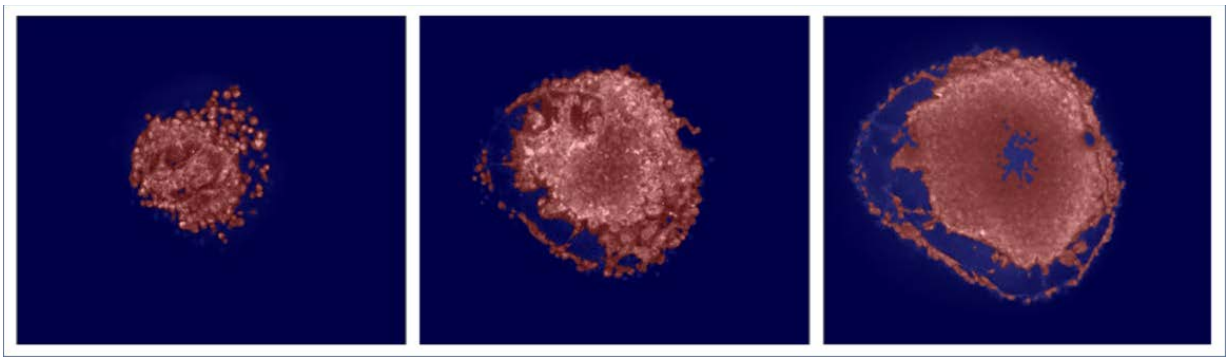

Figure 7. Labelling of organoids after quantification of the fluorescent signals of the secondary antibody Alexa Fluor 647, which has bound to the respective anti-CDH1 antibody. Depicted here is the same organoid (untreated, 20x magnification) for three Z-planes at 10, 50 and 100 µm height (left to right). Red: positive signal corresponding to CDH1 expression; blue: negative signal corresponding to the absence of CDH1 expression/background noise.

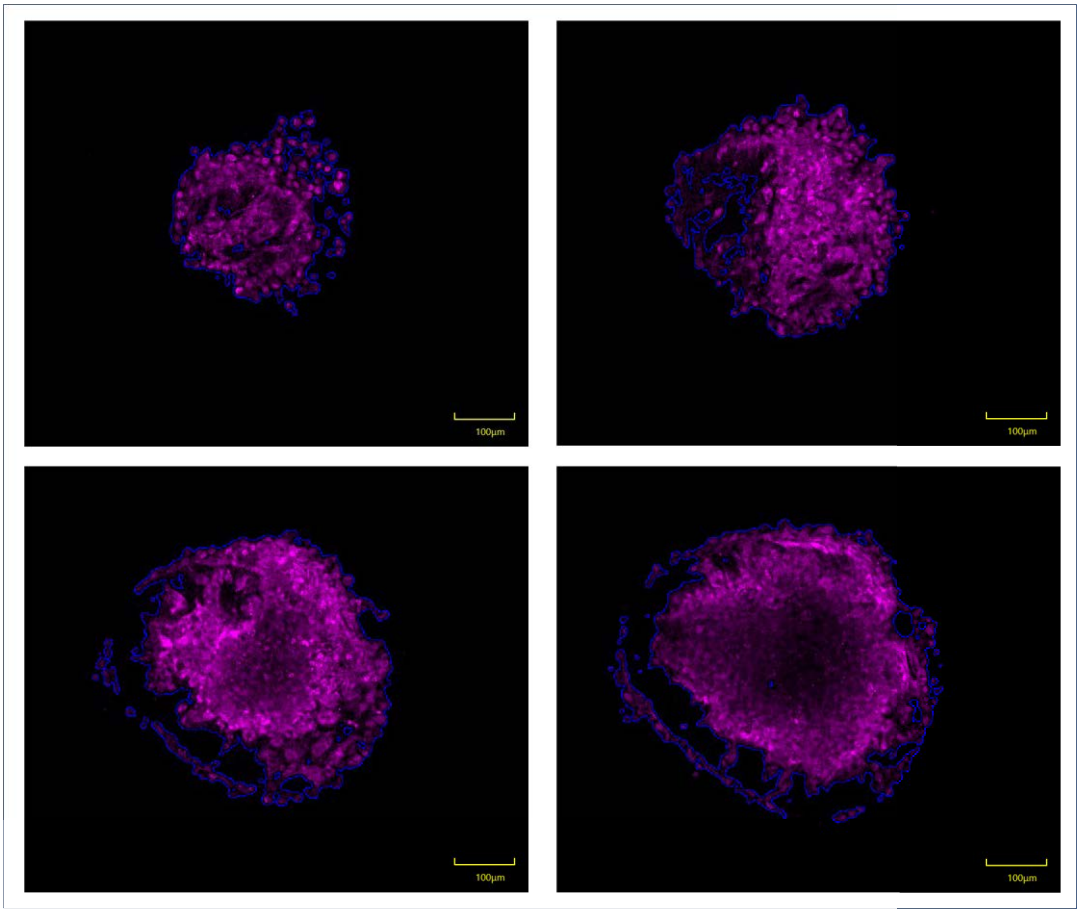

Figure 8. Labelling and quantification of the fluorescent signal of the secondary antibody Alexa Fluor 647, which has bound to the respective anti-CDH1 antibody (640 nm channel), thereby corresponding to the expression of CDH1 in the organoid. The framed areas (coloured in blue) represent the identified positive signal. Depicted here are four different Z-planes (10,25, 50 and 75 µm height, left to right) from the same organoid (untreated, 20x magnification). Reference scale: 100 µm.

The total intensity of the CDH1 signal was then divided by the calculated number of nuclei, to normalize the CDH1 expression in each organoid and receive comparable results. The number of nuclei was determined by the software application and computations described above, by analysing the signals of the DAPI channel (405 nm). Further statistical analysis and graphic presentation was conducted with the GraphPad Prism 8 software. At least three optimal organoids/replicates were needed for each singular approach of analysis.

3.3.5 Tumorsphere Methods and Protocols

Tumorspheres and cancer stem cells (CSCs) were derived from Panc-1 ATCC cells and utilized for cytotoxic evaluation of novel drugs and substances. The following sections detail the methodical processes for tumorsphere handling and their experimental application.

3.3.5.1 Cultivation of Tumorspheres

The manual protocol for the cultivation and generation of Panc-1-derived tumorspheres was adapted and optimized from several publications (Domenichini et al. 2019; Qin et al. 2020; Cao et al. 2011). Tumorspheres were cultivated in DMEM/F-12 medium supplemented with basic fibroblast growth factor (bFGF, Cat. #100-18B, PeproTech), epidermal growth factor (EGF, Cat. #AF-100-15 PeproTech) and B-27 (Cat. #17504044, Thermo Fisher Scientific). The growth factors EGF and bFGF were added in a concentration of 20 mg/mL, the supplement B-27 (Brewer et al. 1994) in a concentration of 1 %. Foetal bovine serum (FBS) was excluded from the medium to prevent cell clustering. The tumorsphere medium was prepared freshly for all methodical steps to ensure supplement activity and efficacy. Dissolved supplements were aliquoted and stored at -20 °C. The B-27 aliquots were never thawed more than once.

To initiate the tumorsphere culture, 10 mL cell suspension ($2.5*10^3$ cells/mL) was seeded in T25 flasks with ultra-low attachment (ULA) surface coating (Cat. #690985, Greiner Bio-One) to prevent cellular adherence. The suspension culture was incubated for two weeks at 37 °C, after which the original cell culture medium was replaced. The medium was then changed every five to seven days, depending on the cell culture and its growth rate. Splitting and harvesting the tumorsphere culture was achieved by transferring the cell suspension to 15 mL Falcon tubes and reducing the total volume down to 5 mL. Following the removal of supernatant medium, the cells were isolated and singularized with 0.5 mg/mL Dispase-II, by adding the enzyme solution to the suspension and pipetting the cells slowly up and down for 5 minutes. Successful dissolution and singularization of tumorsphere cells was verified with

the LUNAII CellCounter device. The cells were split accordingly and seeded back in 10 mL of tumorsphere cultivation medium.

Staining of tumorspheres was conducted in 96-well ULA plates (Cat. #690985, Greiner Bio-One) via the addition of 100 µL staining solution containing 0.2 µg/ml Hoechst 33342 (Chazotte 2011; Latt et al. 1975), and incubated for 30 minutes at 37 °C. Images were recorded with the CQ1 Confocal Imaging Cytometer (Yokogawa Electric Company).

3.3.5.2 Tumorsphere Cytotoxicity Assays

The cytotoxic properties of novel substances on Panc-1-derived tumorsphere cells were evaluated with the CellTiter-Glo Luminescent Cell Viability Assay (Cat. # G7570, Promega) as described above (3.3.3.1). On a 96-Well ULA plate (Cat. #650970, Greiner Bio-One), a total number of 1,000 singularized tumorsphere cells were seeded in a volume of 90 µL and treated with 10 µL substance solution directly afterwards. DRCs and controls were applied and prepared as described in the cytotoxicity assay protocols above. Substance incubation lasted for 48 hours. The CellTiter-Glo assay was initiated by adding 1:1 CellTiter-Glo solution to each well and rotating the plate for 30 minutes, protected from light. The luminescent signals were documented with the Tecan SPARK device. Calculation of the IC_{50} values was performed with the GraphPad PRISM 8 software.

4 Results

4.1 Overview

The obtained experimental results of this thesis will be presented in the sections below. Section 4.2 will detail the cultivation of the different cell types, section 4.3 the generation of three-dimensional organoids, both in 96-well and 384-well format. Section 4.4 to 4.6 will present the assay results for the tylophorinine derivatives (section 4.4), for the artemisinin derivatives (section 4.5) and for the histone deacetylase inhibitors (section 4.6). The results obtained with tumorspheres derived from Panc-1 tumour cells will be presented in section 4.7 separately. A short roundup of the results will be covered in section 4.8.

4.2 Cell Cultivation

4.2.1 Cultivation of Panc-1 Cells

Panc-1 cells, from both ATCC and DSMZ, were cultivated in DMEM medium (10 % FBS, 1 % Pen/Strep). Cells were grown to up to forty passages after thawing before being precautionarily discarded. Morphological changes of Panc-1 cells in higher passages were neither observed nor noted, and experimental results could be replicated and reproduced with Panc-1 cells regardless of their passage. Following initial testing and evaluation (see Figure 9), Panc-1 cells were subjected to a steady splitting rhythm to ensure comparable and verifiable experimental assay results. To determine a cell titre suited for experimental research and testing, Panc-1 cells were seeded in a standard 96-well tissue culture plate at concentrations of 5,000, 10,000 and 20,000 cells per well in 100 µL volume, and incubated in the IncuCyte Zoom device. Quantitative analysis of recorded images revealed that an initial starting concentration of 10,000 and 20,000 cells per well already reached confluence during an incubation timeframe of 24 hours. For cytotoxic evaluation of test substances, lasting for 48 and 72 hours of incubation at 37 °C and 5 % CO_2, an initial cell titre of 5,000 Panc-1 cells per well on 96-well plates was therefore defined and applied.

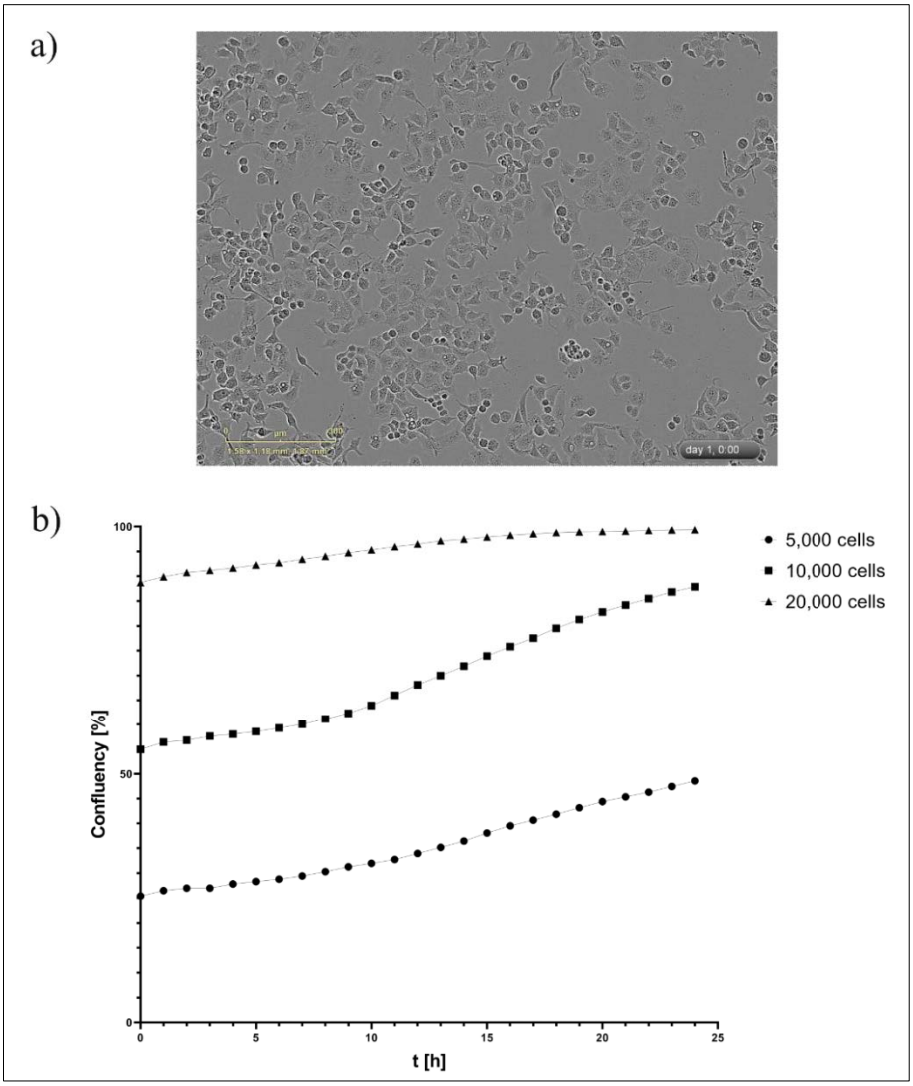

Figure 9. Experimental evaluation of Panc-1 cell growth and cultivation. A) Adherent Panc-1 cells growing on a 96-well tissue culture plate, 24 hours after initial seeding. Start concentration: 5,000 cells/well. Cells were cultivated at 37 °C and 5 % CO_2. Imaging via IncuCyte Zoom. Bottom left: reference scale (300 µm). B) Panc-1 growth rate for initial cell titres of 5,000, 10,000 and 20,000 cells per well. Incubation of Panc-1 cells at 37 °C and 5 % CO_2 lasted for 24 hours and was measured with the IncuCyte Zoom device. X-axis: time (hours); y-axis: confluency of cells (percent). Cell confluency was achieved in wells with an initial cell count of 10,000 and 20,000 after 24 hours, while wells with an initial cell count of 5,000 still exhibited ongoing cell proliferation. Thus, an initial cell titre of 5,000 cells per well was chosen and defined for experimental research. The pictured experiment (b) was conducted once.

4.2.1.1 Panc-1 Cytotoxicity Assays

Cytotoxic efficacy of established chemotherapeutic drugs and novel substances on Panc-1 cells was determined via cell viability assays. As depicted in Figure 10 (see below), this assay was conducted by applying a dose-response curve on the Panc-1 cells 24 hours after seeding,

followed by an incubation period of 48 to 72 hours at 37 °C and 5 % CO_2, to calculate the respective IC_{50} values of three to four independent replicates. Said experimental approach proved to generate valid and reproducible results and was henceforth conducted on all substances presented.

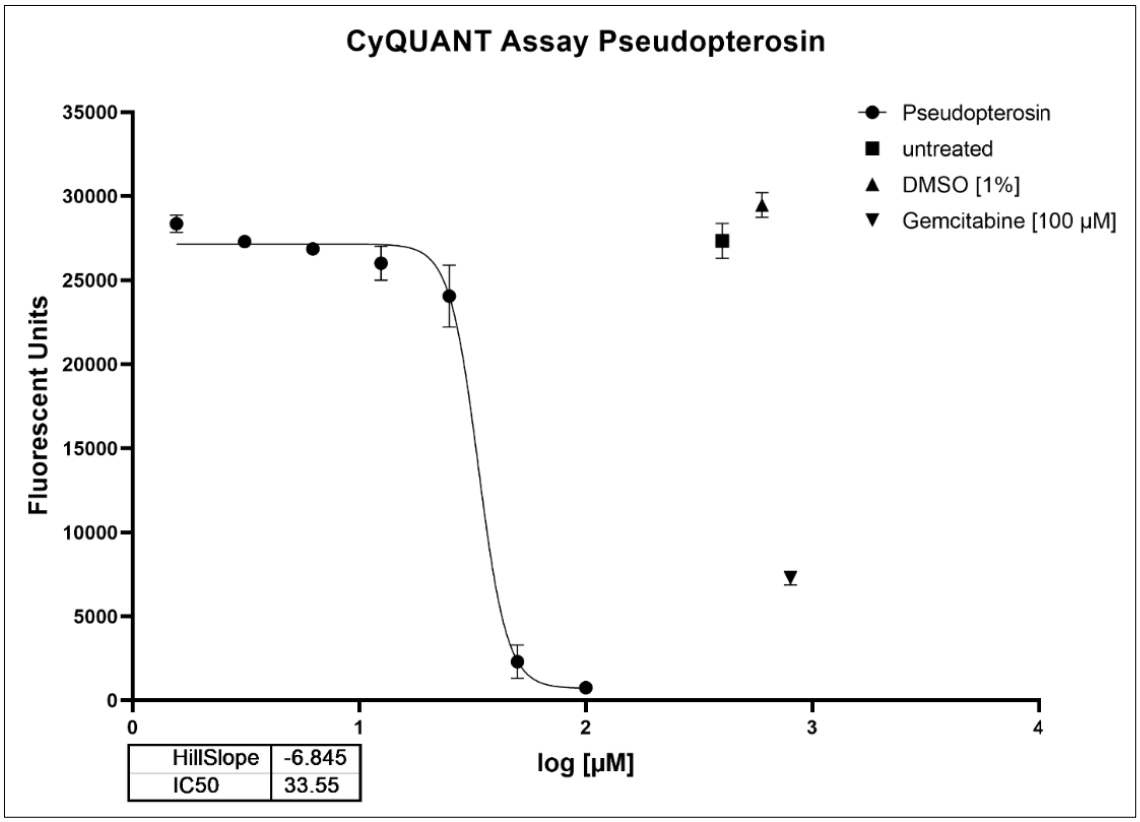

Figure 10. The natural marine product pseudopterosin (PsA-D) exhibited cytotoxic properties on Panc-1 cells. Exemplary dose-response curve (100 to 1.5625 µM), with untreated, solvent (1 % DMSO) and positive (100 µM gemcitabine) control applied. Evaluation of cell viability conducted with the CyQUANT cell proliferation assay. An IC_{50} value of 33.55 µM was measured after 72 hours of incubation. Arithmetic means and their respective standard deviations of triplicates are depicted (Xie et al. 2020).

Pseudopterosin, a natural marine drug (Sperlich and Teusch 2018; Thornton and Kerr 2002), exhibited cytotoxic properties on Panc-1 cells, and showcased an IC_{50} value of 34.02 (±1.35) µM. On Capan-2 cells, another PDAC tumour cell line, an IC_{50} value of 33.94 (±1.02) µM was obtained. These experimental results were published in Xie et al. (2020). The pseudopterosin A-D mixture, isolated from the Caribbean gorgonian *Pseudopterogorgia elisabethae* (Gutiérrez-Rodríguez and Lasker 2004), was kindly provided by Russel Kerr of the Department of Chemistry, University of Prince Edward Island (Canada).

For the two established and clinically applied chemotherapeutic agents gemcitabine (GEM), a cytostatic nucleoside drug (Burris III et al. 1997), and paclitaxel (taxol), a microtubule stabilizer (Xiao et al. 2006) originally derived from the tree plant *Taxus brevifolia* (Wilson et al. 2001),

IC_{50} values of 1.99 (±0.13) µM (Xie et al. 2020) and 13.93 (±0.73) nM were obtained in two-dimensional cell culture models, respectively (see Figure 11 below).

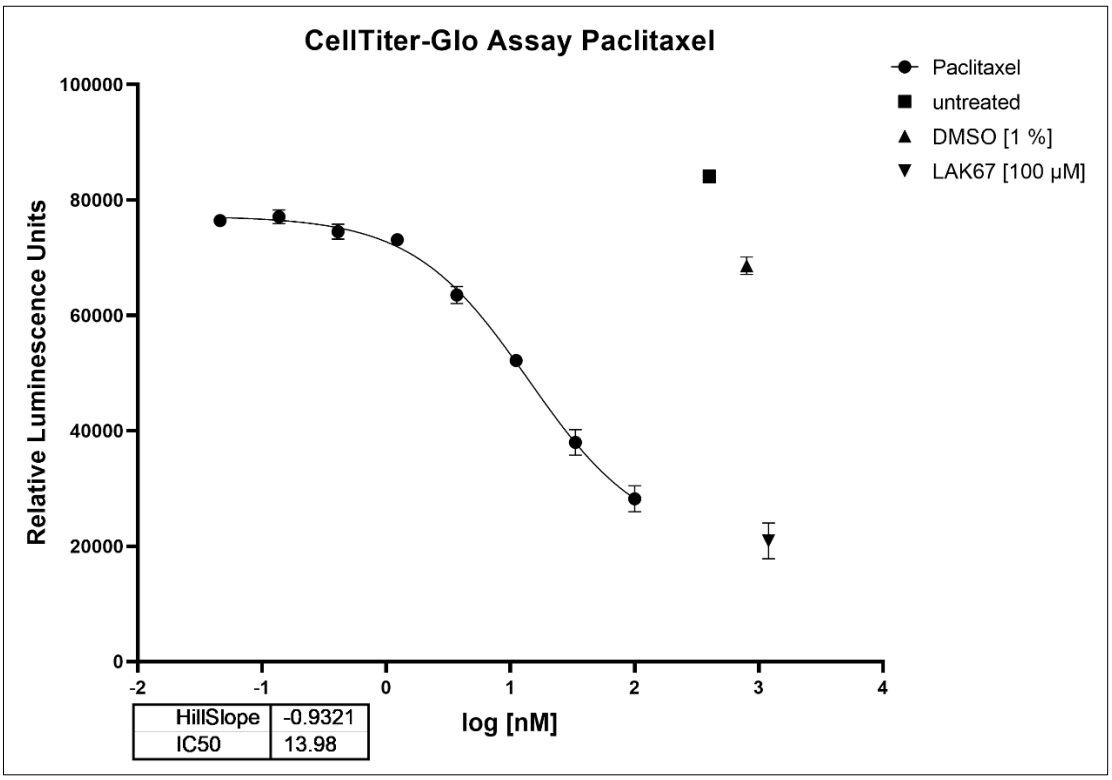

Figure 11. Paclitaxel (taxol) exhibited cytotoxic properties on Panc-1 cells. Exemplary dose-response curve with untreated, solvent (1 % DMSO) and positive control applied. The potent HDAC inhibitor LAK67 (100 µM) was chosen as the positive control. Evaluation of cell viability conducted with the CellTiter-Glo assay. An IC_{50} value of 13.98 nM was measured after 72 hours of incubation. Data points represent the arithmetic means and their respective standard deviations of quadruples. The assay was executed on a 384-well plate format.

The CyQUANT NF Cell Proliferation Assay (Cat. #C35006) from Thermo Fisher Scientific (Jones et al. 2001) was applied to evaluate the cytotoxicity of gemcitabine (GEM), pseudopterosin (PsA-D) and the tylophorinine derivatives (see section 4.4). Following further empirical testing and practical evaluation, the CellTiter-Glo Luminescent Cell Viability Assay (Cat. #G7570) from Promega and the PrestoBlue Cell Viability Reagent assay (Cat. #A13261) from Thermo Fisher Scientific were henceforth utilized due to lower standard deviations and better reproducibility (see results below).

4.2.2 Cultivation of Capan-1 Cells

The established PDAC cell line Capan-1 was originally derived from a hepatic metastasis of pancreatic cancer (Kyriazis et al. 1982) and was successfully cultivated in RPMI medium with 20 % foetal bovine serum and 1 % penicillin/streptomycin over the course of this thesis. Capan-1 cells were applied to evaluate the cytotoxicity of novel chemicals and the initial generation of Capan-1 + HSC microtumour organoids (see section 4.3.3), in order to establish a PDAC hepatic metastasis model.

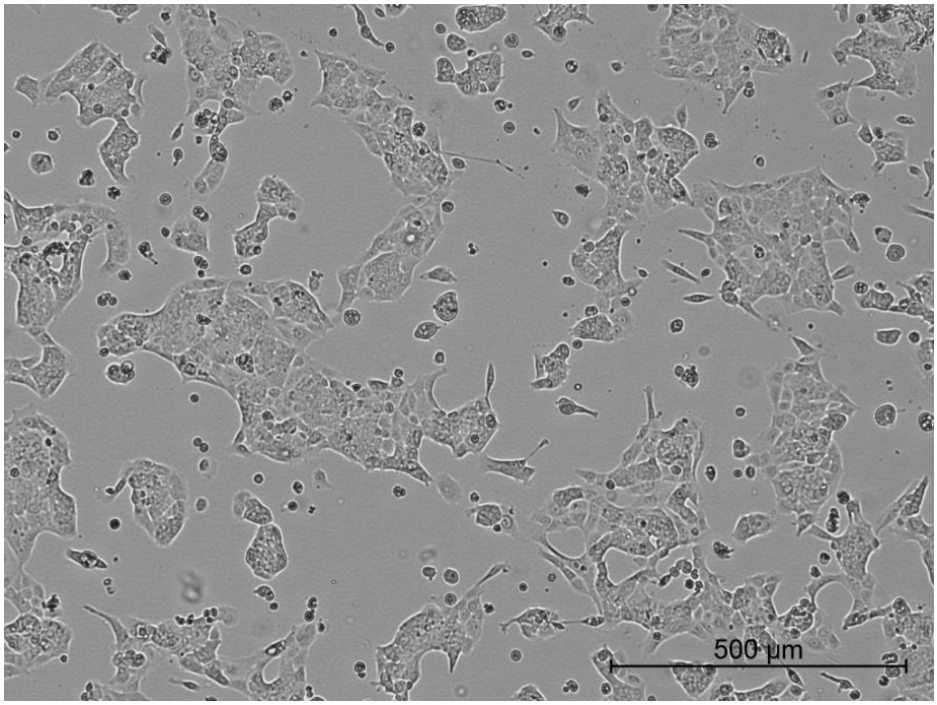

Figure 12. Laboratory cultivation of the pancreatic cancer cell line Capan-1 in T75 tissue culture flasks. Capan-1 cells were grown in RPMI medium (20 % FBS, 1 % Pen/Strep). Exemplary image depicts Capan-1 cells at low confluency 48 hours after initial seeding. Image was recorded with the Axio Vert.A1 microscope and edited with ImageJ. Bottom right scale: 500 µm.

Cytotoxic evaluation of substances and drugs on Capan-1 cells was conducted with the CellTiter-Glo assay, with an initial cell titre of 5,000 cells per well and an incubation period of 72 hours following substance treatment. Due to a shift of focus in the experimental research executed during the thesis, only few substances were tested on Capan-1 cells, one of those being *O*-methyltylophorinidine (internal designation: P05C06), which showcased an IC_{50} value of 22.47 (±1.73) nM (see Figure 13 below). Further experimental data obtained with tylophorinine derivatives is documented in section 4.4.

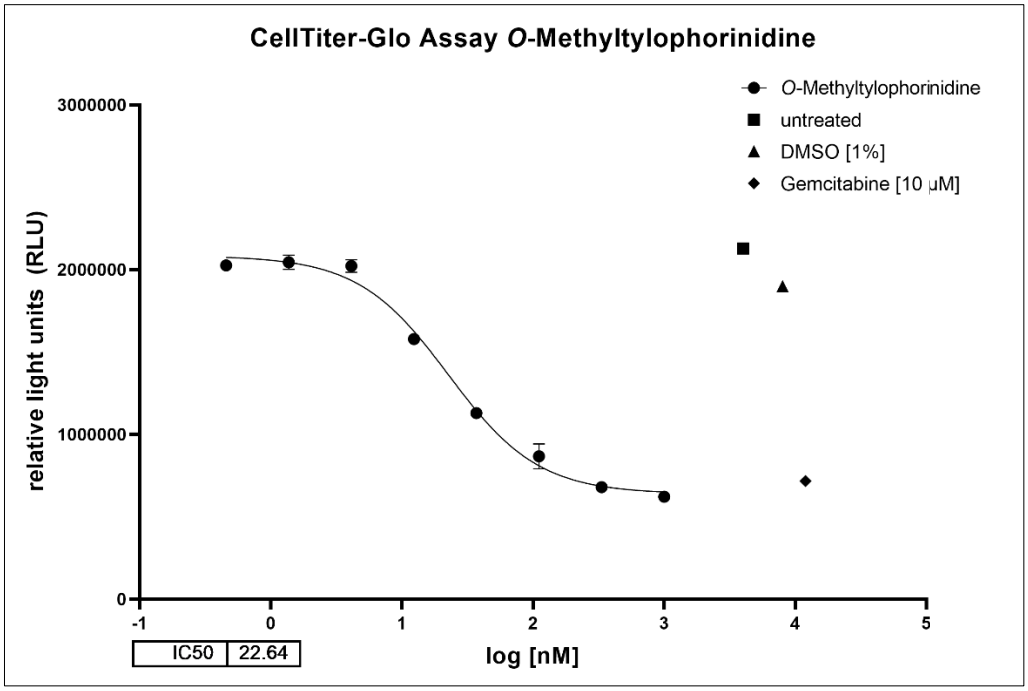

Figure 13. The tylophorinine derivative *O*-methyltylophorinidine exhibited high cytotoxic properties on the PDAC cell line Capan-1. Exemplary dose-response curve (1000 to 0.5 nM), with untreated, solvent (1 % DMSO) and positive control (100 µM gemcitabine). Evaluation of cell viability conducted with the CellTiter-Glo Luminescent Cell Viability Assay (Promega). An IC_{50} value of 22.64 nM was measured after 72 hours of substance treatment. Data points represent the arithmetic means and their respective standard deviations of triplicates.

4.2.3 Cultivation of Patient-derived Cancer-associated Fibroblasts (CAFs)

Cultivation of pancreatic stellate cells (PSC) and hepatic stellate cells (HSC-P) was achieved in DMEM/F-12 medium (20 % FBS, 1 % penicillin/streptomycin). Both patient-derived cell lines were grown to high confluency before being split for experimental research, and exhibited early senescence after 18 to 20 passages, but showcased consistent viability regardless of passage (see Figure 14 below). As KU0020 PSC and NCC06 HSC-P were directly derived from PDAC patients, early senescence was expected and occurred in all cases of cultivation. Both cancer-associated fibroblast (CAF) cell lines were used in three-dimensional (3D) co-culture, together with the PDAC cell lines Panc-1 and Capan-2. PSC cells were furthermore successfully applied in cell viability assays on both 96-well and 384-well formats, thus enabling the evaluation of cytotoxicity of novel substances like the histone deacetylase inhibitors (HDACi) directly on the cancer-associated fibroblasts (CAFs). Following initial optimization of cell density, PSC cells were seeded in a total number of 2,000 cells per well on 96-well plates and 600 cells per well on 384-well plates. Cell viability assays were not conducted with the HSC-P cells.

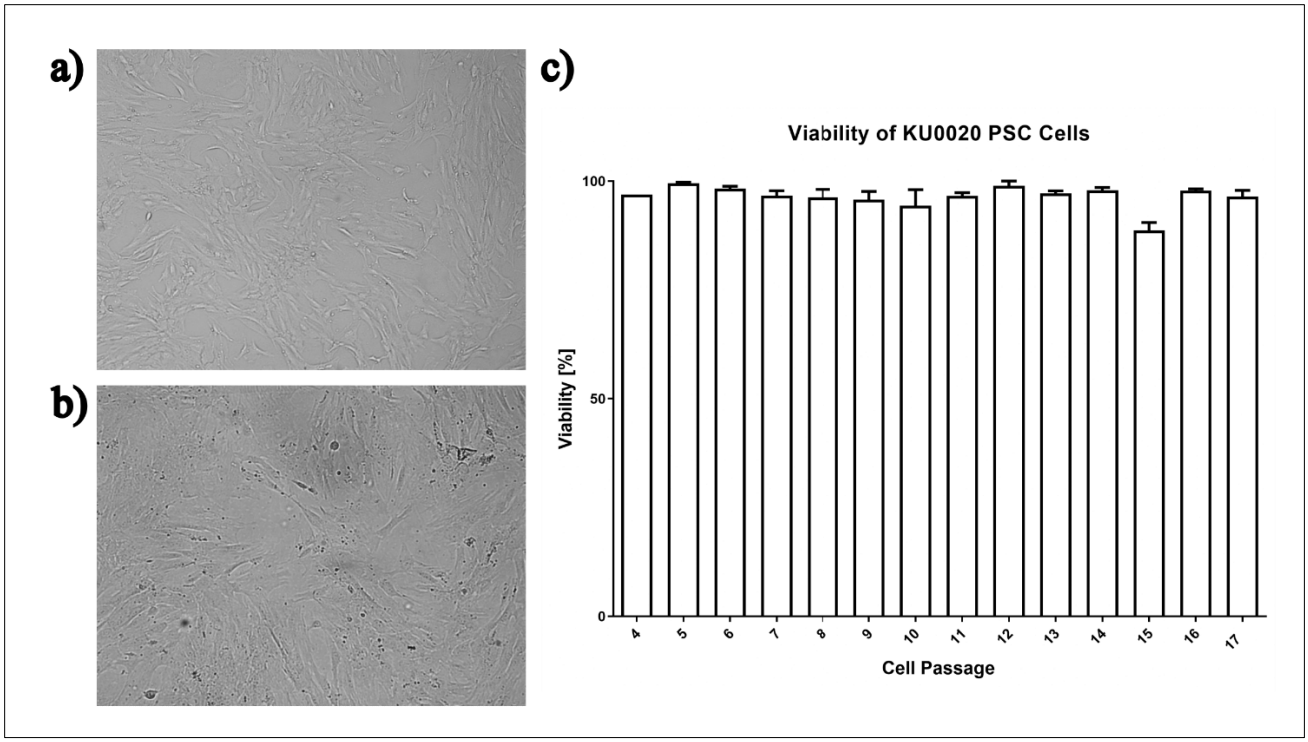

Figure 14. Cultivation of the patient-derived CAF cell line KU0020 PSC. Figures: a) microscopy image of low-density PSC cells; b) microscopy image of high-density PSC cells; c) percentual viability of KU0020 PSC cells (arithmetic means and standard error of the mean) over fourteen consecutive passages, from passage 4 to passage 17. Cell viability was assessed with the LUNA II CellCounter via Trypan Blue and Erythrosin B staining. Images were recorded with the Axio Vert.A1 microscope. PSC cells exhibited high viability over all passages.

Scientific data regarding the cytotoxicity of histone deacetylase inhibitors (HDACi) on PSC cells is presented below in sections 4.6.1 and 4.6.5, summarized in section 4.8. Further results regarding the cytotoxicity of artemisinin derivatives on PSC cells under ultraviolet light illumination are presented in section 4.5.2.

4.3 Three-Dimensional (3D) Co-Culture Organoids

Generation and cultivation of three-dimensional co-culture PDAC organoids was achieved in both 96-well (Xie et al. 2020) and 384-well ultra-low-attachment (ULA) tissue culture plates, as detailed in method section 3.3.4. Organoids were used in cell viability assays to evaluate the cytotoxicity of tylophorinine derivatives, histone deacetylase inhibitors (HDACi) and other natural and synthetic substances, and could be successfully stained with fluorescent antibodies for microscopic confocal imaging. 96-well plate organoids were stable and viable for about nine (216 hours) to twelve days (288 hours) after seeding and showed no observable signs of dissolving or internal cellular apoptosis or detachment. Further results indicate that organoids are stable and viable for up to twenty days following seeding (see outlook section 7.1). 384-well plate organoids were only grown and cultivated for a duration of 144 hours. Variabilities in growth, volume and the ultimate internal number of cells in 96-well plate organoids, which could be indirectly assessed with the relative luminescence units (RLU) obtained with the CellTiter-Glo assay, were noted and documented (see results below). Reproducibility of results was not affected.

4.3.1 Generation and Documentation of Organoids

Panc-1 + PSC co-culture organoids were generated and cultivated as described in method section 3.3.4. Following seeding of Panc-1 and KU0020 PSC cells in DMEM/F-12 (10 % FBS) medium and 0.1 mg/mL collagen-1, organoids both cultivated in 96-well and 384-well ULA plates became stable and compact after 72 to 96 hours of incubation. As seen in Figure 15 to Figure 17 below, organoids were round and spherical after 120 hours of incubation.

The co-culture cells migrated towards the centre of the well 24 hours after seeding and formed a cohesive structure another set of 24 hours later. At 96 hours, the organoid became compact and spherical, and completely stable after 120 hours. Prior to that point, organoids could not be pipetted or transferred from their cultivation plate, due to sticking to the respective pipette tip. Treatment with substances of interest (chemotherapeutic agents, natural products, etc.) was conducted 96 hours after seeding and lasted for 72 hours prior to the execution of the CellTiter-Glo 3D assay. For immunofluorescence staining and subsequent experiments, organoids were subjected to substance treatment at the 120 hours mark. As indicated by the reference scales (featured in the bottom right of the images), the organoids exhibited a width of around 500 to 600 µm. Formation of organoids occurred naturally and resulted in spherical shapes in the majority of all approaches. More detailed images of organoids stained via immunofluorescence, and their cellular composition, recorded via confocal and spinning disc confocal microscopy, are pictured and documented below (see section 4.6.5).

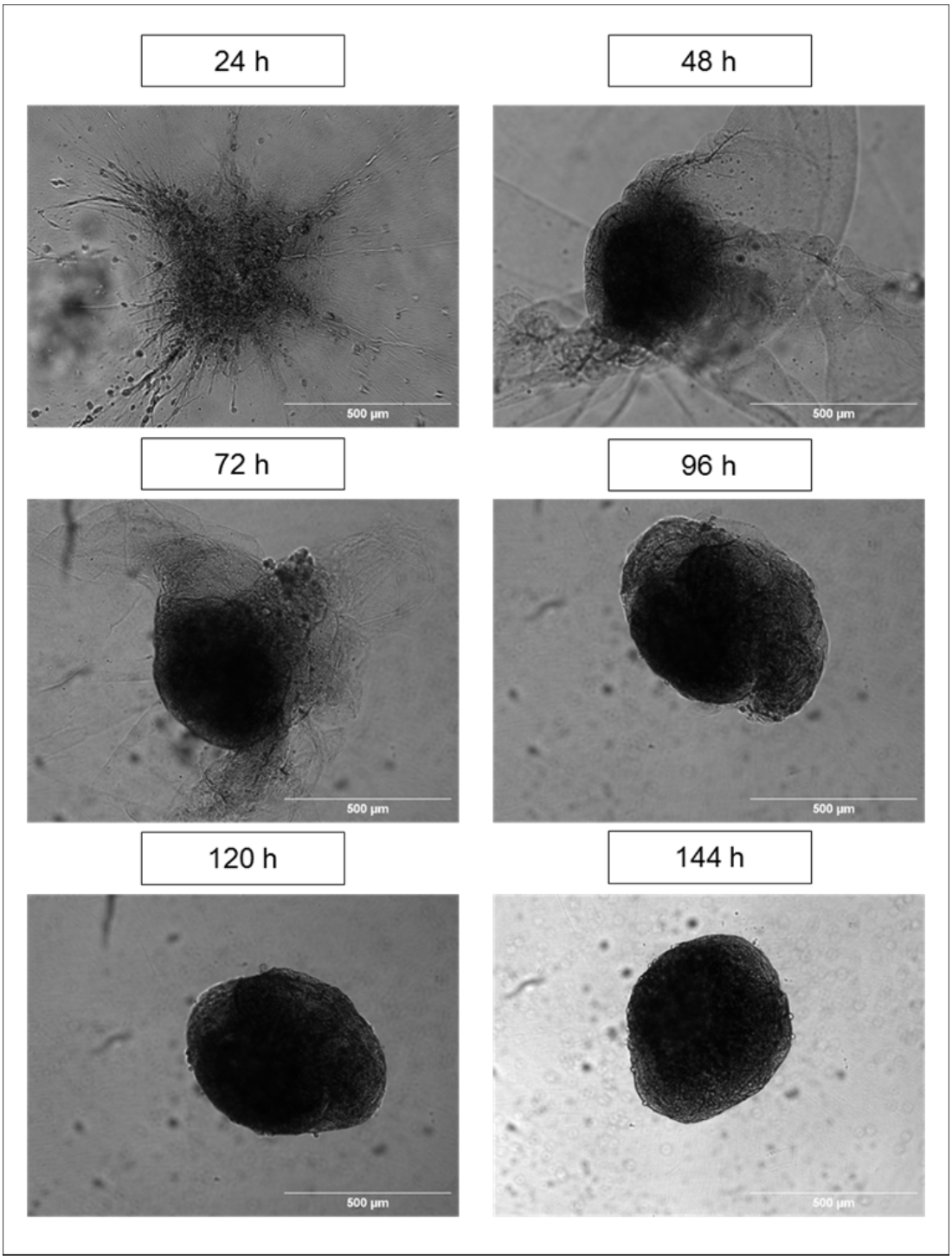

Figure 15. Growth of Panc-1 + PSC organoids on 96-well ULA plates. Organoids become compact and spherical after 96 hours and were stable at 120 hours of cultivation. Images were recorded with the Axio Vert.A1 microscope every 24 hours following seeding and edited with ImageJ. Bottom right: reference scale (500 µm).

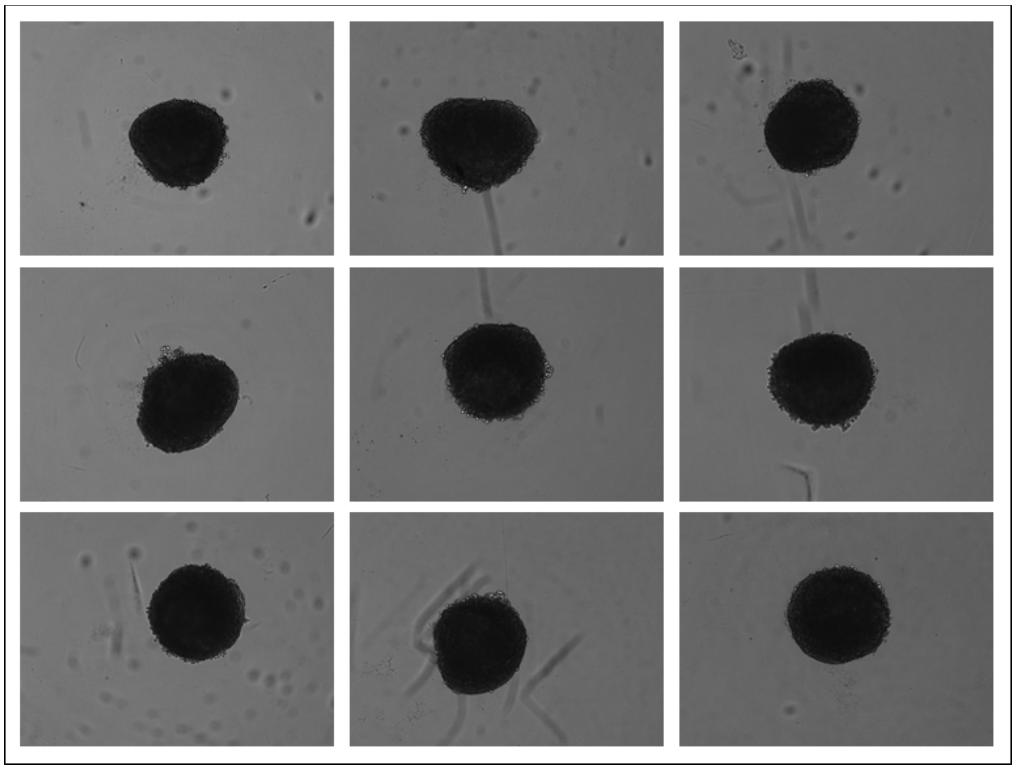

Figure 16. Exemplary images of nine untreated Panc-1 + PSC organoids cultivated on 96-well ULA plates for 144 hours (six days) following manual seeding. All depicted organoids feature a spherical and compact shape. Images recorded with the Axio Vert.A1 microscope and edited with ImageJ.

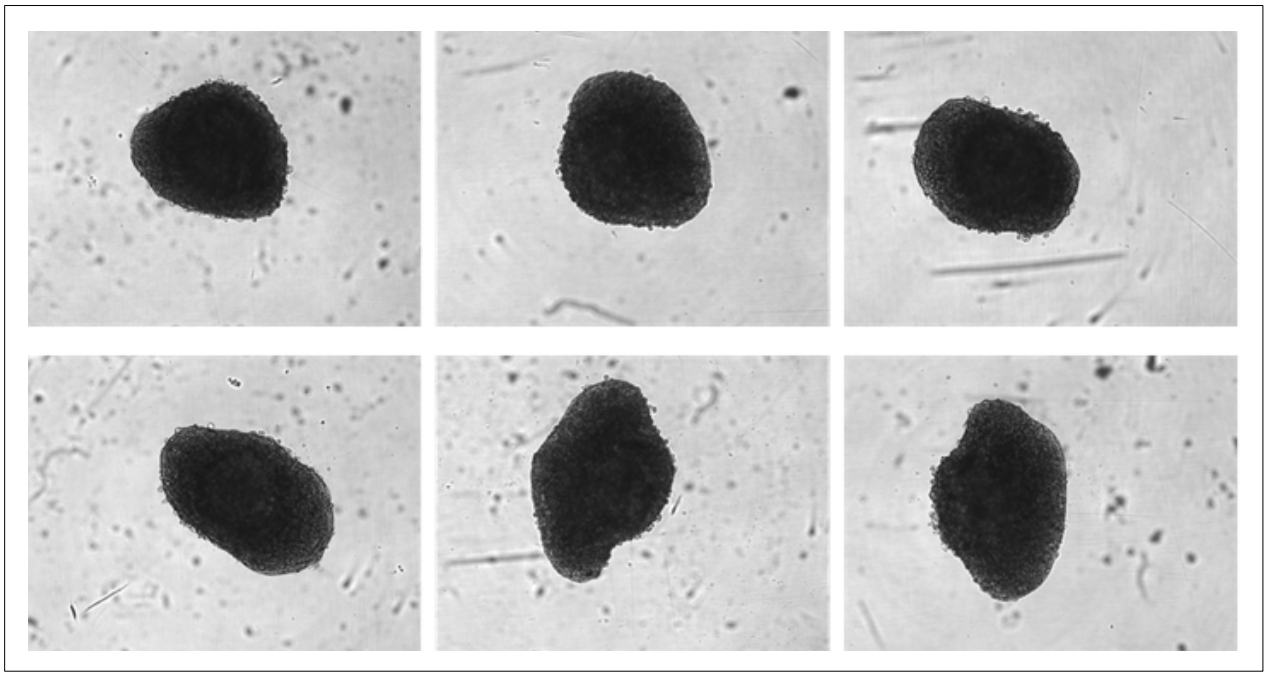

Figure 17. Exemplary images of six untreated Panc-1 + PSC organoids cultivated on 96-well ULA plates for 144 hours (six days) following manual seeding. Differences in shape and size can be observed. Images recorded with the Axio Vert.A1 microscope and edited with ImageJ.

Co-culture Panc-1 + PSC organoids mostly took on a spherical and compact shape after 144 hours of incubation on 96-well plates, as documented in Figure 16, but differences in organoid formation were noted and observed occasionally (see Figures 17 and 47). Via spinning disc confocal microscopy with the Yokogawa CQ1 Confocal Imaging Cytometer, the organoids' spatial parameters could be assessed and quantified, and the volume of different experimental batches were compared, revealing significant variability (see Figure 18 below). However, this data was obtained from experiments conducted for the quantification of protein expression in organoids, detailed and explained in section 4.6.5, only reflecting a 100 µm-wide cut-out of the respective organoid, and should therefore be judged with caution.

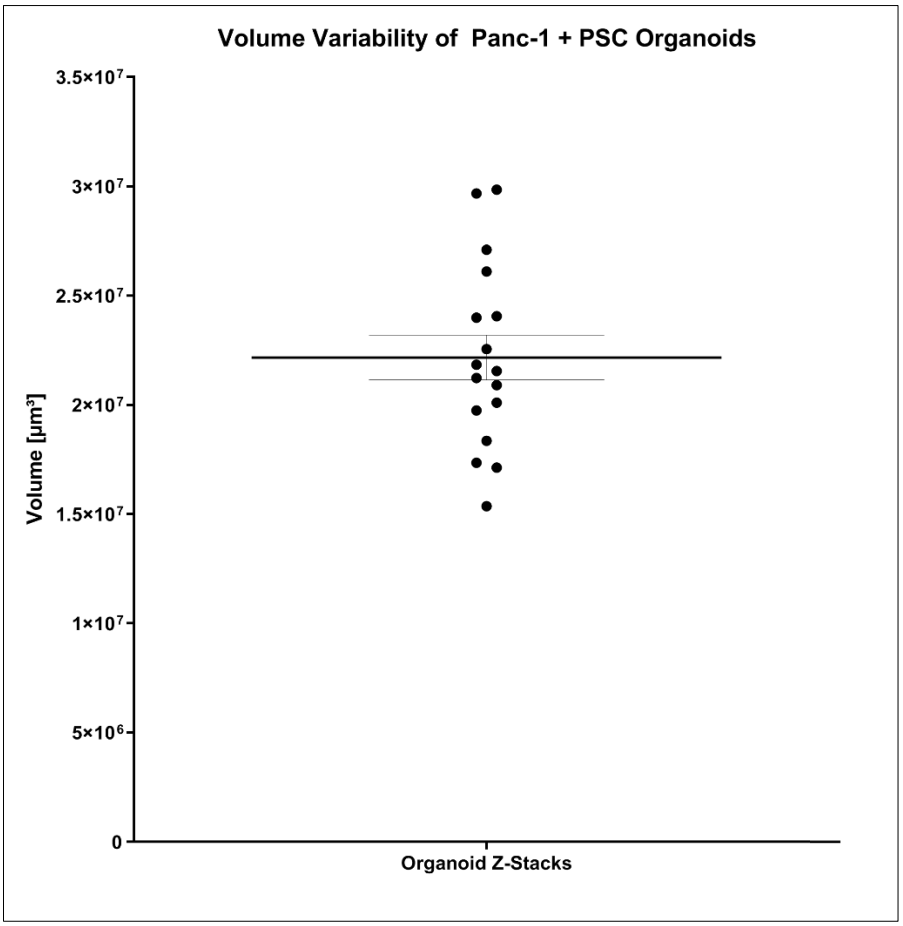

Figure 18. Panc-1 + PSC organoids (cultivated on 96-well plates) from different experimental batches exhibited variability in volume (µm³). Data is depicted as a scatter dot plot of 17 organoids from five batches, with the calculated arithmetic mean and the respective standard errors of the mean. Z-stacks (100 slices, 1 µm/slice) were recorded with the Yokogawa CQ1 Confocal Imaging Cytometer and edited with the respective CellPathfinder software. Statistical analysis with the GraphPad Prism 8 software. See method section 3.3.4.6 for the detailed organoid quantification protocol and volume calculation.

Despite these variabilities in form and size, the intercellular composition of correctly grown organoids (see section 4.3.2), in which pancreatic stellate cells (PSCs) formed a cohesive

surrounding structure around the inner Panc-1 tumour cells, was always observed. Reproducibility of results obtained with the CellTiter-Glo assay was not affected, and organoids seeded either manually or with the CyBio Well vario pipetting robot showed no empirically observable differences, as both internal composition and reaction to cytotoxic drugs and reagents remained consistent and comparable, indicating the stability and reproducibility of data gained and received with the previously described organoid cultivation protocol.

Organoid cultivation on 384-well ULA tissue-culture plate was performed exclusively with the CyBio Well vario pipetting robot. Manual seeding and handling of cell cultures on 384-well plates was unfeasible. The original organoid cultivation protocol, evaluated and established by Bailu Xie (Xie 2018) and Vanessa Mundorf (Mundorf 2018). and detailed in method section 3.3.4.1, was adapted and minimally changed in order to be performed on the CyBio Well vario pipetting robot. Following the successful preparation of the Panc-1 + PSC co-culture in organoid medium (DMEM/F-12 supplemented with 10 % foetal bovine serum and 0.1 mg/mL collagen-1), a diminished volume of 10 µL cell suspension was automatically seeded in each well on the 384-well plate, followed by the addition of 8 µL organoid medium 24 hours later and the subsequent treatment with 10 µL substance solution 72 hours after seeding. Organoid formation proceeded as documented for the 96-well plate organoids (see Figure 19 below), and internal composition and structure, with PSC cancer-associated fibroblast cells (CAFs) forming a surrounding shell and an inner core of Panc-1 tumour cells, was comparable and reproducible (see result section 4.3.2 for immunofluorescence staining of 384-well plate organoids).

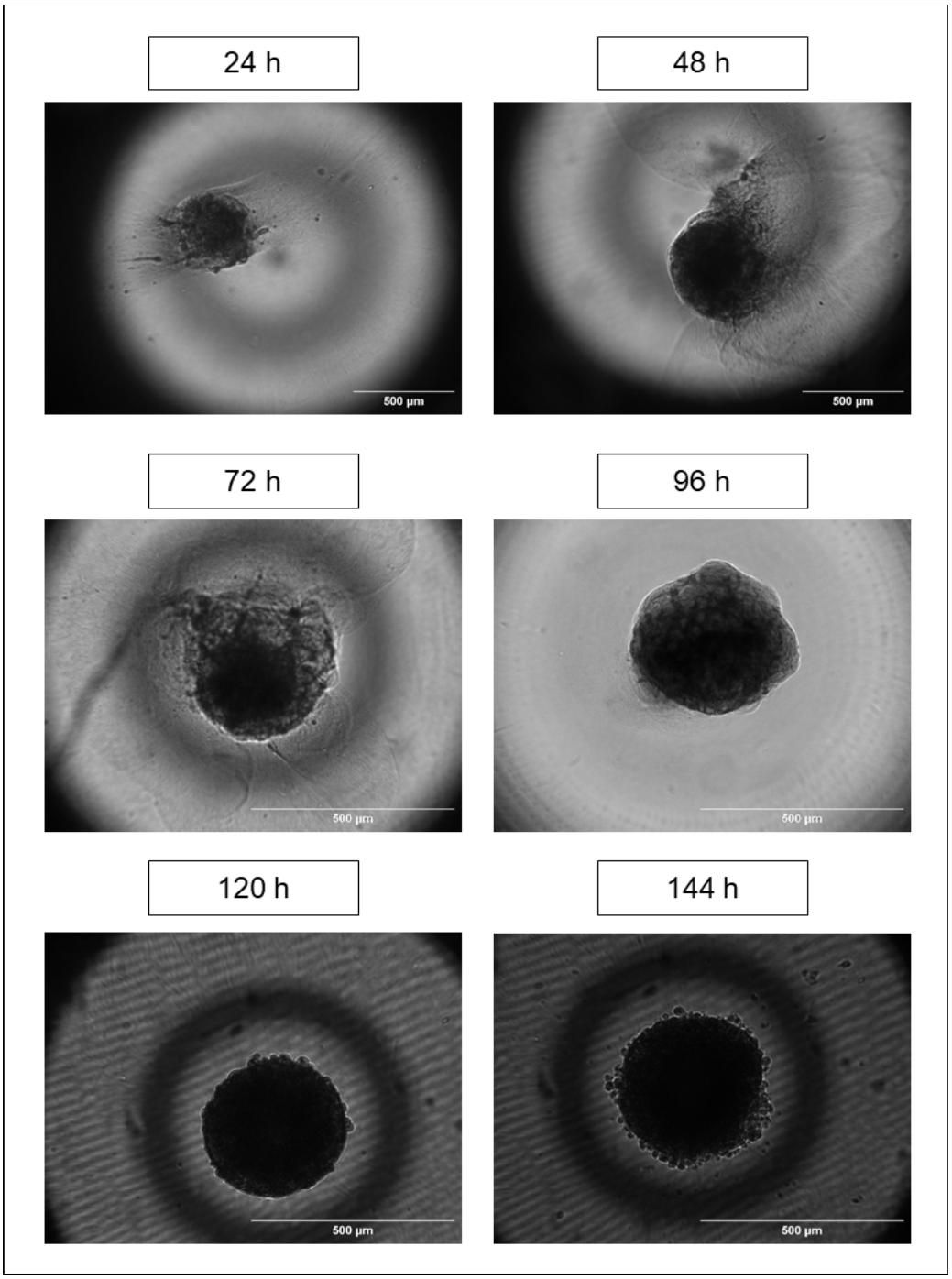

Figure 19. Growth and cultivation of Panc-1 + PSC organoids on 384-well ULA plates. Organoids became compact and spherical after 96 hours and were stable at 120 hours of cultivation. Automatic seeding via the CyBio Well vario pipetting robot (Analytik Jena). Images were recorded with the Axio Vert.A1 microscope every 24 hours following seeding and edited with ImageJ. Bottom right: reference scale (500 µm).

Organoids automatically seeded on 384-well ULA plates via the CyBio Well vario pipetting robot yielded reproducible results comparable to data gained from organoids cultivated on 96-well ULA plates and were used to evaluate the properties and efficacies of natural products and novel substances (see cytotoxicity results below). Staining with immunofluorescent

antibodies was achieved as well, but 384-well plate organoids were not utilized for protein quantification via spinning disc confocal microscopy. Naturally, these organoids featured a much smaller size and volume, but a higher degree of spherical conformity (see Figure 20 below), as expected beforehand. The 384-well approach of organoid cultivation and treatment was favoured once successfully established and standardized in the laboratory, and was applied for the high-throughput screening of histone deacetylase inhibitors (HDACi) and further substances (see section 4.6.1).

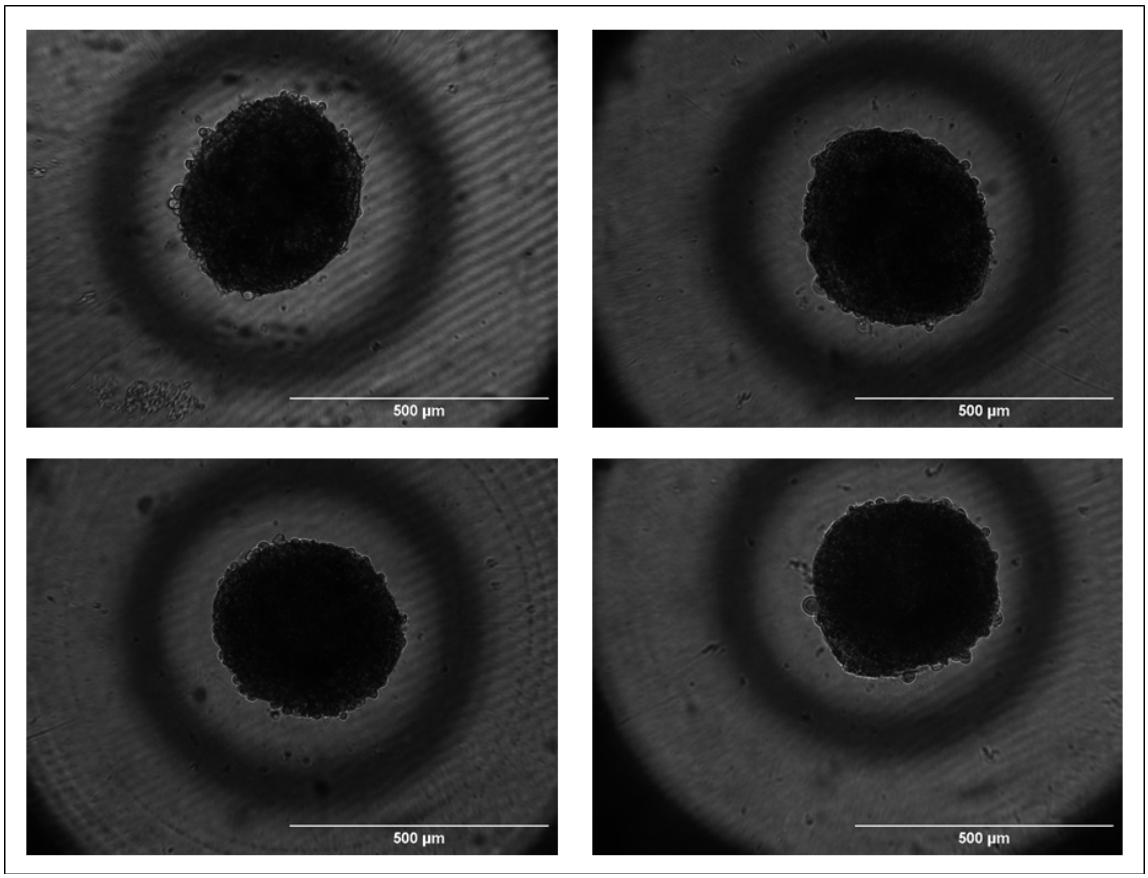

Figure 20. Exemplary images of four untreated Panc-1 + PSC organoids cultivated on 384-well ULA plates for 144 hours (six days) following manual seeding. All depicted organoids featured a spherical and compact shape. Images recorded with the Axio Vert.A1 microscope and edited with ImageJ. Bottom right: reference scale (500 µm).

Organoids consisting of Capan-2 cells and either PSC or hepatic stellate cells (HSC-P), together with organoids consisting of Panc-1 cells and HSC-P cells, were cultivated on 96-well ULA plates as well and exhibited the same cellular composition and structure (see images in the appendix and below). Such organoids were not cultivated on 384-well ULA plates, and initial experiments were not conducted in this thesis. Regarding the successful adaptation of the Panc-1 + PSC organoid cultivation protocol on the 384-well plate format, it can be assumed that the cultivation and incubation of Panc-1 + HSC-P, Capan-2 + PSC and Capan-2 + HSC-

P organoids might be successfully achieved on 384-well ULA plates via automatic pipetting and cell seeding as well.

4.3.2 Microscopical Imaging of Organoids

Multiple different staining methods were performed and conducted with the three-dimensional co-culture organoid models described and depicted above. Organoids were stained with primary antibodies and fluorescent secondary antibodies (see section 4.3.2.1) and imaged via confocal microscopy (Zeiss LSM 880) and spinning disc confocal microscopy (Yokogawa CQ1 Confocal Imaging Cytometer). Three-dimensional Z-stack rendering was conducted as well, visualising the organoids' structure, form and cellular composition. The LIVE/DEAD™ viability stain was also executed with the 3D models, marking dead cells inside the organoid, followed by spinning disc confocal microscopy imaging (see section 4.3.2.2). Microscopical analysis revealed that organoids, both cultivated and incubated in 96-well and 384-well ultra-low attachment (ULA) plates, exhibited a consistent composition of external pancreatic stellate cells (PSCs) and internal PDAC (pancreatic ductal adenocarcinoma) tumour cells.

4.3.2.1 Immunofluorescent Staining of Organoids

The staining protocol of organoids with fluorescent antibodies is described in method section 3.3.4.3.1. Clearance with consecutive ethanol concentrations and benzyl alcohol/benzyl benzoate (BABB, 1:2) was a necessary and essential step in the staining process, and organoids not subjected to clearing were unable to be imaged via confocal and spinning disc confocal microscopy. Organoids were transferred in a volume of 50 µL benzyl alcohol/benzyl benzoate to the respective imaging plate for better handling and storage, as the removal of the BABB solution led to earlier drying of the organoid.

The pancreatic stellate cells (PSCs), which functioned as the inflammatory cancer-associated fibroblasts (CAFi) in the three-dimensional organoid model utilized in this thesis, were always stained, marked and detected with antibodies against the specific alpha smooth muscle actin protein (α-SMA/ACTA2) (Amrutkar et al. 2019; Bu et al. 2019). Favoured tumour markers were the tumour suppressor protein TP53, which was often unregulated and mutated in pancreatic cancer and pancreatic ductal adenocarcinoma (PDAC) (Barton et al. 1991; Czaplinska et al. 2022), and the mitosis marker Ki67 (Fabian et al. 2019; Bouwens 1998). Further proteins of interest were the epithelial marker protein E-cadherin/Cadherin-1 (CDH1) (van Roy and Berx 2008; Kaneta et al. 2020) and the Yes-associated protein 1 (YAP1), a transcriptional coactivator of the Hippo signalling pathway (George et al. 2012; Enrique Rozengurt 2019).

Quantification of CDH1 expression via spinning disc confocal microscopy and the CellPathfinder software is described in section 4.6.5 below.

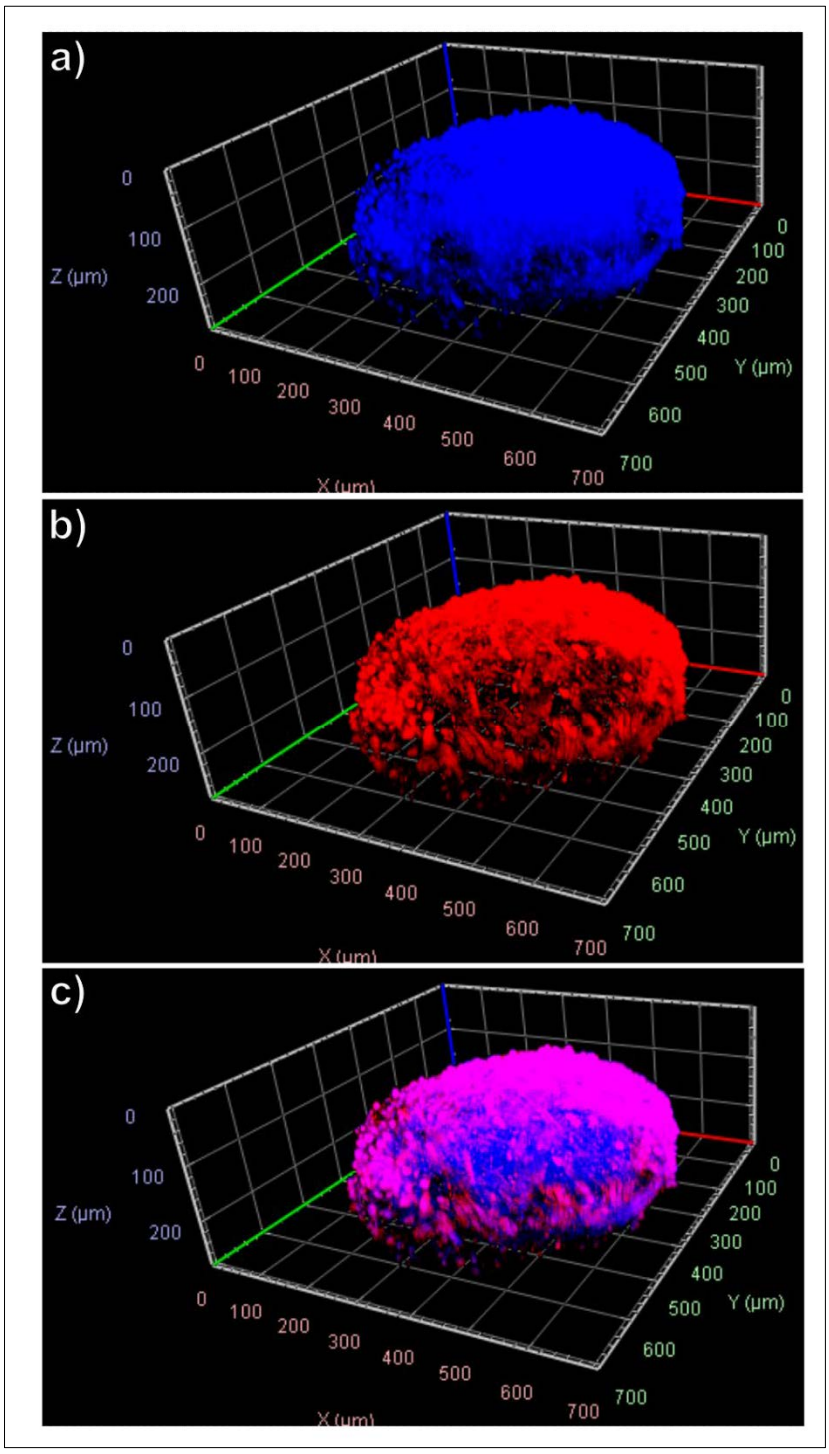

Figure 21. Exemplary three-dimensional rendering of a Panc-1 + PSC organoid. Staining with fluorescent antibodies and DAPI. 3D rendering of 281 recorded slices, with one slice representing 1 µm of height. A) Staining of nuclei with DAPI (405 nm channel); b) staining of pancreatic stellate cells (PSCs) with ACTA2 antibody (561 nm channel); c) merging of both channel. Reference scales in µm. Images recorded via the ZEISS LSM 880 Airy Scan microscope (Carl Zeiss AG) and edited with the ZEISS ZEN 3.6 (blue) software.

As seen in Figure 21 above and Figure 22 below, ACTA2-positive cells (cancer-associated fibroblasts/CAFs) formed a shell-like structure surrounding the internal cellular mass (pancreatic cancer cells) of the organoid model. The respective ACTA2 (alpha smooth muscle actin) signal could also be detected in the inner organoid, although weaker in intensity, as previously documented and presented in the PhD thesis of Bailu Xie (Xie 2018), preceding the work at hand.

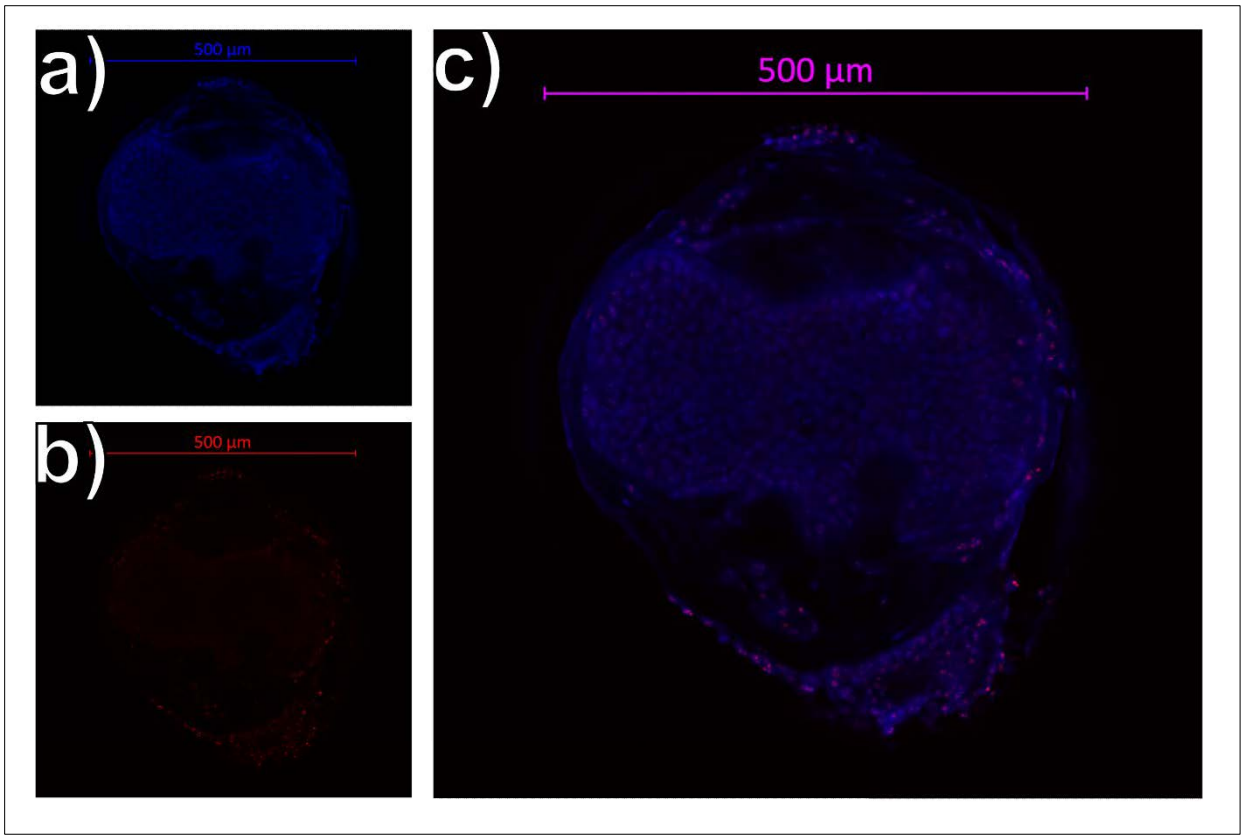

Figure 22. Low expression of ACTA2 (red signal) in Panc-1 tumour cells. Exemplary confocal microscopy images of an IF-stained Panc-1 + PSC organoid. Not identical to the organoid depicted and rendered in Figure 21 above. A) Staining of nuclei with DAPI (405 nm channel); b) staining of pancreatic stellate cells (PSCs) with ACTA2 antibody (561 nm channel); c) merging of both channel. Reference scales: 500 µm. Images recorded with the ZEISS LSM 880 Airy Scan microscope (Carl Zeiss AG) and edited with the ZEISS ZEN 3.6 (blue) software.

The co-culture PDAC organoids, consisting of pancreatic tumour cells and cancer-associated fibroblasts (CAFs), which were utilized in this thesis, thus exhibited the same structural properties as described and evaluated in the preliminary works of Bailu Xie (Xie 2018) and Vanessa Mundorf (Mundorf 2018), proving the three-dimensional model's reproducibility across different laboratories and cell batches. The majority of immunofluorescence staining images and Z-stacks were recorded and processed with the Yokogawa CQ1 Confocal Imaging Cytometer due to an improved and streamlined working process, as applying the Zeiss LSM 880 confocal microscope for quantitative analysis of protein expression in treated organoids

was not feasible. Organoids were always recorded on the ibidi 89626 imaging plate, in a volume of 50 to 100 µL benzyl alcohol/benzyl benzoate (1:2).

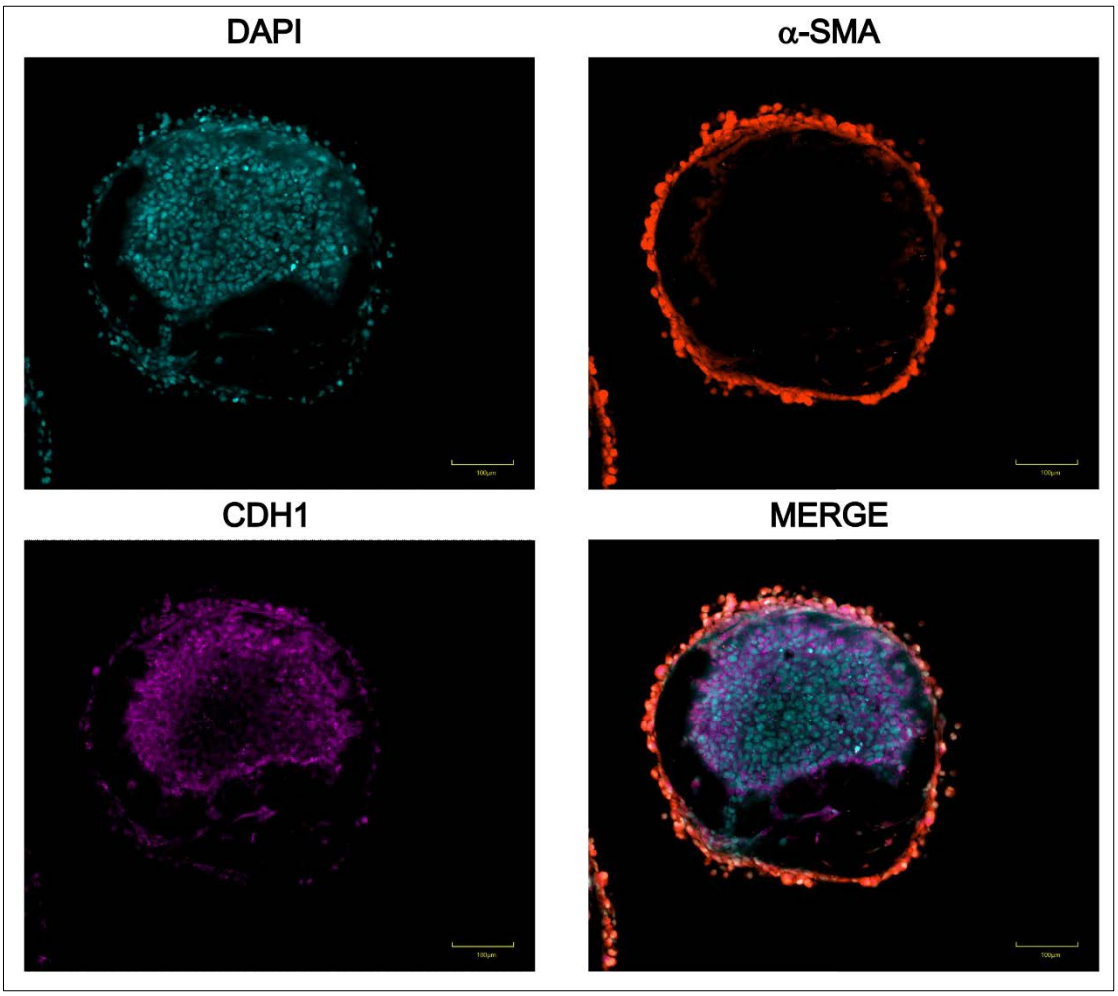

Figure 24. Exemplary spinning disc confocal microscopy images of an IF-stained Panc-1 + PSC organoid. Upper left picture: DAPI-staining of nuclei (405 nm channel); upper right picture: ACTA2-staining with fluorescent antibodies (561 nm channel); bottom left picture: E-cadherin-staining with fluorescent antibodies (640 nm channel); bottom right picture: merging of all three channels. Magnification: 20x. Reference scales (bottom right, yellow): 100 µm. On the bottom left side of the frame, the fringe of another organoid can be seen. Images recorded via the CQ1 Confocal Imaging Cytometer (Yokogawa Electric Corporation) and edited with the CellPathfinder software (Yokogawa).

Quantification of protein signal, especially of the expression of the epithelial marker protein E-cadherin (Burstin et al. 2009), was conducted solely with images recorded by the CQ1 Confocal Imaging Cytometer from Yokogawa. Figure 24 above and Figure 25 below show two exemplary organoids imaged via spinning disc confocal microscopy, in two different magnifications respectively. Imaging with a 40x magnification (see Figure 25 below) was not conducted for quantification and analysis of organoids, as the organoids couldn't be recorded in their totality in a single frame of reference. Further images and quantification results are depicted and described in section 4.6.5.

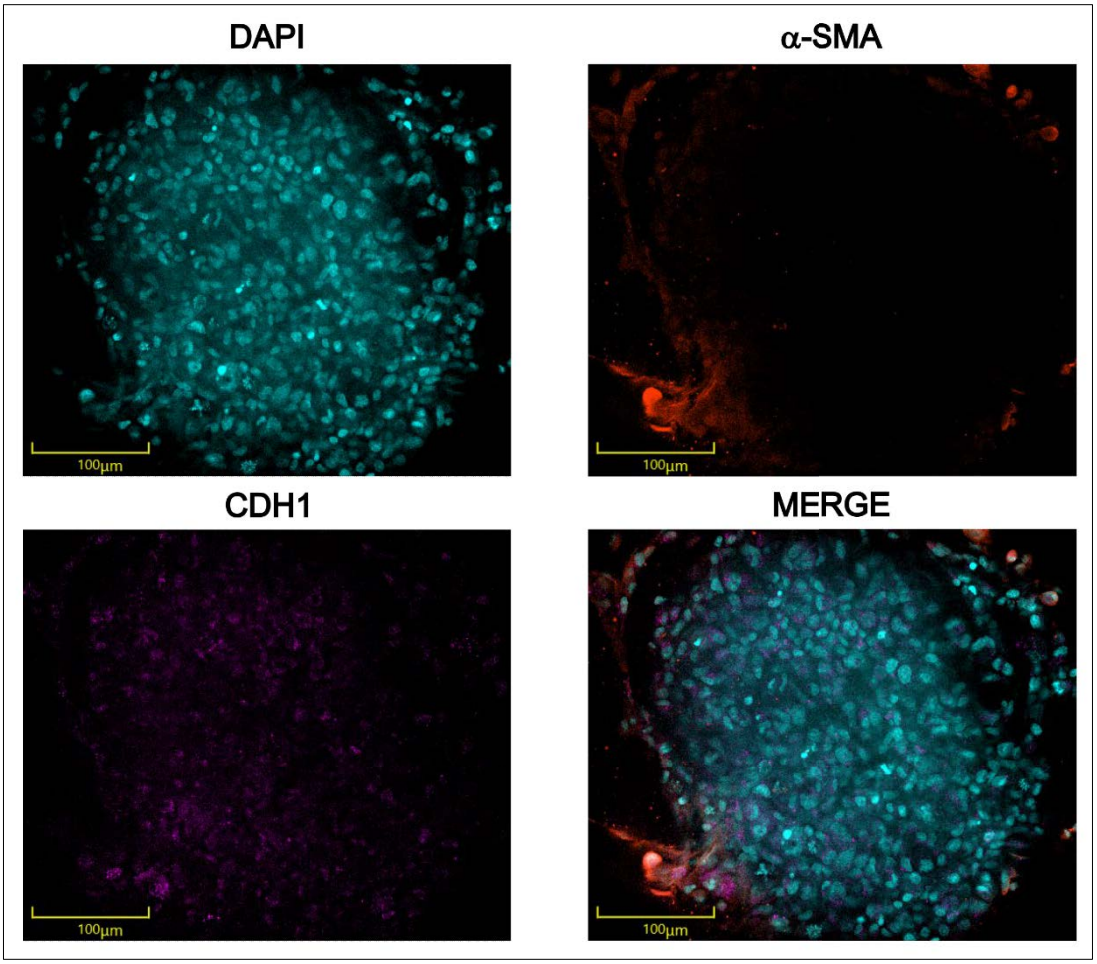

Figure 25. Exemplary spinning disc confocal microscopy images of an IF-stained Panc-1 + PSC organoid. Upper left picture: DAPI-staining of nuclei (405 nm channel); upper right picture: ACTA2-staining with fluorescent antibodies (561 nm channel); bottom left picture: E-cadherin-staining with fluorescent antibodies (640 nm channel); bottom right picture: merging of all three channels. Magnification: 40x. Reference scales (bottom left, yellow): 100 µm. Images recorded via the CQ1 Confocal Imaging Cytometer (Yokogawa Electric Corporation) and edited with the CellPathfinder software (Yokogawa).

Organoids cultivated on 384-well plates were successfully stained, cleared and imaged as well, and documentation via spinning disc confocal microscopy on a 40x magnification (see Figure 26 below) revealed much higher ACTA2 signals in the whole structure of the organoid as observed in organoids cultivated and grown on 96-well plates (see figures above), indicating a possible difference in the overall composition of the organoids or a change in the protein expression in the PDAC tumour cells (Panc-1), though no significant differences between organoids grown on 96-well and 384-well plates regarding cytotoxic results were noted or measured (see cytotoxicity results in section 4.6.1).

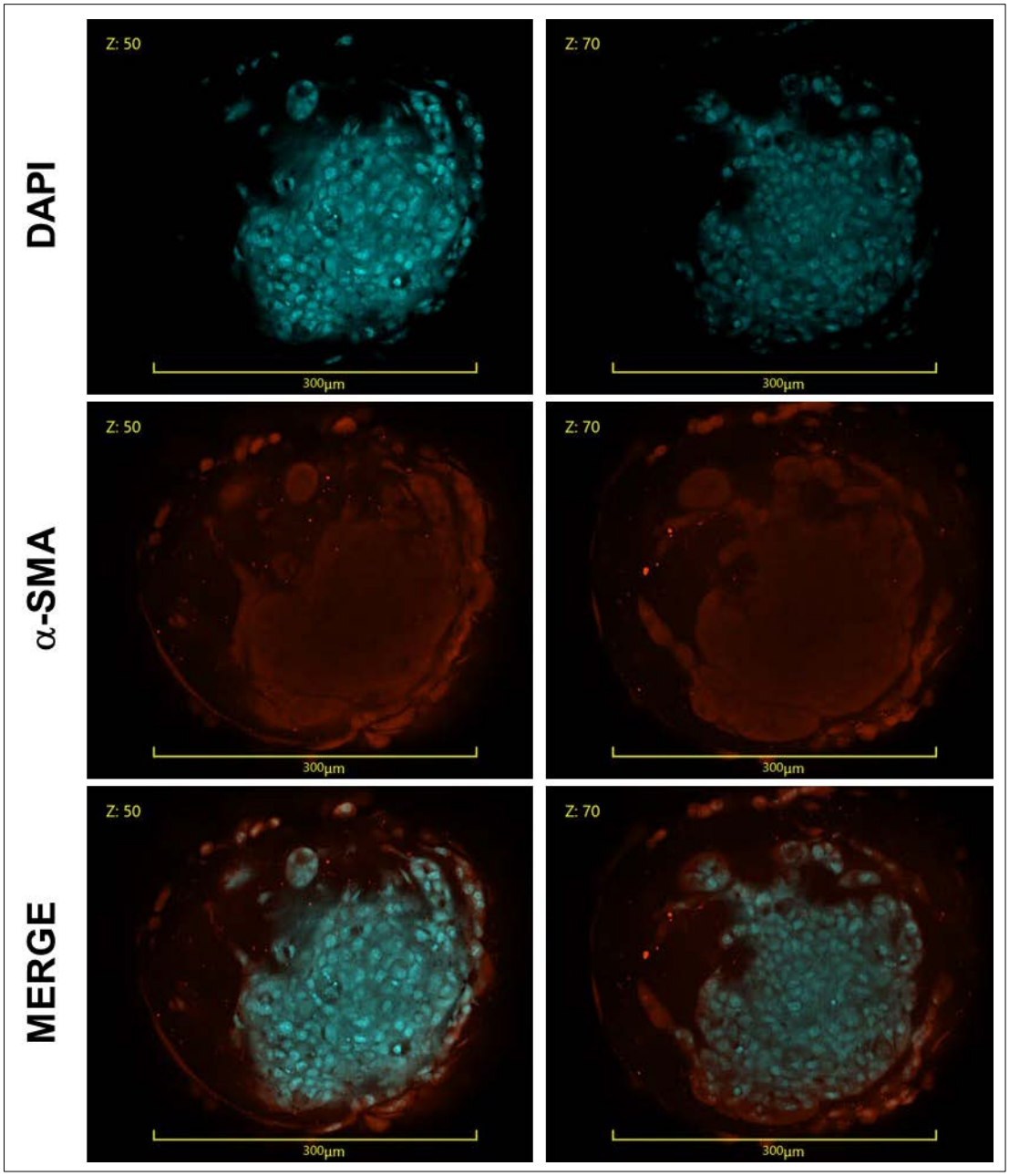

Figure 26. Exemplary spinning disc confocal microscopy images of an IF-stained Panc-1 + PSC organoid cultivated on a 384-well ULA plate. Top: DAPI-staining of nuclei (405 nm); middle: ACTA2-staining with fluorescent antibodies (561 nm channel); bottom: merging of both channels. Two different optical planes from a Z-stack library are depicted here. Left Z-slice: 50 µm height; right Z-slice: 70 µm height. Reference scales: 300 µm. Images recorded via the CQ1 Confocal Imaging Cytometer (Yokogawa Electric Corporation) and edited with the CellPathfinder software (Yokogawa).

4.3.2.2 Live/Dead Staining of Organoids

Organoid models, cultured with Panc-1 and KU0020 PSC cells, were stained with the LIVE/DEAD™ Viability/Cytotoxicity Kit (Cat. #L3224, Thermo Fisher Scientific) to examine the amount of dead cells inside the organoid after incubation with cytotoxic agents. The potent drug staurosporine (Omura et al. 1977) was applied as a control substance, exhibiting high efficacy at low concentrations. Staining of organoids with the dead stain ethidium-homodimer 1 (see Figures 27 to 30 below) revealed minor amounts of dead cells in untreated organoids, contrasted by organoids treated with 1 and 10 µM of staurosporine for 24 hours.

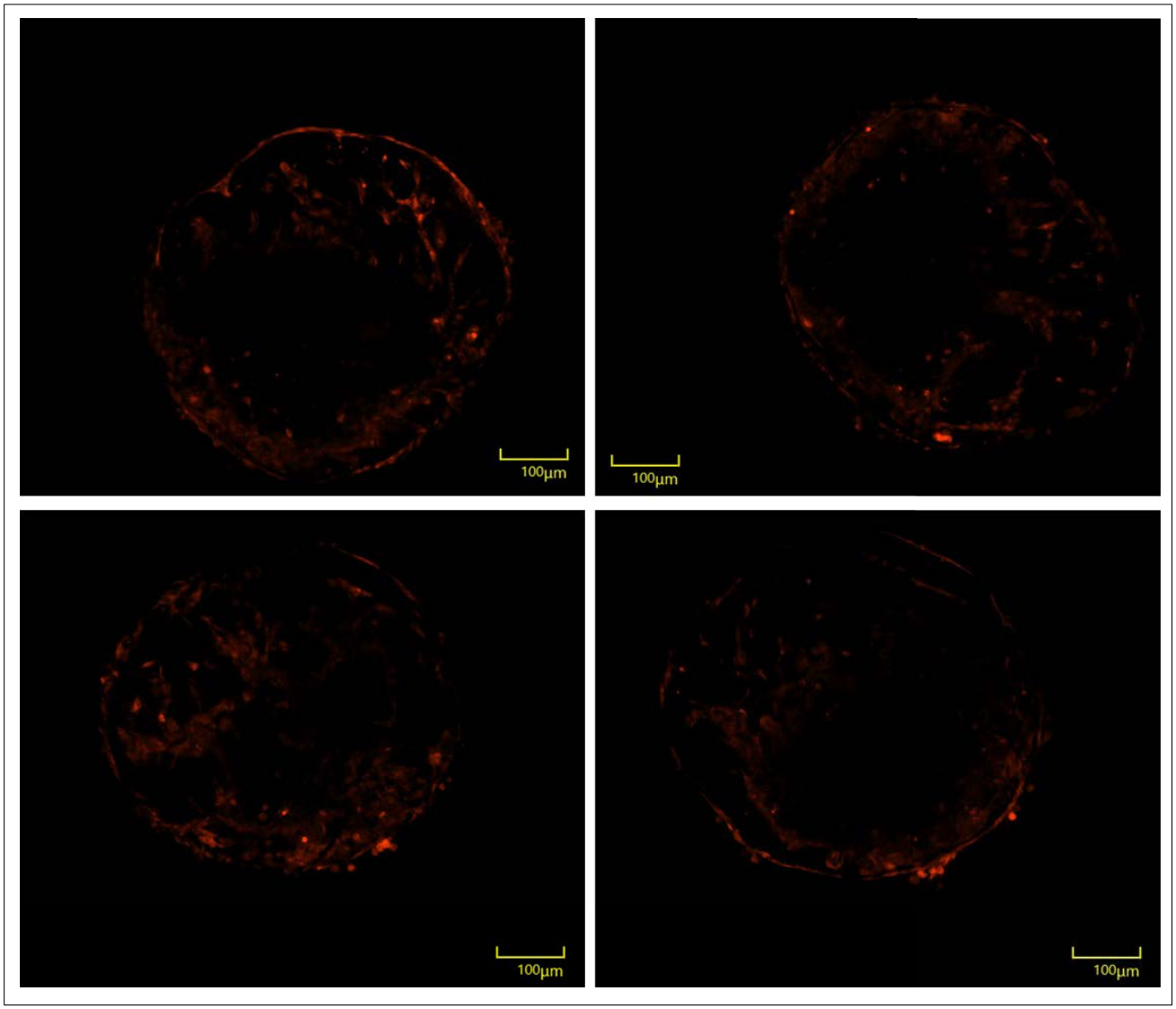

Figure 27. Staining of untreated organoids (Panc-1 + PSC) with ethidium homodimer-1. Organoids were incubated for six days after seeding on 96-well ULA plates. Four different organoids depicted. EthD-1 signal recorded with the 561 nm channel (20x magnification). Reference scale (yellow): 100 µm. Images recorded via the CQ1 Confocal Imaging Cytometer (Yokogawa Electric Corporation) and edited with the CellPathfinder software (Yokogawa).

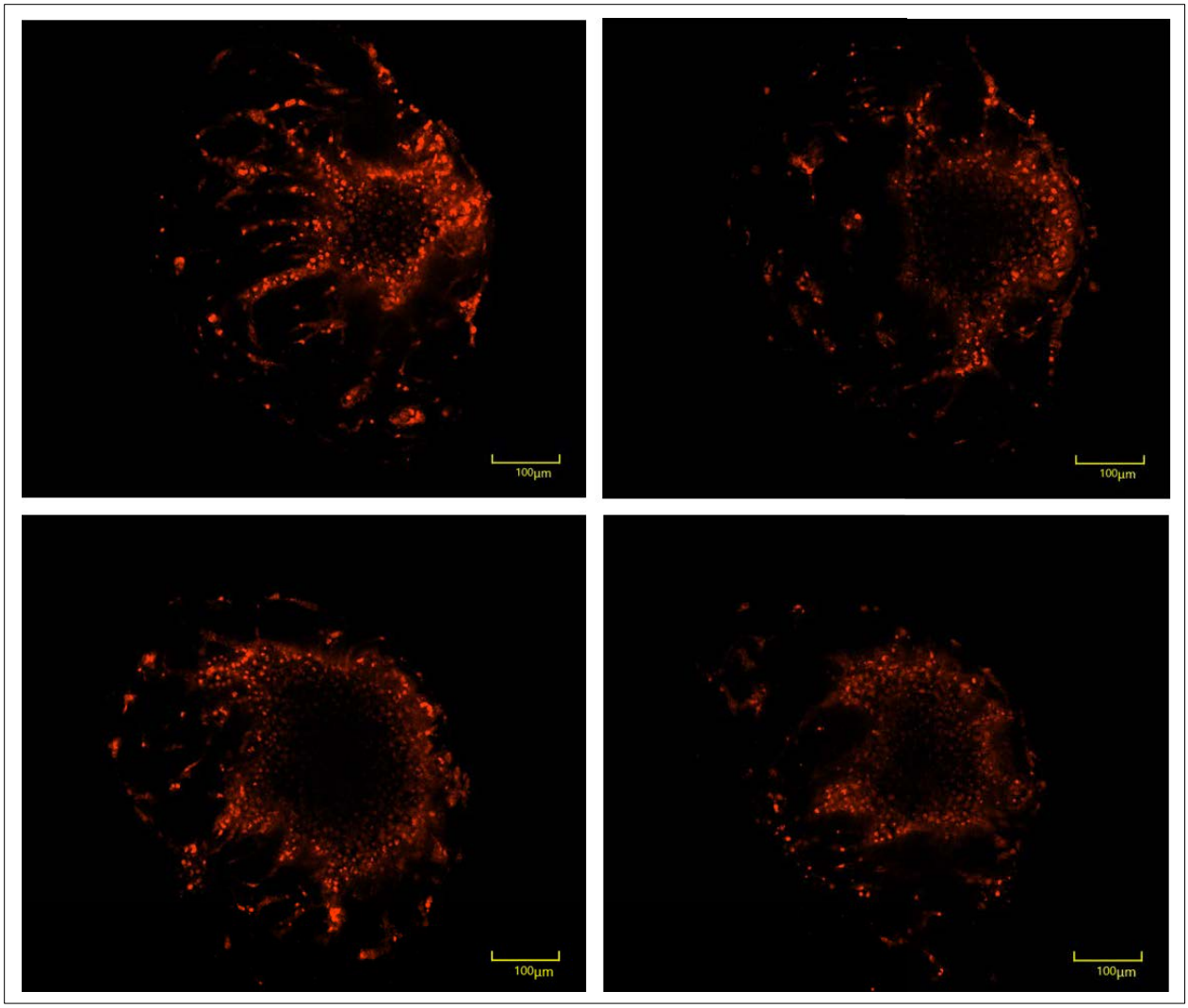

Figure 28. Organoids (Panc-1 + PSC) treated with 1 µM staurosporine for 24 hours. Staining with ethidium homodimer-1. Organoids were incubated for six days after seeding on 96-well ULA plates. Four different organoids depicted. EthD-1 signal recorded with the 561 nm channel (20x magnification). Reference scale (yellow): 100 µm. Images recorded via the CQ1 Confocal Imaging Cytometer (Yokogawa Electric Corporation) and edited with the CellPathfinder software (Yokogawa).

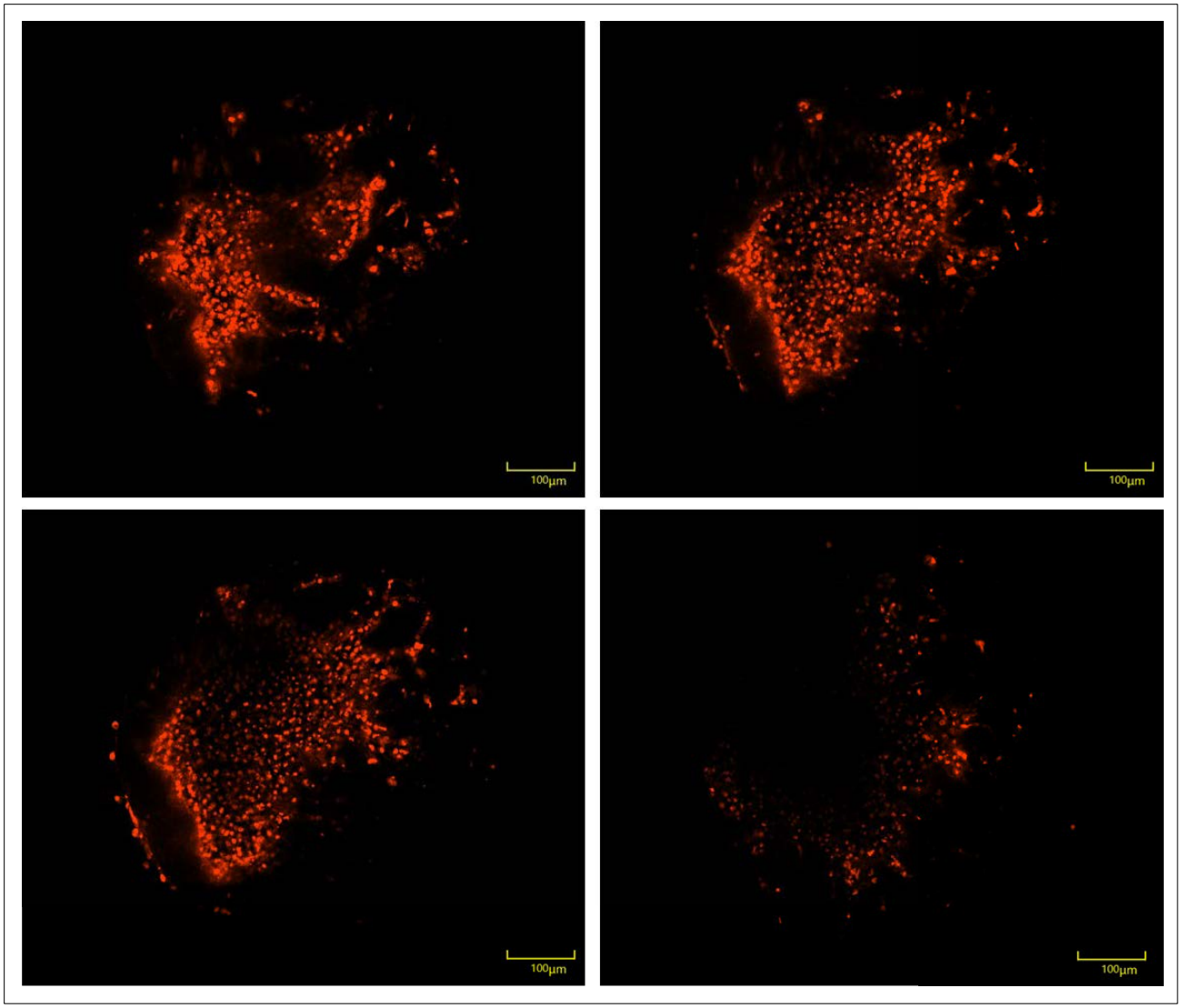

Figure 29. Organoids (Panc-1 + PSC) treated with 10 µM staurosporine for 24 hours. Staining with ethidium homodimer-1. Organoids were incubated for six days after seeding on 96-well ULA plates. Four different organoids depicted. Organoid on the bottom right partially dissolved following the treatment with 10 µM staurosporine. EthD-1 signal recorded with the 561 nm channel (20x magnification). Reference scale (yellow): 100 µm. Images recorded via the CQ1 Confocal Imaging Cytometer (Yokogawa Electric Corporation) and edited with the CellPathfinder software (Yokogawa).

Untreated organoids cultivated on 96-well ULA plates featured insignificant numbers of dead cells (Figure 27) and no distinct staining of cells besides background fluorescence, in comparison to organoids treated with either 1 (Figure 29) or 10 µM (Figure 28) staurosporine, where dead cells could be successfully stained and detected with the LIVE/DEAD™ Viability/Cytotoxicity Kit. Organoids treated with 10 µM staurosporine contained a higher number of dead cells than those treated with 1 µM and partially lost their cohesive structure and shape (see Figure 30 below). Organoids treated with 1 µM staurosporine exhibited an inner core of unaffected cells.

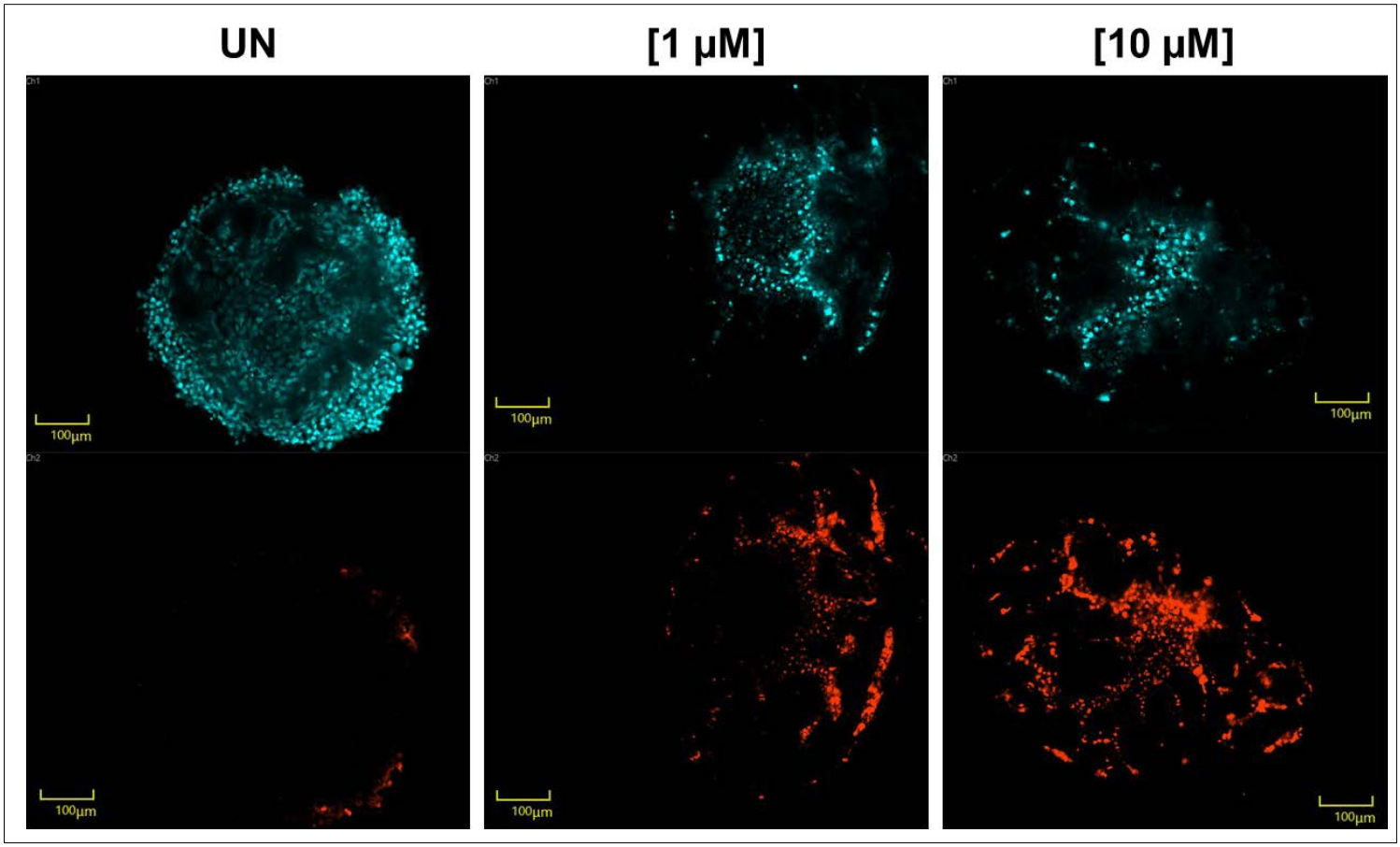

Figure 30. Comparison between organoids stained with ethidium homodimer-1. Organoids were incubated for six days after seeding on 96-well ULA plates. Left: untreated organoid; middle: organoid treated with 1 µM staurosporine; right: organoid treated with 10 µM staurosporine. Treatment with 1 and 10 µM staurosporine lasted for 24 hours. DAPI signal (top) recorded with the 405 nm channel, EthD-1 signal (bottom) recorded with the 561 nm channel (20x magnification). Reference scale (yellow): 100 µm. Images recorded via the CQ1 Confocal Imaging Cytometer (Yokogawa Electric Corporation) and edited with the CellPathfinder software (Yokogawa).

Staining of viable cells with calcein AM could not be achieved for the organoid model due to intense background fluorescence, possibly caused by the large amount of collagen and other components of the extracellular matrix present inside the organoid structure and composition. Calcein staining was only achieved in smaller organoids cultivated on 384-well ULA plates (see Figure 31 below). Staining with DAPI and calcein AM was consistent and validated observations that cells inside co-culture organoids were still viable and exhibited no signs of cellular death.

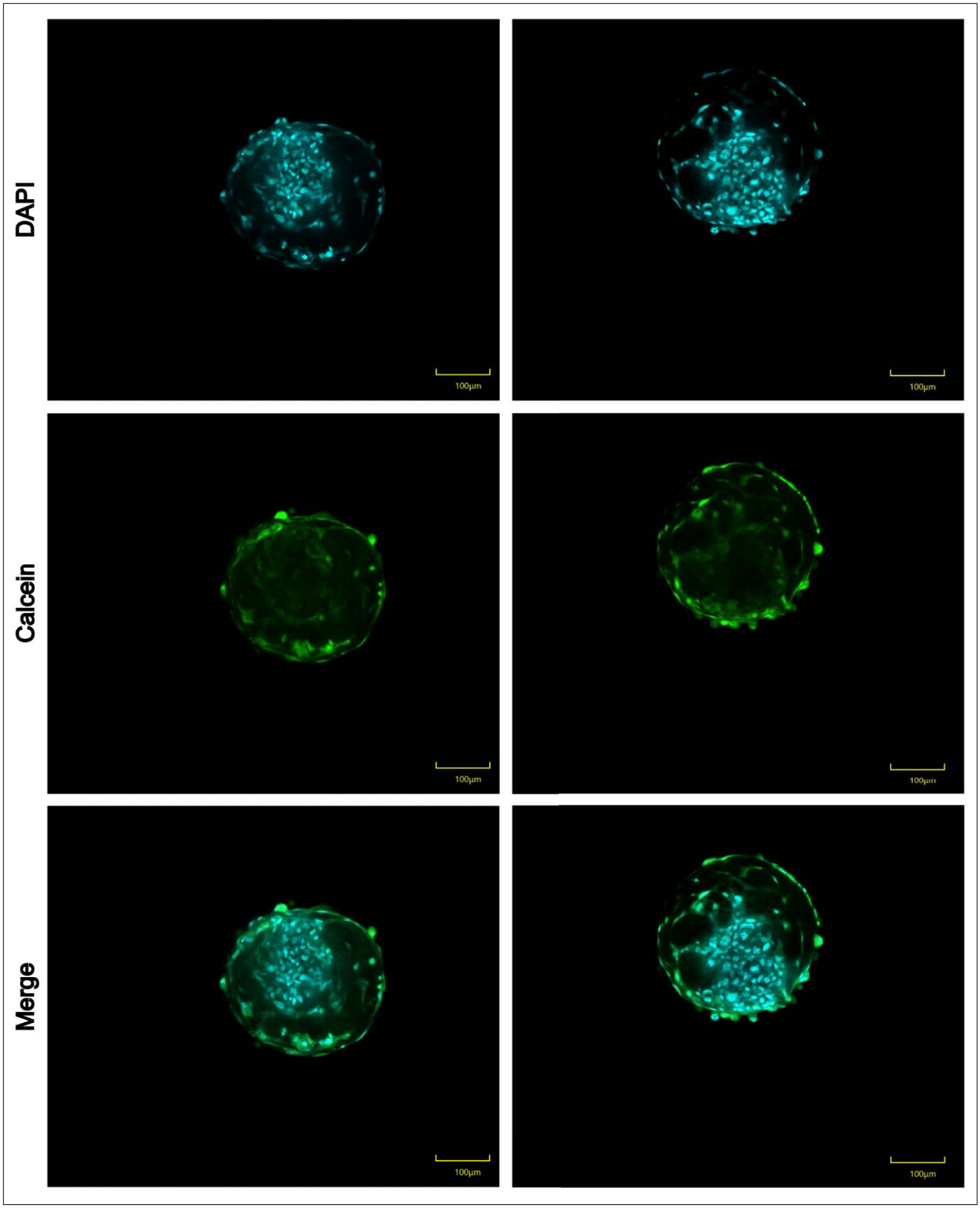

Figure 31. Live-staining of two small organoids (384-well plate-cultivated) with calcein AM. DAPI signal (top) recorded with the 405 nm channel, calcein AM signal (middle) recorded with the 488 nm channel (20x magnification). Bottom images: merging of 405 and 488 nm channel. Reference scale (yellow): 100 µm. Images recorded via the CQ1 Confocal Imaging Cytometer (Yokogawa Electric Corporation) and edited with the CellPathfinder software (Yokogawa).

4.3.3 Cultivation of Capan-1 + HSC-P Organoids

An initial experiment regarding the cultivation of organoids consisting of Capan-1 and NCC06 HSC-P cells on 96-well ultra-low attachment (ULA) plates was conducted to establish a three-dimensional pancreatic ductal adenocarcinoma (PDAC) liver metastasis model. Cells were seeded as defined in the standardized organoid protocol, with cell titres of $1*10^4$ Capan-1 cells/mL and $2*10^4$ HSC-P cells/mL and a collagen-1 matrix of 0.1 mg/mL collagen-1, in an initial volume of 50 µL per well. The successfully formed and grown organoids were cultivated for six days following seeding, and imaged with the Axio Vert.A1 microscope. This experiment was only conducted once and not repeated, but the results described below (see Figure 32 and 33) indicate that Capan-1 + HSC-P organoids can be applied for 3D cell-culture methods and experiments as well.

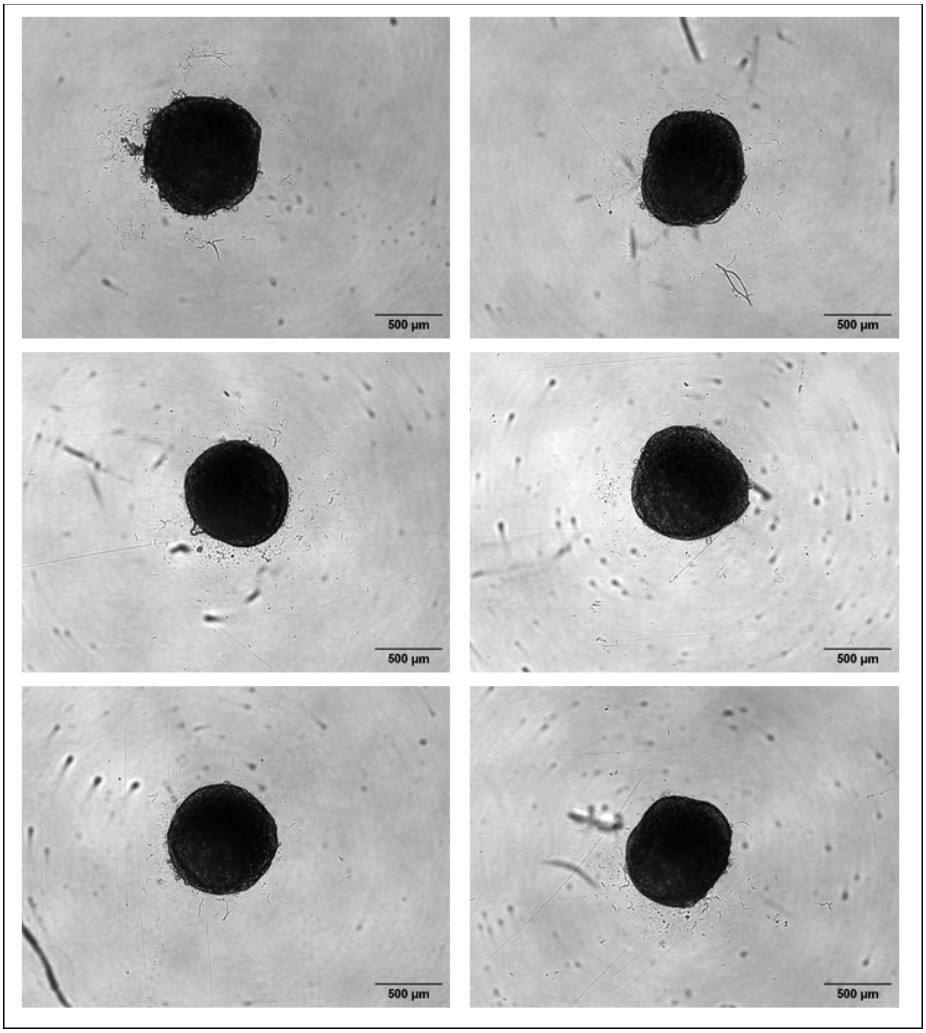

Figure 32. Cultivation of Capan-1 + HSC-P organoids. Six different organoids depicted. Cultivation of organoids lasted for six days following their initial seeding on 96-well ULA plates. Reference scale (bottom right): 500 µm. Images were recorded with the Axio Vert.A1 microscope and edited with the ImageJ software.

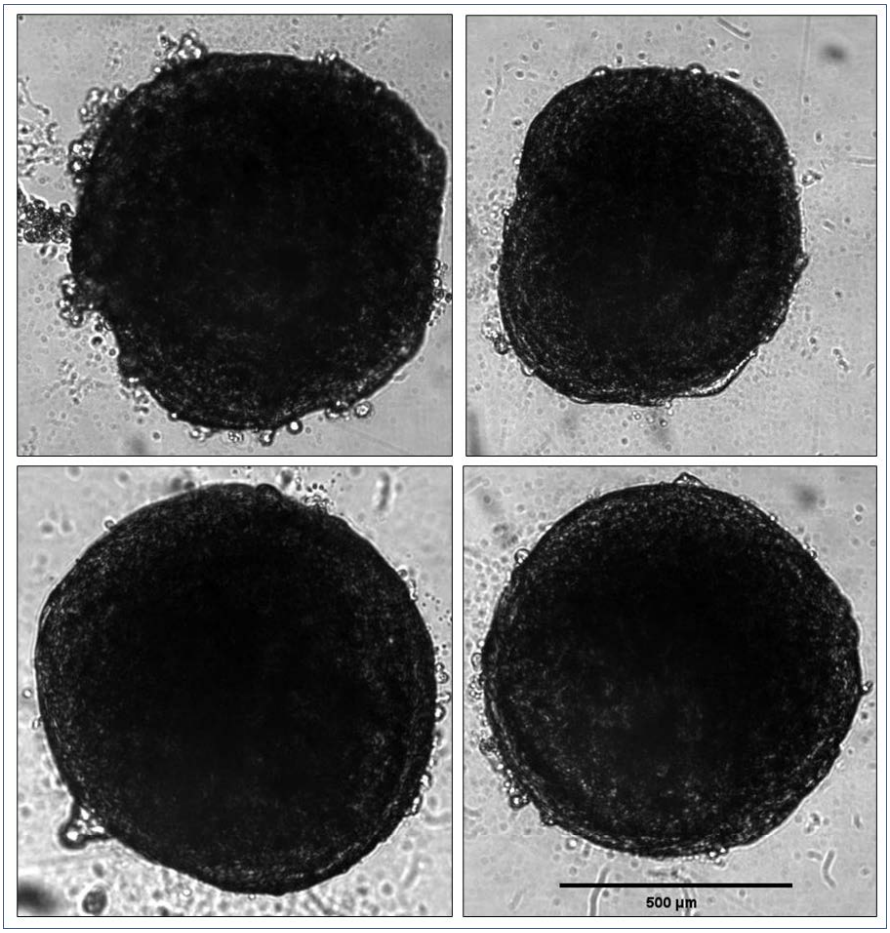

Figure 33. Cultivation of Capan-1 + HSC-P organoids. Four different organoids depicted. Cultivation of organoids lasted for six days following their initial seeding on 96-well ULA plates. Reference scale (bottom right): 500 µm. Images were recorded with the Axio Vert.A1 microscope and edited with the ImageJ software.

To establish the Capan-1 + HSC-P organoid model and generate a validated and standardized protocol of operation for the cultivation and handling of the organoids, further experimental research and testing has to be conducted.

4.4 Experimental Analysis of Tylophorinine Derivatives

Six derivatives of the natural plant product tylophorinine (TYLO), including the most potent agent *O*-methyltylophorinidine (see material section 3.2.1), were isolated and provided by the research group of Professor Proksch from the Institute of Pharmaceutical Biology and Biotechnology of the Heinrich Heine University (Düsseldorf, Germany). These substances were tested and evaluated on pancreatic cancer cells and three-dimensional organoid models via cytotoxicity assays (4.4.1) and live-cell imaging (4.4.2), and results presented here were partially published before (Xie et al. 2020).

4.4.1 Cytotoxic Evaluation of *O*-Methyltylophorinidine

The tylophorinine derivative *O*-methyltylophorinidine was tested and examined on Panc-1 and Capan-2 cells, as well as on Panc-1 + PSC and Panc-1 + HSC-P organoids. On all four models, *O*-methyltylophorinidine exhibited high effectivity and low IC_{50} values, with 4.6 and 5.58 nM on Panc-1 and Capan-2 cells respectively, and 3.57 and 6.39 nM on Panc-1 + PSC and Panc-1 + HSC-P organoids respectively, verifying the natural efficacy of tylophorinine derivatives and substances on tumour cells, and on pancreatic cancer cells specifically. The results presented in the table below (Table 16) were first published in Xie et al. (2020).

Table 16. Cytotoxic evaluation of *O*-methyltylophorinidine on 2D (Panc-1, Capan-2) and 3D (Panc-1+PSC, Panc-1+HSC-P) models. The CyQUANT NF Cell Proliferation (Cat. #C35006, Thermo Fisher Scientific) was used for the 2D models, the CellTiter-Glo 3D Cell Viability Assay (Cat. #G9681, Promega) for the 3D organoid models. Arithmetic means and their respective standard deviations of three repeats are depicted below (Xie et al. 2020).

PDAC Model	IC_{50} [nM]
Panc-1 (2D)	4.60 (±0.47)
Capan-2 (2D)	5.58 (±1.47)
Panc-1 + KU0020 PSC (3D)	3.57 (±1.30)
Panc-1 + NCC06 HSC-P (3D)	6.39 (±2.28)

4.4.2 Anti-Proliferative Effects of Tylophorinine Derivatives

The evaluation of anti-proliferative properties regarding the different tylophorinine derivatives was conducted with the live-cell imaging application of the IncuCyte Zoom device (Sartorius, Germany). Panc-1 cells were seeded out on 96-well tissue culture plates, treated with 10, 100 and 1000 nM of tylophorinine derivatives and incubated for 96 hours (see method section 3.3.3.2). Gemcitabine (100 µM) served as the positive control, DMSO (1 %) as the negative control. Statistical analysis (ANOVA) was conducted with the GraphPad Prism 8 software (see Figure 34 below).

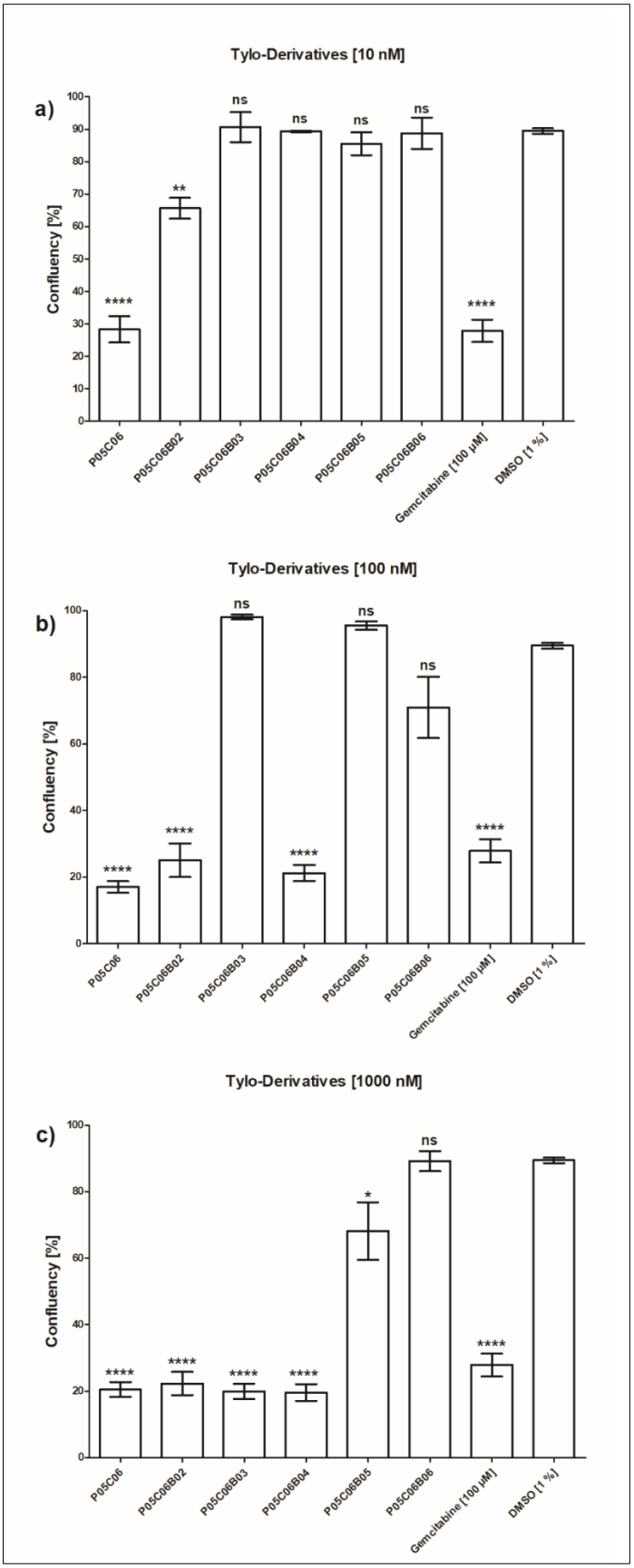

Figure 34. Anti-proliferative effects of tylophorinine derivatives. The y-axis represent the percental confluency of the recorded wells. From left to right: P05C06 (*O*-methyltylophorinidine), P05C06B02 (tylophorinidine), P05C06B03 (tylophoridicine E), P05C06B04 (2-demethoxytylophorine), P05C06B05

(Tylophoridicine D), P05C06B06 (*O*-demethyl-tylophoridicine D). A) treatment with 10 nM derivatives; b) treatment with 100 nM derivatives; c) treatment with 1000 nM derivatives. Controls: gemcitabine (100 µM) and DMSO (1 %). Statistical analysis via ANOVA (compared to DMSO-control). Columns represent the arithmetic means and their respective standard errors of the mean (SEM). Ns: not significant; *: p<0.1; **: p<0.01; ****: p<0.0001.

P05C06B05 and P05C06B06 exhibited the lowest anti-proliferative effects at all tested concentrations. P05C06B04 exhibited high efficacy at both 1000 and 100 nM, but no measurable effect at 10 nM, and P05C06B03 only at 1000 nM. P05C06 (*O*-methyltylophorinidine) showcased the highest effect at all concentrations, with the lowest confluency of all derivatives at even 10 nM, and P05C06B02 showcased similar, but weaker effects at 100 and 1000 nM and significantly diminished effect at 10 nM. These results further empirically validate and confirm the anti-tumorigenic and anti-proliferative properties of tylophorinine derivatives and match the data published previously by our research institute (Reimche et al. 2022).

4.5 Experimental Analysis of Artemisinin Derivatives

The cytotoxic properties of the natural plant metabolite artemisinin (ARS) and its respective derivatives were tested and researched on PDAC cells and organoid models. Several synthetic artemisinin-based drugs were examined with the CellTiter-Glo cell viability assay on Panc-1 cells cultivated on 384-well plates via the CyBio Well vario pipetting robot (see section 4.5.1 below). The CellTiter-Glo assay was conducted after 48 hours of incubation, while the UV-activated artemisinin-hybrid substances were tested with the PrestoBlue assay after 24 hours of incubation (see section 4.5.2 below). Some of the results presented below were previously published in the PhD thesis of Christina Bold, who synthesized these artemisinin compounds (Bold 2022).

4.5.1 Cytotoxic Evaluation of Artemisinin Derivatives

Panc-1 cells were seeded out on 384-well plates as described in method section 3.3.3.1, and subjected to treatment with artemisinin derivatives 24 hours after seeding for an incubation period of 48 hours. All pipetting steps were performed with the CyBio Well vario pipetting robot, and the luminescent signals were measured with the Tecan SPARK device or the POLARstar Optima device, as luminescent values were often too high to be recorded with the Tecan device. All artemisinin drugs were subjected to three independent repeats and analysed with the GraphPad Prism 8 software.

Table 17. Cytotoxic evaluation of artemisinin and several derivatives on Panc-1 cells. The CellTiter-Glo Luminescent Cell Viability Assay (Cat.#G7570, Promega) was applied to the cells after 48 hours of incubation. Depicted values represent the arithmetic means and their respective standard deviations of three repeats.

Artemisinin Derivatives	IC_{50} [µM]
Artemisinin	> 100
Artesunate	13.78 (±2.31)
CB-108	12.57 (±0.96)
CB-110	13.77 (±1.61)
CB-66-Fr1	14.02 (±3.07)
CB-84-Fr1	6.12 (±0.53)
CB-AC-8	17.35 (±4.82)
(CB)-EDV-01	11.99 (±2.96)
CB-Jan	12.11 (±1.39)
Dihydroartemisinin	18.84 (±4.47)

Artemisinin exhibited no cytotoxic effect on Panc-1, while artesunate (ART) and dihydroartemisinin (DHA) exhibited mild cytotoxic properties, with measured IC_{50} values of 13.78 and 18.84 µM, respectively. The artemisinin derivatives synthesized and provided by the research group of Professor Griesbeck from the Department of Chemistry (University of Cologne, Germany) exhibited similar and comparable IC_{50} values. CB-84-Fr1 showcased the lowest IC_{50} value of 6.12 µM on Panc-1 cells. These results indicate that natural and synthetic derivatives of artemisinin might theoretically function as potent chemotherapeutic agents against PDAC.

Within the scope of this thesis, only artesunate (ART) and dihydroartemisinin (DHA) were tested and evaluated on three-dimensional co-culture organoids (Panc-1 + PSC), and both proved to be very efficacious. An IC_{50} value of 3.96 (±0.80) µM was measured for artesunate, and an IC_{50} value of 3.21 (±0.30) µM for dihydroartemisinin (see Figure 35 below), further validating the theoretical application of artemisinin derivatives as anti-tumorigenic substances.

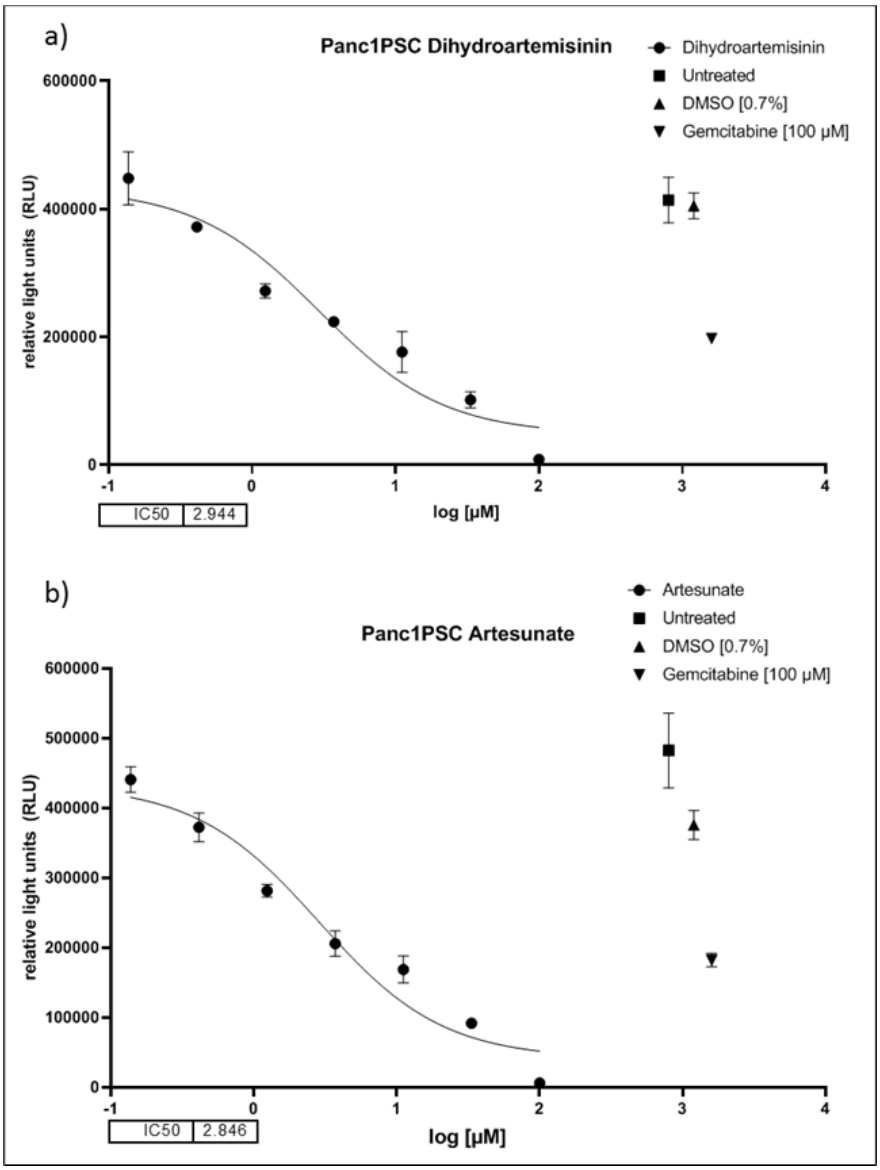

Figure 35. Dihydroartemisinin and artesunate exhibited cytotoxic properties on Panc-1 + PSC organoids. Exemplary dose-response curve (100 to 1.5625 µM), with untreated, solvent (1 % DMSO) and positive control (100 µM gemcitabine) applied. Evaluation of cytotoxicity with the CellTiter-Glo 3D Cell Viability Assay (Cat. #G9681, Promega). For DHA (a), an IC_{50} value of 2.944 µM was measured; for ART (b), an IC_{50} value of 2.846 µM. Data points represent the arithmetic means and their respective standard deviations of triplicates.

4.5.2 Activation of Artemisinin-Hybrids via UV Irradiation

Due to practical constraints, treatment of Panc-1 and KU0020 PSC cells with artemisinin hybrids under ultraviolet irradiation could only last 24 hours following substance treatment to prevent evaporation and contamination of cell medium. Cytotoxicity was assessed using the PrestoBlue assay and measured with the Tecan SPARK device (see Table 18 and Figures 36 to 37 below). As shown before (see Table 17 above), artemisinin exhibited no measurable

cytotoxic properties on Panc-1 cells, and on PSC cells as well (measured only for 24 hours of incubation), with and without incubation under ultraviolet irradiation. Benzophenone alone exhibited weak cytotoxic properties on Panc-1 cells only under UV irradiation, with an IC_{50} value of 43 μM. The derivative "Hybrid 1" was activated by UV irradiation (Bold 2022) and negatively affected cell viability in both Panc-1 and PSC cells, with IC_{50} values of 3.80 μM and 23.24 μM respectively. Artemisinin and Benzophenone (BP) together (not crosslinked) exhibited minor cytotoxic properties on Panc-1 cells only under UV irradiation. These results verify the UV-mediated activation of benzophenone-linked artemisinin derivatives and their selectivity on tumour cells, as they show higher cytotoxic properties on Panc-1 cells than the cancer-associated fibroblast (CAF) cell type KU0020 PSC. Assays for BP under UV irradiation, ART + BP and ART + BP under UV irradiation were not conducted.

Table 18. Cytotoxic evaluation of artemisinin and several derivatives on Panc-1 and KU0020 PSC cells with and without UV radiation (366 nm at 24 hours of incubation). Benzophenone included. The PrestoBlue Cell Viability Reagent (Cat. #A13262, Thermo Fisher Scientific) assay was conducted after 24 hours of incubation. Depicted values represent the arithmetic means and their respective standard deviations of three repeats.

Substance	IC_{50} [μM] on Panc-1	IC_{50} [μM] on KU0020 PSC
Artemisinin	>100	>100
Artemisinin (UV irradiation)	>100	>100
Benzophenone	>100	>100
Benzophenone (UV irradiation)	42.79 (±5.69)	X
Hybrid	>100	>100
Hybrid (UV irradiation)	3.80 (±1.29)	23.24 (±8.78)
Artemisinin + Benzophenone	>100	X
Artemisinin + Benzophenone (UV irradiation)	55.75 (±5.37)	X

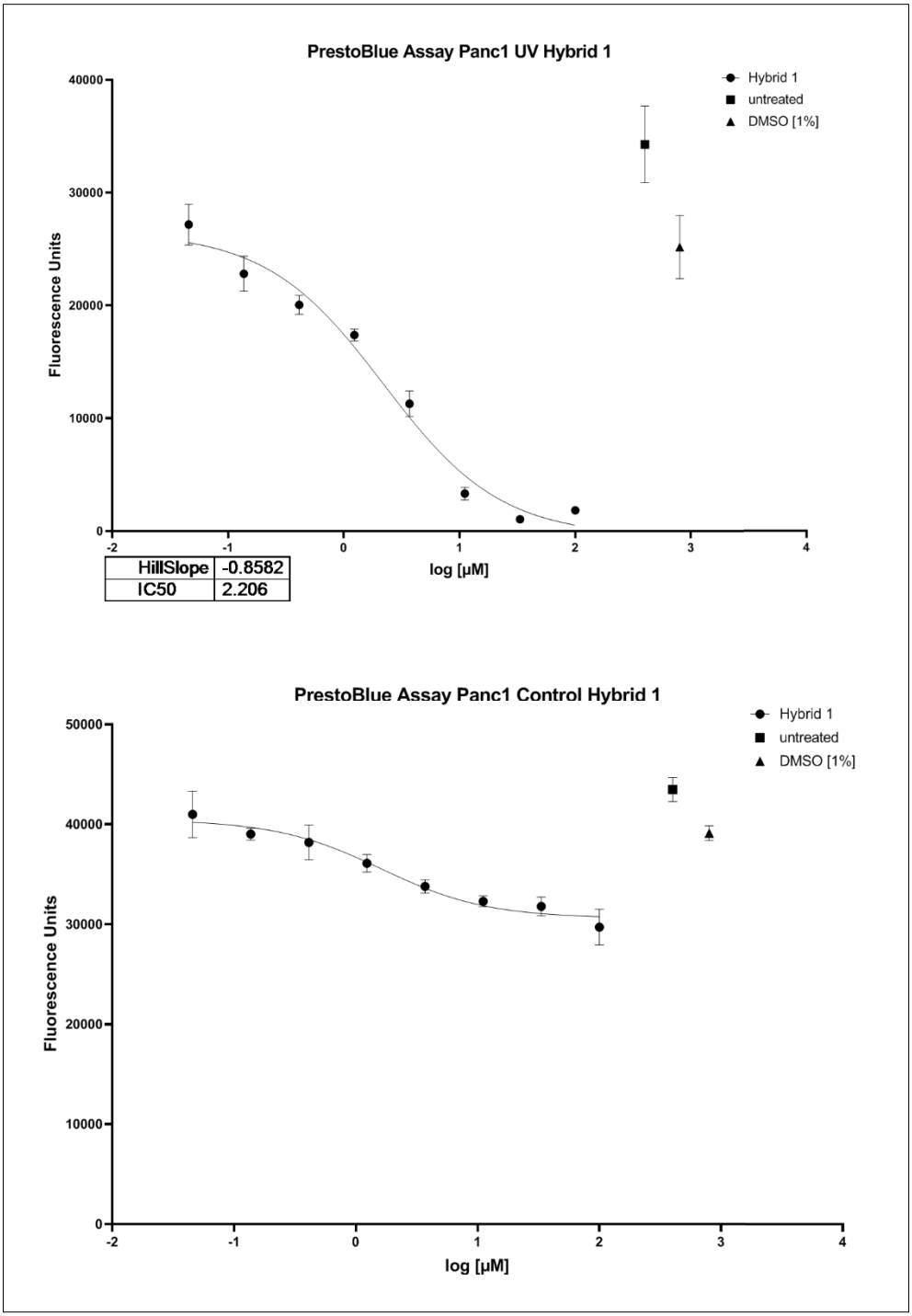

Figure 36. Artemisinin derivative Hybrid 1 (linked with benzophenone) exhibited cytotoxic properties on Panc-1 cells under UV irradiation (366 nm for 24 hours). Exemplary dose-response curve (100 to 1.5625 µM), with untreated and solvent (1 % DMSO) control applied. Evaluation of cytotoxicity with the PrestoBlue Cell Viability Reagent assay. Under UV irradiation, an IC_{50} value of 2.206 µM was measured. Without UV irradiation, no significant cytotoxic effect could be measured after 24 hours of incubation. Data points represent the arithmetic means and their respective standard deviations of triplicates.

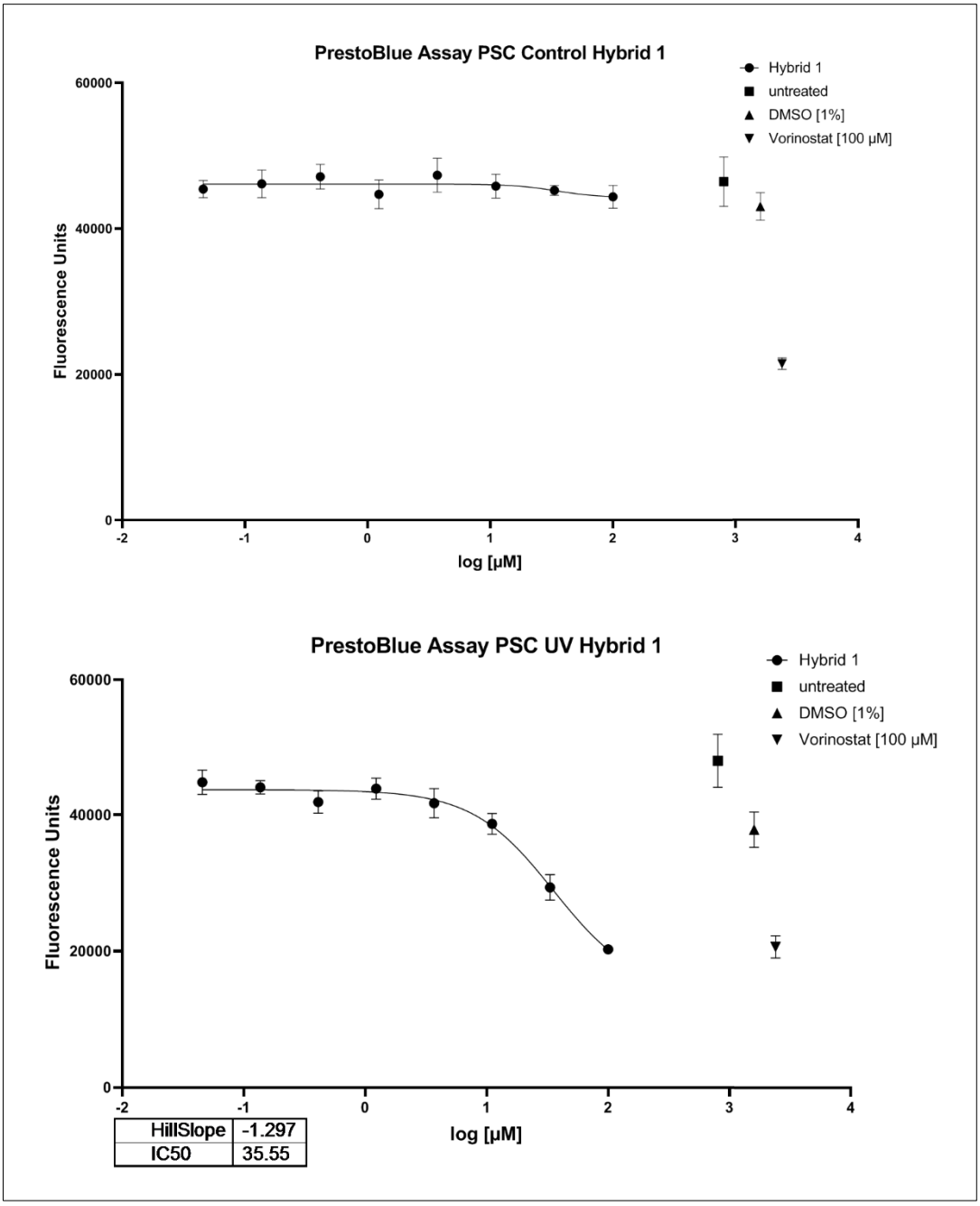

Figure 37. Artemisinin derivative Hybrid 1 (linked with benzophenone) exhibited cytotoxic properties on KU0020 PSC cells under UV irradiation (366 nm for 24 hours). Exemplary dose-response curve (100 to 1.5625 µM), with untreated and solvent (1 % DMSO) control applied. Evaluation of cytotoxicity with the PrestoBlue Cell Viability Reagent assay. Under UV irradiation, an IC_{50} value of 35.55 µM was measured. Without UV irradiation, no significant cytotoxic effect could be measured after 24 hours of incubation. Data points represent the arithmetic means and their respective standard deviations of triplicates.

Multiple derivatives, including UV-activated hybrids, of the anti-malarian drug artemisinin were experimentally proven to exhibit and feature anti-tumorigenic properties on the PDAC cell line Panc-1 and three-dimensional co-culture PDAC organoids (Panc-1 + KU0020 PSC). Further

scientific research is required to examine the effects and pharmaceutical mode of action of artemisinin derivatives in pancreatic cancer.

4.6 Experimental Analysis of Histone Deacetylase Inhibitors

The examination and research of histone deacetylase inhibitors (HDACi) and their effect on pancreatic cancer cells and organoids represent a major component of the thesis at hand. HDAC inhibitors were evaluated on their cytotoxic properties on Panc-1 cells, KU0020 PSC cells and 3D organoids (see section 4.6.1 below) in several approaches, and the effects of potent HDAC inhibitors on the expression of proteins of interests in Panc-1 cells were examined via western blotting (see section 4.6.3) and real-time quantitative PCR (RT-qPCR; see section 4.6.4). Further anti-proliferative properties were examined via Panc-1 colony formation assays (see section 4.6.2). The expression of E-cadherin (CDH1) in three-dimensional Panc-1 + KU0020 PSC organoids was examined at last via immunofluorescence (IF) staining and spinning disc confocal microscopy with the Yokogawa CQ1 Confocal Imaging Cytometer, and machine learning - assisted quantification was conducted for analysis. Some of the results presented and described below were first published in the master thesis of Daria Janßen (Janßen 2021), which was part of the HDACi research project at the Institute of Health Research and Education, (University of Osnabrück, Germany) and supervised by the author of this thesis.

4.6.1 Cytotoxic Evaluation of Histone Deacetylase Inhibitors

Multiple histone deacetylase inhibitors (HDACi), synthesized and provided for examination by the research group of Professor Kurz of the Institute of Pharmaceutical and Medical Chemistry of the Heinrich Heine University (Düsseldorf, Germany), were subjected to cytotoxic evaluation on the pancreatic ductal adenocarcinoma (PDAC) cell line Panc-1, the cancer-associated fibroblast (CAF) cell line KU0020 PSC cells, and organoid models (Panc-1 + PSC). Different periods of incubation (48 to 72 hours) were tested, and assays were conducted on 96-well and 384-well tissue culture (TC) plates, both via manual handling and pipetting with the CyBio Well vario pipetting robot. Table 19 (see below) summarizes the final and conclusive cytotoxicity results gained with commercially available HDAC inhibitors and novel synthetic substances on two-dimensional (2D) cell culture models (Panc-1 cells and KU0020 PSC cells) and three-dimensional (3D) organoid models (Panc-1 + PSC) after 72 hours of substance treatment. These results were gained from cells seeded both manually and automatically with the CyBio Well vario pipetting robot, on 96-well and 384-well plates. Measurement of luminescence values was conducted with the Tecan SPARK and the POLARstar Optima device. The

established drug vorinostat/suberoylanilide hydroxamic acid (Grant et al. 2007) was used as a suitable positive control, together with three commercially available HDAC6 inhibitors: citarinostat (Bae et al. 2018), ricolinostat (Lee et al. 2018a) and tubastatin A (Vishwakarma et al. 2013).

Table 19. Cytotoxic evaluation of histone deacetylase inhibitors (HDACi) on PDAC culture models after 72 hours of incubation. This table summarizes the result obtained with commercially available HDAC inhibitors (citarinostat, ricolinostat, tubastatin A and vorinostat) and those obtained with the novel substances (provided by the research group of Professor Kurz by the Institute of Pharmaceutical and Medical Chemistry), sorted alphabetically. Cytotoxicity assays (CellTiter-Glo) were conducted on both 96-well and 384-well tissue culture (TC) plates. Depicted values represent the arithmetic means and their respective standard deviations of three to four repeats. ATCC Panc-1 cells were utilized. Some results listed below were first published in the master thesis of Daria Janßen (Janßen 2021)

		KU0020 PSC	Panc-1 (ATCC)	3D (Panc-1 + PSC)
Source	**HDAC Inhibitors**	**IC_{50} [µM]**		
Commercially available	Citarinostat	16.13 (±5.32)	39.03 (±5.03)	16.20 (±1.66)
	Ricolinostat	13.39 (±1.73)	58.72 (±4.73)	16.31 (±3.75)
	Tubastatin A	79.17 (±5.58)	24.64 ±(5.97)	32.46 (±5.40)
	Vorinostat (SAHA)	3.62 (±0.43)	6.89 (±0.24)	2.06 (±0.42)
AG Kurz (Heinrich Heine University Düsseldorf)	KSK64	14.87 (±4.55)	7.04 (±0.58)	3.30 (±0.58)
	KSK75	>100	> 100	X
	LAK41	2.41 (±0.41)	9.18 (±1.31)	2.51 (±0.99)
	LAK53	44.90 (±7.34)	25.16 (±3.17)	12.80 (±2.77)
	LAK61	74.83 (±6.86)	86.93 (±0.87)	23.94 (±2.17)
	LAK67	10.34 (±5.64)	15.97 (±0.58)	6.46 (±1.34)
	LAK92	>100	60.33 (±6.54)	39.93 (±10.71)
	LAK107	>100	>100	X
	LAK110	>100	>100	X
	LAK121	>100	>100	X
	LAK127	59.45 (±11.89)	48.82 (±2.59)	33.96 (±4.18)
	LAK-ZnFD	>100	>100	X
	MPK264	40.59 (±4.07)	15.45 (±2.77)	5.54 (±1.30)
	MPK265	24.33 (±1.96)	27.02 (±5.05)	14.06 (±3.49)
	MPK324	20.89 (±3.13)	24.94 (±5.00)	14.25 (±3.80)
	MPK544	3.01 (±0.84)	6.96 (±1.03)	1.05 (±0.10)

Sixteen novel HDAC inhibitors (see Table 19 above and material section 3.3.1) were examined and evaluated in total, exhibiting both high (e.g. KSK64) and low cytotoxic efficacies (e.g. LAK92). No HDAC inhibitor featured IC_{50} values under 1 µM, or values comparable to the tylophorinine derivatives (see section 4.4 above). Except for the five HDAC inhibitors KSK75, LAK107, LAK110, LAK121 and LAK-ZnFD, which showcased low potency on Panc-1 and KU0020 PSC cells, with no significant cytotoxicity measured in the applied dose-response

curves (DRC), CellTiter-Glo assays were conducted on all two applied cell lines and 3D organoids for each HDAC inhibitor.

All three HDAC6 inhibitors (citarinostat, ricolinostat and tubastatin A) exhibited low cytotoxic efficacy on Panc-1 cells and average efficacy on KU0020 PSC cells. Tubastatin featured the highest measured IC_{50} values on KU0020 PSC cells and 3D organoids (79.17 µM and 32.46 µM, respectively) among the HDAC6 inhibitors, but the lowest IC_{50} value on Panc-1 cells (24.64 µM), indicating that inducing cell death in PSC cells coincides with causing cytotoxic effects in the organoids. Citarinostat and Ricolinostat exhibited higher cytotoxic efficacy on the PSC cells (16.13 µM and 13.39 µM, respectively), low efficacy on Panc-1 cells (39.03 µM and 58.72 µM, respectively), but lower IC_{50} values on 3D organoids than Tubastatin A (16.20 µM and 16.31 µM, respectively). Vorinostat/SAHA, a pan-HDAC inhibitor, showcased very high cytotoxic properties on all tested cells and models, as expected, with an IC_{50} value of 3.62 µM on PSC cells, 6.89 µM on Panc-1 cells and 3.30 µM on 3D organoids. The pan-HDACi was also tested on Capan-1 cells in a 2D model and exhibited an IC_{50} value of 4.05 (±0.27) µM.

Four novel HDAC inhibitors featured low IC_{50} values and high cytotoxic potential and were subjected to further experimental analysis: KSK64, LAK41, MPK264 and MPK544 (in alphabetical order). MPK264, a derivative of the potent HDAC6 inhibitor nexturastat A (Pflieger et al. 2021), exhibited very low cytotoxic potential on PSC cells, with an IC_{50} value of 40.59 µM, and average efficacy on Panc-1 cells (IC_{50} value of 15.45 µM), but very high efficacy on organoids (IC_{50} value of 5.54 µM). KSK64, an HDAC1/6-specific inhibitor (Alves Avelar et al. 2021), featured average cytotoxicity on PSC cells (IC_{50} value of 14.87 µM), but high cytotoxic potential on both Panc-1 cells and 3D organoids (IC_{50} values of 7.04 µM and 3.30 µM, respectively). LAK41, an HDAC2/6-specific inhibitor, exhibited very high cytotoxic properties on all tested models (IC_{50} values of 2.41, 9.18 and 2.51 µM for PSC, Panc-1 and organoids respectively), together with MPK544, another HDAC2/6-specific inhibitor, which showcased IC_{50} values comparable to vorinostat/SAHA (3.01, 6.96 and 1.05 µM for PSC, Panc-1 and 3D organoids respectively), therefore being the most potent of the novel sixteen substances (Pflieger 2020; Alves Avelar et al. 2021).

4.6.2 Colony Formation Assay (Panc-1)

The colony formation assay, or clonogenic assay, was conducted to further examine the cytotoxic and anti-proliferative properties of potent HDAC inhibitors. KSK64, MPK264 and MPK544 were chosen to be evaluated via this procedure, with the HDAC6i tubastatin A and the highly efficacious pan-HDACi vorinostat/SAHA serving as the respective negative and positive control. Following initial testing and protocol optimization, based on the assay

procedure described in Chen et al. (2019), 1,000 Panc-1 cells per well were seeded on 6-well tissue-culture plates and treated with the substances at concentrations of 100, 250 and 500 nM after 24 hours of initial cultivation. Incubation lasted for ten days in total, followed by crystal violet staining and counting of colonies. The assay results are presented and described in Figure 38 below.

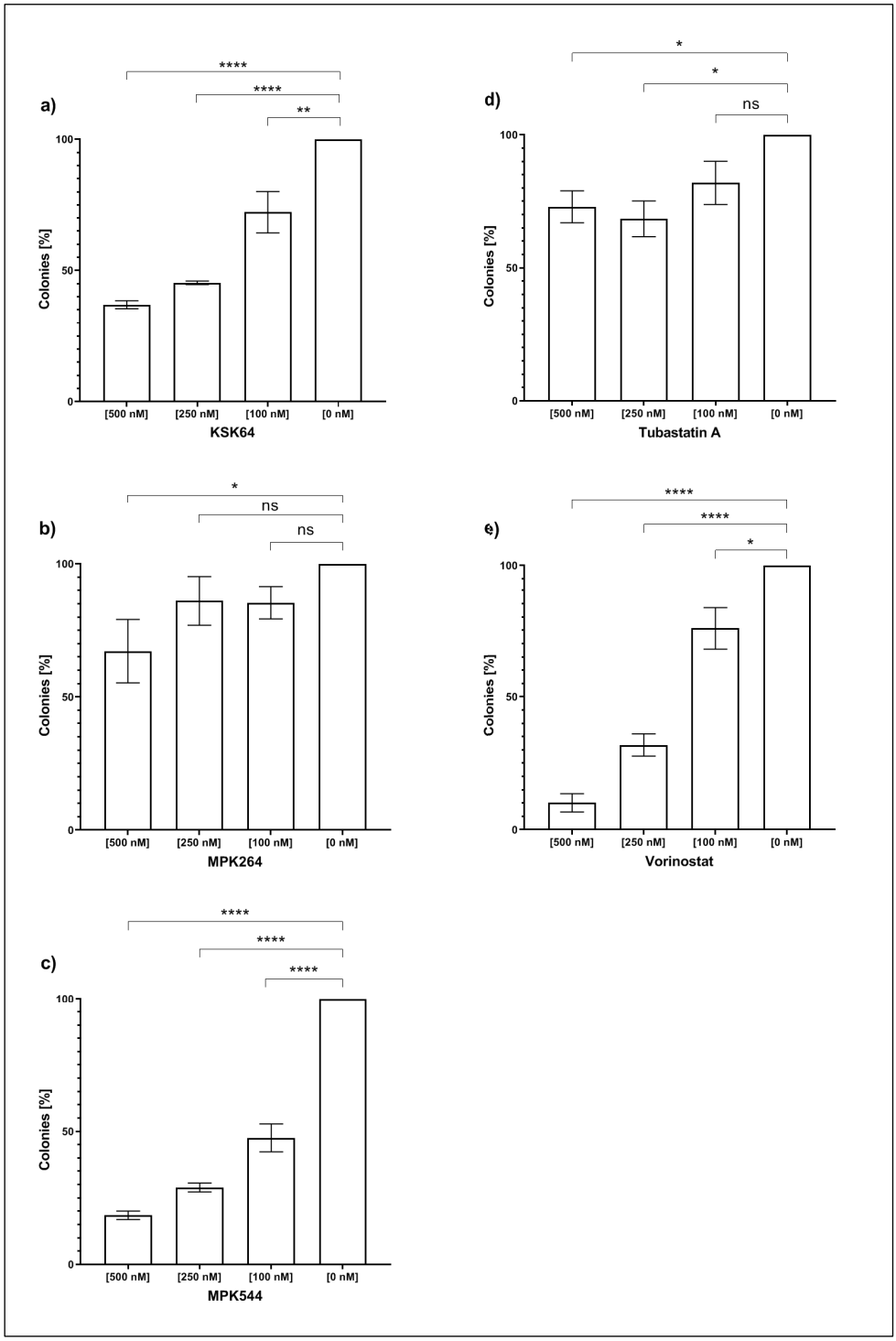

Figure 38. Colony formation of Panc-1 cells over 10 days of treatment with HDAC inhibitors. A) assay results for HDACi KSK64; b) assay results for MPK264; c) assay results for MPK544; d) assay results for the established HDAC6 inhibitor tubastatin A; e) assay results for the established pan-HDAC

inhibitor vorinostat (SAHA). Colony growth was normalized [%] and compared via one-way ANOVA (Dunnett's multiple comparison test). The depicted columns represent the arithmetic means of three to four experimental repeats and their respective standard errors of the mean. Ns: not significant; *: p<0.1; **: p<;0.001; ****: p<0.0001.

Treatment of Panc-1 cells with the negative control tubastatin A, an established inhibitor of the enzyme HDAC6 (Gradilone et al. 2013), only resulted in slight decrease of formed colonies after 10 days of incubation, whereas colony formation was significantly decreased under treatment with the pan-HDAC inhibitor vorinostat/SAHA, at both 250 and 500 nM of substance concentration. Of the three tested novel HDAC inhibitors, MPK264 proved to be the least effective and only significantly decreased colony formation at a concentration of 500 nM. KSK64 and MPK544 exhibited the highest potential, with MPK544 showcasing the strongest effects at all measured concentrations, comparable to the results gained with vorinostat/SAHA. The colony formation assay data matched the cytotoxicity assay results and proved the potency and efficacy of vorinostat, KSK64 and MPK544, as well as the lower efficacy of MPK264 and tubastatin A.

4.6.3 Western Blotting

The potent HDAC2/6 inhibitor MPK544 (see experimental results above) was chosen for further experimental evaluation via western blotting and RT-qPCR (see section 4.6.4 below), to evaluate its effect on the expression of the epithelial marker protein E-cadherin (Tsuchiya et al. 2006), which is downregulated in pancreatic ductal adenocarcinoma (Wang et al. 2018), and to test the hypothesis that treatment with HDAC inhibitors induces reversal of epithelial-mesenchymal transition (EMT) in pancreatic cancer cells (Ropero and Esteller 2007; Polireddy et al. 2016; Mishra et al. 2017; Loh et al. 2019). The pancreatic cancer cell line Panc-1 was utilized and seeded in an amount of $3*10^5$ cells per well on 6-well plates and treated with MPK544 after six hours of initial incubation, at concentrations of 1, 4 and 7 µM. Substance treatment lasted for 24 hours, after which the Panc-1 cells were harvested and lysed to conduct SDS-PAGE and western blotting. The essential housekeeping protein glyceraldehyde 3-phosphate dehydrogenase (GAPDH) was chosen and used as the necessary loading control for the blotting procedure (Zhang et al. 2015; Silver et al. 2006). Initial western blotting results for E-cadherin (CDH1) were first achieved with the housekeeping protein beta-actin (Thellin et al. 1999), but exhibited reduced reproducibility and are therefore not included in this thesis. As depicted in Figure 39 below, protein expression of E-cadherin (CDH1) was significantly upregulated in Panc-1 cells treated with 7 µM MPK544, while only non-significant upregulation was measured in Panc-1 cells treated with 1 and 4 µM MPK544.

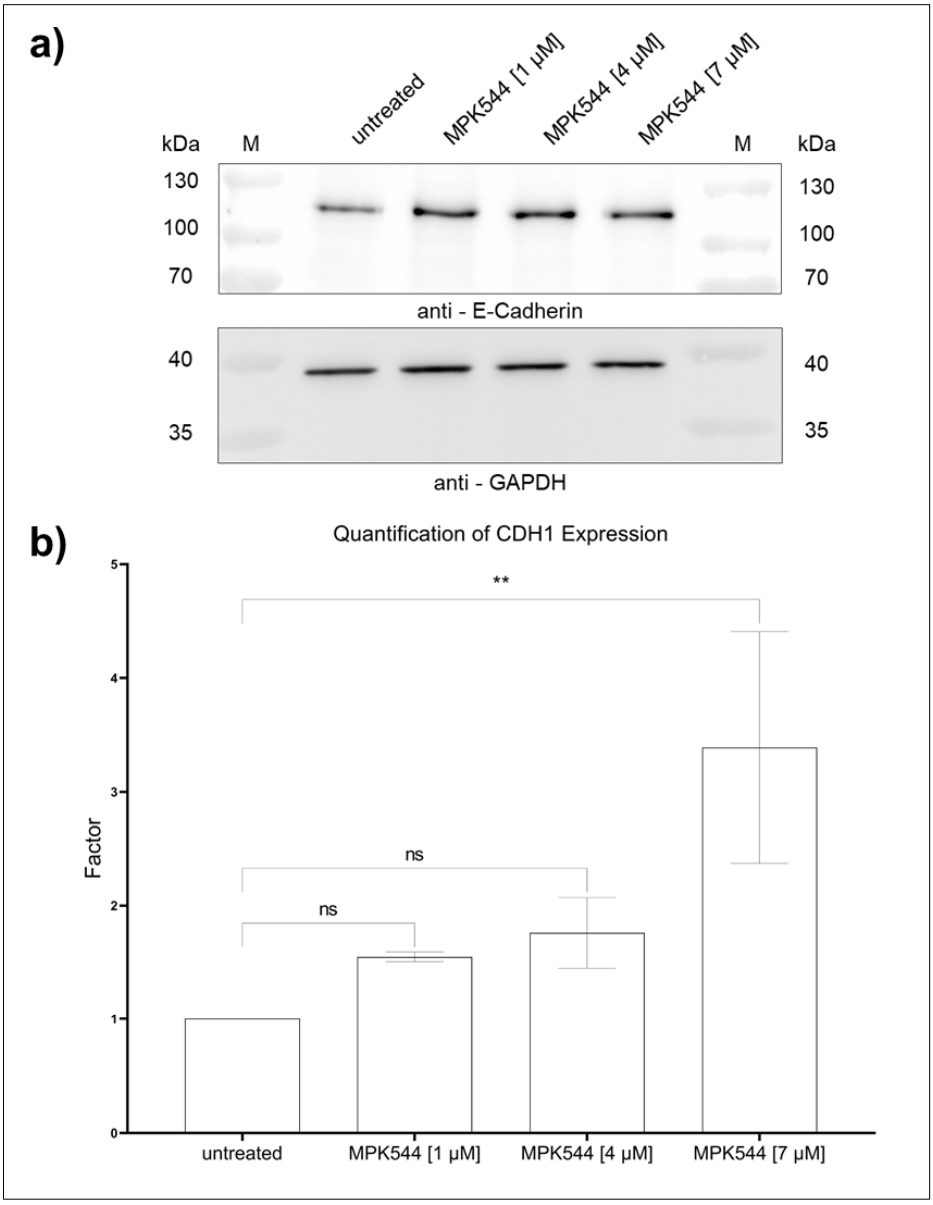

Figure 39. Upregulation of the epithelial marker protein E-cadherin (CDH1) in Panc-1 cells following treatment with the novel HDAC inhibitor MPK544. Substance treatment lasted for 24 hours. A) exemplary western blot (upper blot: CDH1; lower blot: GAPDH serving as the loading control); b) quantification of protein expression. Y-axis: factor of protein expression (normalized against the untreated control). Statistical analysis of CDH1 protein expression conducted via one-way ANOVA. The depicted columns represent the arithmetic means of three experimental repeats and their respective standard errors of the mean. Ns: non-significant; **: $p<0.01$. Prior initial results were first published in the master thesis of D. Janßen (Janßen 2021).

A control western blotting approach with gemcitabine (GEM), paclitaxel (taxol) and tubastatin A (TubaA), compared to the pan-HDAC inhibitor vorinostat (SAHA) and the potent HDAC inhibitor KSK64 was conducted as well and revealed that the protein expression of E-cadherin (CDH1) was not significantly upregulated under treatment with 1 µM gemcitabine and 5 nM paclitaxel. Treatment with 10 µM tubastatin A resulted in the upregulation of E-cadherin

(CDH1), but significantly lower compared to treatment with 1 µM KSK64 and 3 µM vorinostat (SAHA), verifying that upregulation of CDH1 in the PDAC cell line Panc-1 is specific for HDACi incubation.

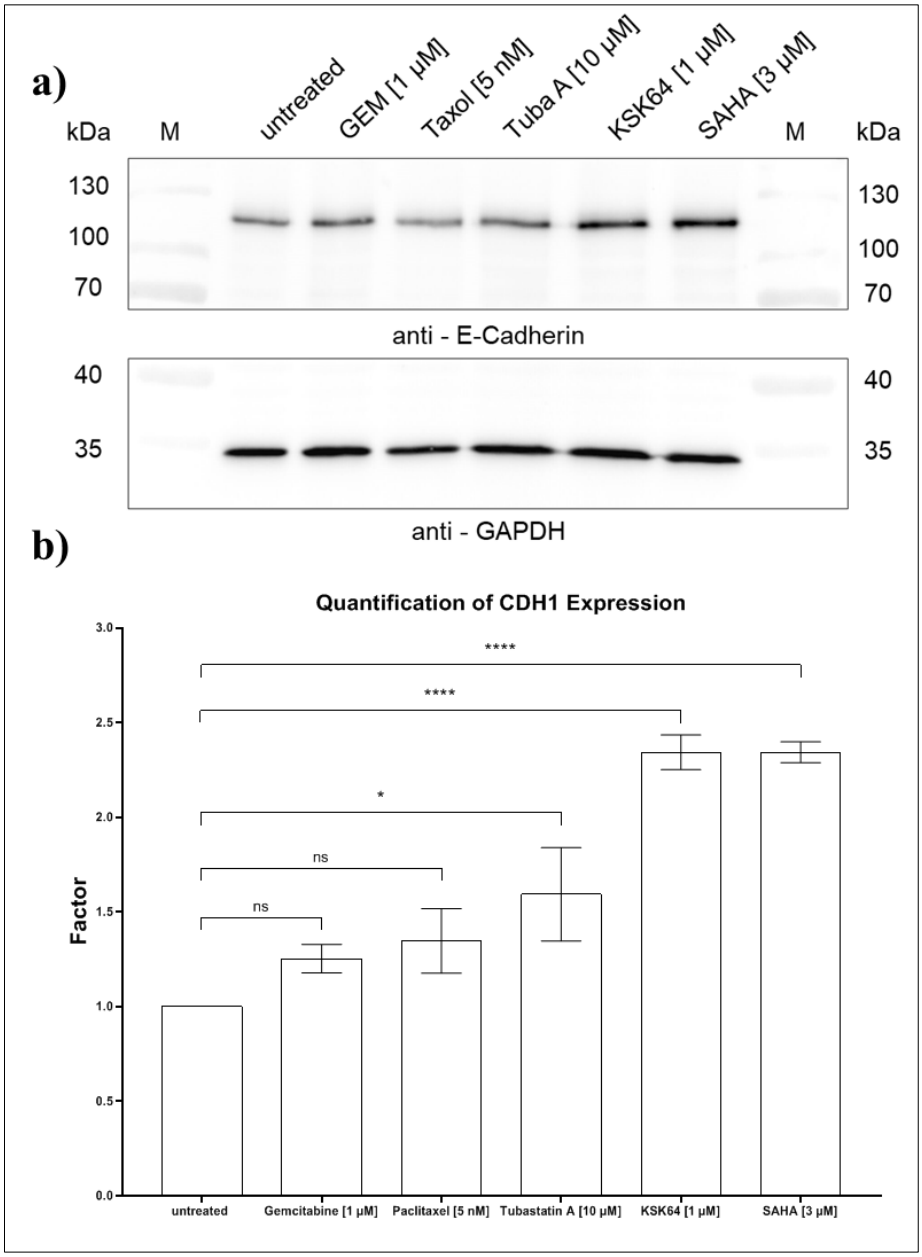

Figure 40. Upregulation of the epithelial marker protein E-cadherin (CDH1) in Panc-1 cells following treatment with established chemotherapeutic agents (gemcitabine, paclitaxel), HDAC inhibitors (tubastatin A, vorinostat) and the novel substance KSK64. Substance treatment lasted for 24 hours. A) exemplary western blot (upper blot: CDH1; lower blot: GAPDH serving as the loading control); b) quantification of protein expression. Y-axis: factor of protein expression (normalized against the untreated control). Statistical analysis of CDH1 protein expression conducted via one-way ANOVA. The depicted columns represent the arithmetic means of three experimental repeats and their respective standard errors of the mean. Ns: non-significant; *: $p<0.1$; ****: $p<0.0001$. Prior initial results were first published in the master thesis of D. Janßen (Janßen 2021).

The upregulation of the epithelial marker protein E-cadherin (CDH1) in the pancreatic cancer cell line Panc-1 via treatment with the HDAC inhibitor MPK544 and an incubation period of 24 hours could be proven, and was further examined utilizing RT-qPCR analysis (see below).

4.6.4 Real-time quantitative PCR (RT-qPCR)

RT-qPCR analysis was conducted and performed as described in method section 3.3.3.4 above. Following initial protocol optimization, a total of $1*10^6$ Panc-1 cells were seeded in 6 cm x 1.5 cm tissue-culture dishes and subjected to 24 hours of substance treatment before cells were harvested and lysed. Isolation of RNA and RT-qPCR was conducted as described and detailed in the respective kit protocols.

As presented in the western blotting results obtained from Panc-1 (see section 4.6.3 above), the protein expression of E-cadherin (CDH1) could be upregulated via treatment with the novel HDAC2/6 inhibitor MPK544 after 24 hours of incubation. This finding was further verified and substantiated in the RT-qPCR analysis, as the upregulation of E-cadherin mRNA transcription in Panc-1 cells, following treatment with 1 and 4 µM MPK544,could be demonstrated likewise (see Figure 41 below), as well as the downregulation of the mesenchymal protein vimentin (VIM), another tumour marker associated with poor survival (Maehira et al. 2019), indicating that the process of epithelial-mesenchymal transition (EMT) can indeed be partially reversed via medical treatment with drugs and substances exhibiting inhibitory activity against histone deacetylase proteins. MPK544, which showcased high cytotoxic efficacy (see results above), might emerge as a potential new chemotherapeutic agent effective against pancreatic cancer and pancreatic ductal adenocarcinoma.

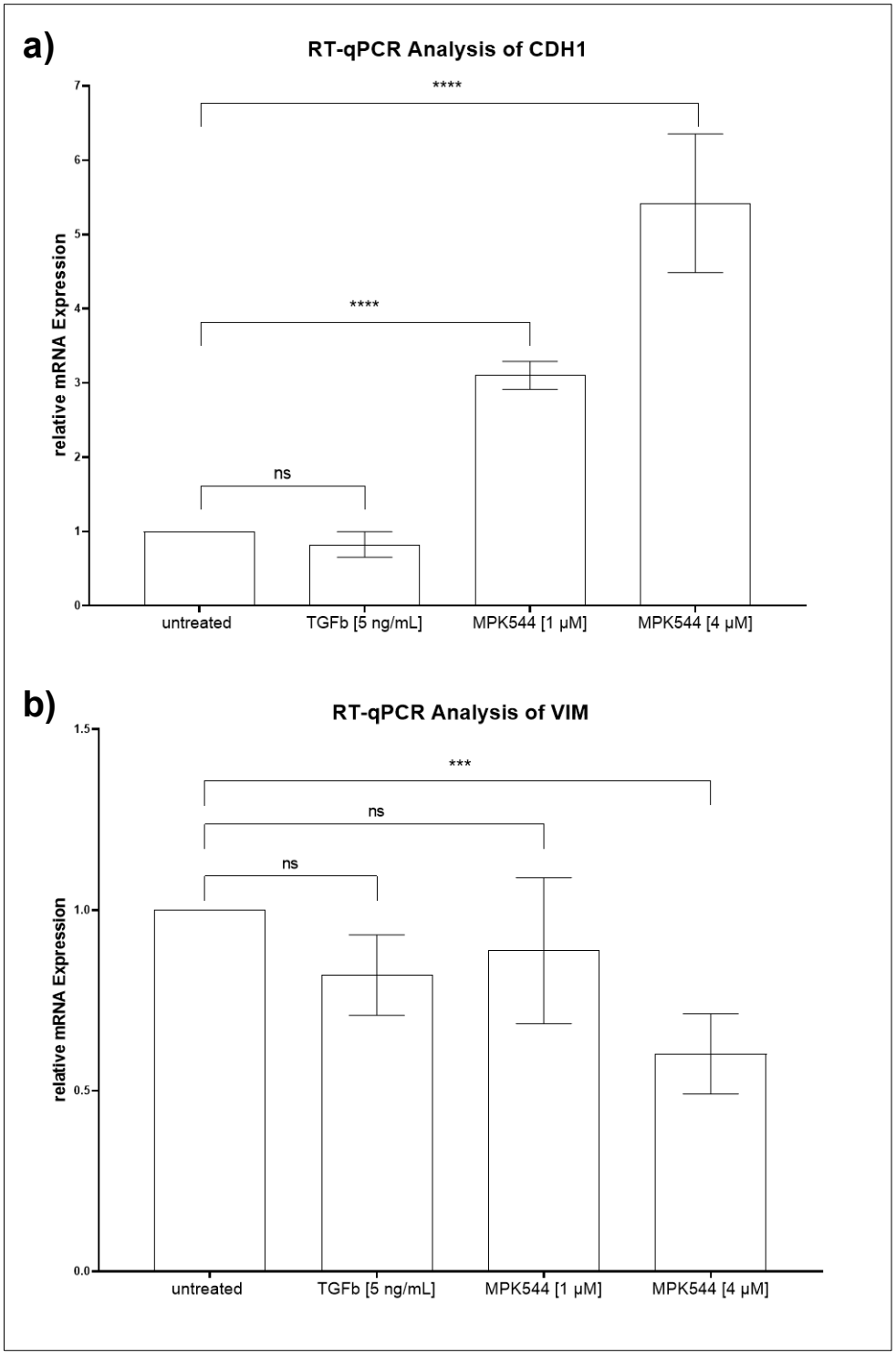

Figure 41. Treatment of Panc-1 cells with the novel HDAC inhibitor MPK544 induced upregulation of CDH1 gene transcription and downregulation of vimentin (VIM) gene transcription. Panc-1 cells were treated with 1 and 4 µM of MPK544 and 5 ng/mL of TGFb. Levels of gene transcription were analysed via real-time quantitative polymerase chain reaction (RT-qPCR). A) upregulation of CDH1 transcription in Panc-1 cells; b) downregulation of vimentin gene transcription in Panc-1 cells. The arithmetic means of five experimental repeats and their respective standard errors of the mean are depicted. Statistical evaluation conducted via one-way ANOVA. Ns: non-significant; ***: p<0.001; ****: p<0.0001.

4.6.5 Quantification of Protein Expression in Three-Dimensional Organoids

On the basis of the protein expression results obtained from Panc-1 cells treated with HDAC inhibitors, specifically MPK544 (see results above), we attempted to establish and optimize an experimental protocol to quantify and analyse the expression of the epithelial marker protein E-cadherin (CDH1) in three-dimensional (3D) co-culture organoids (Panc-1 + PSC) subjected to treatment with HDAC inhibitors. As MPK544 induced the upregulation of CDH1 protein expression in the two-dimensional (2D) Panc-1 cell culture model, it was theorized that a similar effect could be observed and verified in the 3D organoid model, further validating and substantiating the efficacy of MPK544. Initial quantification results prior to the optimization of the protocol, which is described in method section 3.3.4.6 and was applied in the experiments documented further below, were published in the master thesis of D. Janßen (Janßen 2021) and served as the first trial experiments, which are not included in this thesis.

The Panc-1 + KU0020 PSC organoids were cultivated and grown according to custom, and subjected to substance treatment on day 6 (120 hours after seeding). Incubation lasted for either 24 or 72 hours, after which the organoids were fixated, stained with primary antibodies targeting proteins of interests and fluorescent secondary antibodies, as well as with the nuclear stain DAPI, cleared and recorded via spinning disc confocal microscopy, followed by analysis with the CellPathfinder software (see method section 3.3.4.6). The obtained data was then normalized and visualized with the GraphPad Prism 8 software. Below, several exemplary images (Figures 42 to 49) of Panc-1 + KU0020 PSC organoids, recorded via spinning disc confocal microscopy, are depicted to exemplify the practical process of the experimental setup and to visualize the diverse shapes and forms of the examined 3D co-culture models.

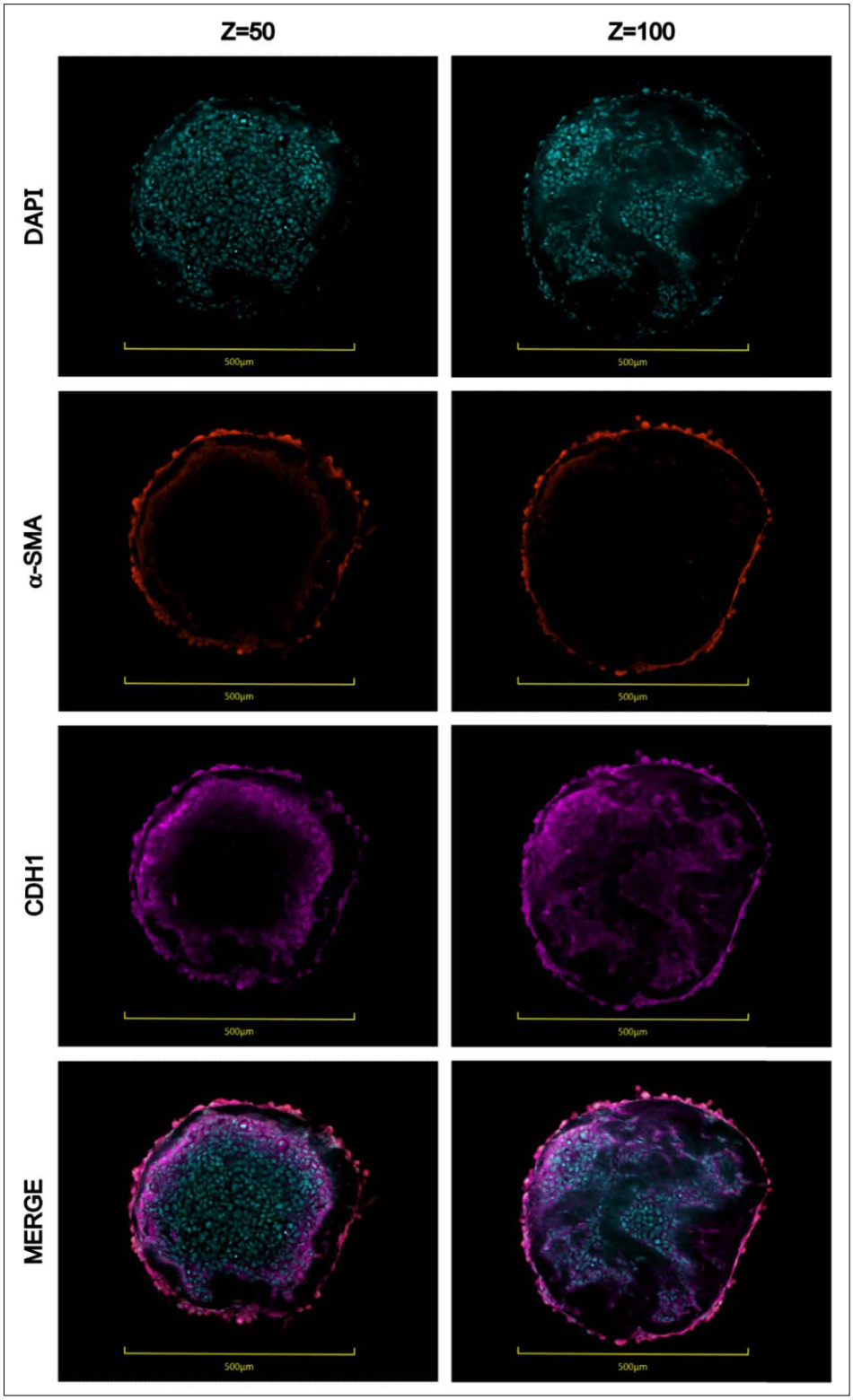

Figure 42. Exemplary spinning disc confocal microscopy images of an IF-stained Panc-1 + PSC organoid. Left: Z-slice at 50 µm height; right; Z-slice at 100 µm height. From top to bottom: 1) DAPI-staining of nuclei (405 nm channel); 2) ACTA2-staining with fluorescent antibodies (561 nm channel); 3) E-cadherin-staining with fluorescent antibodies (640 nm channel); 4) merging of all three channels. Magnification: 20x. Reference scales: 500 µm. Images recorded via the CQ1 Confocal Imaging Cytometer (Yokogawa Electric Corporation) and edited with the CellPathfinder software (Yokogawa).

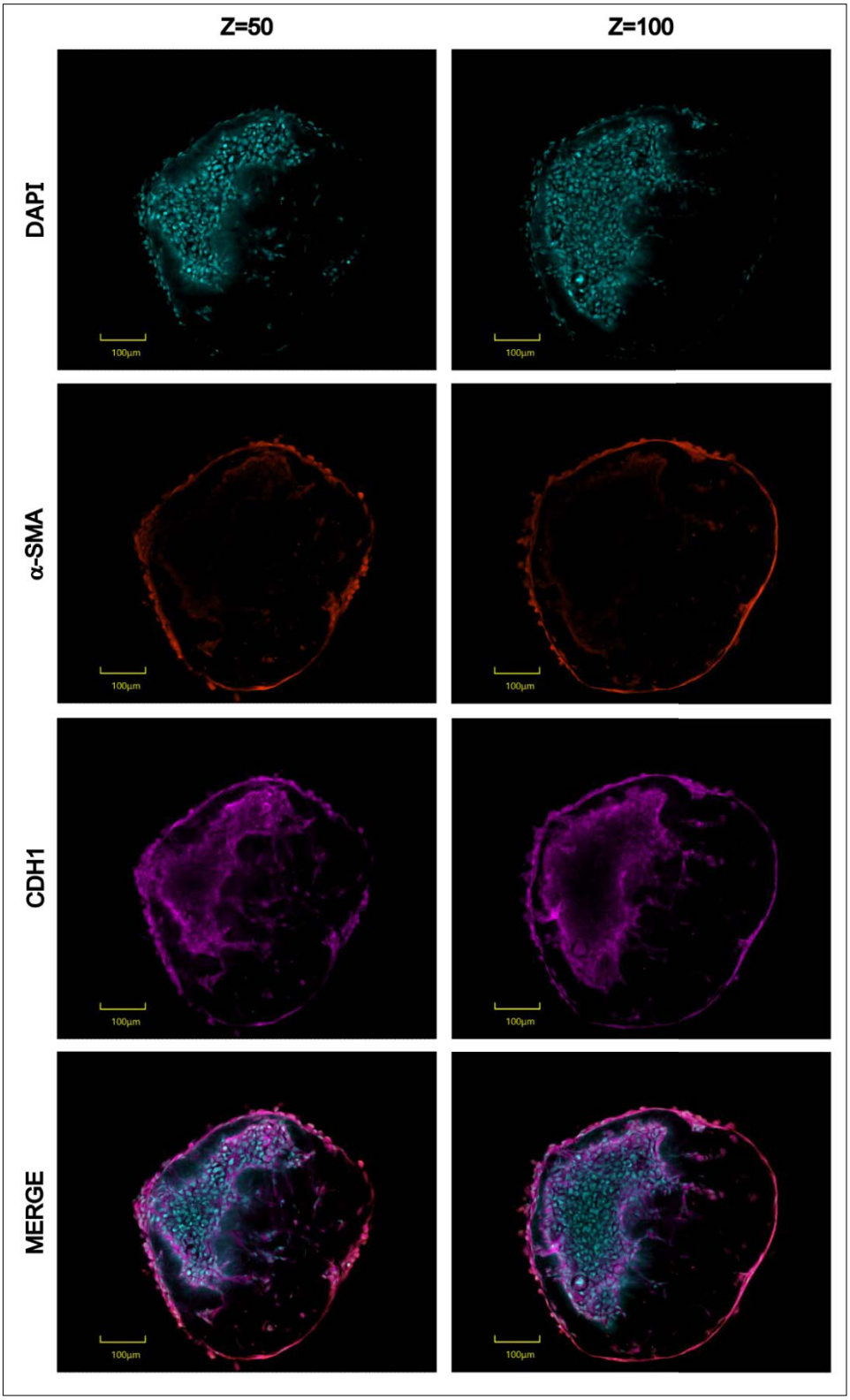

Figure 43. Exemplary spinning disc confocal microscopy images of an IF-stained Panc-1 + PSC organoid. Left: Z-slice at 50 µm height; right; Z-slice at 100 µm height. From top to bottom: 1) DAPI-staining of nuclei (405 nm channel); 2) ACTA2-staining with fluorescent antibodies (561 nm channel); 3) E-cadherin-staining with fluorescent antibodies (640 nm channel); 4) merging of all three channels. Magnification: 20x. Reference scales: 100 µm. Images recorded via the CQ1 Confocal Imaging Cytometer (Yokogawa Electric Corporation) and edited with the CellPathfinder software (Yokogawa).

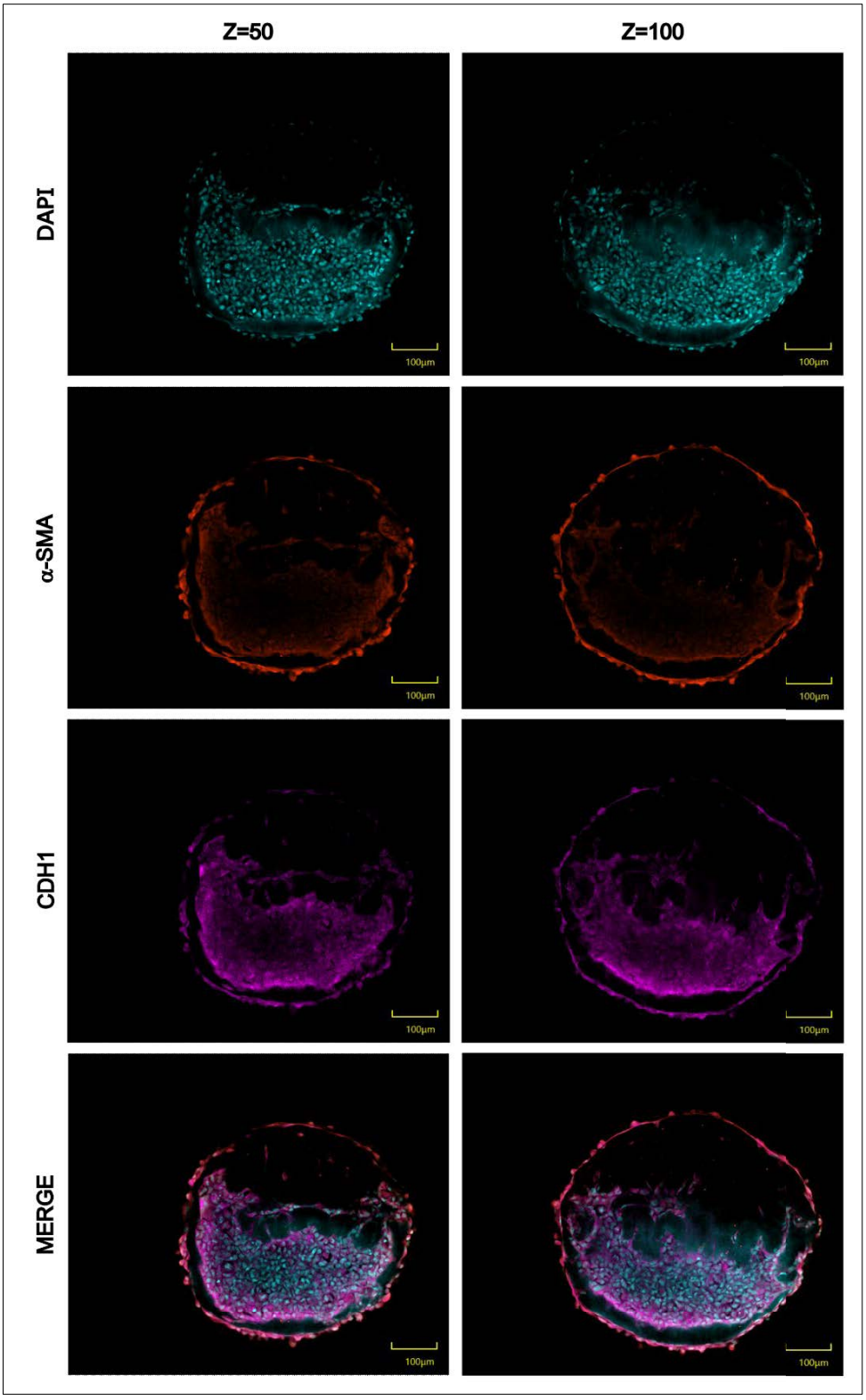

Figure 44. Exemplary spinning disc confocal microscopy images of an IF-stained Panc-1 + PSC organoid. Left: Z-slice at 50 µm height; right; Z-slice at 100 µm height. From top to bottom: 1) DAPI-staining of nuclei (405 nm channel); 2) ACTA2-staining with fluorescent antibodies (561 nm channel); 3) E-cadherin-staining with fluorescent antibodies (640 nm channel); 4) merging of all three channels. Magnification: 20x. Reference scales: 100 µm. Images recorded via the CQ1 Confocal Imaging Cytometer (Yokogawa Electric Corporation) and edited with the CellPathfinder software (Yokogawa).

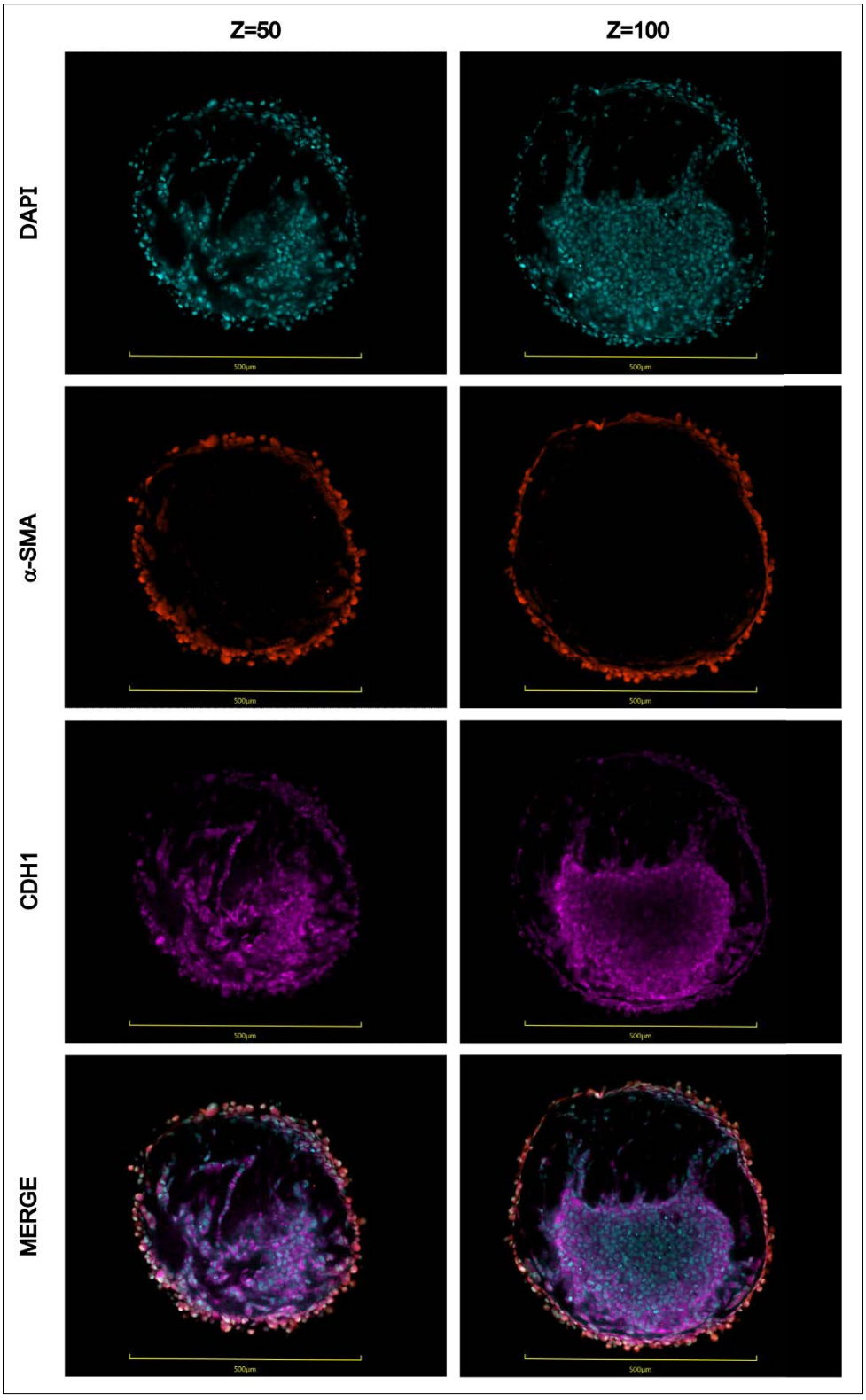

Figure 45. Exemplary spinning disc confocal microscopy images of an IF-stained Panc-1 + PSC organoid. Left: Z-slice at 50 µm height; right; Z-slice at 100 µm height. From top to bottom: 1) DAPI-staining of nuclei (405 nm channel); 2) ACTA2-staining with fluorescent antibodies (561 nm channel); 3) E-cadherin-staining with fluorescent antibodies (640 nm channel); 4) merging of all three channels. Magnification: 20x. Reference scales: 500 µm. Images recorded via the CQ1 Confocal Imaging Cytometer (Yokogawa Electric Corporation) and edited with the CellPathfinder software (Yokogawa).

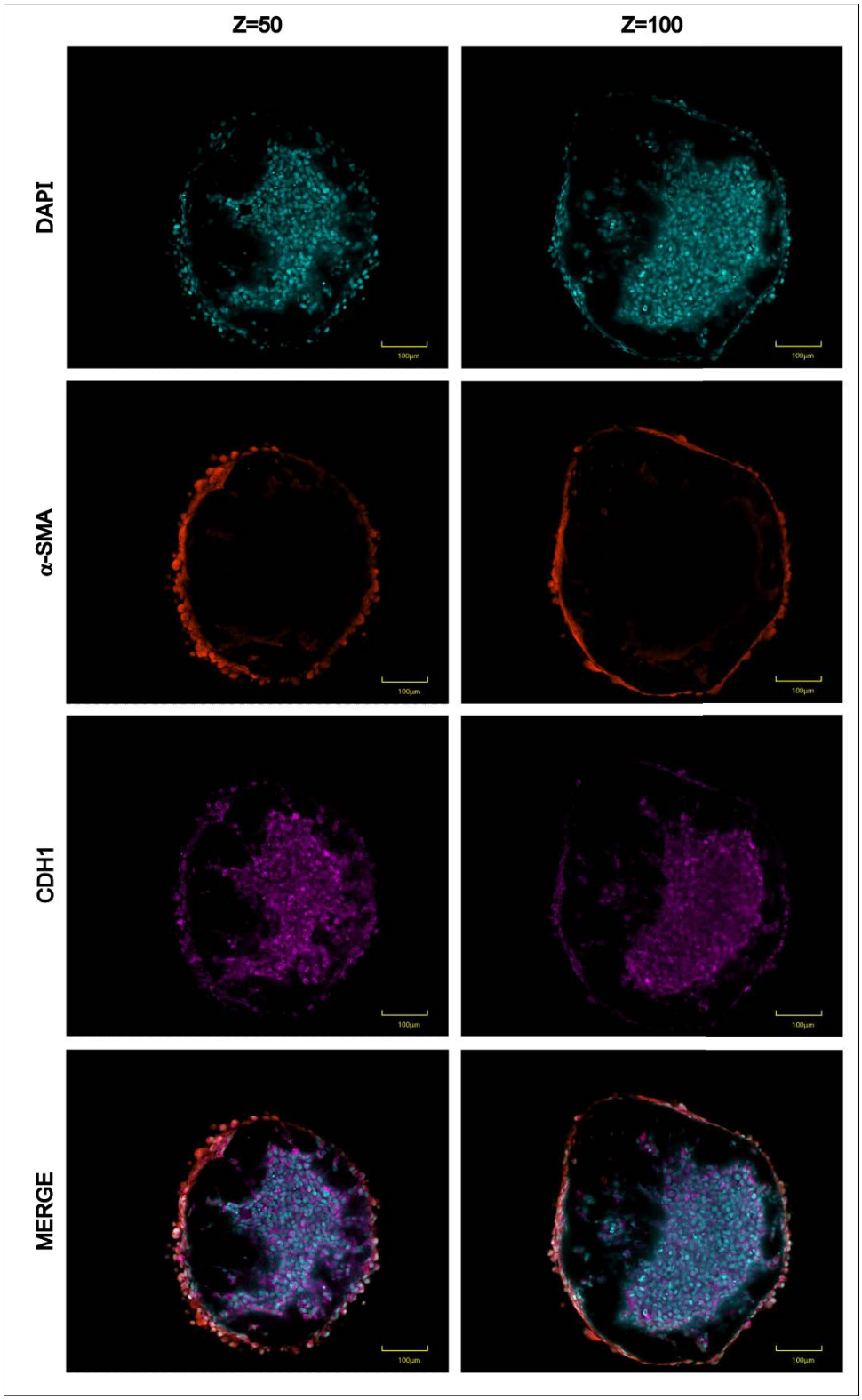

Figure 46. Exemplary spinning disc confocal microscopy images of an IF-stained Panc-1 + PSC organoid. Left: Z-slice at 50 µm height; right; Z-slice at 100 µm height. From top to bottom: 1) DAPI-staining of nuclei (405 nm channel); 2) ACTA2-staining with fluorescent antibodies (561 nm channel); 3) E-cadherin-staining with fluorescent antibodies (640 nm channel); 4) merging of all three channels. Magnification: 20x. Reference scales: 100 µm. Images recorded via the CQ1 Confocal Imaging Cytometer (Yokogawa Electric Corporation) and edited with the CellPathfinder software (Yokogawa).

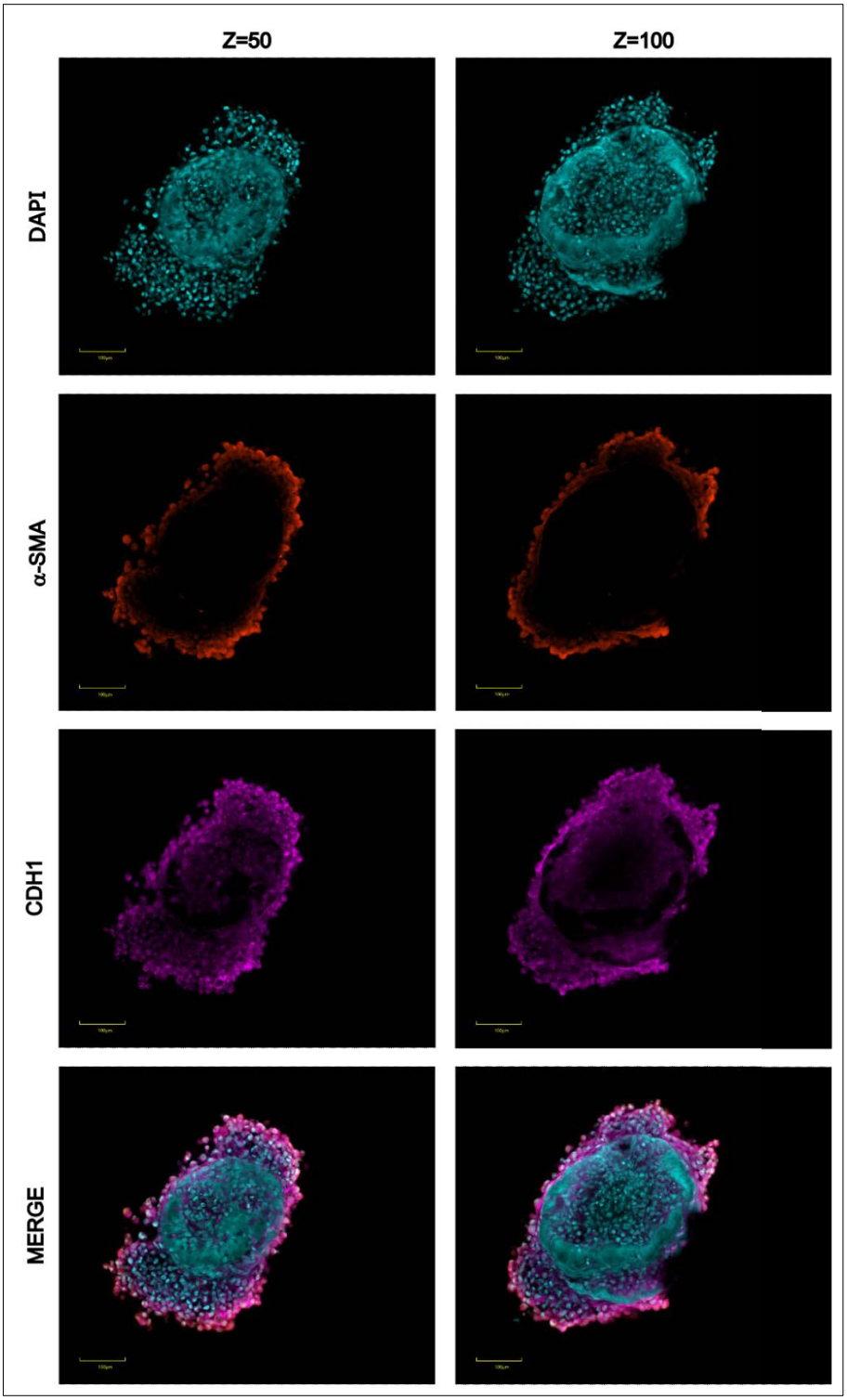

Figure 47. Exemplary spinning disc confocal microscopy images of an irregularly formed, IF-stained Panc-1 + PSC organoid. Left: Z-slice at 50 µm height; right; Z-slice at 100 µm height. From top to bottom: 1) DAPI-staining of nuclei (405 nm channel); 2) ACTA2-staining with fluorescent antibodies (561 nm channel); 3) E-cadherin-staining with fluorescent antibodies (640 nm channel); 4) merging of all three channels. Magnification: 20x. Reference scales: 100 µm. Images recorded via the CQ1 Confocal Imaging Cytometer (Yokogawa Electric Corporation) and edited with the CellPathfinder software (Yokogawa).

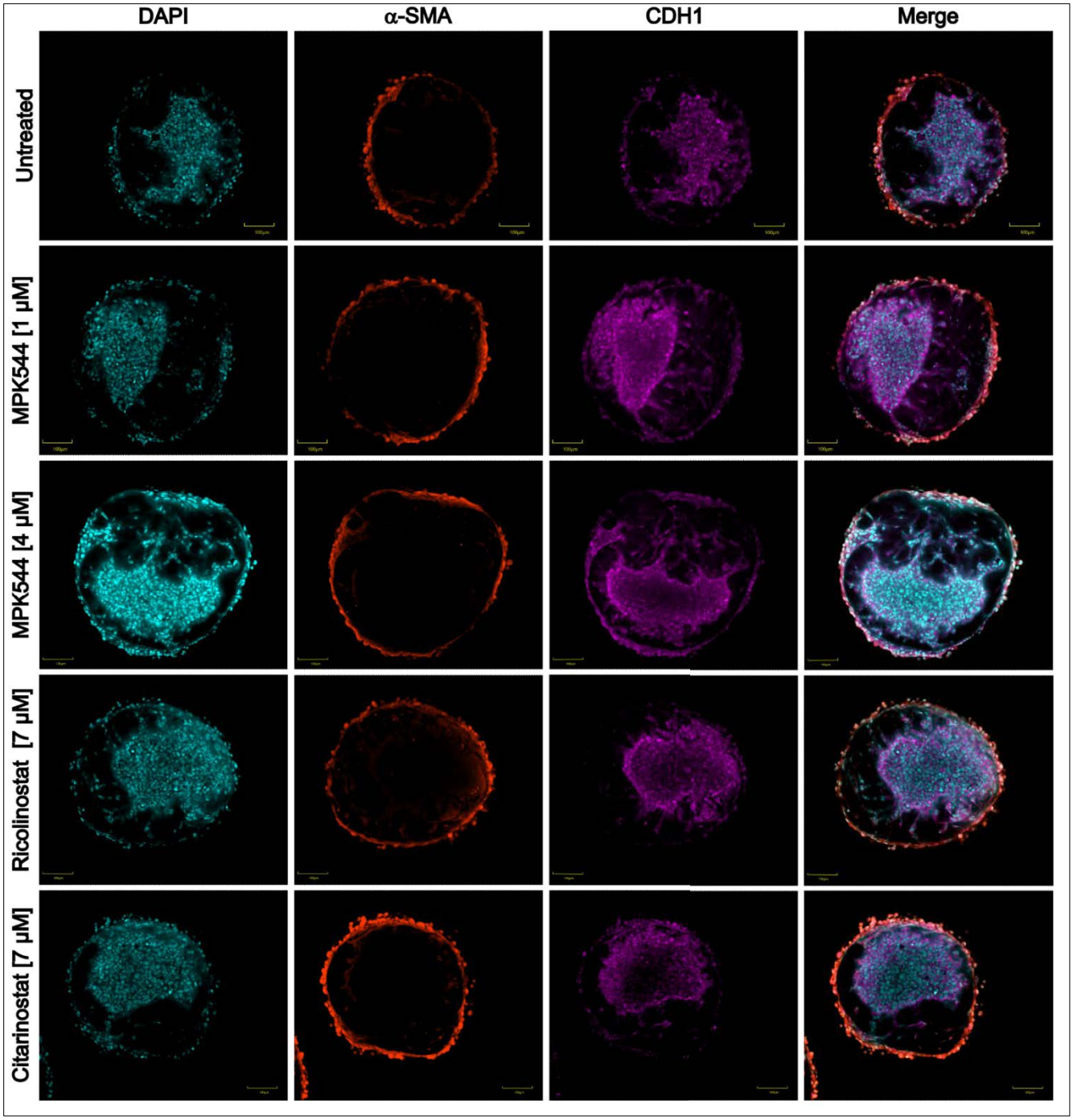

Figure 48. Exemplary spinning disc confocal microscopy images of several Panc-1 + PSC organoids. Treatment with different HDAC inhibitors for 24 hours. Staining from left to right: 1) DAPI-staining of nuclei (405 nm channel); 2) ACTA2-staining with fluorescent antibodies (561 nm channel); 3) E-cadherin-staining with fluorescent antibodies (640 nm channel); 4) merging of all three channels. From top to bottom (organoids): 1) untreated organoid; 2) organoid treated with 1 µM MPK544; 3) organoid treated with 4 µM MPK544; 4) organoid treated with the HDAC6 inhibitor ricolinostat (7 µM); 5) organoid treated with the HDAC6 inhibitor citarinostat (7 µM).Magnification: 20x. Reference scales: 100 µm. Images recorded via the CQ1 Confocal Imaging Cytometer (Yokogawa Electric Corporation) and edited with the CellPathfinder software (Yokogawa).

Organoids derived from Panc-1 and KU0020 PSC cells mainly featured a round and compact shape, but could also exhibit irregular forms and internal cellular makeup, as shown in the exemplary images and collages above. Only correctly formed and spherical organoids were chosen and used for the quantification of the fluorescence signal corresponding to the CDH1-antibody, in order to analyse the levels of protein expression under different treatments and concentrations of HDAC inhibitors. Figure 49 below recaps this process, as detailed and described in method section 3.3.4.6.

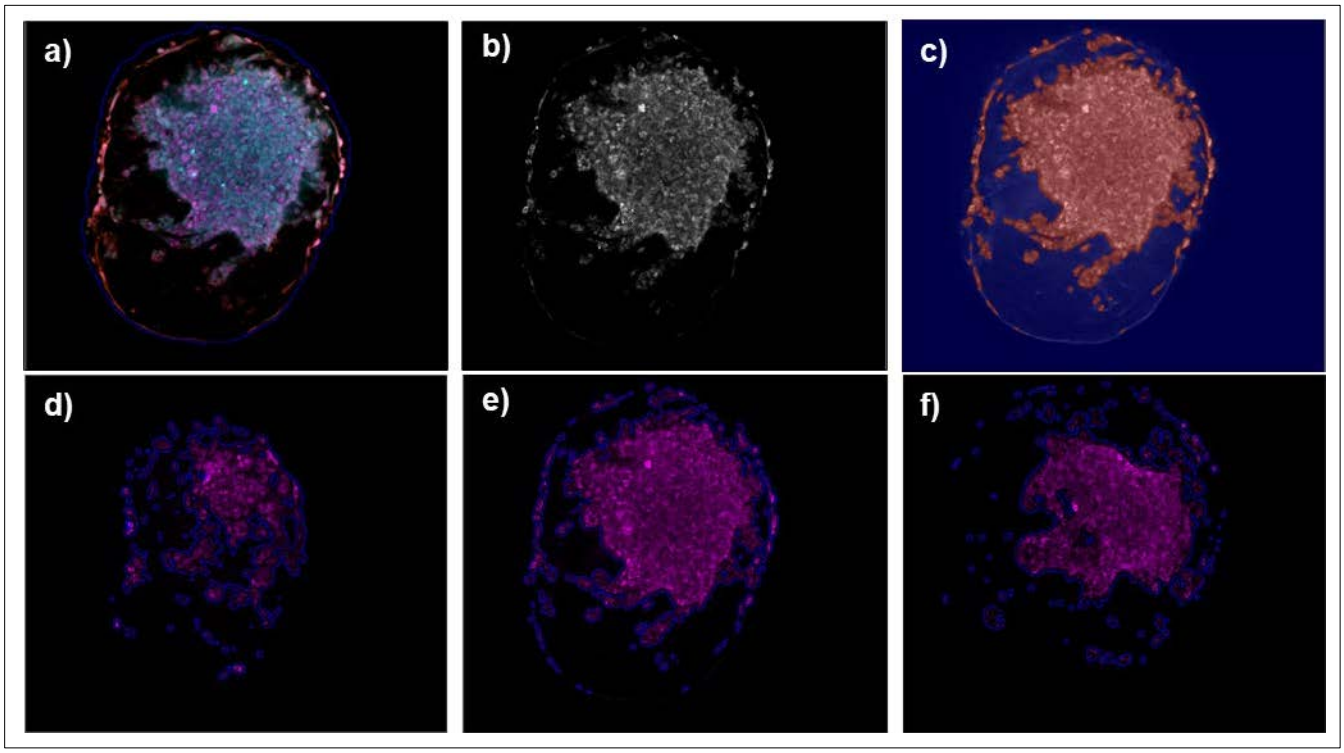

Figure 49. Quantification of fluorescence signals recorded by the CQ1 Confocal Imaging Cytometer (Yokogawa Electric Corporation) via the CellPathfinder software (Yokogawa). A) merged image of three channels (blue: DAPI; red: ACTA2; purple: E-cadherin), with the outlined organoid shape (blue); b) fluorescence signal representing the protein expression of E-cadherin (CDH1); c) signal identification via a machine learning-assisted approach; d) - f) quantification of CDH1 protein expression (640 nm channel) of three different Z-slices. Pictures a), b), c) and e) depict the same Z-slice.

Visual differentiation of CDH1 protein expression was not possible and feasible (see recorded spinning disc confocal microscopy images above). Panc-1 + PSC organoids treated with MPK544 at a concentration of 1 µM (see Figure 50 below) exhibited a significant upregulation of CDH1 protein expression, but showcased no significant upregulation when treated with 4 µM MPK544, as well as with 7 µM of ricolinostat and citarinostat.

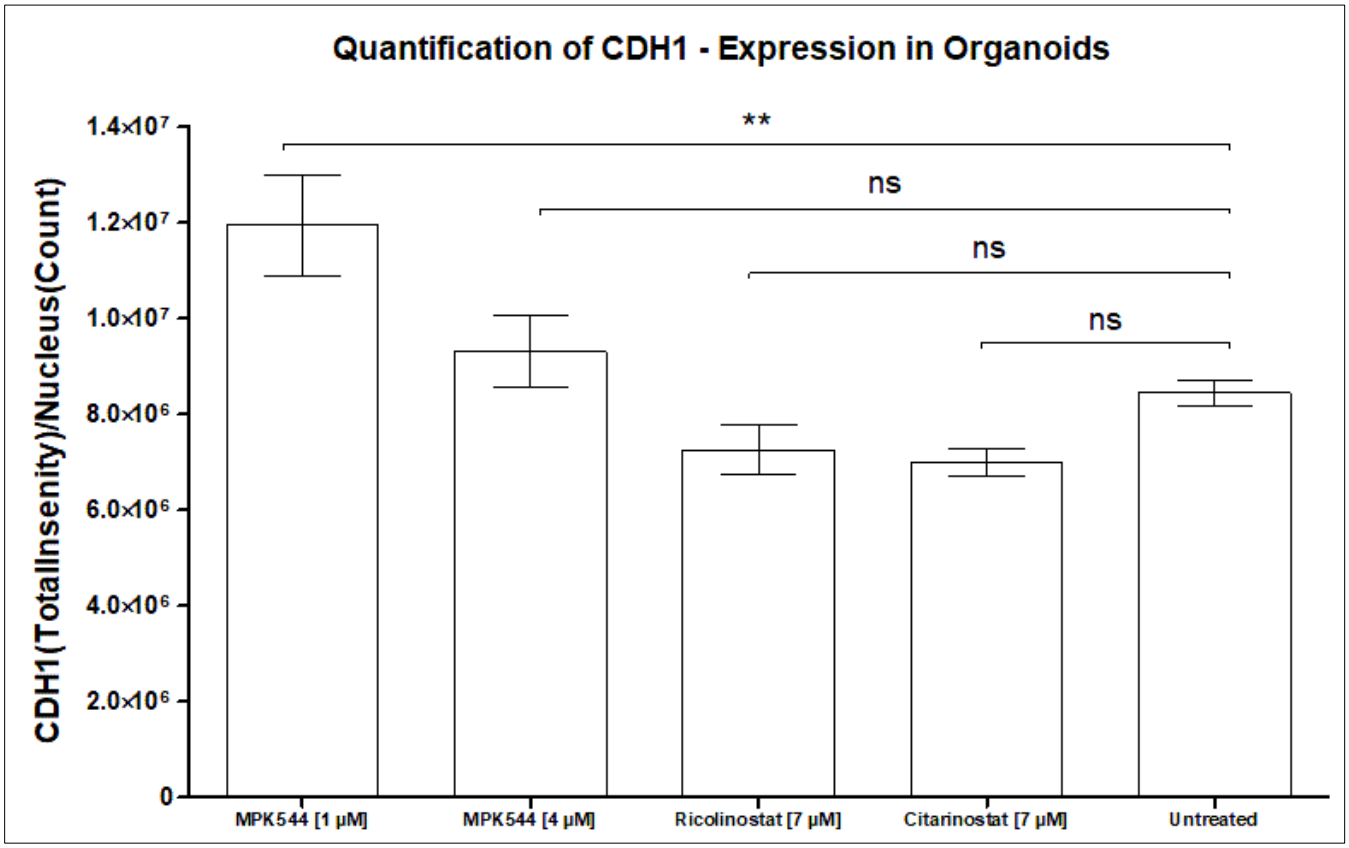

Figure 50. Quantification of the expression of the epithelial marker protein E-cadherin (CDH1) in organoids (Panc-1 + KU0020 PSC) via analysis with the CellPathfinder software (Yokogawa Electric Company). Organoid treatment (from left to right): MPK544 (1 µM), MPK544 (4 µM), ricolinostat (7 µM), citarinostat (7 µM), and untreated organoids. The y-axis represent the total intensity of the CDH1 signal, divided by the calculated number of the nuclei. Substance treatment lasted 24 hours. Columns depict the arithmetic means and their respective standard errors of the mean of three to four measured organoids. Ns: non-significant; **: $p<0.01$.

A control approach, where organoids were treated with 5 ng/mL TGF-beta for both 24 and 72 hours (after 6 days of cultivation) to induce epithelial-mesenchymal transition (EMT), showed that the protein expression of the epithelial marker protein E-cadherin (CDH1) could be downregulated in Panc-1 + PSC organoids as well, but only after 72 hours of incubation.

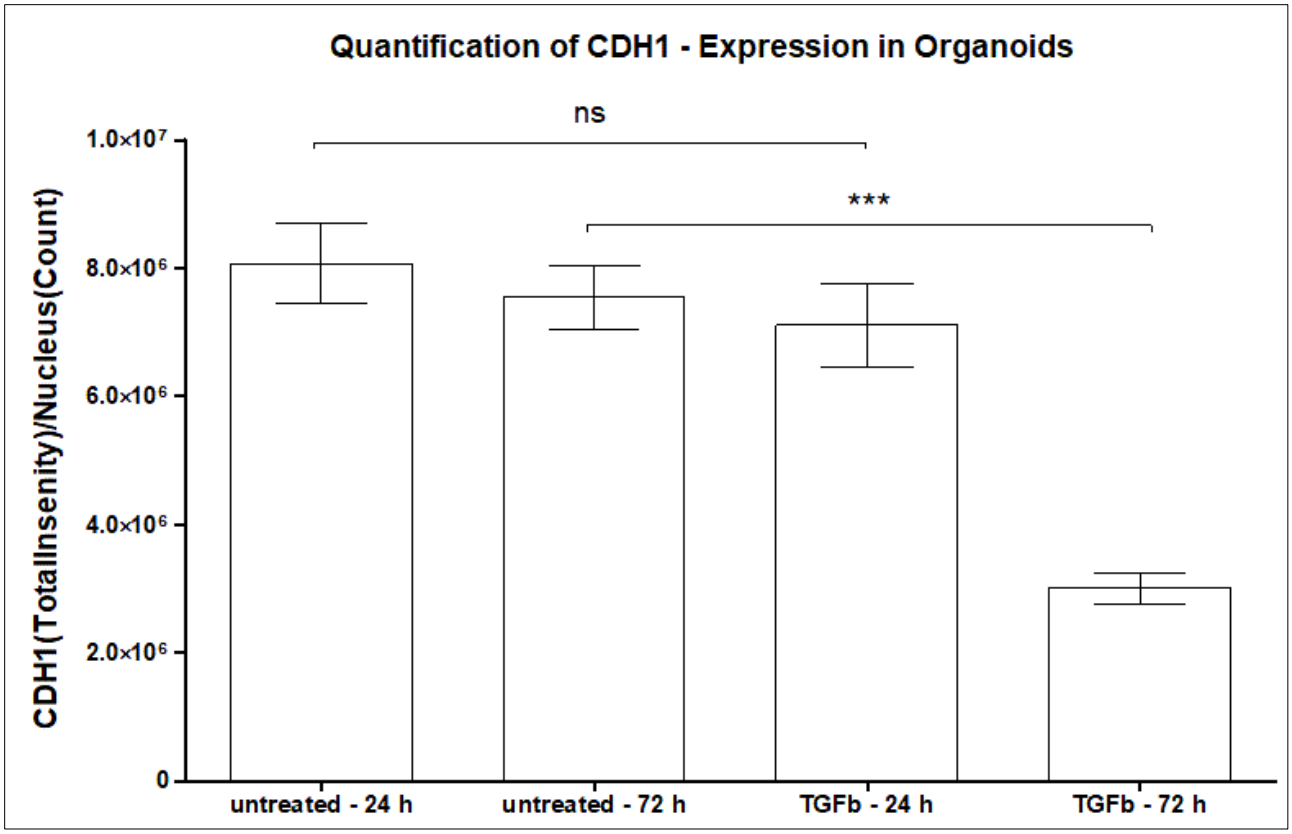

Figure 51. Quantification of the expression of the epithelial marker protein E-cadherin (CDH1) in organoids (Panc-1 + KU0020 PSC) via analysis with the CellPathfinder software (Yokogawa Electric Company). Organoid treatment (from left to right): untreated organoids (24 hours incubation); untreated organoids (72 hours incubation); 5 ng/mL TGF-beta (24 hours incubation; 5 ng/mL TGF-beta (72 hours incubation). Columns depict the arithmetic means and their respective standard errors of the mean of five measured organoids. Ns: non-significant; ***: $p<0.001$.

The quantification results further substantiate the efficacy and potency of the novel HDAC2/6 inhibitor MPK544, and the hypothesis that the process of epithelial-mesenchymal transition (EMT) can be reverted in pancreatic cancer (PC) cells via treatment with HDAC inhibitors. Due to several methodical complications and practical difficulties, which will be discussed and clarified in section 5.5 (see discussion below), further intensive experimental research and analysis regarding the internal composition of organoids (Panc-1 + KU0020 PSC), the biological interaction between the composing cells and the expression of E-cadherin and other associated proteins relevant to the process of EMT and mesenchymal-epithelial transition (MET) must be conducted to assess and evaluate the pharmacological effects of MPK544.

4.7 Cultivation of Panc-1 - derived Tumorspheres

Tumorspheres were cultivated and handled as specified in method section 3.3.5 above. Panc-1 cells were seeded in tissue culture flasks featuring ultra-low attachment (ULA) surfaces (Greiner Bio-One, Cat. #690985) and cultivated for two weeks, enzymatically isolated with Dispase II (Sigma Aldrich, Cat. #D4693) and transferred to 96-well ULA plates (Greiner Bio-One, Cat. #650970) for cytotoxic treatment and testing. Initial results obtained from Panc-1 - derived tumorspheres were first published in the master thesis of D. Janßen (Janßen 2021), and are not included in this thesis.

Panc-1 cells were observed to quickly form cohesive clusters in suspension culture conditions (see Figures 52 and 53), which aggravated and impeded the cultivation of Panc-1 - derived tumorspheres, and subsequently the seeding and execution of the cytotoxicity assay. To prevent this phenomenon, the treatment of cells with 0.2 µg/mL Dispase II every seven days of incubation was introduced, to ensure a continuous supply with fresh tumorsphere medium and supplements and to prevent the accumulation of cellular debris and clumps. With this approach, tumorspheres could be reliably cultivated and handled, and tumorsphere cells were used to further evaluate the cytotoxic properties of novel histone deacetylase inhibitors (HDACi).

Tumorspheres were dyed with the nuclear stain Hoechst 33342 (Latt et al. 1975; Chazotte 2011) and imaged via spinning disc confocal microscopy with the CQ1 Confocal Imaging Cytometer (Yokogawa Electric Company). Cytotoxic evaluation of novel substances was successfully achieved (see Table 20 below) and was conducted for novel HDAC inhibitors (see HDACi result section 4.6 above). The potent HDAC inhibitors KSK64 (IC_{50} on Panc-1: 7.04 µM), MPK264 (IC_{50} on Panc-1: 15.45 µM) and MPK544 (IC_{50} on Panc-1: 6.96 µM) were screened for their cytotoxicity, together with LAK61 (IC_{50} on Panc-1: 86.93 µM) serving as a negative control.

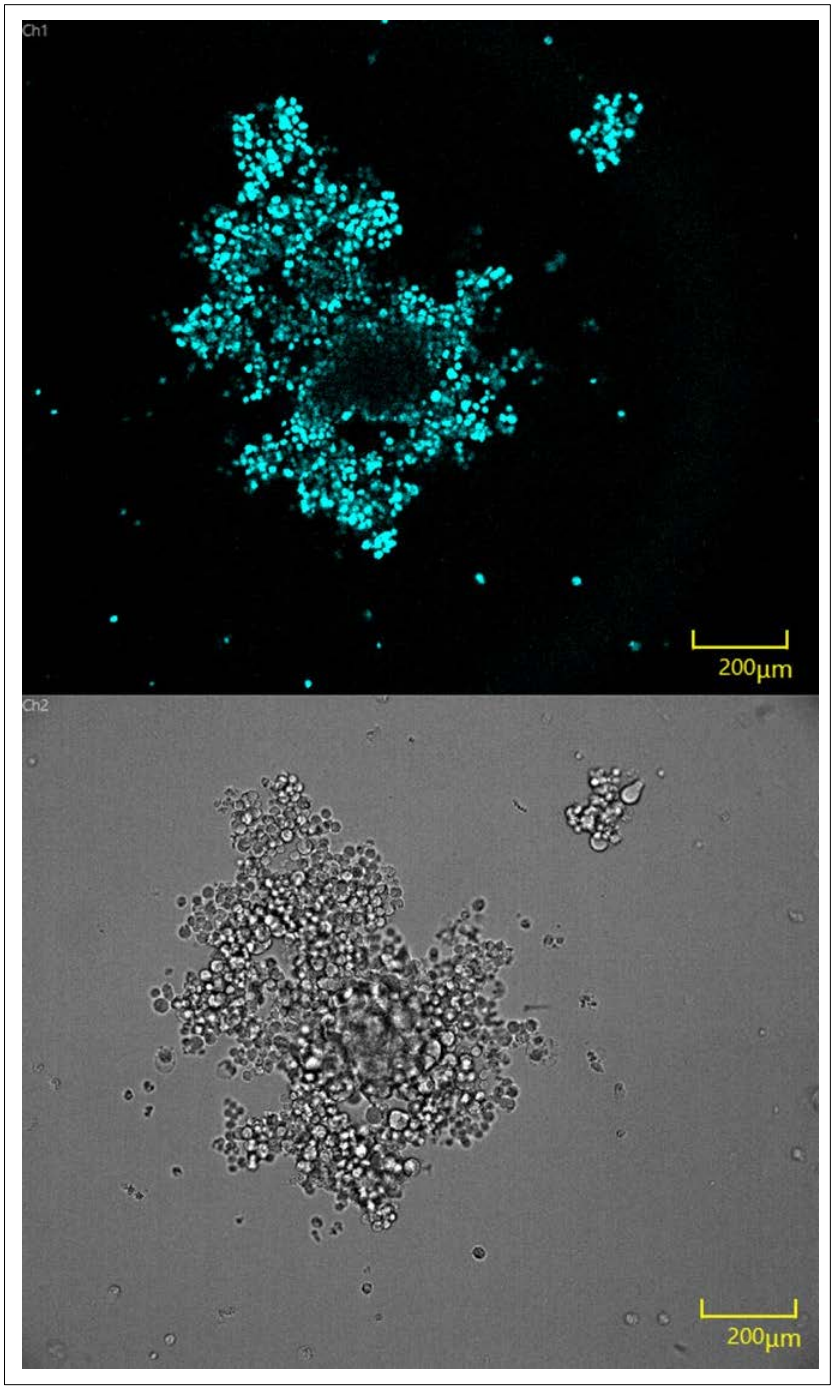

Figure 52. Nuclear staining of tumorsphere cells derived from Panc-1 (ATCC) with Hoechst 33342 (0.2 µg/mL). Top image: Hoechst staining (405 nm channel); bottom image: brightfield channel. Tumorspheres were incubated for 48 hours on 96-well ULA plates. Images were recorded with the CQ1 Confocal Imaging Cytometer (Yokogawa Electric Company). Reference scale: 200 µm.

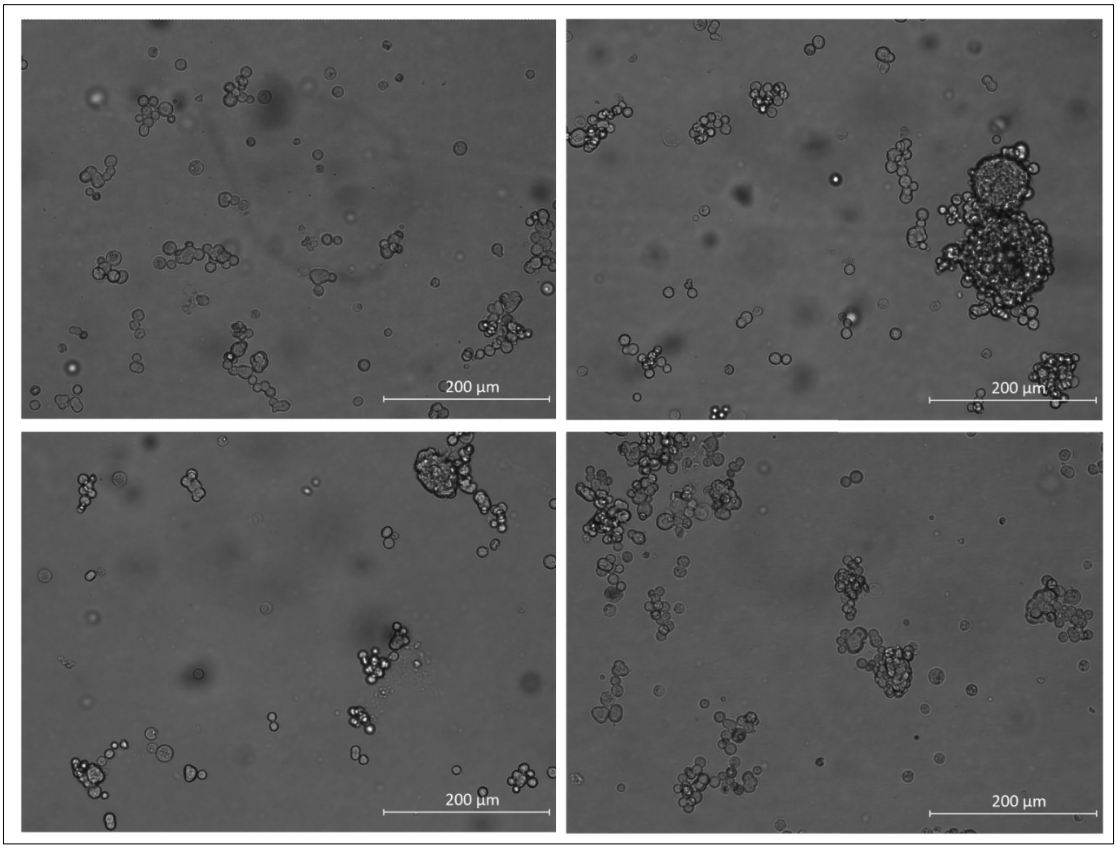

Figure 53. Tumorsphere suspension culture in supplemented DMEM/F-12 medium. Tumorspheres were subjected to Dispase II treatment and seeded back in T25 ULA flasks (10 mL medium) 24 hours before recording. In the picture on the top right, a large cell cluster next to a tumorsphere can be seen. Reference scale (bottom right): 200 µm. Images were recorded with the Axio Vert.A1 microscope and edited with the ImageJ software.

Table 20. Cytotoxic evaluation of novel histone deacetylase inhibitors on tumorspheres derived from Panc-1 (ATCC) cells. The CellTiter-Glo 3D Cell Viability Assay (Cat. #G9681, Promega) was conducted after 48 hours of incubation. Depicted values represent the arithmetic means and their respective standard deviations of three repeats

HDAC Inhibitor	IC_{50} [µM]
KSK64	2.07 (±1.17)
LAK61	15.79 (±1.39)
MPK264	12.33 (±2.74)
MPK544	0.54 (±0.18)

All four HDAC inhibitors exhibited lower IC_{50} values on tumorspheres derived from Panc-1 cells than on the two-dimensional (2D) Panc-1 model. The lowest values were measured with KSK64 and MPK544, in accordance with the results described above (see section 4.6). A drastic difference was observed for LAK61, which showcased an IC_{50} value of 86.93 µM on Panc-1 cells, but a much lower IC_{50} value of 15.79 µM on tumorspheres. The IC_{50} value measured for MPK264 (12.33 µM), was in contrast very close to the value measured on Panc-1 cells (15.45 µM). Further experiments and adjustments of the cultivation protocol are needed and required to evaluate and correctly assess these results. Overall, tumorspheres grown in suspension culture showcased higher sensitivity both to handling, cultivation and cytotoxic treatment than adherent Panc-1 cells.

4.8 Roundup

Several chemotherapeutic and cytotoxic agents (e.g. gemcitabine and vorinostat) and novel substances, both natural and synthetic, were screened and evaluated on two-dimensional (2D) and three-dimensional (3D) pancreatic cancer models. 3D organoids (Panc-1 + KU0020 PSC) were cultivated and incubated on 96-well and 384-well ultra-low attachment (ULA) plates via manual and automated pipetting with the CyBio Well vario robot (Analytik Jena), and proved to be viable and stable for up to twelve days following seeding. The natural substance *O*-methyltylophorinidine exhibited high cytotoxic efficacy in both the CyQuant assay and in live-cell imaging, as well as on 3D co-culture organoids (Xie et al. 2020). Derivates of the established anti-malarian drug artemisinin exhibited cytotoxic properties on Panc-1 and Panc-1 + PSC organoids, and the activation of benzophenone-linked hybrids via ultraviolet irradiation was proven and documented as well. Several novel histone deacetylase inhibitors (HDACi) were tested and screened on Panc-1 cells, KU0020 PSC cells and 3D organoids, both on 96-well and 384-well formats, which KSK64 and MPK544 emerging as the most potent substances. MPK544 was capable of inducing the upregulation of E-cadherin, an epithelial marker protein, in Panc-1 cells, both on the mRNA and on the protein level. A protocol for the quantification of protein expression in pancreatic cancer organoids was established and further optimized, and delivered first promising results for MPK544 and the expression of E-cadherin. An experimental approach on the cultivation of tumorspheres, derived from adherent Panc-1 cells, was conducted and optimized, and tumorsphere-like cells could be harvested and successfully utilized to perform cytotoxicity screening assays.

5 Discussion of Results

5.1 Overview

The following section covers the discussion, review and critical assessment of the experimental methods, established scientific protocols, received results and data described and presented in the previous sections and paragraphs above. Section 5.2 covers the generation and cultivation of three-dimensional organoid models, as well as their application for drug screening. Section 5.3 covers the results for the natural product tylophorinine/*O*-methyltylophorinidine and its derivatives, obtained via cytotoxicity assays and live-cell imaging. Section 5.4 covers the drug screening and ultraviolet (UV) irradiation experiments conducted with artemisinin and its derivates, which were provided by the research group of Professor Griesbeck from the Department of Chemistry (University of Cologne, Germany). Section 5.5 covers the histone deacetylase inhibitors provided by the research group of Professor Kurz of the Institute of Pharmaceutical and Medical Chemistry of the Heinrich Heine University (Düsseldorf, Germany). Section 5.6 covers the generation and cultivation of tumorspheres from Panc-1 cells, and their application for drug screening experiments.

5.2 Three-Dimensional Organoids

The creation, cultivation and growth of three-dimensional organoids from PDAC cell lines (Panc-1/Capan-2) and patient-derived cancer-associated fibroblasts (pancreatic/hepatic stellate cells; KU0020 PSC/NCC06 HSC-P) was already evaluated and optimized by the works of Bailu Xie and Vanessa Mundorf (Mundorf 2018; Xie 2018). We were able to replicate these results for Panc-1 + PSC, Panc-1 + HSC, Capan-2 + PSC and Capan-2 + HSC organoids without further difficulty, verifying the stability and replicability of these models, and applied them for the screening of gemcitabine, pseudopterosin and *O*-methyltylophorinidine (Xie et al. 2020). In result sections 4.3 and 4.6.5, several organoids stained via immunofluorescent antibodies were presented and described. As clearly documented, the cellular composition of these organoids is largely uniform and consistent, with pancreatic cancer cells located in the inside of the organoids, surrounded by a sheet of ACTA2-positive cancer-associated fibroblasts (CAFs). This composition remains the same in organoids cultivated on 384-well ULA plates, despite their smaller dimensions. Cultivation of Panc-1 + PSC organoids on these plates via the application of the CyBio Well vario pipetting robot was achieved without further complications and enabled the high-throughput drug screening of HDAC inhibitors. As seen in Table 19 (section 4.6.1), where cytotoxicity results gained from 96-well and 384-well organoids are combined, IC_{50} values from both models were comparable with low standard deviations. For example, vorinostat (SAHA) exhibited an IC_{50} value of 2.06 (±0.42) µM, LAK127 an IC_{50}

value of 33.96 (±4.18) µM and MPK544, the most potent HDACi measured, an IC_{50} value of 1.05 (±0.10) µM. Utilization of 384-well plates and the CyBio Well vario pipetting robot significantly accelerated the measurement of novel substances and their cytotoxic screening, not only for organoids, but for pancreatic cancer (Panc-1) and CAF (KU0020 PSC) cells as well.

In the scientific paper of 2020, where the cytotoxic efficacy of pseudopterosin and *O*-methyltylophorinidine was evaluated (Xie et al. 2020), we used and documented organoids created from Capan-2 and hepatic stellate cells (NCC06 HSC-P) as well, with four organoid variants in total: Panc-1 + KU0020 PSC, Panc-1 + NCC06 HSC-P, Capan-2 + KU0020 PSC and Capan-2 + NCC06 HSC-P. Only Panc-1 + KU0020 PSC organoids were cultivated on 384-well ULA plates via the CyBio Well vario pipetting robot, and no initial experiments regarding the cultivation of the other three variants were conducted. Based on the obtained results and the immunofluorescence staining of these organoids, it is very likely that the cultivation of Panc-1 + NCC06 HSC-P, Capan-2 + KU0020 PSC and Capan-2 + NCC06 HSC-P organoids can be achieved as well, without larger modifications of the seeding and cultivation protocol for 3D organoids.

For the seeding of 3D organoids on the 384-well ULA plates, we started with 10 µL volume for each well (100 Panc-1 cells + 200 CAF cells). Higher volumes were not evaluated, but are probably possible, as the formed organoids possessed a size of 300 µm, not filling out their respective wells and leaving enough space for growth (see sections 4.3.1 and 4.3.2.1). So far, these organoids were only seeded and incubated in ultra-low attachment cell culture plates, but not in normal 384-well tissue culture plates treated with polyHEMA or other surface coating agents (Xie 2018). Such experiments were not conducted, because the coating of 384-well tissue culture plates with such agents was considered to be unfeasible and resulting in low reproducibility. Further optimizations and modifications for the cultivation and handling of organoids on 384-well ULA plates, as well as initial experiments regarding Panc-1 + NCC06 HSC-P, Capan-2 + KU0020 PSC and Capan-2 + NCC06 HSC-P organoids must be conducted in the future, e.g. the usage of matrigel instead of collagen and the conduction of matrigel invasion experiments on 384-well plate organoids (Ferretti et al. 2021; Kleinman and Martin 2005).

Panc-1 + PSC organoids exhibited stability and viability, and could be cultivated for up to twenty days following initial seeding (see the results presented in the outlook section). As proven by the staining with EthD-1 (see result section 4.3.2.2), most cells inside the organoids were vital and did not exhibit cellular damage or apoptosis. That calcein staining of 96-well plate organoids was unfeasible (data not shown) might be caused by the large amount of collagen and ECM components in the organoid body, which exhibited autofluorescence in the

488 nm channel. In contrast, 384-well organoids could be successfully stained with calcein, probably due to their smaller size and lower amounts of collagen and ECM components. Organoids did not lose their form and shape with prolonged cultivation, and the cellular composition did not change either. Longer incubations and experiments exceeding time periods of 72 hours are therefore possible and might improve the examination of biological processes in these organoids.

Future experiments utilizing these 3D models, besides matrigel invasion assays, which were not conducted during the course of this thesis, involve the analysis of organoids via flow cytometry and fluorescence-activated cell sorting (FACS). In this approach, organoids would first be cultivated as usual, followed by their pooling, trypsinization and transfer to a suitable cytometry device. Organoid cells could be separated back in cancer-associated fibroblasts (KU0020 PSC, NCC06 HSC-P) and tumour cells (Panc-1, Capan-2) and seeded back in two-dimensional cell culture models, to examine their changed biological properties. Another experiment could involve the analysis of surface proteins and the screening for potential cancer stem cells by looking for the elevated expression of proteins such as CD24, CD44, CD133 and EpCAM (Domenichini et al. 2019), or to examine the process of epithelial-mesenchymal transition (EMT) by comparing the expression of E-cadherin, N-cadherin, vimentin and other epithelial and mesenchymal markers (Quail and Joyce 2013). Besides EMT and the development of CSCs, another essential process of PDAC tumorigenesis and progression that has to be analysed in this 3D model is hypoxia. An initial experiment with the Hypoxyprobe-Green Kit (Hypoxyprobe, Cat.# HP6-100Kit), where Panc-1 + PSC organoids were incubated with 200 µM pimonidazole for 2 hours was started, but no hypoxic signals could be measured via spinning disc confocal microscopy (data not shown), and future trials must be executed, as hypoxia is a major driving factor of PDAC chemoresistance, angiogenesis and metastasis.

Further important and interesting factors to be examined in organoids are metabolic intermediates, the expression and secretion of extracellular matrix (ECM) components and proteins, the expression of oncogenes and tumour-suppressor genes, the Hippo-YAP pathway, which is associated with mechanic stress and enhanced malignancy, the NF-κB pathway and the secretion of exosomes and oncosomes. Exosomes are known to be present in the growth medium of PDAC cultures, capable of inducing the formation of pre-metastatic niches and influencing the tumour microenvironment (Basso et al. 2017; Costa-Silva et al. 2015). The supernatant medium of organoids, which are cultivated in up to 200 µL DMEM/F-12 medium, could be harvested and screened for exosomal proteins and factors such as tetraspanins, which regulate metastasis (Malla et al. 2018). Regarding the Hippo-YAP pathway, a planned experiment was the cultivation of PDAC organoids with Panc-1 and Capan-2 cells carrying inactivating mutations of the YAP gene, to analyse the effects of the signalling pathway in drug screening. Such genetically altered cells were generated, cloned

and gifted by the research team of Professor Randall Mrsny of the University of Bath (United Kingdom), but no organoids were grown, as these cells could not be cultivated successfully in the research laboratories, probably due to cellular damage caused by the transport.

Panc-1 + PSC organoids were utilized to successfully screen the cytotoxic properties of artesunate derivatives (see section 4.5), tylophorinine derivatives (see section 4.4) and histone deacetylase inhibitors (see section 4.6). The IC_{50} values obtained with the 3D CellTiter-Glo assays were reproducible and comparable, but were, in almost all cases, lower than the values of the same substances measured on 2D Panc-1 cells, e.g. for MPK264, a value of 15.45 µM was measured on Panc-1 cells, and a value of 5.54 µM on organoids. This observation was documented for organoids grown on both 96-well and 384-well plates. Even for ineffective substances such as LAK127 (Panc-1: 48.82 µM; 3D organoids: 33.96 µM), lower values were measured on organoids than on the 2D cell culture models. The same finding was documented for the substances artesunate (Panc-1: 13.78 µM; 3D organoids: 3.96 µM) and dihydroartemisinin (Panc-1: 18.84 µM; 3D organoids: 3.21 µM). Panc-1 + PSC organoids thus appear to be more sensitive against treatment with cytotoxic substances as cells grown in two-dimensional models. This observation seemingly contradicts the results gained for gemcitabine (Xie et al. 2020) and leads to the assumption that the chemoresistant properties of Panc-1 + PSC organoids do not cover the effects of artemisinins and histone deacetylase inhibitors (HDACi), or that the organoid model itself is more sensitive towards substance treatment in general. The reasons behind this finding are unclear. A hypothetical answer to this question might be the lack of mechanic and fibrotic stress in the organoids, which is necessary for the chemoresistant and malignant properties of PDAC, and that the sole presence of cancer-associated fibroblasts (CAFs) alone is not enough to induce these effects in our model (Rice et al. 2017). The application of collagen or matrigel on fully-grown organoids might be able to create such a microenvironment and enhance chemoresistance and further malignant/metastatic properties in the organoid system.

In section 4.3.3, a short initial experiment was documented: the cultivation and generation of Capan-1 + NCC06 HSC-P organoids, a potential PDAC liver metastasis model. Only one attempt was conducted, but resulted in the successful growth of a full 96-well plate of Capan-1 + NCC06 HSC-P organoids in the same conditions as for the Panc-1 + PSC organoids. More experiments must be done to evaluate this protocol and to examine the cellular composition of these organoids. A functioning Capan-1 + NCC06 HSC-P organoid should exhibit the same cellular structure, with an internal mass of tumour cells (Capan-2) surrounded by ACTA2-positive cancer-associated fibroblasts (HSCs). Organoids consisting of Capan-1 + KU0020 PSC cells are possible as well, but were not cultivated in the course of this thesis. The application of these organoids for drug screening could support the characterization of novel substances like HDAC inhibitors and artesunates, and differences between PDAC tumours of

the pancreatic body and liver metastases could be examined and analysed (see suggestions above). Miniaturisation on 384-well plates via the CyBio Well vario pipetting robot might be possible as well, but remains to be proven experimentally.

5.3 Tylophorinines

Derivatives of tylophorinine exhibited high efficacy on all tested models. *O*-methyl-tylophorinidine is the most potent of the six tested derivatives on PDAC cell lines and 3D organoids, as previously published (Xie et al. 2020), and proved its effect as an anti-proliferative substance via live-cell imaging experiments on Panc-1 cells, conducted with the IncuCyte Zoom device. The derivatives P05C06B02 and P05C06B04 showcased similar efficacy at 1 µM and 100 nM, although considerable weaker at a concentration of 10 nM. P05C06B05 and P05C06B06 proved to be completely ineffective. Of note is that the efficacious derivatives showcased their anticancer potential at very low concentrations when compared to the positive control gemcitabine (GEM), and *O*-methyltylophorinidine was active even at 10 nM on Panc-1 cells. These results coincide with the experimental data previously published by Irene Reimche, where the same derivatives were screened on breast cancer models, especially on triple-negative breast cancer (TNBC) cells and organoids (Reimche et al. 2022). An IC_{50} value of 27.81 (±2.83) nM was measured for P05C06B04 on Panc-1 cells (72 hours of substance treatment) by Shaliny Sothyrathnam with the CellTiter-Glo assay, conducted during her bachelor thesis at the Institute of Health Research and Education of the University of Osnabrück (Germany), but no further experiments regarding the effects and mechanisms of these tylophorinine derivatives were executed.

P05C06, P05C06B02 and P05C06B04 are the most potent and interesting of the six tylophorinine derivatives, requesting further examination and experimental research. Inhibition of the NF-κB signalling pathway and the expression and regulation of hypoxia-inducible factor 1 (HIF-1), both of which contribute to the malignant nature of pancreatic ductal adenocarcinoma (PDAC), might reveal the pharmaceutical mechanisms behind the efficacy of these derivatives (Chen et al. 2016; Lin et al. 2009). The application of these derivatives might be especially beneficial for the study of the molecular interactions between pancreatic stellate cells (PSCs) and pancreatic cancer cells in the organoid models. As anti-inflammatory agents, tylophorinine derivatives could be applied as chemotherapeutic agents for the treatment of non-metastasized pancreatic cancer.

5.4 Artemisinins and Artesunates

Artemisinin derivatives were tested on Panc-1 cells, both manually and with the CyBio Well vario pipetting robot, and showcased moderate cytotoxic efficacy when compared to the results obtained with tylophorinine derivatives. Artemisinin itself proved to be ineffective against Panc-1, with no measurable cytotoxic effect, but is suited as a comparable negative control for the correct assessment and evaluation of drug screening experiments and assays. For artesunate (ART) and dihydroartemisinin (DHA), the only two derivatives tested on the Panc-1 + KU0020 PSC organoid model so far, IC_{50} values of 13.78 and 18.84 µM were measured, respectively. The most potent artemisinin derivative was CB-84-Fr1, with an IC_{50} value of 6.12 µM, and all screened substances exhibited a value below 20 µM, thus being, on average, more potent on Panc-1 cells than most of the tested histone deacetylase inhibitors (HDACi) (see HDACi results in section 4.6.1).

The effect of artesunate treatment on the processes of ferroptosis and inflammation remains to be examined. As the most potent derivative, CB-84-Fr1 might induce ferroptosis in pancreatic cancer cells via the generation of radical oxygen species (ROS) at a considerably higher rate then artemisinin and the other screened substances. Artesunate and dihydroartemisinin have proven their anti-proliferative capabilities in initial clonogenic cell assay experiments (data not shown) and should be tested on their potency regarding induction of ferroptosis as well. Ferroptosis itself, which is an important factor regarding pancreatic cancer tumorigenesis, can be inhibited by suppressing the functions of the transferrin receptor, glutaminase 2 (GLS2) and enzymes involved in the regulation of intracellular iron levels, and can be induced via suppression of glutathione peroxidase 4 (GPX4) in cancer cells (Hassannia et al. 2019; Chen et al. 2020). Via knockdown experiments (transfection of cancer cells with siRNA) the biological mechanisms behind the derivatives' efficacies could be further evaluated in PDAC models. Further experiments involve the screening of the remaining derivatives on Panc-1 + PSC organoids, as well as on PDAC CAF cell lines (KU0020 PSC, NCC06 HSC-P).

The photochemical activation of the artemisinin hybrid (see result section 4.5.1) was successful and revealed high efficacy on Panc-1 cells and moderate cytotoxic potential on KU0020 PSC cells. The reasoning behind the distinct activation of the hybrid molecule through UV irradiation, as detailed in the PhD thesis of Christina Bold (Bold 2022), could be proven, as both benzophenone alone and artemisinin plus benzophenone showcased significantly lower cytotoxic efficacy. Further evaluation of UV-activated artemisinin derivatives on other PDAC cell lines (Capan-1, Capan-2, etc.) and patient-derived CAF cell lines (NCC06 HSC-P) remains to be conducted. Initial UV-activation experiments on 3D organoids were attempted with 384-well ULA plates, but were not feasible due to the low volume and evaporation effects. Evaporation itself limited the duration of substance treatment to only 24 hours, as the tissue

culture plates had to be incubated without their cover plates to ensure UV activation. UV-irradiation yielded no effects with the cover plate on top of the cells (data not shown). Experiments with Panc-1 + KU0020 PSC organoids on 96-well ULA plates should be accomplishable without further intricacies due to the higher volume of growth medium, but were not conducted in the course of this thesis. Incubation periods longer than 24 hours could induce genetic damage in the cells, caused by the extended ultraviolet irradiation, and are not planned to be conducted for further research.

Overall, the experimental results confirmed the cytotoxic and anticancer potential of artemisinin derivatives on pancreatic cancer and their efficacy as UV-activated substances. Phototherapy is a new alternative method for the medical treatment of pancreatic ductal adenocarcinoma, and such methods are indeed capable to sensitize pancreatic cancer cells against gemcitabine treatment, indicating their potential to improve cancer treatment and overall survival rate. Future experiments and results might elucidate the efficacy of artemisinin derivatives in such applications and clinical usages (Hamblin 2020; Sun et al. 2022).

5.5 Histone Deacetylase Inhibitors and Epithelial-Mesenchymal Transition

We screened sixteen novel substances exhibiting HDACi activity for their cytotoxic potential on Panc-1, KU0020 PSC and 3D organoids, with citarinostat, ricolinostat, tubastatin A and vorinostat (SAHA) as controls. As expected, SAHA exhibited high efficacy on all models. KSK64, LAK41, LAK67 and MPK544 were the most potent novel inhibitors, all showcasing high cytotoxic efficacy on all three models. Concordant results for KSK64 were previously published and coincide with the data presented here (Lee et al. 2020). MPK264 is another interesting HDAC inhibitor that was used for experimental evaluation. The three HDAC6 inhibitors all showcased low to moderate efficacy, with tubastatin A being the least potent on PSC cells and organoids. Tubastatin was therefore applied as a negative control for further assays. Based on these results, it can be concluded that inhibition of HDAC6 alone is not sufficient in inducing cell death in PDAC.

Of note and scientific interest is the observation that all HDAC inhibitors showcased lower IC_{50} values on the 3D organoid model as on the 2D Panc-1 models (with the sole exception of tubastatin A, whose values were in the same close range). Most HDAC inhibitors also showcased lower values on the organoids than on the KU0020 PSC cells as well. This is the case for both effective and ineffective inhibitors, and possible reasons behind this finding were discussed above (see discussion section 5.2). Clarification might be achieved by conducting the drug screening assays on other organoid models (Panc-1 + HSC, Capan-2 + PSC and Capan-2 + HSC), as well as on the theorized liver metastasis model Capan-1 + HSC (see

above), and by analysing the biological mechanisms behind the functions of the HDAC inhibitors. Screenings can also be performed on Capan-1, Capan-2 and NCC06 HSC-P cells alone. The only HDAC inhibitor tested on Capan-1 cells was vorinostat (SAHA), with an IC_{50} value of 22.47 (±1.73) µM, being considerably higher and therefore less active than on PSC, Panc-1 and Panc-1 + PSC organoids. No further HDACi cytotoxicity assays on Capan-1 were conducted.

Colony formation assay results were in accordance with the cytotoxicity results. MPK544, an HDAC2/6 inhibitor, was the most potent drug, followed by KSK64 and MPK264. Tubastatin A showcased the lowest potency. MPK544 even exceeded vorinostat (SAHA) regarding the inhibition of colony formation, at all three concentrations, thus being the most effective HDACi tested in this approach. Other HDACi were not examined with the colony formation assay, which remains to be conducted. Interesting candidates are LAK41 and LAK67, as well as the two HDAC6 inhibitors citarinostat and ricolinostat. Colony formation assays were not performed with Capan-1 and Capan-2 cells, and no initial experiments where executed. The protocol has to be adapted for both cell lines due to their different sizes and proliferation rates (Deer et al. 2010). An interesting approach would be the application of colony formation assays for KU0020 PSC and NCC06 HSC-P cells. Both cell lines secrete massive amounts of collagen and extracellular matrix (ECM) components, so it remains debatable if such an approach would yield conclusive results.

Examination of epithelial-mesenchymal transition (EMT) was confined to the expression of the epithelial marker E-cadherin (CDH1) and the mesenchymal marker vimentin (VIM). Western blotting with lysates gained from MPK544-treated Panc-1 cells verified that HDAC inhibitors are capable of partially reversing EMT processes in cancer cells, though only at 7 µM of substance concentration. Control blots with gemcitabine, paclitaxel, tubastatin A, KSK64 and SAHA further validated this hypothesis. The RT-qPCR data showed an upregulation of CDH1 for 4 µM MPK544, and a downregulation of vimentin (VIM) at 4 µM as well. Western blotting of vimentin and N-cadherin was inconclusive (data not shown). Though these results strongly support the potential of MPK544 to reverse EMT by inhibiting the expression of E-cadherin and inducing the expression of vimentin, further experiments are necessary for substantive evaluation. Panc-1 cells might be subjected to longer substance treatments to showcase measurable EMT reversal, as Panc-1 cells were only incubated for 24 hours. Longer incubation periods are possible without adjustment of cell titre numbers. Based on the data presented above, the HDAC2/6 inhibitor MPK544 can be considered as an effective agent for inducing epigenetic changes in pancreatic cancer cells, and an interesting candidate for the sensitisation of cancer cells towards chemotherapeutic intervention. Initial experiments regarding the synergistic effects between MPK544 and gemcitabine were conducted, but

revealed no measurable improvement regarding cytotoxicity (data not shown). More western blot data is documented in the appendix section.

The quantification of CDH1 expression in Panc-1 + KU0020 PSC organoids revealed a high degree of variability between the organoids. Following optimization of the treatment and measurement protocols, a moderate effect of the upregulation of CDH1 protein expression could be verified for MPK544 at 1 µM, but not for 4 µM, and none for citarinostat and ricolinostat at 7 µM as well. The control approach with TGF-beta revealed a strong measurable effect after 72 hours, but none after 24 hours. An incubation of 24 hours might not be enough to induce the desired effect of CDH1 upregulation in 3D organoids. It should be noted that the established measuring protocol with the CellPathfinder software resulted in huge standard deviations and variances, indicating a low efficacy of all substances in this approach and a huge diversity and variability of the organoids regarding their CDH1 expression levels regardless of treatment. The IF-staining galleries depicted in result section 4.6.5 show different organoid shapes and forms, but no visible differences in CDH1 expression. In some cases, a lack of CDH1 expression in the middle of the organoid was observed. This finding might be caused by an actual lack of CDH1 expression in this area of the organoid, or by an insufficient antibody staining, which must be resolved following further experimental research. The staining process itself yielded good results and usable images recorded with the CQ1 Confocal Imaging Cytometer (Yokogawa) and the LSM880 confocal microscope (Zeiss), and does not appear to be in need of optimization and adaptation. An interesting finding is the expression of CDH1 in all detected cells, both Panc-1 and KU0020 PSC cells. The CDH1 quantification results should be viewed with caution, but the obtained data indicate the potential of MPK544 to induce epigenetic changes in 3D organoids and to potentially reverse epithelial-mesenchymal transition (EMT). Future experiments must establish both a working negative and positive control for this approach and a suitable incubation period for the substance treatment, and should prove that EMT does occur in these organoid models to a measurable degree, either via IF-staining or by RT-qPCR analysis. Besides E-cadherin (CDH1), the expression of N-cadherin (CDH2), vimentin (VIM) and EpCAM could also be examined and quantified.

Other experimental approaches to evaluate the efficacy of MPK544, KSK64, LAK41 and LAK67 include migration assays and transwell migration assays. We tested the effect of KSK64, MPK264 and MPK544 on Panc-1 cell migration via the IncuCyte Zoom live-cell imaging application, at concentrations of 1, 4 and 7 µM, with SAHA and tubastatin A as the positive and negative controls in an initial experimental setup, in which no measurable effect on cell migration was observed for any applied substance (data not shown). A working standard protocol has to be established beforehand, to evaluate the effects of MPK544 on migration and invasion, which remains to be conducted. Initial data published in the master

thesis of D. Janßen (Janßen 2021) indicate that MPK544 is capable to inhibit the migration of Panc-1 cells in a transwell assay setup.

5.6 Tumorspheres and Cancer Stem Cells

Cultivation of tumorspheres from Panc-1 (ATCC) cells proved complicated, and required several approaches before the protocol described above (see method section 3.3.5) was established. Initial experiments were conducted on 6-well tissue culture plates with cell-repellent surface coating, where Panc-1 cells were cultivated for several weeks and observed to evaluate and estimate the induction and growth of tumorspheres. Following these experiments, which yielded unsatisfactory results, the 6-well plates were replaced with appropriate T25 flasks, and tumorsphere suspension cultures were subjected to Dispase II treatment every seven days, which resulted in a significant increase of visible tumorspheres. Panc-1 cells were henceforth seeded in T25 flasks with cell-repellent surface coating for up to two weeks prior to experimental application. Cytotoxicity assay results were consistent and reproducible, and further confirmed the anticancer efficacy of MPK544 and KSK64, the two most potent HDAC inhibitors screened and evaluated. Although these data could be generated and replicated, the cultivation process itself proved to be difficult and often resulted in the complete loss of viable cells in the suspension culture, demanding the simultaneous incubation of two to four T25 flasks. One T25 flasks did not yield enough cells for harvesting and cell seeding, due to the high amount of dead cells and cell clusters in the suspension culture. The presence of clustered cells especially did complicate the cultivation process and aggravated the assessment of the culture's status prior to harvesting and cell counting with the LUNAII device. The cultivation method therefore requires further intensive optimization and modification, to ensure a reproducible and simple standard protocol.

Besides cytotoxicity assays, several other experiments to examine these tumorspheres were conducted. The protein expression of the mesenchymal markers N-cadherin (CDH2) and EpCAM (CD326), the epithelial marker E-cadherin (CDH1) and the stem cell markers Oct4 and Sox2 were analysed via western blotting (see results presented in the appendix). N-cadherin (western blot data not shown) was only minimally expressed in both Panc-1 cells and derived tumorspheres, and no increase of N-cadherin expression in tumorspheres could be verified in this model. EpCAM and CDH1 expression in tumorspheres was stronger than in adherent Panc-1 cells, Oct4 expression was equal in both cultures. RT-qPCR analysis for the cancer stem cell (CSC) markers CD24, CD44, CD133 and Nanog was conducted as well, with mRNA obtained from KU0020 PSC cells as a suitable negative control, but no upregulation of any markers in tumorspheres could be observed (data not included due to low reproducibility).

These results are inconclusive and indicate the requirement to optimize and evaluate the methodical handling.

Optimization might involve the evaluation of the tumorsphere cultivation medium, by including growth factors to induce stemness (e.g. N-2 supplement from Thermo Fisher, Cat. #17502048) or the application of more sensitive enzymes (e.g. accutase) for the isolation of tumorspheres (Mishra et al. 2017; Domenichini et al. 2019). According to published data, PDAC cancer stem cells exhibit expression of CD24, CD44, CD133, EpCAM, Nanog, Oct4, Sox2, Snail and Slug, and such factors should be used as controls in future research based on the findings presented here (Zhou et al. 2021; Shankar et al. 2011). Despite these methodical challenges, a working protocol to harvest and utilize tumorsphere cells for drug screening and staining procedures could be established, which can be further adjusted to tumorspheres formed under different cultivation protocols and conditions.

6 Summary of Results

We evaluated the cytotoxic potential of tylophorinine derivatives, artemisinin derivatives and histone deacetylase inhibitors (HDACi) on established pancreatic cancer cells (Panc-1, Capan-1, Capan-2), cancer-associated fibroblasts (CAFs) (KU0020 PSC, NCC06 HSC-P) and three-dimensional organoids cultivated from these cell lines. Miniaturisation of Panc-1 + PSC organoids on 384-well ULA plates via application of the CyBio Well vario pipetting robot of Analytik Jena was achieved and standardized, resulting in high-throughput screening of all novel HDAC inhibitors presented above. The three tylophorinine derivatives P05C06, P05C06B02 and P05C06B04 exhibited the strongest anti-proliferative effects in Panc-1 cells, and P05C06 showcased high cytotoxic efficacy on 3D organoids (Xie et al. 2020). Artemisinin derivatives were less potent, with CB-84-Fr1 being the most effective and cytotoxic derivative tested, but did induce cell death in Panc-1 cells and Panc-1 + PSC organoids, and UV-activation of benzophenone-linked artemisinin hybrids was proven and verified on Panc-1 and PSC cells. The four novel substances LAK41, LAK67, KSK64 and MPK544 were the most effective HDAC inhibitors, screened on Panc-1, KU0020 PSC and Panc-1 + PSC cells and organoids, further evaluated via colony formation assays. MPK544 induced upregulation of the epithelial marker E-cadherin on the protein and mRNA level, and downregulation of the mesenchymal marker vimentin on the mRNA level. Tubastatin A revealed low efficacy on all models, thus being suited as a negative control for further experimentation, with vorinostat (SAHA) as a highly effective positive control. Quantification of E-cadherin protein expression in Panc-1 + PSC organoids via IF-staining, spinning disc confocal microscopy and the CellPathfinder software indicate that MPK544 is capable of inducing the reversal of epithelial-mesenchymal transition (EMT) in the organoid model, but these results should be viewed cautiously and require further evaluation and experimentation. Cultivation of tumorspheres from Panc-1 (ATCC) cells was achieved, and tumorsphere cells could be harvested for drug screening assays, but cancer stem cells (CSCs) could not be verified inside these cultures via western blotting and RT-qPCR. Optimization and strict evaluation of the tumorsphere cultivation protocol is therefore required to generate a viable and malignant CSC population.

Co-culture organoids cultivated on 384-well ULA plates could be applied for standardized drug screening assays, yielding good reproducibility and verifiable results. Staining with fluorescent antibodies and other markers was feasible as well, proving the validity of this organoid model and its aptitude for experimental application. The high-throughput screening, supported by the CyBio Well vario pipetting robot, significantly accelerated drug screening procedures and generated valid and usable data for all tested substances and drugs.

O-methyltylophorinidine (P05C06), KSK64, LAK41 and MPK544 emerged as novel substances of interests, with high cytotoxic potential and efficacy on Panc-1 and Panc-1 + PSC

organoids, as well as on PSC cells. In future experiments and projects, these drugs will be further examined and utilized.

7 Outlook

7.1 Biochip Applications for Organoid Research

The transfer of tumour organoids on biochip models was successfully accomplished in several studies, to examine the interactions between tumour cells and their tumour microenvironment (TME) regarding chemoresistance and angiogenesis (Tomás-Bort et al. 2020; Lim et al. 2021). In cooperation with the biotechnology company Dynamic42 (Jena, Germany), who specialise in biochip technology and application, a novel organoid-on-chip model was established, where the Panc-1 + KU0020 PSC organoids would be transferred to a specialized biochip, with an upper cell layer of endothelial cells (HUVECs), and subjected to drug treatment and screening (Raasch et al. 2016; Raasch et al. 2019). The structure and schematic of said biochip, developed by Dynamic42, has not been published yet, and will not be presented in this thesis. In Figure 54, the organoid-on-chip system is depicted, with the respective pumps in the background. The chips were incubated at 37 °C, connected to the pumps to ensure constant medium exchange and flow across the endothelial cell layer. HUVECS were seeded on the chips five days before the transfer of the organoids (day 6 of cultivation) from their 96-well ULA plates to the chips' cavities, which were especially designed to hold the organoids in place. Substance treatment started 24 hours later and lasted for 72 hours in total, followed by evaluation of cell viability with the CellTiter-Glo 3D assay.

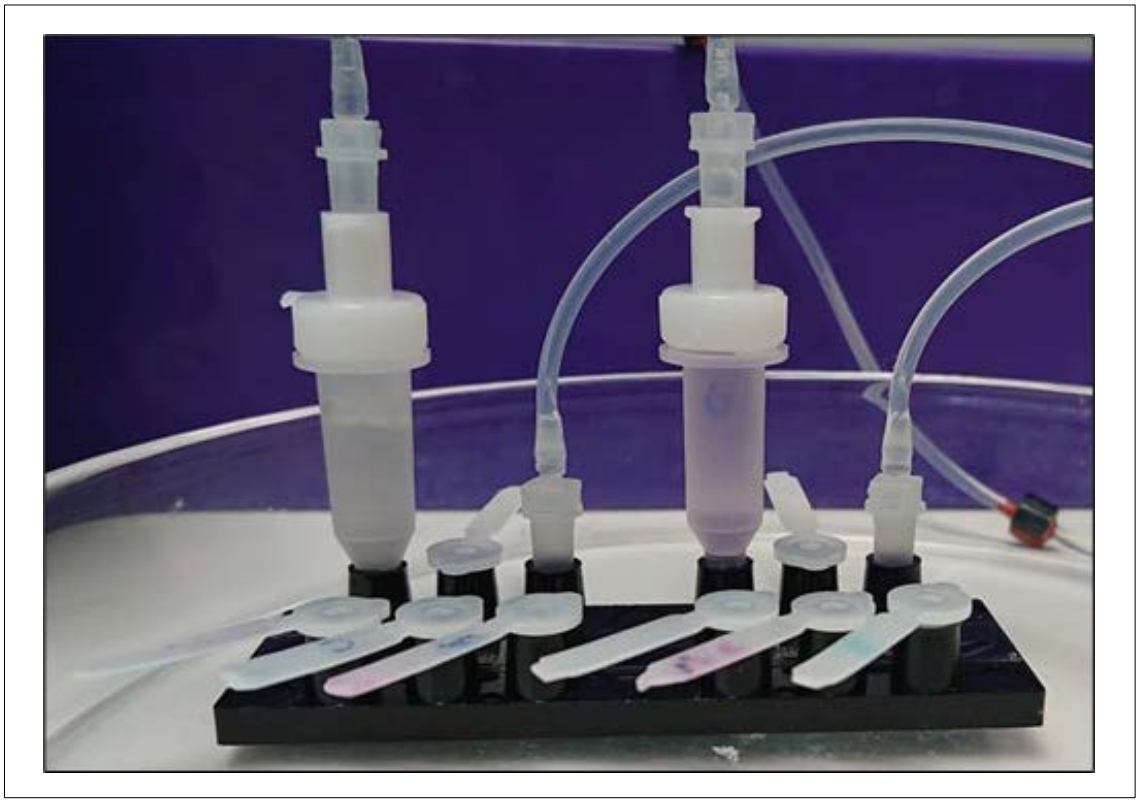

Figure 54. Organoid-on-chip model, developed and established by Dynamic42. In this exemplary image, the two separate cell culture chambers were subjected to different treatments; the left one

received no medium change, the right one received complete medium change every 24 hours. The channels' openings are closed with white clips. Only the endothelial layer received medium flow. Pumps out of frame. A clear change of pH value in the respective media can be observed.

In an initial experiment, Panc-1 + KU0020 PSC organoids were subjected to 72 hours of substance treatment with paclitaxel at concentrations of 25 and 10 nM. Exemplary images of organoids and endothelial cells are depicted in the figures below. Evaluation of cell viability with the CellTiter-Glo assay revealed that the organoids were not affected by paclitaxel treatment, but that they featured significantly lower viability than the remaining organoids on the 96-well ULA plates. These organoids were still viable twenty days after their initial seeding. The endothelial HUVEC cells however detached from their respective layer, probably being affected by the chemotherapeutic and cytotoxic agent paclitaxel (taxol). Figures 55 to 59 below depict the Panc-1 + KU0020 PSC organoids and the HUVEC cells on the biochip layers.

Viability of organoids and endothelial cells was compared between cells receiving medium exchange (1 mL organoid medium plus substances/DMSO) every 24 hours and cells receiving no medium exchange. Redosing and medium change had no measurable effect on cell viability, as seen in Figure 59 below. Paclitaxel did not induce cell death and apoptosis in the biochip organoids, but did induce the detachment of HUVEC cells from their respective surface layer (see Figure 58). Biochip organoids were overall less viable than those remaining in their original 96-well ULA plates (Greiner Cat. #650970). Apparently, the drug paclitaxel did not get dissolved into the biochip organoid layer, thus only affecting the endothelial cells in the upper layer.

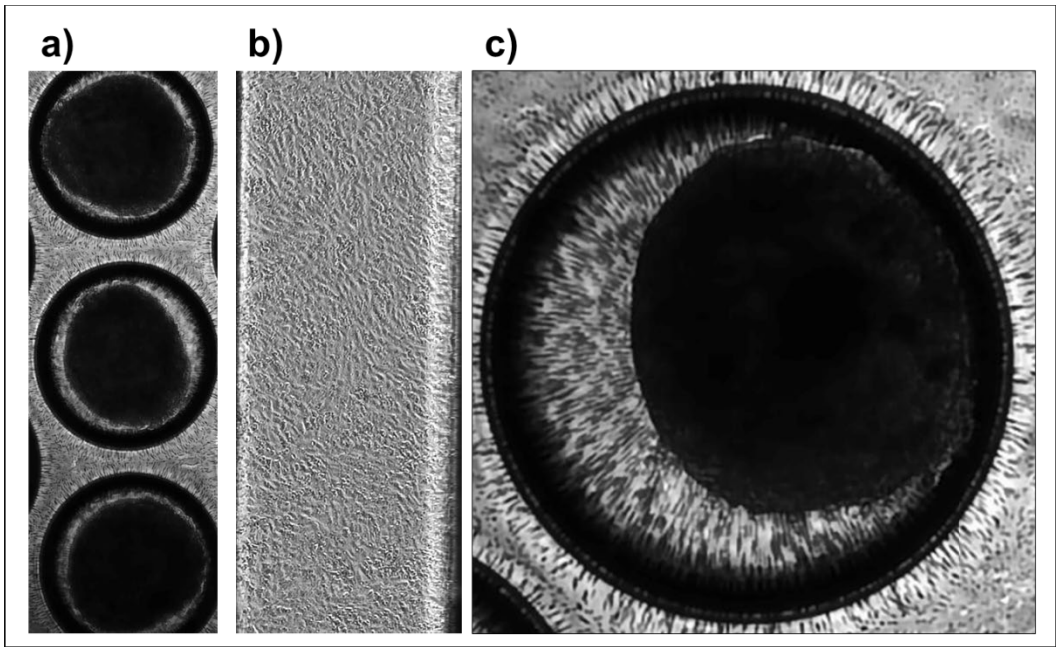

Figure 55. Organoids and HUVEC cells on the Dynamic42 biochip model. Images recorded with the Axio Vert.A1 microscope. A) three organoids in the cavities of the lowest layer; b) endothelial cells (72 hours after seeding); c) organoid in cavity (24 hours after transfer).

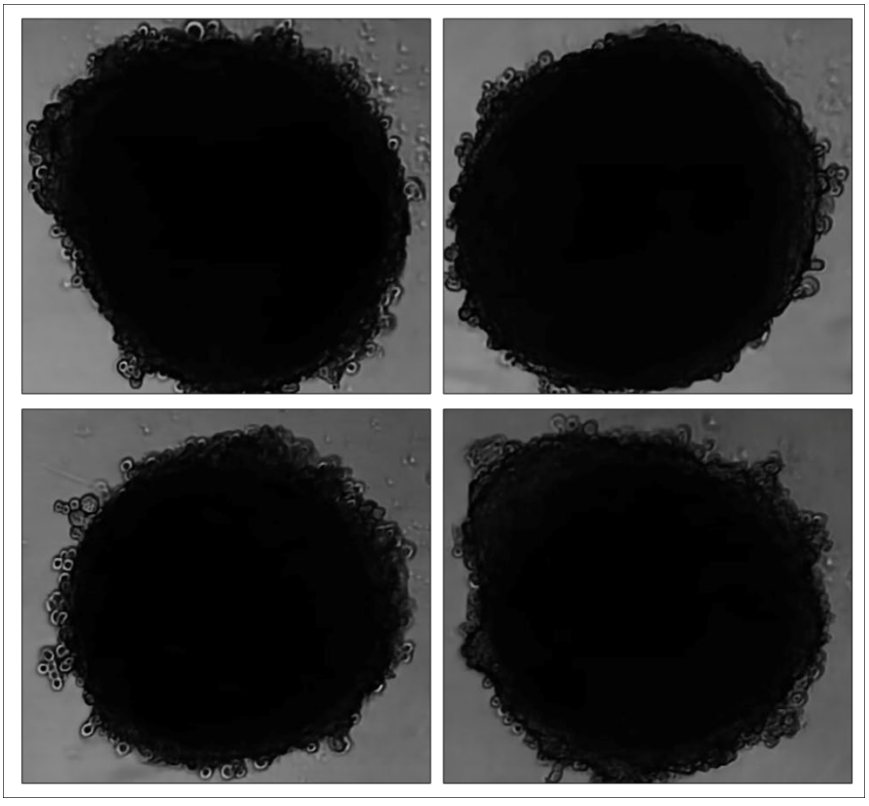

Figure 56. Panc-1 + KU0020 PSC organoids on a 96-well ULA plate (Greiner Cat. #657970) 240 hours after initial seeding. Four distinct organoids depicted. Images recorded with the Axio Vert.A1 microscope. Organoids were viable and exhibited cell proliferation.

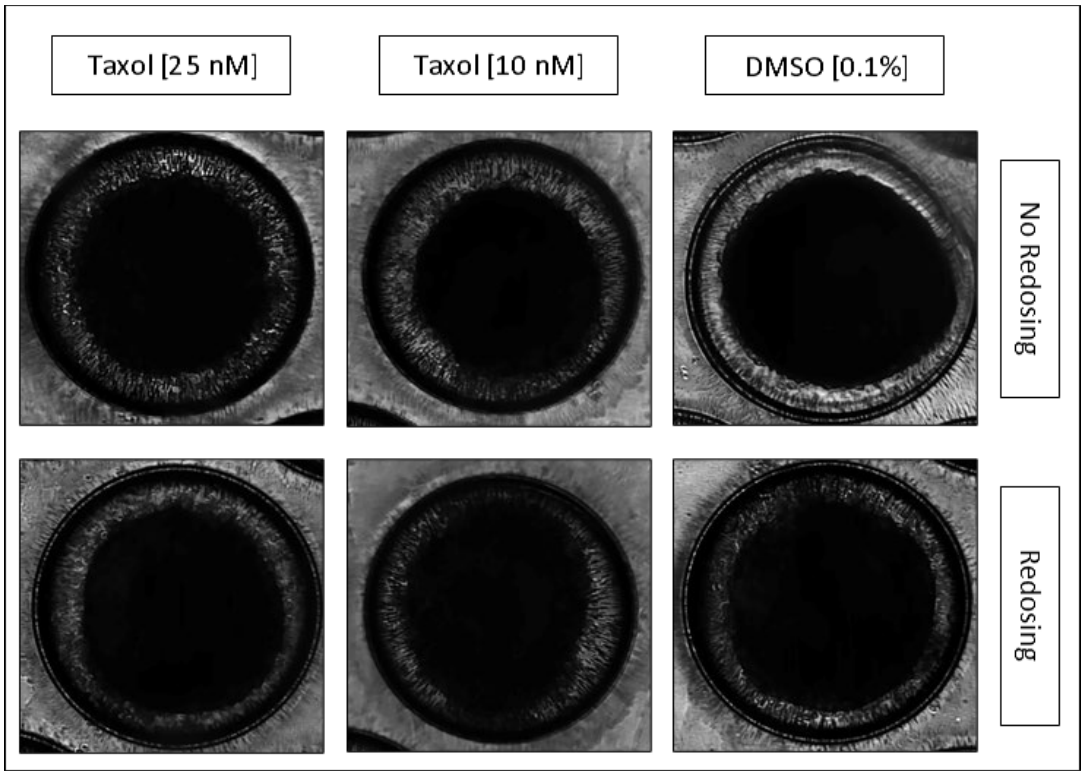

Figure 57. Panc-1 + KU0020 PSC organoids on the biochip layer after 72 hours of substance treatment. From left to right: paclitaxel (25 nM), paclitaxel (10 nM) and DMSO (0.1 %). Upper images: no redosing of medium; bottom images: redosing of medium every 24 hours. No cytotoxic effects are visible in this initial approach. Images recorded with the Axio Vert.A1 microscope.

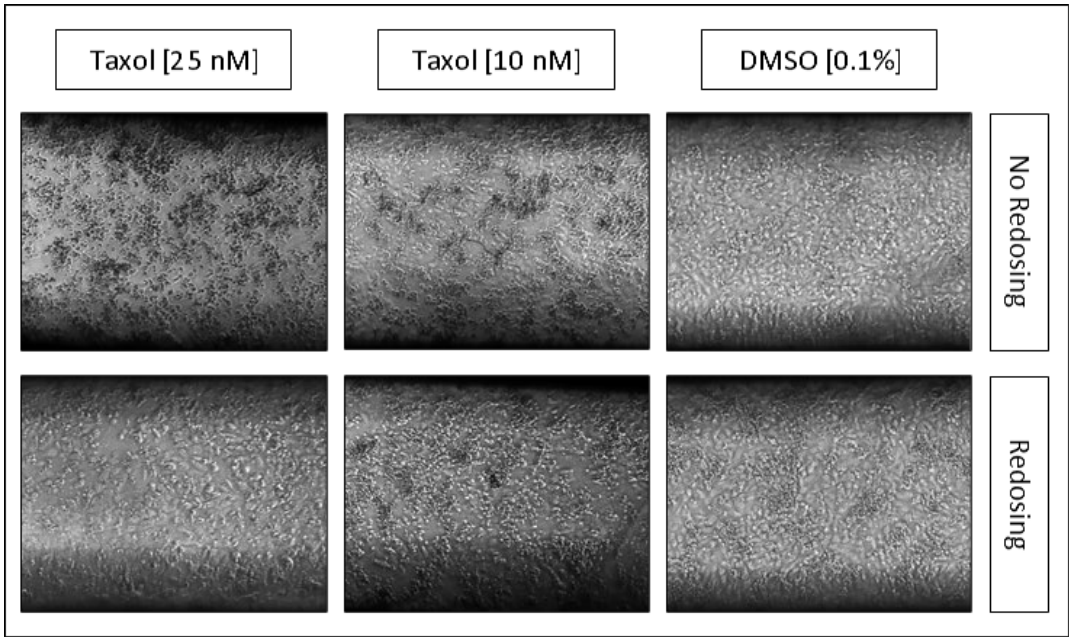

Figure 58. HUVEC cells on the biochip layer after 72 hours of substance treatment. From left to right: paclitaxel (25 nM), paclitaxel (10 nM) and DMSO (0.1 %). Upper images: no redosing of medium; bottom images: redosing of medium every 24 hours. HUVECs detached from the surface layer due to paclitaxel incubation. Images recorded with the Axio Vert.A1 microscope.

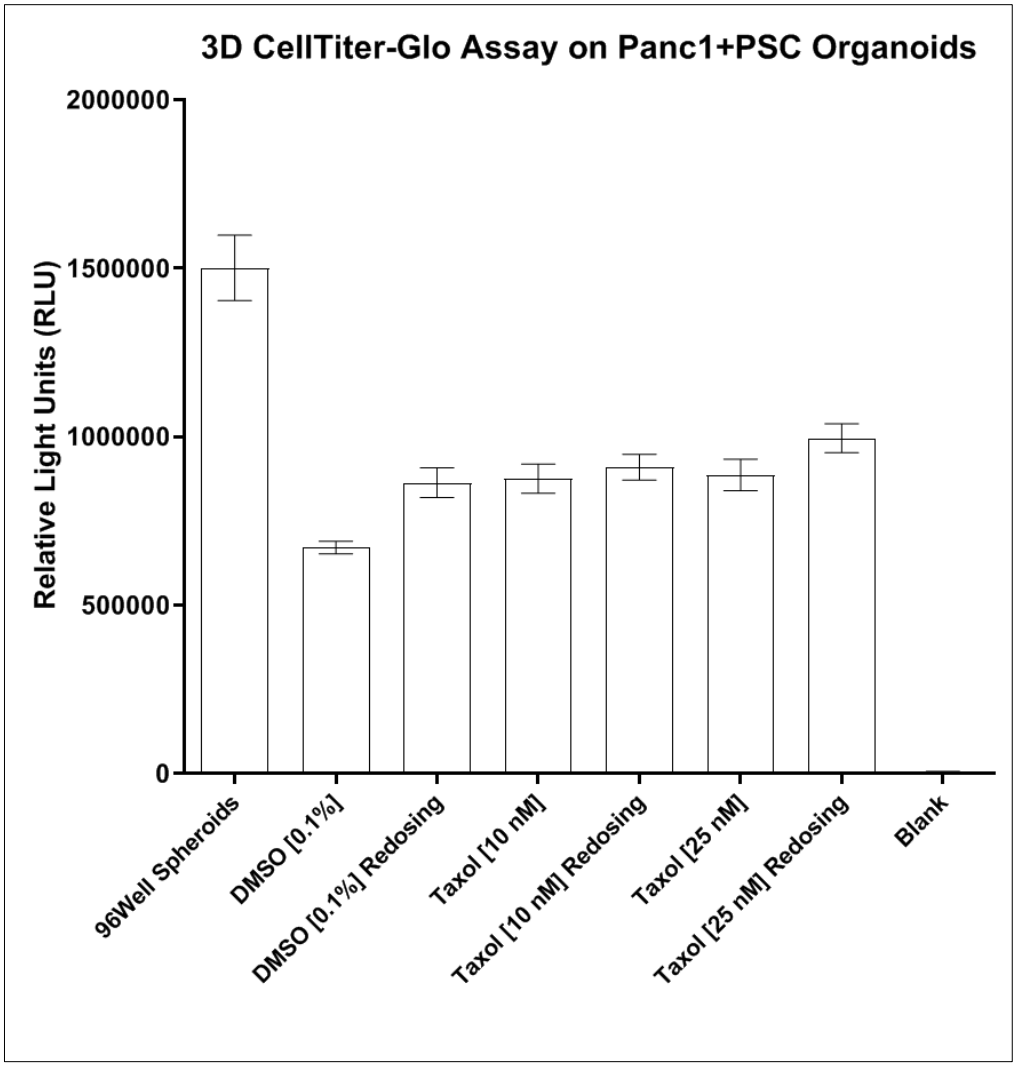

Figure 59. Cell viability results of Panc-1 + KU0020 PSC organoids, obtained with the CellTiter-Glo 3D assay (Promega). The remaining organoids of the 96-well ULA plate were applied as a control, and exhibited high RLU values. Organoids transferred to the biochip were significantly less viable than the remaining organoids. Neither redosing nor paclitaxel treatment had significant effects on cell viability, and organoids subjected to 0.1 % DMSO without any medium exchange exhibited the lowest values. Y-axis: relative luminescence units (RLU). Depicted data represent the arithmetic means and the respective standard deviations of five measured organoids. This experiment was only conducted once. Results were measured with the Tecan infinite 200Pro device.

These results depict initial experiments. This biochip model will be further optimized and evaluated by Dynamic42 and the Institute of Pharmaceutical Biology and Biotechnology (Heinrich Heine University, Düsseldorf), to standardize drug screening and cultivation of patient-derived pancreatic endothelial cells, establishing a vascularized PDAC organoid-on-chip model. The HUVEC cells will be eventually replaced with human pancreatic microvascular endothelial cells (HPaMEC), to establish a more lifelike vascularized organoid chip model, as HUVEC cells are derived from umbilical blood. The HPaMEC cells were originally applied, but

were observed to detach from the endothelial surface layer 24 hours after seeding, and appeared to be less stable on the chip model (data not shown).

7.2 Advanced Organoid Models and Cell Culture Experiments

We presented a 3D organoid model cultivated from established pancreatic cancer cell lines (Panc-1, Capan-1 and Capan-2) and patient-derived, non-immortalized cancer-associated fibroblasts (KU0020 PSC; NCC06 HSC-P). The Capan-1 + NCC06 HSC-P model was shortly introduced and requires further evaluation. Only the Panc-1 + KU0020 PSC model was miniaturised on 384-well ULA plates with the CyBio Well vario pipetting robot (Analytik Jena), and Panc-1 + NCC06 HSC-P, Capan-2 + KU0020 PSC and Capan-2 + NCC06 HSC-P remain to be examined in this approach. Based on the findings documented above, the miniaturisation of these three organoid models should be achieved without any larger technical issues.

The organoid model only consists of two separate cell lines. As described in section 2.1.4, the tumour microenvironment (TME) of pancreatic ductal adenocarcinoma (PDAC) is composed of many more different cell types. The organoid model can thus be progressed and advanced by introducing other cell lines, such as immune cells and endothelial cells. For immune cells, the established monocyte cell line THP-1 could be utilized and inserted into the organoid, as tumour-associated macrophages (TAMs) represent one of the most important factors regarding the development of chemoresistance, metastasis, angiogenesis and immune evasion in the progression of malignant PDAC (Ferreira Garcia Rodrigues 2022; Ireland and Mielgo 2018; Liou et al. 2013). THP-1 cells could be added to the organoid culture 72 hours following initial seeding, when the organoids have formed completely, but initial experiments have not been conducted in the course of the thesis. Besides monocytes, endothelial cells can also be added to the organoid model (see biochip assay above), as angiogenesis, the formation of new, often malformed, blood vessels is an essential process in pancreatic cancer and is fuelled by hypoxia and inflammation via the NF–κB pathway, and PDAC tumours are often hypovascular (Adams and Alitalo 2007; Guo et al. 2020; Werno et al. 2010).

So far, the organoids were only cultivated in a collagen-1 matrix, and did not receive further treatment. Organoids growth could be supported by the application of matrigel, or by adding growth factors such as B-27, EGF and FGF, which are used in the cultivation of cancer stem cells in tumorspheres (Domenichini et al. 2019; Cai et al. 2018). Upregulation of enzymes such as the focal adhesion kinase (FAK), which promote cancer stemness, is induced by factors of the extracellular matrix (ECM), and could be reconstructed in the organoid model by reorganizing the matrix solution (Begum et al. 2017). The Hippo-YAP pathway, activated by matrix stiffness and mechanical stress, is known to induce chemoresistance in PDAC tumour

cells as well, and Panc-1 and Capan-2 cells carrying YAP1 mutations were constructed by research partners from the University of Bath (see discussion above), which remain to be utilized for organoid cultivation and 3D drug screening (Gujral and Kirschner 2017). Co-culture organoids might also be generated and grown from PDAC cell lines that were desensitised against gemcitabine and obtained chemoresistant properties (Su et al. 2023).

As seen above, organoids remain stable and viable up to twenty days in cell culture conditions. Longer time periods are likely possible, and PDAC tumour cells might gain novel malignant properties in these long-term approaches via interaction with the pancreatic and hepatic stellate cells (Erkan et al. 2010). Medium exchange for organoids grown on 96-well ULA plates can be executed easily by discarding and adding 100 µL of volume. In a theoretical setup, organoids could be grown for different time periods and subjected to drug treatments, comparing the obtained IC_{50} values to evaluate possible changes in the organoids' sensitivity towards the respective chemotherapeutic agents (e.g. gemcitabine, paclitaxel etc.). Another possible approach would be the digestion of organoids via trypsine, accutase or dispase, and returning the 3D culture cells back to 2D cell cultivation, requiring isolation and separation of the two different cell types, which could be achieved via FACS.

PDAC tumour cells are known to secrete exosomes, which interact with immune cells (B cells) and inflammatory CAFs and induce the formation of pre-metastatic niches in hepatic tissue (Allenson et al. 2017; Capello et al. 2019; Han and Duan 2019). The supernatant medium of 3D co-culture organoids can be harvested, stored and used to analyse the concentration of exosomes, mRNA content and exosomal markers (Khushman et al. 2019; Mikamori et al. 2017). 2D pancreatic cancer cells could be treated with supernatant medium from organoid cultures and examined on their chemoresistance towards cytotoxic agents like gemcitabine and paclitaxel, as well as on the development of cancer stem cells and cancer-initiating cells (Stefanius et al. 2019; Valcz et al. 2020).

Utilized compounds not included in this thesis are the nucleolipids, a class of promising substances with potential anticancer activity and chemotherapeutic efficacy on glioblastoma cells (Rosemeyer et al. 2019; Knies et al. 2016). The Institute of Pharmaceutical Biology and Biotechnology received multiple derivatives, synthesized by the Institute of Chemistry of New Materials of the University of Osnabrück, in cooperation with Professor Helmut Rosemeyer and Mona Lünswilken, which were screened on Panc-1 cells via the CellTiter-Glo assay by Shaliny Sothyratnam as part of her bachelor thesis (Sothyratnam 2020). These compounds were not screened on PSC cells or 3D organoids, remaining to be conducted.

8 Appendix

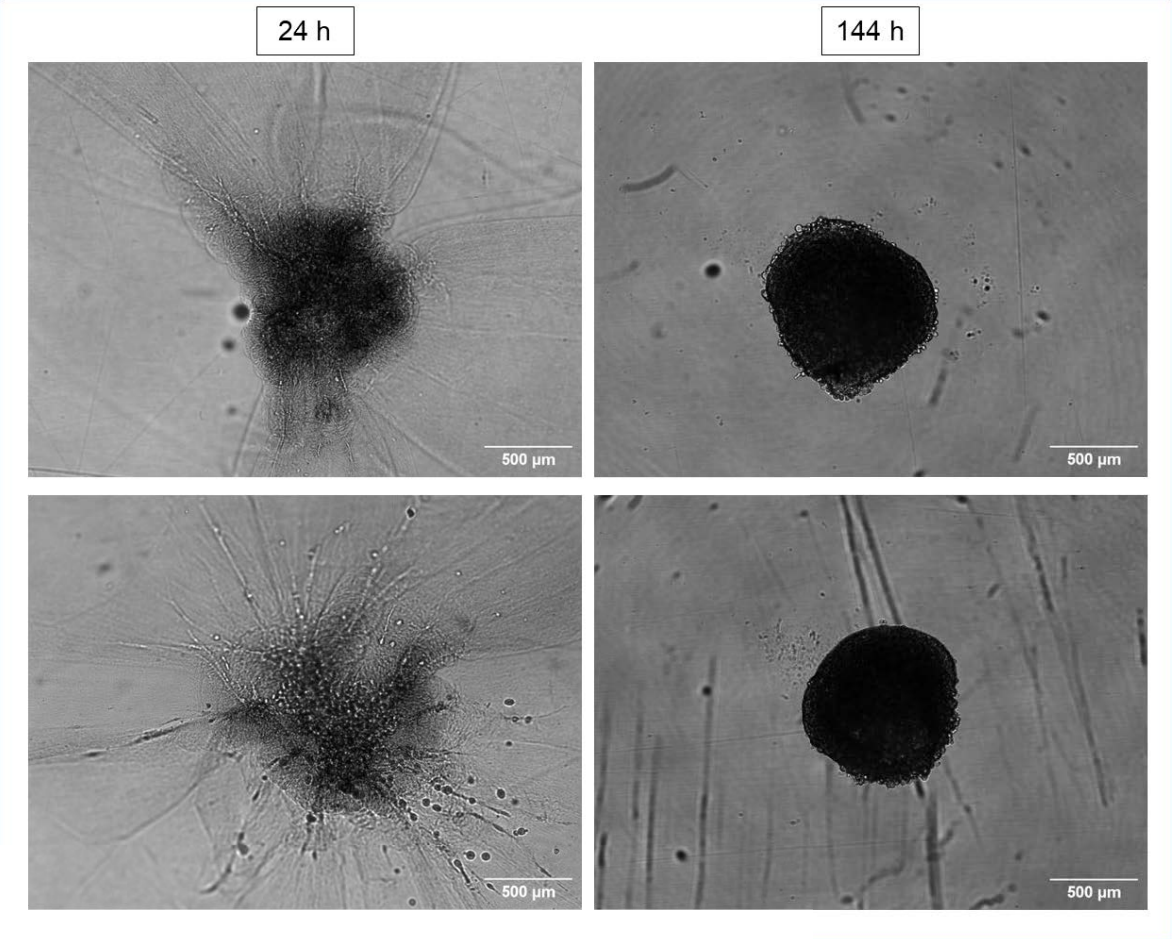

Figure 60. Organoid growth over the course of 144 hours on 96-well ULA plates (Greiner Cat. #650970). Two Panc-1 + KU0020 PSC organoids on the same plate are depicted, 24 hours (left images) and 144 hours (right images) after seeding. The pancreatic stellate cells (PSCs) can be seen migrating towards the inner core of the organoid, together with the collagen-1 matrix spread out around the tumour mass. Images recorded with the Axio Vert.A1 microscope and edited with ImageJ. Scale of reference: 500 µm.

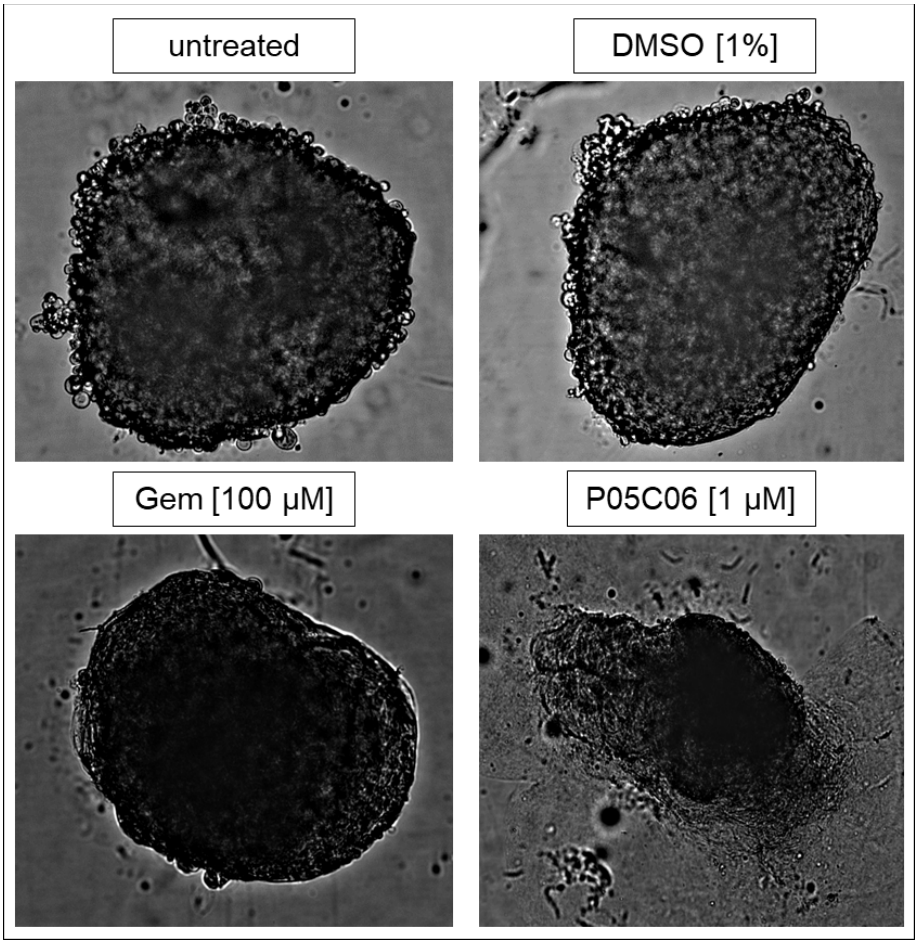

Figure 61. Exemplary images of four Panc-1 + KU0020 PSC organoids cultivated on 96-well ULA (Greiner Cat. #650970) plates for 144 hours (six days) following manual seeding. Organoids were subjected to drug treatment (72 hours of incubation) on day 4. DMSO (1 % solvent control) had no adverse effect on organoid growth, while gemcitabine (100 µM) halted cell proliferation significantly, and P05C06/*O*-methyltylophorinidine (1000 nM) induced cell death and the disruption of the organoid. Images recorded with the Axio Vert.A1 microscope and edited with ImageJ.

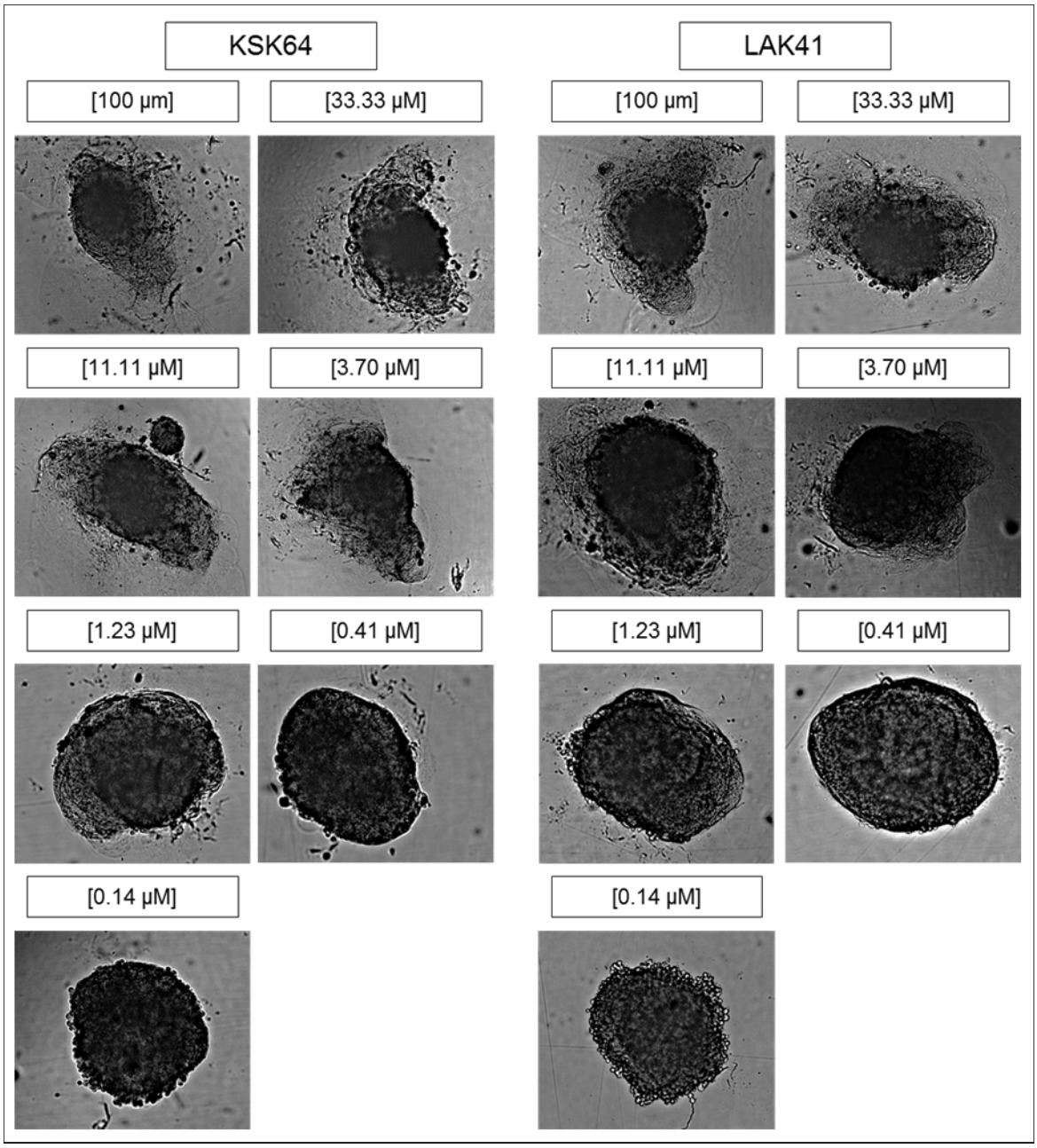

Figure 62. Exemplary images of a dose-response curve (DRC) for cytotoxicity assays. Organoids were manually cultivated and treated with seven decreasing concentrations of the two potent HDAC inhibitors KSK64 (left) and LAK41 (right), from 100 to 0.14 µM (1:3 steps). One organoid per substance concentration. Cytotoxic effects of KSK64 and LAK41 at 100 to 1.23 µM are observable and detectable. Images recorded with the Axio Vert.A1 microscope and edited with ImageJ.

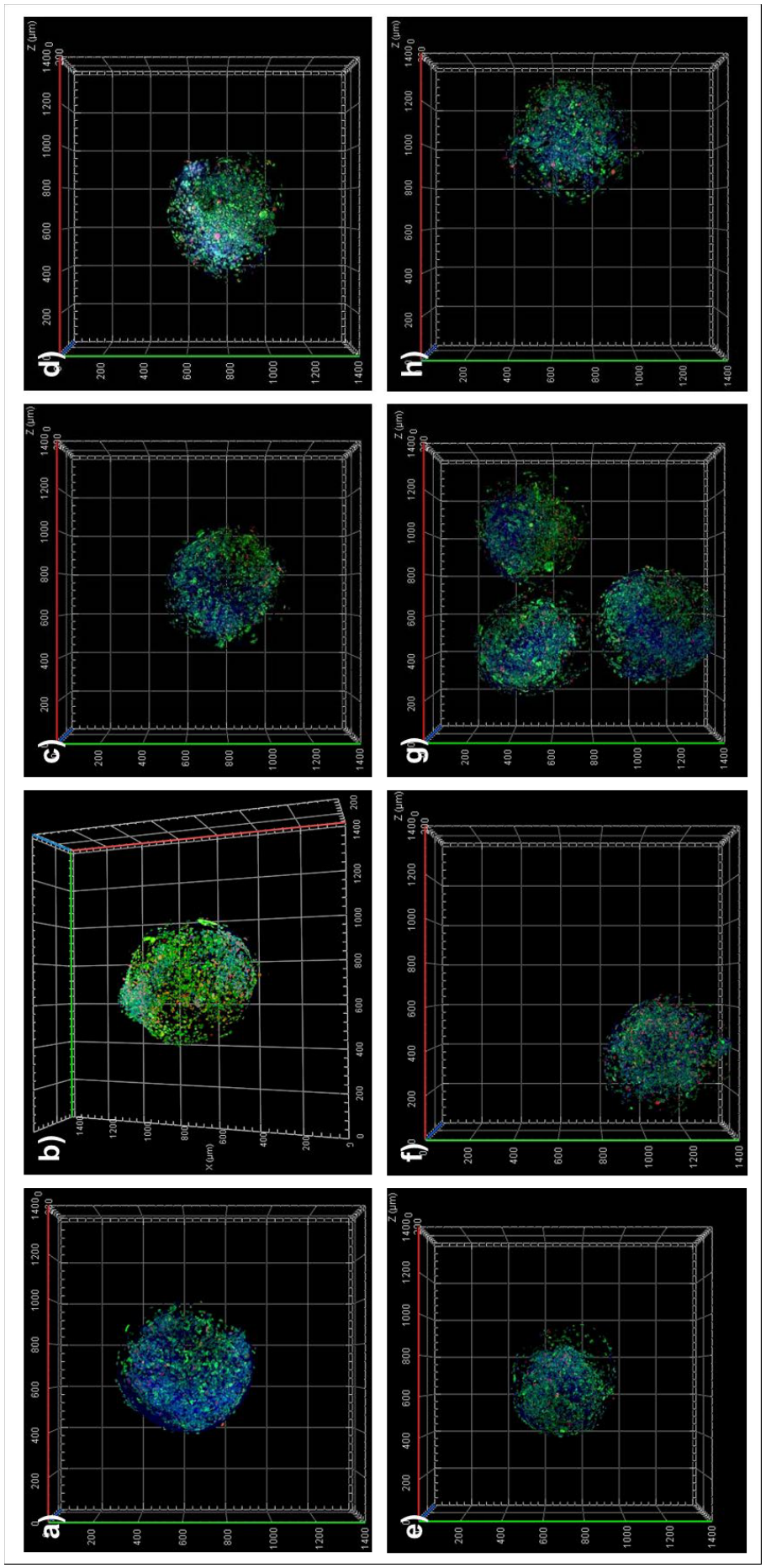
a)
b)
c)
d)
e)
f)
g)
h)
Z (µm)
X (µm)

Figure 63. PDAC organoids cultured with Panc-1 cells and either pancreatic (PSC) or hepatic stellate cells (HSC). Staining with fluorescent antibodies against Ki67 (546 nm channel, red), p53 (488 nm channel, green) and DAPI (405 nm channel, blue). Rendering of ca. 100 recorded slices (depending on organoid), with one slice representing 1 µm of height. A) Panc-1 + KU0020 PSC organoid (untreated); b) Panc-1 + NCC06 HSC-P organoid (untreated); c) Panc-1 + KU0020 PSC organoid treated with DMSO (0.2 %); d) Panc-1 + NCC06 HSC-P organoid treated with DMSO (0.2 %); e) Panc-1 + KU0020 PSC organoid treated with DMSO (0.7 %); f) Panc-1 + NCC06 HSC-P organoid treated with DMSO (0.7 %); g) three Panc-1 + KU0020 PSC organoids treated with DMSO (1 %); h) Panc-1 + NCC06 HSC-P organoid treated with DMSO (1 %). Treatment was conducted on day 4 of cultivation and lasted for 72 hours. Reference scales in µm. Images recorded with an image size of 512x512 pixels and a bit depth of 8 bit via the ZEISS LSM 880 Airy Scan microscope (Carl Zeiss AG) and edited with the ZEISS ZEN 3.6 (blue) software.

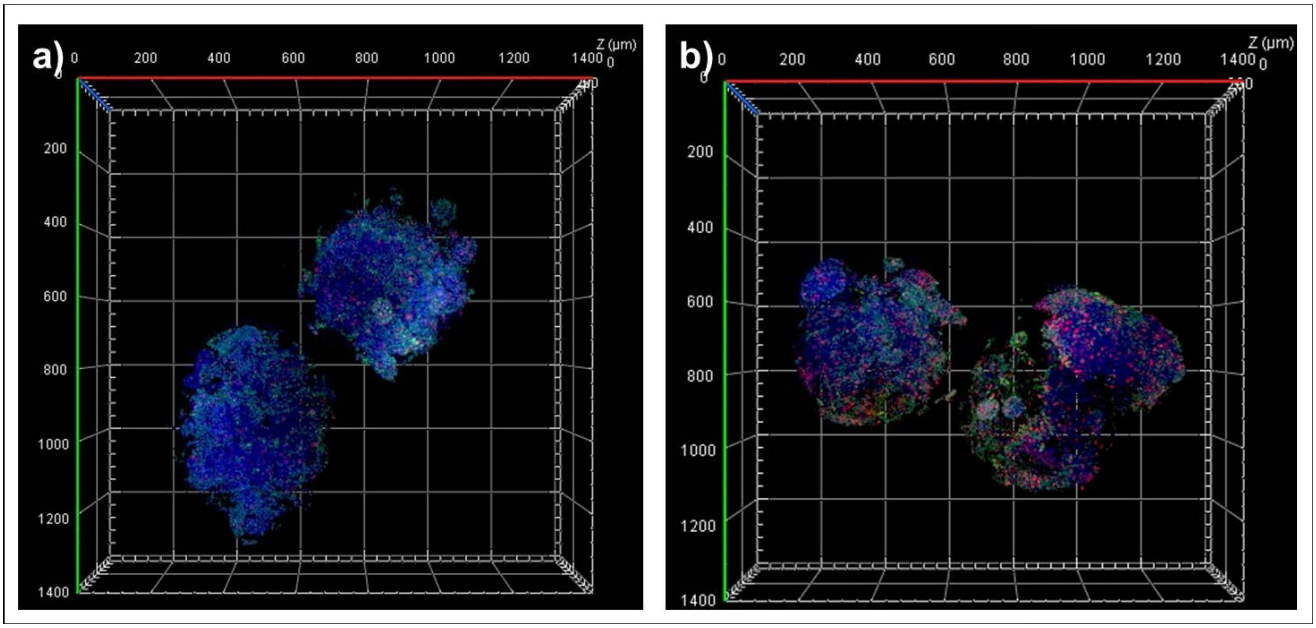

Figure 64. PDAC organoids cultured with Capan-2 cells and either pancreatic (PSC) or hepatic stellate cells (HSC). Staining with fluorescent antibodies against Ki67 (546 nm channel, red), p53 (488 nm channel, green) and DAPI (405 nm channel, blue). Rendering of ca. 100 recorded slices (depending on organoid), with one slice representing 1 µm of height. A) Capan-2 + KU0020 PSC organoids treated with DMSO (1 %); b) Panc-1 + NCC06 HSC-P organoids treated with DMSO (1 %). Treatment was conducted on day 4 of cultivation and lasted for 72 hours. Reference scales in µm. Images recorded with an image size of 512x512 pixels and a bit depth of 8 bit via the ZEISS LSM 880 Airy Scan microscope (Carl Zeiss AG) and edited with the ZEISS ZEN 3.6 (blue) software.

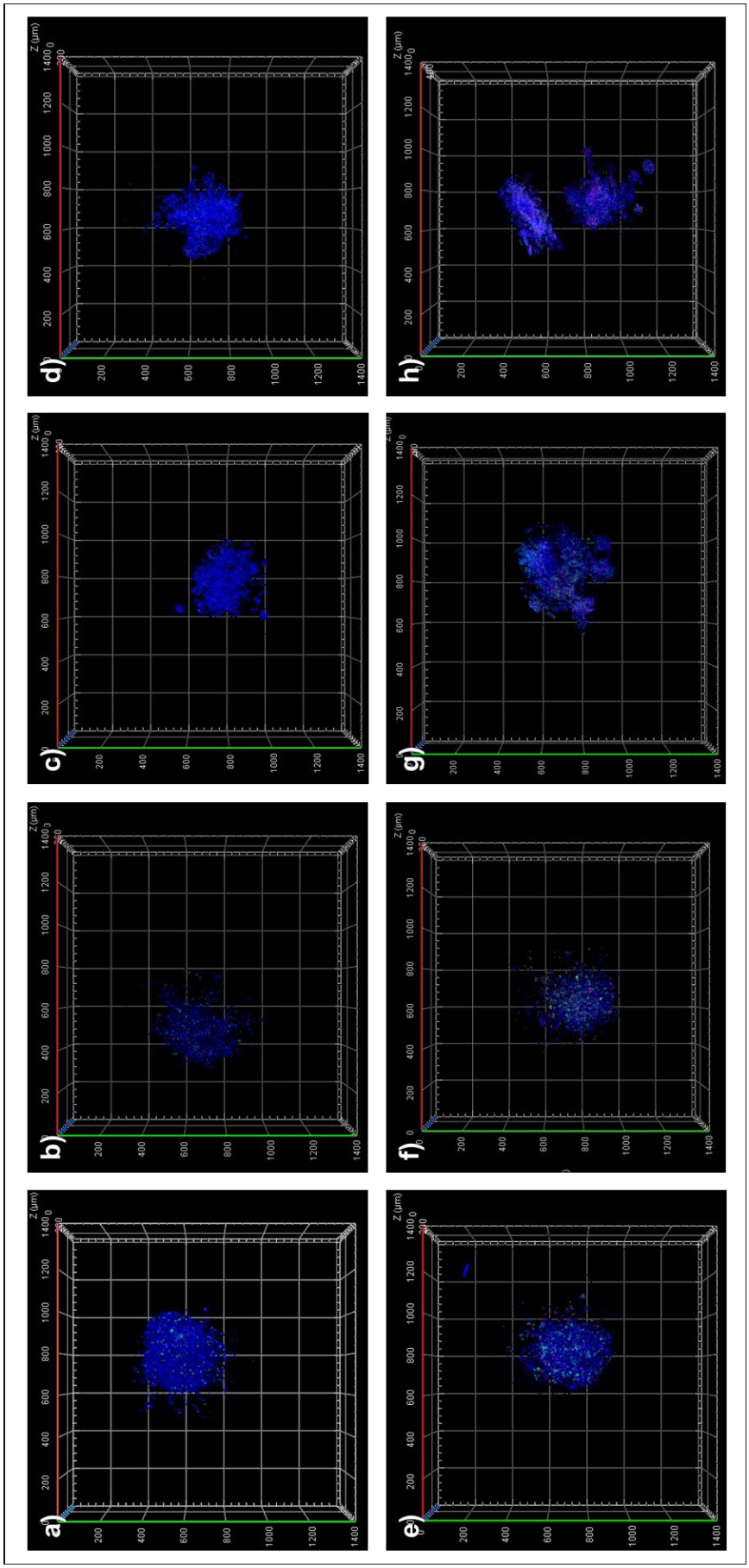
a)
b)
c)
d)
e)
f)
g)
h)
Z (µm)

Figure 65. PDAC organoids cultured with Panc-1 or Capan-2 cells and either pancreatic (PSC) or hepatic stellate cells (HSC), treated with staurosporine and *O*-methyltylophorinidine (P05C06). Staining with fluorescent antibodies against Ki67 (546 nm channel, red), p53 (488 nm channel, green) and DAPI (405 nm channel, blue). Rendering of ca. 100 recorded slices (depending on organoid), with one slice representing 1 µm of height. A) Panc-1 + KU0020 PSC organoid treated with staurosporine (10 µM); b) Panc-1 + NCC06 HSC-P organoid treated with staurosporine (10 µM); c) Capan-2 + KU0020 PSC organoid treated with staurosporine (10 µM); d) Capan-2 + NCC06 HSC-P organoid treated with staurosporine (10 µM); e) Panc-1 + KU0020 PSC organoid treated with P05C06 (1 µM); f) Panc-1 + NCC06 HSC-P organoid treated with P05C06 (1 µM); g) Capan-2 + KU0020 PSC organoids treated with P05C06 (1 µM); h) Capan-2 + NCC06 HSC-P organoid treated with P05C06 (1 µM). Treatment was conducted on day 4 of cultivation and lasted for 72 hours. Reference scales in µm. Images recorded with an image size of 512x512 pixels and a bit depth of 8 bit via the ZEISS LSM 880 Airy Scan microscope (Carl Zeiss AG) and edited with the ZEISS ZEN 3.6 (blue) software.

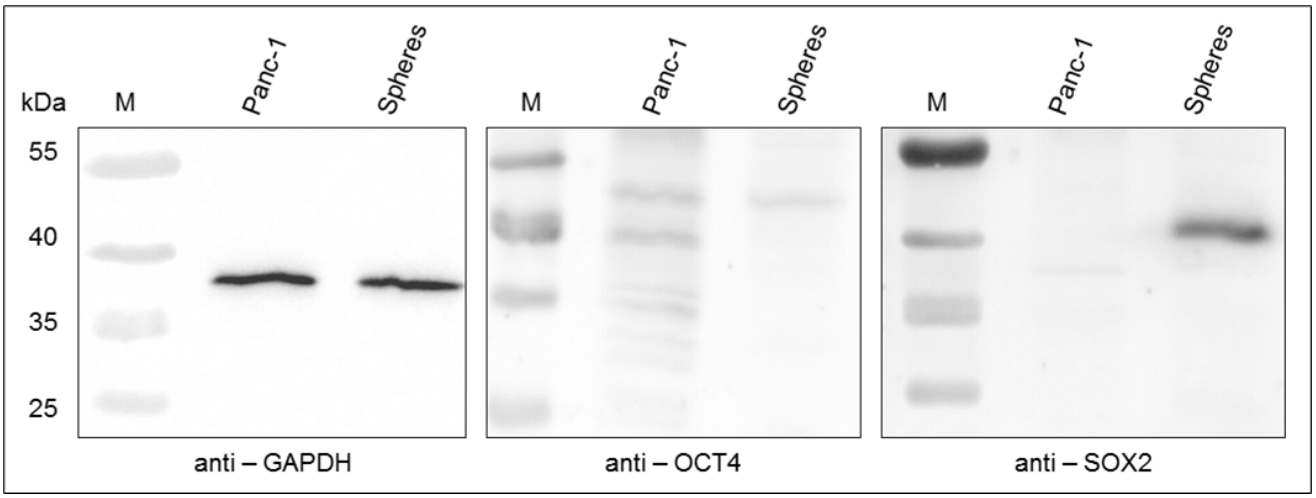

Figure 66. Expression of the stem cell markers and transcription factors Oct4 and Sox2 in Panc-1 cells and tumorspheres (derived from Panc-1). Left blot: GAPDH loading control; middle blot: Oct4 blot; right blot: Sox2 blot. Comparison between Panc-1 (ATCC) cells (left lane) and tumorspheres (right lane) derived from Panc-1 cells (see method section 3.3.5) reveals upregulation of Sox2 in tumorsphere cells. Initial blot results.

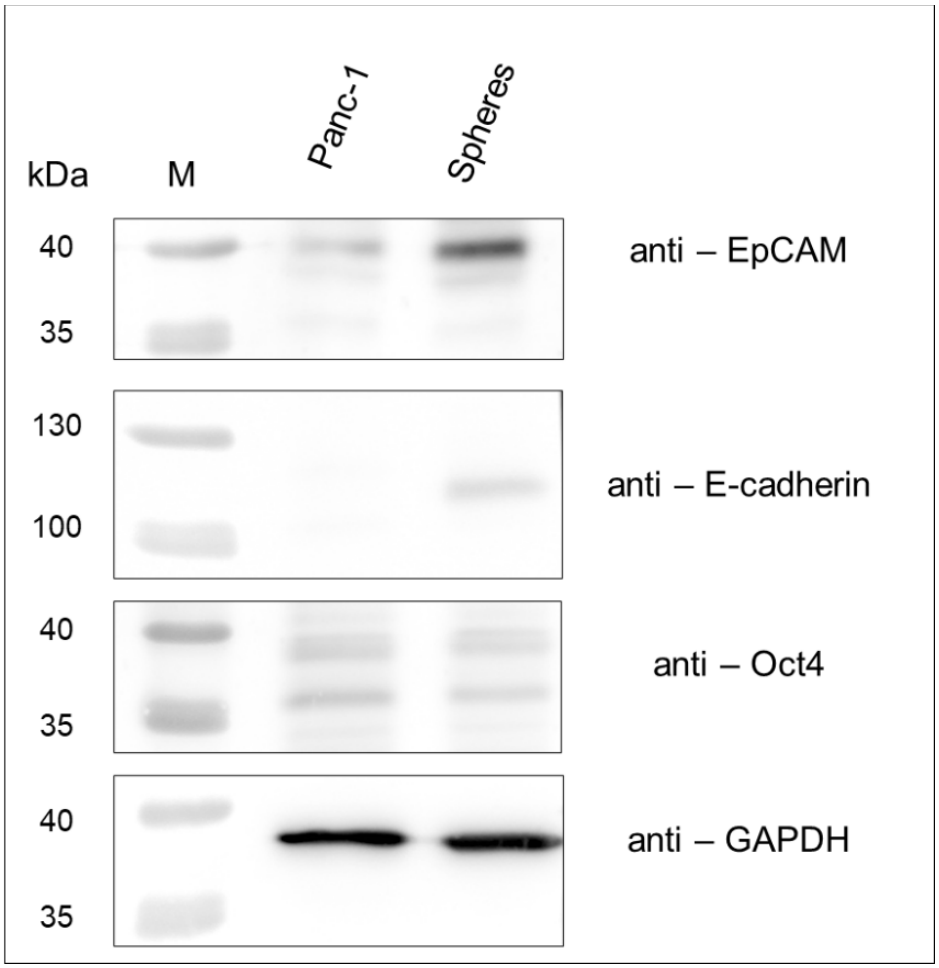

Figure 67. Expression of the EMT markers EpCAM, E-cadherin (CDH1) and the stem cell marker Oct4 in Panc-1 cells and tumorspheres (derived from Panc-1). Blot descriptions, from top to bottom: EpCAM detection, E-cadherin detection, Oct4 detection, GAPDH loading control. Comparison between Panc-1 (ATCC) cells (left lane) and tumorspheres (right lane) derived from Panc-1 cells (see method section 3.3.5) reveals upregulation of E-cadherin and EpCAM in tumorsphere cells.

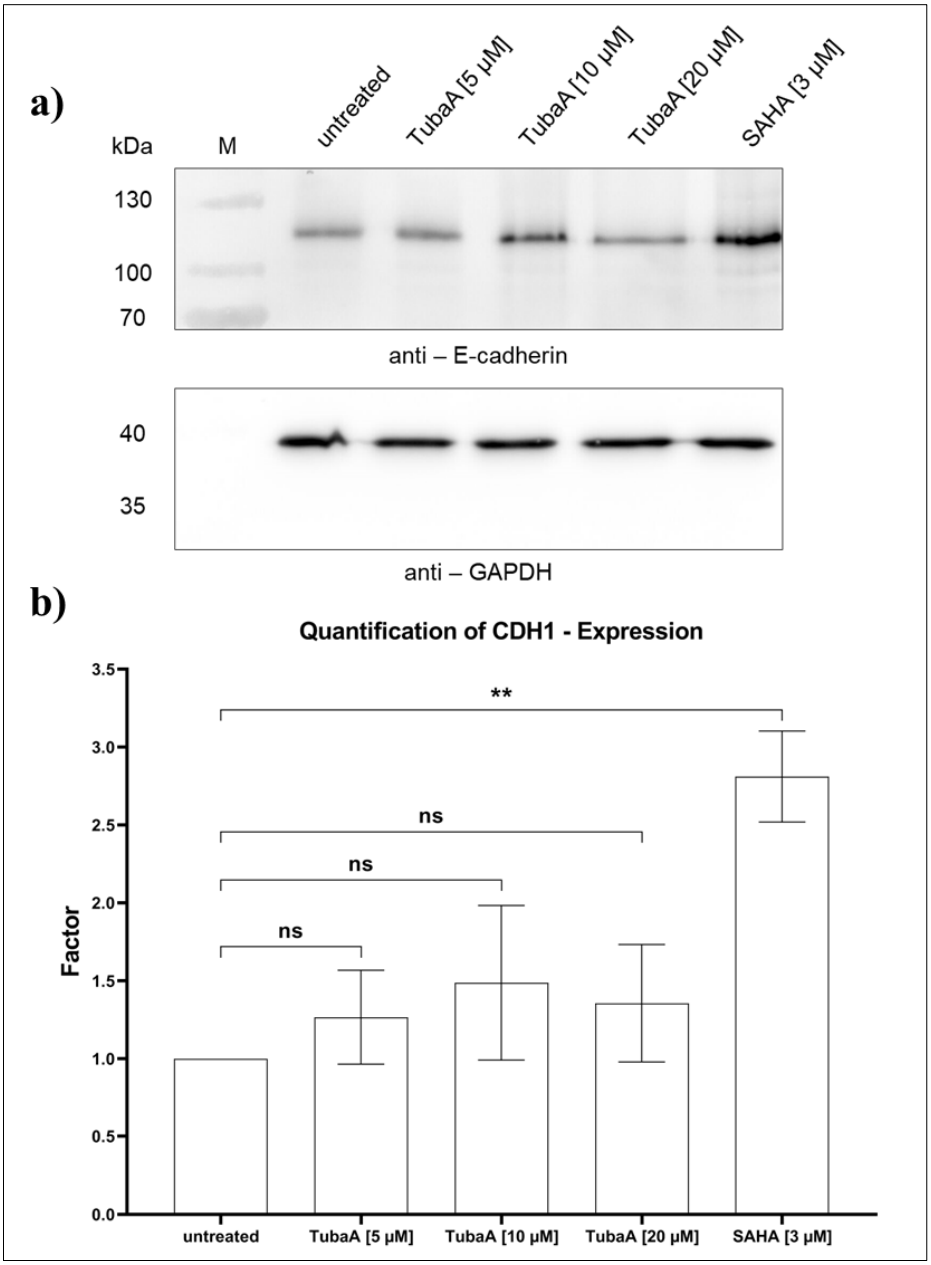

Figure 68. Treatment of Panc-1 cells with the established HDAC6 inhibitor tubastatin A only resulted in minimal and non-significant upregulation of the epithelial marker protein E-cadherin (CDH1). The pan-HDAC inhibitor vorinostat (SAHA) served as the positive control. Substance treatment lasted for 24 hours. A) exemplary western blot (upper blot: CDH1; lower blot: GAPDH serving as the loading control); b) quantification of protein expression. Y-axis: factor of protein expression (normalized against the untreated control). Statistical analysis of CDH1 protein expression conducted via one-way ANOVA. The depicted columns represent the arithmetic means of three experimental repeats and their respective standard errors of the mean. Ns: non-significant; **: $p<0.001$.

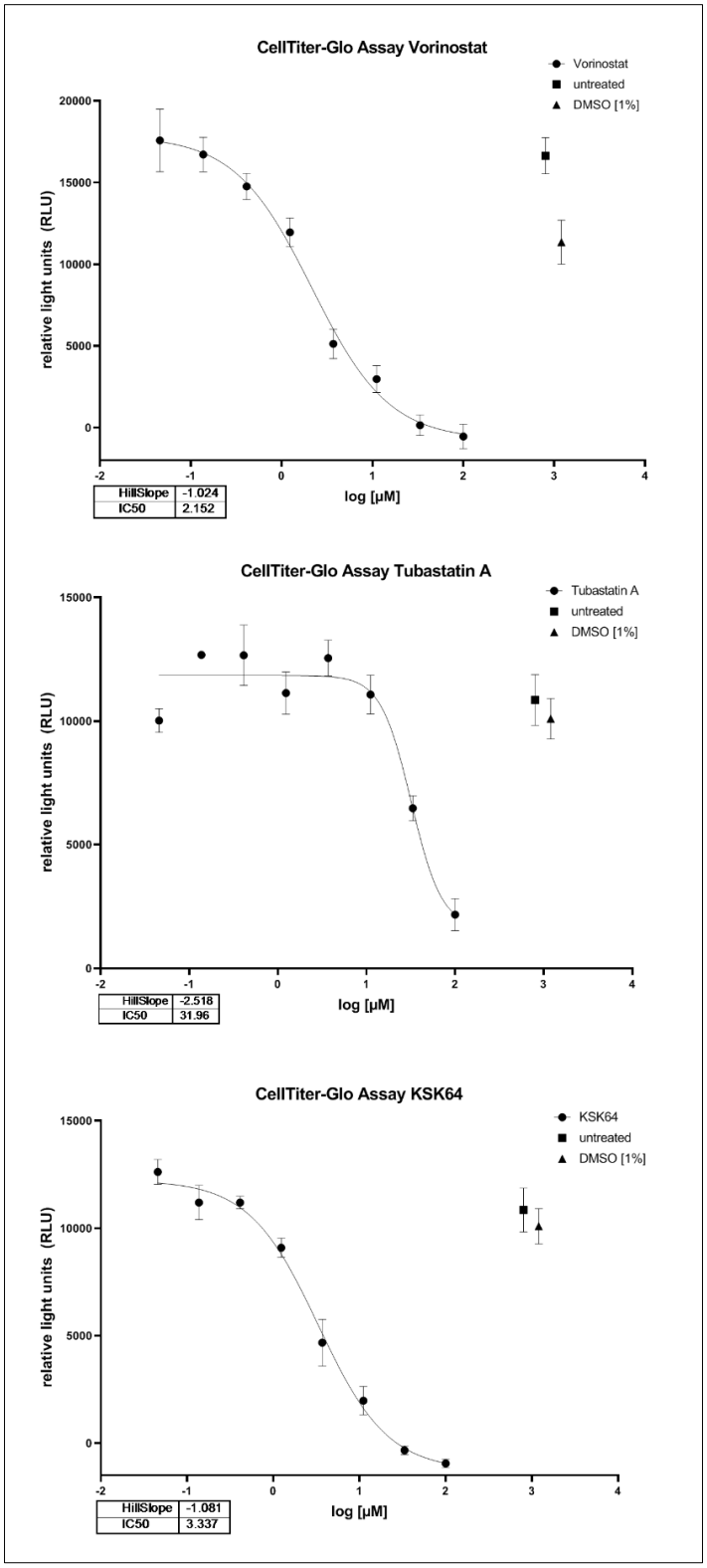

Figure 69. Cytotoxic screening of the pan-HDAC inhibitor vorinostat (SAHA), the HDAC6 inhibitor tubastatin A and the novel HDAC inhibitor KSK64 on Panc-1 (ATCC) cells. The assay was conducted on 384-well plates via automated pipetting with the CyBio Well vario pipetting robot (Analytik Jena). Exemplary dose-response curve (100 to 0.05 µM), with untreated and solvent (1 % DMSO) control. The SAHA dose-response curve served as the positive control for the 384-well plate measurement. Evaluation of cell viability conducted with the CellTiter-Glo Luminescent Cell Viability Assay

(Promega). IC_{50} values of 2.152, 31.96 and 3.337 µM were measured for SAHA, tubastatin A and KSK64 after 72 hours of substance treatment, respectively. KSK64 exhibited high cytotoxic efficacy on Panc-1 cells, comparable to SAHA, while tubastatin A exhibited low efficacy. Data points represent the arithmetic means and their respective standard deviations of quadruples.

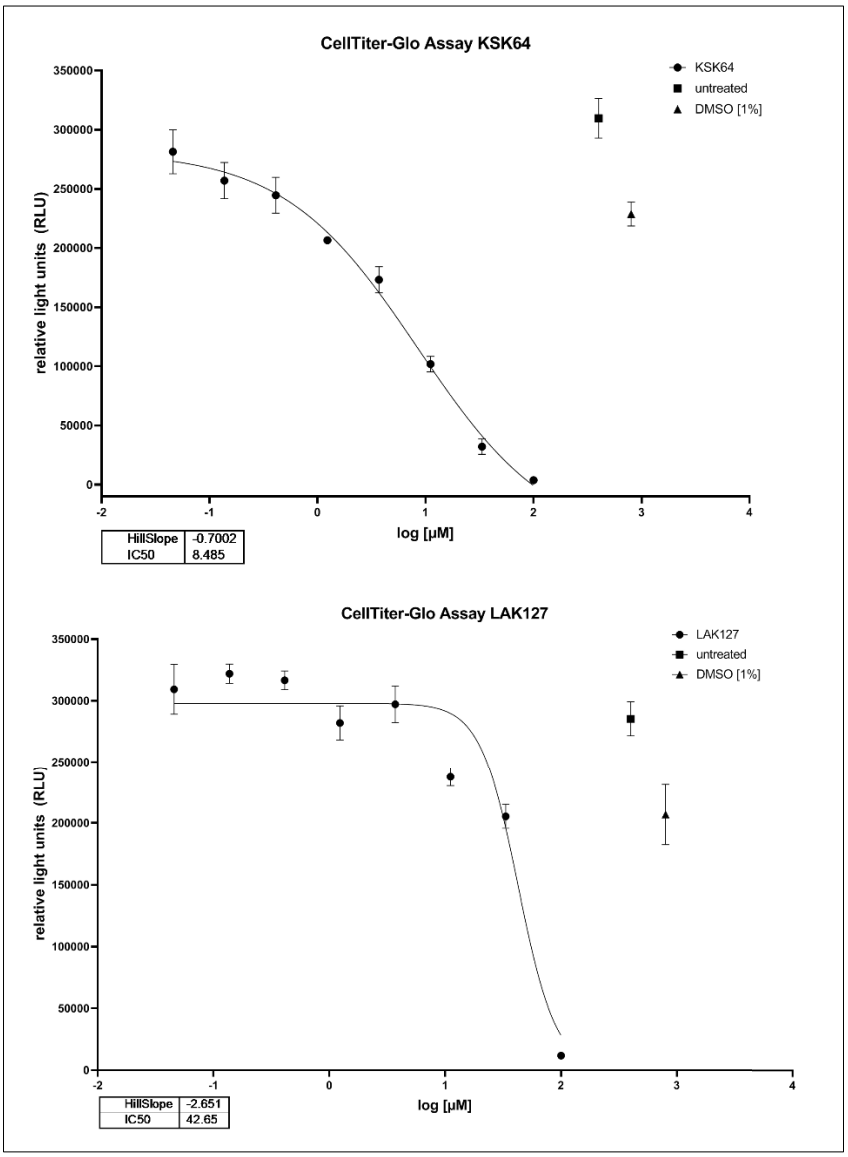

Figure 70. Cytotoxic screening of the novel HDACi drugs KSK64 and LAK127 on KU0020 PSC cells. The assay was conducted on 384-well plates via automated pipetting with the CyBio Well vario pipetting robot (Analytik Jena). Exemplary dose-response curve (100 to 0.05 µM), with untreated and solvent (1 % DMSO) control. Evaluation of cell viability conducted with the CellTiter-Glo Luminescent Cell Viability Assay (Promega). IC_{50} values of 8.485 and 42.65 µM were measured for KSK64 and LAK127 after 72 hours of substance treatment, respectively. KSK64 exhibited high cytotoxic efficacy on Panc-1 cells, while LAK127 exhibited low efficacy. Data points represent the arithmetic means and their respective standard deviations of quadruples.

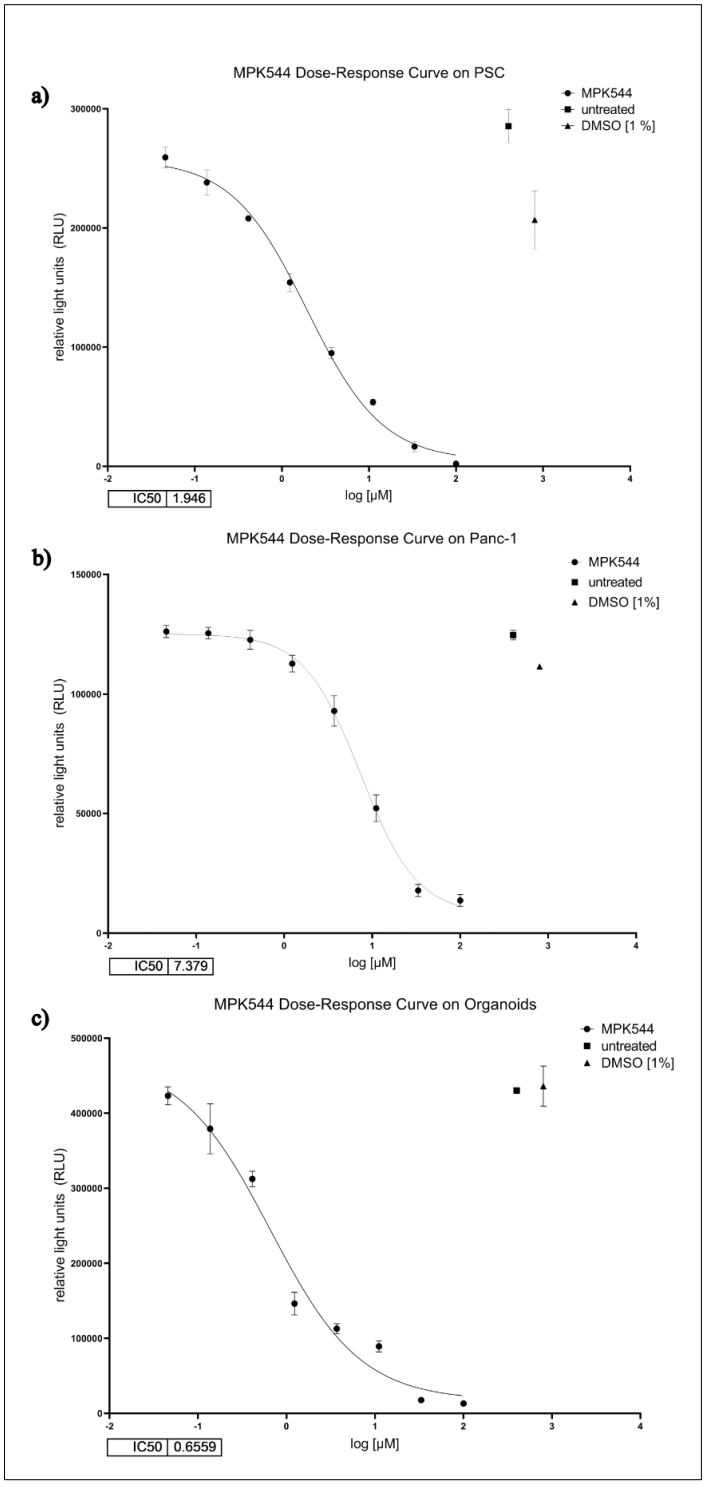

Figure 71. Cytotoxic drug screening of the potent HDAC inhibitor MPK544 on different PDAC models. Exemplary dose-response curves (100 to 0.14 µM) on a) Panc-1 cells, b) KU0020 PSC cells and c) Panc-1 + PSC organoids. Only the untreated and solvent controls (DMSO 1 %) are present in this layout, as MPK544 itself was utilized as the positive control for each 384-well plate measurement with the CellTiter-Glo cell viability assays (Promega). IC_{50} values of 1.946, 7.379 and 0.6559 µM were measured for MPK544 on Panc-1 cells, PSC cells and organoids after 72 hours of substance treatment, respectively. MPK544 showcased high cytotoxic efficacy on all three PDAC models. Depicted values represent the arithmetic mean and standard deviation of quadruples.

9 Bibliography

Adams, Ralf H.; Alitalo, Kari (2007): Molecular regulation of angiogenesis and lymphangiogenesis. In *Nature reviews. Molecular cell biology* 8 (6), pp. 464–478. DOI: 10.1038/nrm2183.

Aghdassi, Ali; Sendler, Matthias; Guenther, Annett; Mayerle, Julia; Behn, Claas-Olsen; Heidecke, Claus-Dieter et al. (2012): Recruitment of histone deacetylases HDAC1 and HDAC2 by the transcriptional repressor ZEB1 downregulates E-cadherin expression in pancreatic cancer. In *Gut* 61 (3), pp. 439–448. DOI: 10.1136/gutjnl-2011-300060.

Ahuja, Nidhi; Schwer, Bjoern; Carobbio, Stefania; Waltregny, David; North, Brian J.; Castronovo, Vincenzo et al. (2007): Regulation of insulin secretion by SIRT4, a mitochondrial ADP-ribosyltransferase. In *The Journal of biological chemistry* 282 (46), pp. 33583–33592. DOI: 10.1074/jbc.M705488200.

Allenson, K.; Castillo, J.; San Lucas, F. A.; Scelo, G.; Kim, D. U.; Bernard, V. et al. (2017): High prevalence of mutant KRAS in circulating exosome-derived DNA from early-stage pancreatic cancer patients. In *Annals of oncology : official journal of the European Society for Medical Oncology* 28 (4), pp. 741–747. DOI: 10.1093/annonc/mdx004.

Altschul, S. F.; Madden, T. L.; Schäffer, A. A.; Zhang, J.; Zhang, Z.; Miller, W.; Lipman, D. J. (1997): Gapped BLAST and PSI-BLAST: a new generation of protein database search programs. In *Nucleic acids research* 25 (17), pp. 3389–3402. DOI: 10.1093/nar/25.17.3389.

Altschul, Stephen F.; Gish, Warren; Miller, Webb; Myers, Eugene W.; Lipman, David J. (1990): Basic Local Alignment Search Tool. In *Journal of molecular biology* (215), pp. 403–410.

Alves Avelar, Leandro A.; Schrenk, Christian; Sönnichsen, Melf; Hamacher, Alexandra; Hansen, Finn K.; Schliehe-Diecks, Julian et al. (2021): Synergistic induction of apoptosis in resistant head and neck carcinoma and leukemia by alkoxyamide-based histone deacetylase inhibitors. In *European journal of medicinal chemistry* 211, p. 113095. DOI: 10.1016/j.ejmech.2020.113095.

Amrutkar, Manoj; Aasrum, Monica; Verbeke, Caroline S.; Gladhaug, Ivar P. (2019): Secretion of fibronectin by human pancreatic stellate cells promotes chemoresistance to gemcitabine in pancreatic cancer cells. In *BMC cancer* 19 (1), p. 596. DOI: 10.1186/s12885-019-5803-1.

Amrutkar, Manoj; Berg, Kjersti; Balto, Aina; Skilbrei, Miguel G.; Finstadsveen, Anette V.; Aasrum, Monica et al. (2023): Pancreatic stellate cell-induced gemcitabine resistance in pancreatic cancer is associated with LDHA- and MCT4-mediated enhanced glycolysis. In *Cancer cell international* 23 (1), p. 9. DOI: 10.1186/s12935-023-02852-7.

Amrutkar, Manoj; Gladhaug, Ivar P. (2017): Pancreatic Cancer Chemoresistance to Gemcitabine. In *Cancers* 9 (11), p. 157. DOI: 10.3390/cancers9110157.

Asfaha, Yodita; Schrenk, Christian; Alves Avelar, Leandro A.; Hamacher, Alexandra; Pflieger, Marc; Kassack, Matthias U.; Kurz, Thomas (2019): Recent advances in class IIa histone deacetylases research. In *Bioorganic & medicinal chemistry* 27 (22), p. 115087. DOI: 10.1016/j.bmc.2019.115087.

Askan, Gokce; Sahin, Ibrahim Halil; Chou, Joanne F.; Yavas, Aslihan; Capanu, Marinela; Iacobuzio-Donahue, Christine A. et al. (2021): Pancreatic cancer stem cells may define tumor stroma characteristics and recurrence patterns in pancreatic ductal adenocarcinoma. In *BMC cancer* 21 (1), p. 385. DOI: 10.1186/s12885-021-08123-w.

Bae, Jooeun; Hideshima, Teru; Tai, Yu-Tzu; Song, Yan; Richardson, Paul; Raje, Noopur et al. (2018): Histone deacetylase (HDAC) inhibitor ACY241 enhances anti-tumor activities of antigen-specific central memory cytotoxic T lymphocytes against multiple myeloma and solid tumors. In *Leukemia* 32 (9), pp. 1932–1947. DOI: 10.1038/s41375-018-0062-8.

Bailey, Peter; Chang, David K.; Nones, Katia; Johns, Amber L.; Patch, Ann-Marie; Gingras, Marie-Claude et al. (2016): Genomic analyses identify molecular subtypes of pancreatic cancer. In *Nature* 531 (7592), pp. 47–52. DOI: 10.1038/nature16965.

Balamurugan, Kuppusamy (2016): HIF-1 at the crossroads of hypoxia, inflammation, and cancer. In *International journal of cancer* 138 (5), pp. 1058–1066. DOI: 10.1002/ijc.29519.

Barton, C. M.; Staddon, S. L.; Hughes, C. M.; Hall, P. A.; O'Sullivan, C.; Klöppel, G. et al. (1991): Abnormalities of the p53 tumour suppressor gene in human pancreatic cancer. In *Br J Cancer* 64 (6), pp. 1076–1082. DOI: 10.1038/bjc.1991.467.

Basso, Daniela; Gnatta, Elisa; Padoan, Andrea; Fogar, Paola; Furlanello, Sara; Aita, Ada et al. (2017): PDAC-derived exosomes enrich the microenvironment in MDSCs in a SMAD4-dependent manner through a new calcium related axis. In *Oncotarget* 8 (49), pp. 84928–84944. DOI: 10.18632/oncotarget.20863.

Batabyal, Pikli; Vander Hoorn, Stephen; Christophi, Christopher; Nikfarjam, Mehrdad (2014): Association of diabetes mellitus and pancreatic adenocarcinoma: a meta-analysis of 88 studies. In *Annals of surgical oncology* 21 (7), pp. 2453–2462. DOI: 10.1245/s10434-014-3625-6.

Becker, Andrew E.; Hernandez, Yasmin G.; Frucht, Harold; Lucas, Aimee L. (2014): Pancreatic ductal adenocarcinoma. Risk factors, screening, and early detection. In *World journal of gastroenterology* 20 (32), pp. 11182–11198. DOI: 10.3748/wjg.v20.i32.11182.

Begum, Asma; Ewachiw, Theodore; Jung, Clinton; Huang, Ally; Norberg, K. Jessica; Marchionni, Luigi et al. (2017): The extracellular matrix and focal adhesion kinase signaling regulate cancer stem cell function in pancreatic ductal adenocarcinoma. In *PLoS ONE* 12 (7), e0180181. DOI: 10.1371/journal.pone.0180181.

Bengtsson, Axel; Andersson, Roland; Ansari, Daniel (2020): The actual 5-year survivors of pancreatic ductal adenocarcinoma based on real-world data. In *Sci Rep* 10 (1), p. 16425. DOI: 10.1038/s41598-020-73525-y.

Bengtsson, Axel; Andersson, Roland; Rahm, Jonas; Ganganna, Karthik; Andersson, Bodil; Ansari, Daniel (2021): Organoid technology for personalized pancreatic cancer therapy. In *Cellular oncology (Dordrecht)* 44 (2), pp. 251–260. DOI: 10.1007/s13402-021-00585-1.

Bernard, Vincent; Semaan, Alexander; Huang, Jonathan; San Lucas, F. Anthony; Mulu, Feven C.; Stephens, Bret M. et al. (2019): Single-Cell Transcriptomics of Pancreatic Cancer Precursors Demonstrates Epithelial and Microenvironmental Heterogeneity as an Early Event in Neoplastic Progression. In *Clinical cancer research : an official journal of the American Association for Cancer Research* 25 (7), pp. 2194–2205. DOI: 10.1158/1078-0432.CCR-18-1955.

Bianchi, V.; Borella, S.; Calderazzo, F.; Ferraro, P.; Chieco Bianchi, L.; Reichard, P. (1994): Inhibition of ribonucleotide reductase by 2'-substituted deoxycytidine analogs: possible application in AIDS treatment. In *Proceedings of the National Academy of Sciences of the United States of America* 91 (18), pp. 8403–8407. DOI: 10.1073/pnas.91.18.8403.

Blanchard II., John A.; Barve, Shirish; Joshi-Barve, Swati; Talwalker, Ramesh; Gates Jr., Lawrence K. (2000): Cytokine Production by CAPAN-1 and CAPAN-2 Cell Lines. In *Digestive Diseases and Sciences* 45 (5), pp. 927–932.

Bold, Christina (2022): Photochemische Transformation eines pharmakologisch aktiven Naturstoffs: Ein neuer, lichtinduzierter Ansatz zur Aktivierung von Artemisinin. Inaugural-Dissertation. Universität Köln, Köln.

Bouwens, L. (1998): Cytokeratins and cell differentiation in the pancreas. In *J. Pathol.* 184 (3), pp. 234–239. DOI: 10.1002/(SICI)1096-9896(199803)184:3<234::AID-PATH28>3.0.CO;2-D.

Bradner, James E.; West, Nathan; Grachan, Melissa L.; Greenberg, Edward F.; Haggarty, Stephen J.; Warnow, Tandy; Mazitschek, Ralph (2010): Chemical phylogenetics of histone deacetylases. In *Nature chemical biology* 6 (3), pp. 238–243. DOI: 10.1038/nchembio.313.

Bradney, Michael J.; Venis, Stephanie M.; Yang, Yi; Konieczny, Stephen F.; Han, Bumsoo (2020): A Biomimetic Tumor Model of Heterogeneous Invasion in Pancreatic Ductal Adenocarcinoma. In *Small* 16 (10), e1905500. DOI: 10.1002/smll.201905500.

Breslin, Susan; O'Driscoll, Lorraine (2016): The relevance of using 3D cell cultures, in addition to 2D monolayer cultures, when evaluating breast cancer drug sensitivity and resistance. In *Oncotarget* 7 (29), pp. 45745–45756. DOI: 10.18632/oncotarget.9935.

Brewer, Gregory J.; Torricelli, John; Evege, Ethel K.; Price, Paul J. (1994): NEUROBASAL™ MEDIUM/B27 SUPPLEMENT: A NEW SERUM–FREE MEDIUM COMBINATION FOR SURVIVAL OF NEURONS. In *Focus* 16 (1).

Broutier, Laura; Andersson-Rolf, Amanda; Hindley, Christopher J.; Boj, Sylvia F.; Clevers, Hans; Koo, Bon-Kyoung; Huch, Meritxell (2016): Culture and establishment of self-renewing human and mouse adult liver and pancreas 3D organoids and their genetic manipulation. In *Nature protocols* 11 (9), pp. 1724–1743. DOI: 10.1038/nprot.2016.097.

Bryant, Kirsten L.; Mancias, Joseph D.; Kimmelman, Alec C.; Der, Channing J. (2014): KRAS: feeding pancreatic cancer proliferation. In *Trends in Biochemical Sciences* 39 (2), pp. 91–100. DOI: 10.1016/j.tibs.2013.12.004.

Bu, Luke; Baba, Hideo; Yoshida, Naoya; Miyake, Keisuke; Yasuda, Tadahito; Uchihara, Tomoyuki et al. (2019): Biological heterogeneity and versatility of cancer-associated fibroblasts in the tumor microenvironment. In *Oncogene* 38 (25), pp. 4887–4901. DOI: 10.1038/s41388-019-0765-y.

Bulle, Ashenafi; Dekervel, Jeroen; Deschuttere, Lise; Nittner, David; Libbrecht, Louis; Janky, Rekin's et al. (2020): Gemcitabine Recruits M2-Type Tumor-Associated Macrophages into the Stroma of Pancreatic Cancer. In *Translational oncology* 13 (3), p. 100743. DOI: 10.1016/j.tranon.2020.01.004.

Burris III, Howard A.; Moore, Malcolm J.; Andersen, John; Green, Mark R.; Rothenberg, Mace L.; Modiano, Manuel R. et al. (1997): Improvements in Survival and Clinical Benefit With Gemcitabine as First-Line Therapy for Patients With Advanced Pancreas Cancer: A Randomized Trial. In *Journal of clinical oncology* 15 (6).

Burstin, Johannes von; Eser, Stefan; Paul, Mariel C.; Seidler, Barbara; Brandl, Martina; Messer, Marlena et al. (2009): E-cadherin regulates metastasis of pancreatic cancer in vivo and is suppressed by a SNAIL/HDAC1/HDAC2 repressor complex. In *Gastroenterology* 137 (1), 361-71, 371.e1-5. DOI: 10.1053/j.gastro.2009.04.004.

Butler, Kyle V.; Kalin, Jay; Brochier, Camille; Vistoli, Guilio; Langley, Brett; Kozikowski, Alan P. (2010): Rational design and simple chemistry yield a superior, neuroprotective HDAC6 inhibitor, tubastatin A. In *J. Am. Chem. Soc.* 132 (31), pp. 10842–10846. DOI: 10.1021/ja102758v.

Cai, Mao-Hua; Xu, Xiao-Gang; Yan, Shi-Li; Sun, Ze; Ying, Yin; Wang, Bai-Kui; Tu, Yue-Xing (2018): Depletion of HDAC1, 7 and 8 by Histone Deacetylase Inhibition Confers Elimination of Pancreatic Cancer Stem Cells in Combination with Gemcitabine. In *Scientific reports* 8 (1), p. 1621. DOI: 10.1038/s41598-018-20004-0.

Cai, Xing Fu; Jin, Xuejun; Lee, Dongho; Yang, Young Taek; Lee, Kyeong; Hong, Young-Soo et al. (2006): Phenanthroquinolizidine alkaloids from the roots of Boehmeria pannosa potently inhibit hypoxia-inducible factor-1 in AGS human gastric cancer cells. In *Journal of natural products* 69 (7), pp. 1095–1097. DOI: 10.1021/np060081y.

Calvo, Fernando; Ege, Nil; Grande-Garcia, Araceli; Hooper, Steven; Jenkins, Robert P.; Chaudhry, Shahid I. et al. (2013): Mechanotransduction and YAP-dependent matrix remodelling is required for the generation and maintenance of cancer-associated fibroblasts. In *Nature cell biology* 15 (6), pp. 637–646. DOI: 10.1038/ncb2756.

Cannon, Andrew; Thompson, Christopher; Hall, Bradley R.; Jain, Maneesh; Kumar, Sushil; Batra, Surinder K. (2018): Desmoplasia in pancreatic ductal adenocarcinoma: insight into pathological function and therapeutic potential. In *Genes & cancer* 9 (3-4), pp. 78–86. DOI: 10.18632/genesandcancer.171.

Cao, Lu; Zhou, Yanming; Zhai, Beibei; Liao, Jian; Xu, Wen; Zhang, Ruixiu et al. (2011): Sphere-forming cell subpopulations with cancer stem cell properties in human hepatoma cell lines. In *BMC gastroenterology* 11, p. 71. DOI: 10.1186/1471-230X-11-71.

Capello, Michela; Vykoukal, Jody V.; Katayama, Hiroyuki; Bantis, Leonidas E.; Wang, Hong; Kundnani, Deepali L. et al. (2019): Exosomes harbor B cell targets in pancreatic adenocarcinoma and

exert decoy function against complement-mediated cytotoxicity. In *Nature communications* 10 (1), p. 254. DOI: 10.1038/s41467-018-08109-6.

Cavaco, Ana C. Martins; Eble, Johannes A. (2019): A 3D Spheroid Model as a More Physiological System for Cancer-Associated Fibroblasts Differentiation and Invasion In Vitro Studies. In *Journal of visualized experiments : JoVE* (150). DOI: 10.3791/60122.

Chazotte, Brad (2011): Labeling nuclear DNA with hoechst 33342. In *Cold Spring Harb Protoc* 2011 (1), pdb.prot5557. DOI: 10.1101/pdb.prot5557.

Chen, Cheng-Yu; Zhu, Guo-Yuan; Wang, Jing-Rong; Jiang, Zhi-Hong (2016): Phenanthroindolizidine alkaloids from Tylophora atrofolliculata with hypoxia-inducible factor-1 (HIF-1) inhibitory activity. In *RSC Adv.* 6 (83), pp. 79958–79967. DOI: 10.1039/C6RA16455B.

Chen, Chi-Yuan; Yang, Shuenn-Chen; Lee, Kuo-Hsiung; Yang, Xiaoming; Wei, Lin-Yi; Chow, Lu-Ping et al. (2014): The antitumor agent PBT-1 directly targets HSP90 and hnRNP A2/B1 and inhibits lung adenocarcinoma growth and metastasis. In *Journal of medicinal chemistry* 57 (3), pp. 677–685. DOI: 10.1021/jm401686b.

Chen, Gang; Guo, Guangqi; Zhou, Xiaodong; Chen, Hongxia (2020): Potential mechanism of ferroptosis in pancreatic cancer. In *Oncology letters* 19 (1), pp. 579–587. DOI: 10.3892/ol.2019.11159.

Chen, Hua; Sun, Bei; Wang, Shuangjia; Pan, Shangha; Gao, Yue; Bai, Xuewei; Xue, Dongbo (2010): Growth inhibitory effects of dihydroartemisinin on pancreatic cancer cells: involvement of cell cycle arrest and inactivation of nuclear factor-kappaB. In *Journal of Cancer Research and Clinical Oncology* 136 (6), pp. 897–903. DOI: 10.1007/s00432-009-0731-0.

Chen, Wei; Wang, Huizhi; Liu, Yawen; Xu, Wei; Ling, Chen; Li, Yafang et al. (2019): Linc-RoR promotes proliferation, migration, and invasion via the Hippo/YAP pathway in pancreatic cancer cells. In *J Cell Biochem*. DOI: 10.1002/jcb.29308.

Chen, Xueman; Song, Erwei (2019): Turning foes to friends: Targeting cancer-associated fibroblasts. In *Nature Reviews Drug Discovery* 18 (2), p. 99. DOI: 10.1038/s41573-018-0004-1.

Cheng, Vinton; Esteves, Filomena; Chakrabarty, Aruna; Cockle, Julia; Short, Susan; Brüning-Richardson, Anke (2015): High-content analysis of tumour cell invasion in three-dimensional spheroid assays. In *Oncoscience* 2 (6), pp. 596–606. DOI: 10.18632/oncoscience.171.

Chernyavska, M.; Schmid, M.; Freitag, P. C.; Palacio-Castañeda, V.; Piruska, A.; Huck, W. T. S. et al. (2019): Unravelling Receptor and RGD Motif Dependence of Retargeted Adenoviral Vectors using Advanced Tumor Model Systems. In *Scientific reports* 9 (1), p. 18568. DOI: 10.1038/s41598-019-54939-9.

Cho, Ha Young; Lee, Sang Wu; Jeon, Yu Hyun; Lee, Dong Hoon; Kim, Go Woon; Yoo, Jung et al. (2020): Combination of ACY-241 and JQ1 Synergistically Suppresses Metastasis of HNSCC via Regulation of MMP-2 and MMP-9. In *International journal of molecular sciences* 21 (18). DOI: 10.3390/ijms21186873.

Choi, Jae-Il; Jang, Sung Ill; Hong, Jaehyun; Kim, Chul Hoon; Kwon, Soon Sung; Park, Joon Seong; Lim, Jong-Baeck (2020): Cancer-initiating cells in human pancreatic cancer organoids are maintained by interactions with endothelial cells. In *Cancer letters*. DOI: 10.1016/j.canlet.2020.10.012.

Clocchiatti, Andrea; Florean, Cristina; Brancolini, Claudio (2011): Class IIa HDACs: from important roles in differentiation to possible implications in tumourigenesis. In *Journal of cellular and molecular medicine* 15 (9), pp. 1833–1846. DOI: 10.1111/j.1582-4934.2011.01321.x.

Conroy, Thierry; Hammel, Pascal; Hebbar, Mohamed; Ben Abdelghani, Meher; Wei, Alice C.; Raoul, Jean-Luc et al. (2018): FOLFIRINOX or Gemcitabine as Adjuvant Therapy for Pancreatic Cancer. In *The New England journal of medicine* 379 (25), pp. 2395–2406. DOI: 10.1056/NEJMoa1809775.

Costa-Silva, Bruno; Aiello, Nicole M.; Ocean, Allyson J.; Singh, Swarnima; Zhang, Haiying; Thakur, Basant Kumar et al. (2015): Pancreatic cancer exosomes initiate pre-metastatic niche formation in the liver. In *Nature cell biology* 17 (6), pp. 816–826. DOI: 10.1038/ncb3169.

Crawford, Howard C.; Di Pasca Magliano, Marina; Banerjee, Sulagna (2019): Signaling Networks That Control Cellular Plasticity in Pancreatic Tumorigenesis, Progression, and Metastasis. In *Gastroenterology* 156 (7), pp. 2073–2084. DOI: 10.1053/j.gastro.2018.12.042.

Crespo, Miguel; Vilar, Eduardo; Tsai, Su-Yi; Chang, Kyle; Amin, Sadaf; Srinivasan, Tara et al. (2017): Colonic organoids derived from human induced pluripotent stem cells for modeling colorectal cancer and drug testing. In *Nature medicine* 23 (7), pp. 878–884. DOI: 10.1038/nm.4355.

Czaplinska, Dominika; Ialchina, Renata; Andersen, Henriette Berg; Yao, Jiayi; Stigliani, Arnaud; Dannesboe, Johs et al. (2022): Crosstalk between tumor acidosis, p53 and extracellular matrix regulates pancreatic cancer aggressiveness. In *International journal of cancer*. DOI: 10.1002/ijc.34367.

Dai, Xiaoshuo; Zhang, Xiaoyan; Chen, Wei; Chen, Yihuan; Zhang, Qiushuang; Mo, Saijun; Lu, Jing (2021): Dihydroartemisinin: A Potential Natural Anticancer Drug. In *International journal of biological sciences* 17 (2), pp. 603–622. DOI: 10.7150/ijbs.50364.

D'Arcangelo, Elisa; Wu, Nila C.; Cadavid, Jose L.; McGuigan, Alison P. (2020): The life cycle of cancer-associated fibroblasts within the tumour stroma and its importance in disease outcome. In *British Journal of Cancer*. DOI: 10.1038/s41416-019-0705-1.

D'Costa, Zenobia; Jones, Keaton; Azad, Abul; van Stiphout, Ruud; Lim, Su Y.; Gomes, Ana L. et al. (2017): Gemcitabine-Induced TIMP1 Attenuates Therapy Response and Promotes Tumor Growth and Liver Metastasis in Pancreatic Cancer. In *Cancer research* 77 (21), pp. 5952–5962. DOI: 10.1158/0008-5472.CAN-16-2833.

DeBerardinis, Ralph J.; Lum, Julian J.; Hatzivassiliou, Georgia; Thompson, Craig B. (2008): The Biology of Cancer: Metabolic Reprogramming Fuels Cell Growth and Proliferation. In *Cell metabolism* 7 (1), pp. 11–20. DOI: 10.1016/j.cmet.2007.10.002.

Deer, Emily L.; González-Hernández, Jessica; Coursen, Jill D.; Shea, Jill E.; Ngatia, Josephat; Scaife, Courtney L. et al. (2010): Phenotype and genotype of pancreatic cancer cell lines. In *Pancreas* 39 (4), pp. 425–435. DOI: 10.1097/MPA.0b013e3181c15963.

Dhiman, Mini; Parab, Rajashri R.; Manju, Sreedharannair L.; Desai, Dattatraya C.; Mahajan, Girish B. (2012): Antifungal activity of hydrochloride salts of tylophorinidine and tylophorinine. In *Natural product communications* 7 (9), pp. 1171–1172.

Di, Zi; Klop, Maarten J. D.; Rogkoti, Vasiliki-Maria; Le Dévédec, Sylvia E.; van de Water, Bob; Verbeek, Fons J. et al. (2014): Ultra high content image analysis and phenotype profiling of 3D cultured micro-tissues. In *PLoS ONE* 9 (10), e109688. DOI: 10.1371/journal.pone.0109688.

Di Modugno, Francesca; Colosi, Cristina; Trono, Paola; Antonacci, Giuseppe; Ruocco, Giancarlo; Nisticò, Paola (2019): 3D models in the new era of immune oncology: focus on T cells, CAF and ECM. In *Journal of experimental & clinical cancer research : CR* 38 (1), p. 117. DOI: 10.1186/s13046-019-1086-2.

Ding, Jinsheng; Li, Hui; Liu, Yang; Xie, Yongjie; Yu, Jie; Sun, Huizhi et al. (2021): OXCT1 Enhances Gemcitabine Resistance Through NF-κB Pathway in Pancreatic Ductal Adenocarcinoma. In *Frontiers in oncology* 11, p. 698302. DOI: 10.3389/fonc.2021.698302.

Domenichini, Alice; Edmands, Jeanne S.; Adamska, Aleksandra; Begicevic, Romana-Rea; Paternoster, Silvano; Falasca, Marco (2019): Pancreatic cancer tumorspheres are cancer stem-like cells with increased chemoresistance and reduced metabolic potential. In *Advances in biological regulation* 72, pp. 63–77. DOI: 10.1016/j.jbior.2019.02.001.

Douglas, Julia E.; Liu, Suyu; Ma, Junsheng; Wolff, Robert A.; Pant, Shubham; Maitra, Anirban et al. (2022): PIONEER-Panc: a platform trial for phase II randomized investigations of new and emerging therapies for localized pancreatic cancer. In *BMC cancer* 22 (1), p. 14. DOI: 10.1186/s12885-021-09095-7.

Du, Ji-Hui; Zhang, Hou-De; Ma, Zhen-Jian; Ji, Kun-Mei (2010): Artesunate induces oncosis-like cell death in vitro and has antitumor activity against pancreatic cancer xenografts in vivo. In *Cancer chemotherapy and pharmacology* 65 (5), pp. 895–902. DOI: 10.1007/s00280-009-1095-5.

Du, Jing; Wang, Xu; Li, Yanchun; Ren, Xueying; Zhou, Yi; Hu, Wanye et al. (2021): DHA exhibits synergistic therapeutic efficacy with cisplatin to induce ferroptosis in pancreatic ductal adenocarcinoma via modulation of iron metabolism. In *Cell death & disease* 12 (7), p. 705. DOI: 10.1038/s41419-021-03996-y.

Dufau, Isabelle; Frongia, Céline; Sicard, Flavie; Dedieu, Laure; Cordelier, Pierre; Ausseil, Frédéric et al. (2012): Multicellular tumor spheroid model to evaluate spatio-temporal dynamics effect of chemotherapeutics: Application to the gemcitabine/CHK1 inhibitor combination in pancreatic cancer. In *BMC cancer* 12, p. 15. DOI: 10.1186/1471-2407-12-15.

Eckschlager, Tomas; Plch, Johana; Stiborova, Marie; Hrabeta, Jan (2017): Histone Deacetylase Inhibitors as Anticancer Drugs. In *International journal of molecular sciences* 18 (7). DOI: 10.3390/ijms18071414.

Edderkaoui, Mouad; Xu, Shiping; Chheda, Chintan; Morvaridi, Susan; Hu, Robert W.; Grippo, Paul J. et al. (2016): HDAC3 mediates smoking-induced pancreatic cancer. In *Oncotarget* 7 (7), pp. 7747–7760. DOI: 10.18632/oncotarget.6820.

Edmondson, Rasheena; Broglie, Jessica Jenkins; Adcock, Audrey F.; Yang, Liju (2014): Three-dimensional cell culture systems and their applications in drug discovery and cell-based biosensors. In *Assay and drug development technologies* 12 (4), pp. 207–218. DOI: 10.1089/adt.2014.573.

Egeblad, Mikala; Nakasone, Elizabeth S.; Werb, Zena (2010): Tumors as organs: complex tissues that interface with the entire organism. In *Developmental cell* 18 (6), pp. 884–901. DOI: 10.1016/j.devcel.2010.05.012.

Ehrenberg, Karl Roland; Gao, Jianpeng; Oppel, Felix; Frank, Stephanie; Kang, Na; Dieter, Sebastian M. et al. (2019): Systematic Generation of Patient-Derived Tumor Models in Pancreatic Cancer. In *Cells* 8 (2). DOI: 10.3390/cells8020142.

Eling, Nils; Reuter, Lukas; Hazin, John; Hamacher-Brady, Anne; Brady, R. Nathan (2015): Identification of artesunate as a specific activator of ferroptosis in pancreatic cancer cells. In *Oncoscience* 2 (5).

Enrique Rozengurt, Guido Eibl (2019): Central role of Yes-associated protein and WW-domain-containing transcriptional co-activator with PDZ-binding motif in pancreatic cancer development. In *World journal of gastroenterology* 25 (15), pp. 1797–1816. DOI: 10.3748/wjg.v25.i15.1797.

Erkan, Mert; Weis, Nadine; Pan, Zheng; Schwager, Christian; Samkharadze, Tamar; Jiang, Xiaohua et al. (2010): Organ-, inflammation- and cancer specific transcriptional fingerprings of pancreatic and hepatic stellate cells. In *BioMed Central*.

Esteller, Manel (2008): Epigenetics in cancer. In *The New England journal of medicine* 358 (11), pp. 1148–1159. DOI: 10.1056/NEJMra072067.

Fabian, Alexander; Stegner, Simon; Miarka, Lauritz; Zimmermann, Johannes; Lenk, Lennart; Rahn, Sascha et al. (2019): Metastasis of pancreatic cancer: An uninflamed liver micromilieu controls cell growth and cancer stem cell properties by oxidative phosphorylation in pancreatic ductal epithelial cells. In *Cancer letters* 453, pp. 95–106. DOI: 10.1016/j.canlet.2019.03.039.

Fan, Yuhui; Lesina, Marina; Algül, Hana (2020): Subtypes of pancreatic stellate cells and distant metastasis of pancreatic ductal adenocarcinoma. In *Annals of translational medicine* 8 (11), p. 671. DOI: 10.21037/atm.2020.03.136.

Farrow, Buckminster; Rowley, David; Dang, Truong; Berger, David H. (2009): Characterization of tumor-derived pancreatic stellate cells. In *The Journal of surgical research* 157 (1), pp. 96–102. DOI: 10.1016/j.jss.2009.03.064.

Fatehullah, Aliya; Tan, Si Hui; Barker, Nick (2016): Organoids as an *in vitro* model of human development and disease. In *Nature cell biology* 18 (3), p. 246. DOI: 10.1038/ncb3312.

Ferdek, Pawel E.; Jakubowska, Monika A. (2017): Biology of pancreatic stellate cells - more than just pancreatic cancer. In *Pflugers Archiv : European journal of physiology* 469 (9), pp. 1039–1050. DOI: 10.1007/s00424-017-1968-0.

Ferreira Garcia Rodrigues, Daniela (2022): Gut feelings. Towards a better understanding of the transcriptomic & molecular signatures of drug-induced intestinal toxicity in human 3D organoids. Maastricht University, Maastricht.

Ferretti, Roberta; Baldassarre, Antonella; Billy, Emmanuel de; M Carcaboso, Angel; Moore, Andrew; Carai, Andrea et al. (2021): Tumor cell invasion into Matrigel: optimized protocol for RNA extraction. In *BioTechniques*. DOI: 10.2144/btn-2021-0001.

Fischbach, Claudia; Chen, Ruth; Matsumoto, Takuya; Schmelzle, Tobias; Brugge, Joan S.; Polverini, Peter J.; Mooney, David J. (2007): Engineering tumors with 3D scaffolds. In *Nature methods* 4 (10), pp. 855–860. DOI: 10.1038/nmeth1085.

Fogh, J. (1986): Human tumor lines for cancer research. In *Cancer investigation* 4 (2), pp. 157–184. DOI: 10.3109/07357908609038260.

Foty, Ramsey (2011): A simple hanging drop cell culture protocol for generation of 3D spheroids. In *Journal of visualized experiments : JoVE* (51). DOI: 10.3791/2720.

Friedman, Scott L. (2008): Hepatic stellate cells: Protean, multifunctional, and enigmatic cells of the liver. In *Physiological reviews* 88 (1), pp. 125–172. DOI: 10.1152/physrev.00013.2007.

Fukumoto, Takeshi; Fatkhutdinov, Nail; Zundell, Joseph A.; Tcyganov, Evgenii N.; Nacarelli, Timothy; Karakashev, Sergey et al. (2019): HDAC6 Inhibition Synergizes with Anti-PD-L1 Therapy in ARID1A-Inactivated Ovarian Cancer. In *Cancer research* 79 (21), pp. 5482–5489. DOI: 10.1158/0008-5472.CAN-19-1302.

Ganguly, T.; Khar, A. (2002): Induction of apoptosis in a human erythroleukemic cell line K562 by tylophora alkaloids involves release of cytochrome c and activation of caspase 3. In *Phytomedicine : international journal of phytotherapy and phytopharmacology* 9 (4), pp. 288–295. DOI: 10.1078/0944-7113-00146.

Gao, Jin-Ming; Yang, Sheng-Xiang; Qin, Jian-Chun (2013): Azaphilonoids: Chemistry and biology. In *Chemical reviews* 113 (7), pp. 4755–4811. DOI: 10.1021/cr300402y.

Gao, Wenli; Bussom, Scott; Grill, Susan P.; Gullen, Elizabeth A.; Hu, You-Cai; Huang, Xueshi et al. (2007): Structure-activity studies of phenanthroindolizidine alkaloids as potential antitumor agents. In *Bioorganic & medicinal chemistry letters* 17 (15), pp. 4338–4342. DOI: 10.1016/j.bmcl.2007.05.021.

Gaugain, Bernard; Barbet, Jacques; Capelle, Nicole; Roques, Bernard P.; Le Pecq, Jean-Bernard (1978): DNA bifunctional intercalators. 2. Fluorescence properties and DNA binding interaction of an ethidium homodimer and an acridine ethidium heterodimer. Appendix: Numerical solution of McGhee and von Hippel equations for competing ligands. In *American Chemical Society* 17 (24).

George, Nicholas M.; Day, Caroline E.; Boerner, Brian P.; Johnson, Randy L.; Sarvetnick, Nora E. (2012): Hippo signaling regulates pancreas development through inactivation of Yap. In *Molecular and cellular biology* 32 (24), pp. 5116–5128. DOI: 10.1128/MCB.01034-12.

Giaginis, Constantinos; Damaskos, Christos; Koutsounas, Ioannis; Zizi-Serbetzoglou, Adamantia; Tsoukalas, Nicolaos; Patsouris, Efstratios et al. (2015): Histone deacetylase (HDAC)-1, -2, -4 and -6 expression in human pancreatic adenocarcinoma: associations with clinicopathological parameters, tumor proliferative capacity and patients' survival. In *BMC gastroenterology* 15, p. 148. DOI: 10.1186/s12876-015-0379-y.

Goldstein, David; El-Maraghi, Robert Hassan; Hammel, Pascal; Heinemann, Volker; Kunzmann, Volker; Sastre, Javier et al. (2015): nab-Paclitaxel plus gemcitabine for metastatic pancreatic cancer: Long-term survival from a phase III trial. In *Journal of the National Cancer Institute* 107 (2). DOI: 10.1093/jnci/dju413.

Gong, Xue; Lin, Chao; Cheng, Jian; Su, Jiansheng; Zhao, Hang; Liu, Tianlin et al. (2015): Generation of Multicellular Tumor Spheroids with Microwell-Based Agarose Scaffolds for Drug Testing. In *PLoS ONE* 10 (6), e0130348. DOI: 10.1371/journal.pone.0130348.

Govindachari, T. R.; Pai, B. R.; Ragade, I. S.; Rajappa, S.; Viswanathan, N. (1961): Chemical examination of Tylophora asthmatica—V. In *Tetrahedron* 14 (3-4), pp. 288–295. DOI: 10.1016/S0040-4020(01)92178-7.

Gradilone, Sergio A.; Radtke, Brynn N.; Bogert, Pamela S.; Huang, Bing Q.; Gajdos, Gabriella B.; LaRusso, Nicholas F. (2013): HDAC6 inhibition restores ciliary expression and decreases tumor growth. In *Cancer Res* 73 (7), pp. 2259–2270. DOI: 10.1158/0008-5472.CAN-12-2938.

Grant, Cliona; Rahman, Fahd; Piekarz, Richard; Peer, Cody; Frye, Robin; Robey, Robert W. et al. (2010): Romidepsin: a new therapy for cutaneous T-cell lymphoma and a potential therapy for solid tumors. In *Expert review of anticancer therapy* 10 (7), pp. 997–1008. DOI: 10.1586/era.10.88.

Grant, Steven; Easley, Chris; Kirkpatrick, Peter (2007): Vorinostat. In *Nature reviews. Drug discovery* 6 (1), pp. 21–22. DOI: 10.1038/nrd2227.

Greenshields, Anna L.; Fernando, Wasundara; Hoskin, David W. (2019): The anti-malarial drug artesunate causes cell cycle arrest and apoptosis of triple-negative MDA-MB-468 and HER2-enriched SK-BR-3 breast cancer cells. In *Experimental and molecular pathology* 107, pp. 10–22. DOI: 10.1016/j.yexmp.2019.01.006.

Gujral, Taranjit S.; Kirschner, Marc W. (2017): Hippo pathway mediates resistance to cytotoxic drugs. In *PNAS* 144 (18). DOI: 10.1073/pnas.1703096114.

Guo, Zengya; Wang, Xiaofeng; Yang, Yuhan; Chen, Weiwei; Zhang, Kundong; Teng, Buwei et al. (2020): Hypoxic Tumor-Derived Exosomal Long Noncoding RNA UCA1 Promotes Angiogenesis via miR-96-5p/AMOTL2 in Pancreatic Cancer. In *Molecular therapy. Nucleic acids* 22, pp. 179–195. DOI: 10.1016/j.omtn.2020.08.021.

Gupta, Sumati; Albertson, Daniel J.; Parnell, Timothy J.; Butterfield, Andrew; Weston, Alexis; Pappas, Lisa M. et al. (2019): Histone Deacetylase Inhibition Has Targeted Clinical Benefit in ARID1A-Mutated Advanced Urothelial Carcinoma. In *Molecular cancer therapeutics* 18 (1), pp. 185–195. DOI: 10.1158/1535-7163.MCT-17-0957.

Gutiérrez-Rodríguez, Carla; Lasker, Howard R. (2004): Reproductive biology, development, and planula behavior in the Caribbean gorgonian Pseudopterogorgia elisabethae. In *Invertebrate Biology* 123 (1), pp. 54–67. DOI: 10.1111/j.1744-7410.2004.tb00141.x.

Halbrook, Christopher J.; Pontious, Corbin; Kovalenko, Ilya; Lapienyte, Laura; Dreyer, Stephan; Lee, Ho-Joon et al. (2019): Macrophage-Released Pyrimidines Inhibit Gemcitabine Therapy in Pancreatic Cancer. In *Cell metabolism*. DOI: 10.1016/j.cmet.2019.02.001.

Hamblin, Michael R. (2020): Photodynamic Therapy for Cancer: What's Past is Prologue. In *Photochemistry and photobiology* 96 (3), pp. 506–516. DOI: 10.1111/php.13190.

Han, Weijia; Duan, Zhongping (2019): Roles of exosomes in liver metastases: Novel diagnosis and treatment choices. In *Journal of cellular physiology* 234 (12), pp. 21588–21600. DOI: 10.1002/jcp.28785.

Han, Yumei; Zhou, Shi; Coetzee, Sonja; Chen, Anping (2019): SIRT4 and Its Roles in Energy and Redox Metabolism in Health, Disease and During Exercise. In *Frontiers in physiology* 10, p. 1006. DOI: 10.3389/fphys.2019.01006.

Hassannia, Behrouz; Vandenabeele, Peter; Vanden Berghe, Tom (2019): Targeting Ferroptosis to Iron Out Cancer. In *Cancer cell* 35 (6), pp. 830–849. DOI: 10.1016/j.ccell.2019.04.002.

Hidalgo, Manuel (2010): Pancreatic Cancer. In *New England Journal of Medicine* (362), pp. 1605–1617. DOI: 10.1046/j.0013-0427.2003.00027.x.

Ho, Terence C. S.; Chan, Alex H. Y.; Ganesan, A. (2020): Thirty Years of HDAC Inhibitors: 2020 Insight and Hindsight. In *Journal of medicinal chemistry* 63 (21), pp. 12460–12484. DOI: 10.1021/acs.jmedchem.0c00830.

Hölken, Johanna.; Teusch, Nicole (2020): Recent developments of 3D models of the tumor microenvironment for cutaneous melanoma: Bridging the gap between the bench and the bedside? In *Journal of translational science* 7, pp. 1–7. DOI: 10.15761/JTS.1000388.

Homolya, L.; Holló, Z.; Germann, U. A.; Pastan, I.; Gottesman, M. M.; Sarkadi, B. (1993): Fluorescent cellular indicators are extruded by the multidrug resistance protein. In *Journal of Biological Chemistry* 268 (29), pp. 21493–21496. DOI: 10.1016/S0021-9258(20)80566-3.

Hood, Katelyn; Shah, Arpita (2016): Belinostat for Relapsed or Refractory Peripheral T-Cell Lymphoma. In *Journal of the advanced practitioner in oncology* 7 (2), pp. 209–218. DOI: 10.6004/jadpro.2016.7.2.6.

Hou, Pei-Pei; Chen, Hang-Zi (2021): Extracellular vesicles in the tumor immune microenvironment. In *Cancer letters* 516, pp. 48–56. DOI: 10.1016/j.canlet.2021.05.032.

Houg, Demi S.; Bijlsma, Maarten F. (2018): The hepatic pre-metastatic niche in pancreatic ductal adenocarcinoma. In *Mol Cancer* 17 (1), p. 95. DOI: 10.1186/s12943-018-0842-9.

Hruban, Ralph H.; Gaida, Matthias M.; Thompson, Elizabeth; Hong, Seung-Mo; Noë, Michaël; Brosens, Lodewijk Aa et al. (2019): Why is pancreatic cancer so deadly? The pathologist's view. In *The Journal of pathology* 248 (2), pp. 131–141. DOI: 10.1002/path.5260.

Huang, Ya-Fang; Xie, Wen-Jie; Fan, Hai-Yu; Du, Juan (2020): Comparative Risks of High-Grade Adverse Events Among FDA-Approved Systemic Therapies in Advanced Melanoma: Systematic Review and Network Meta-Analysis. In *Frontiers in oncology* 10, p. 571135. DOI: 10.3389/fonc.2020.571135.

Hughes, Chris S.; Postovit, Lynne M.; Lajoie, Gilles A. (2010): Matrigel: A complex protein mixture required for optimal growth of cell culture. In *Proteomics* 10 (9), pp. 1886–1890. DOI: 10.1002/pmic.200900758.

Hull, Elizabeth E.; Montgomery, McKale R.; Leyva, Kathryn J. (2016): HDAC Inhibitors as Epigenetic Regulators of the Immune System: Impacts on Cancer Therapy and Inflammatory Diseases. In *BioMed research international* 2016, p. 8797206. DOI: 10.1155/2016/8797206.

Hwang, Hyun Ju; Oh, Min-Suk; Lee, Dong Woo; Kuh, Hyo-Jeong (2019): Multiplex quantitative analysis of stroma-mediated cancer cell invasion, matrix remodeling, and drug response in a 3D co-culture model of pancreatic tumor spheroids and stellate cells. In *Journal of experimental & clinical cancer research : CR* 38 (1), p. 258. DOI: 10.1186/s13046-019-1225-9.

Imamura, Yoshinori; Mukohara, Toru; Shimono, Yohei; Funakoshi, Yohei; Chayahara, Naoko; Toyoda, Masanori et al. (2015): Comparison of 2D- and 3D-culture models as drug-testing platforms in breast cancer. In *Oncology reports* 33 (4), pp. 1837–1843. DOI: 10.3892/or.2015.3767.

Incio, Joao; Liu, Hao; Suboj, Priya; Chin, Shan M.; Chen, Ivy X.; Pinter, Matthias et al. (2016): Obesity-Induced Inflammation and Desmoplasia Promote Pancreatic Cancer Progression and Resistance to Chemotherapy. In *Cancer Discov* 6 (8), pp. 852–869. DOI: 10.1158/2159-8290.CD-15-1177.

Ingenhoff, Luisa; Häberle, Lena; Esposito, Irene (2020): Subtypes of Pancreatic Adenocarcinoma. In Christoph W. Michalski, Jonas Rosendahl, Patrick Michl, Jörg Kleeff (Eds.): TRANSLATIONAL PANCREATIC CANCER RESEARCH. From understanding of. [S.l.]: SPRINGER NATURE (Molecular and Translational Medicine), pp. 3–16.

Ireland, Lucy V.; Mielgo, Ainhoa (2018): Macrophages and Fibroblasts, Key Players in Cancer Chemoresistance. In *Frontiers in cell and developmental biology* 6, p. 131. DOI: 10.3389/fcell.2018.00131.

Ismail, Hanafy M.; Barton, Victoria; Phanchana, Matthew; Charoensutthivarakul, Sitthivut; Wong, Michael H. L.; Hemingway, Janet et al. (2016): Artemisinin activity-based probes identify multiple molecular targets within the asexual stage of the malaria parasites Plasmodium falciparum 3D7. In *Proceedings of the National Academy of Sciences of the United States of America* 113 (8), pp. 2080–2085. DOI: 10.1073/pnas.1600459113.

Ito, Genta; Kawakami, Kazuyoshi; Aoyama, Takeshi; Yokokawa, Takashi; Nakamura, Masashi; Ozaka, Masato et al. (2021): Risk factors for severe neutropenia in pancreatic cancer patients treated with gemcitabine/nab-paclitaxel combination therapy. In *PLoS ONE* 16 (7), e0254726. DOI: 10.1371/journal.pone.0254726.

Jaganathan, Hamsa; Gage, Jacob; Leonard, Fransisca; Srinivasan, Srimeenakshi; Souza, Glauco R.; Dave, Bhuvanesh; Godin, Biana (2014): Three-dimensional in vitro co-culture model of breast tumor using magnetic levitation. In *Scientific reports* 4, p. 6468. DOI: 10.1038/srep06468.

Jang, Imjoo; Beningo, Karen A. (2019): Integrins, CAFs and Mechanical Forces in the Progression of Cancer. In *Cancers* 11 (5), p. 721. DOI: 10.3390/cancers11050721.

Jang, So-Dam; Song, Jeeyeun; Kim, Hyun-Ah; Im, Chang-Nim; Khawar, Iftikhar Ali; Park, Jong Kook; Kuh, Hyo-Jeong (2021): Anti-Cancer Activity Profiling of Chemotherapeutic Agents in 3D Co-Cultures of Pancreatic Tumor Spheroids with Cancer-Associated Fibroblasts and Macrophages. In *Cancers* 13 (23), p. 5955. DOI: 10.3390/cancers13235955.

Janßen, Daria (2021): Pharmakologische Charakterisierung neuer Histon-Deacetylase (HDAC)-Inhibitoren in 3D Tumormodellen des Pankreasadenokarzinoms. Universität Osnabrück, Osnabrück. Institut für Gesundheitswissenschaft und Bildung.

Jena, Bikash Chandra; Das, Chandan Kanta; Bharadwaj, Deblina; Mandal, Mahitosh (2020): Cancer associated fibroblast mediated chemoresistance: A paradigm shift in understanding the mechanism of tumor progression. In *Biochimica et biophysica acta. Reviews on cancer* 1874 (2), p. 188416. DOI: 10.1016/j.bbcan.2020.188416.

Jesus, Victor H. F. de; Camandaroba, Marcos P. G.; Calsavara, Vinicius F.; Riechelmann, Rachel P. (2020): Systematic review and meta-analysis of gemcitabine-based chemotherapy after FOLFIRINOX in advanced pancreatic cancer. In *Therapeutic advances in medical oncology* 12, 1758835920905408. DOI: 10.1177/1758835920905408.

Ji, Peng; Huang, Haiqin; Yuan, Shirui; Le Wang; Wang, Siqi; Chen, Yiwei et al. (2019): ROS-Mediated Apoptosis and Anticancer Effect Achieved by Artesunate and Auxiliary Fe(II) Released from Ferriferous Oxide-Containing Recombinant Apoferritin. In *Advanced healthcare materials* 8 (23), e1900911. DOI: 10.1002/adhm.201900911.

Jiang, Feng; Zhou, Jin-Yong; Zhang, Dan; Liu, Ming-Hao; Chen, Yu-Gen (2018): Artesunate induces apoptosis and autophagy in HCT116 colon cancer cells, and autophagy inhibition enhances the artesunate-induced apoptosis. In *International Journal of Molecular Medicine* 42 (3), pp. 1295–1304. DOI: 10.3892/ijmm.2018.3712.

Jin, Ming-Zhu; Jin, Wei-Lin (2020): The updated landscape of tumor microenvironment and drug repurposing. In *Signal Transduction and Targeted Therapy* 5 (1), p. 166. DOI: 10.1038/s41392-020-00280-x.

Jones, Laurie J.; Gray, Matthew; Yue, Stephen T.; Haugland, Richard P.; Singer, Victoria L. (2001): Sensitive determination of cell number using the CyQUANT® cell proliferation assay. In *Journal of Immunological Methods* 254 (1-2), pp. 85–98. DOI: 10.1016/S0022-1759(01)00404-5.

Kabacaoglu, Derya; Ruess, Dietrich A.; Ai, Jiaoyu; Algül, Hana (2019): NF-κB/Rel Transcription Factors in Pancreatic Cancer: Focusing on RelA, c-Rel, and RelB. In *Cancers* 11 (7). DOI: 10.3390/cancers11070937.

Kaneta, Yoshihiro; Sato, Takeshi; Hikiba, Yohko; Sugimori, Makoto; Sue, Soichiro; Kaneko, Hiroaki et al. (2020): Loss of Pancreatic E-Cadherin Causes Pancreatitis-Like Changes and Contributes to Carcinogenesis. In *Cellular and molecular gastroenterology and hepatology* 9 (1), pp. 105–119. DOI: 10.1016/j.jcmgh.2019.09.001.

Kapuscinski, J. (1995): DAPI: a DNA-specific fluorescent probe. In *Biotechnic & histochemistry : official publication of the Biological Stain Commission* 70 (5), pp. 220–233. DOI: 10.3109/10520299509108199.

Kenny, Paraic A.; Lee, Genee Y.; Myers, Connie A.; Neve, Richard M.; Semeiks, Jeremy R.; Spellman, Paul T. et al. (2007): The morphologies of breast cancer cell lines in three-dimensional assays correlate with their profiles of gene expression. In *Molecular Oncology* 1 (1), pp. 84–96. DOI: 10.1016/j.molonc.2007.02.004.

Khushman, Moh'd; Patel, Girijesh Kumar; Laurini, Javier Ariel; Bhardwaj, Arun; Roveda, Kelly; Donnell, Robert et al. (2019): Exosomal markers (CD63 and CD9) expression and their prognostic significance using immunohistochemistry in patients with pancreatic ductal adenocarcinoma. In *Journal of gastrointestinal oncology* 10 (4), pp. 695–702. DOI: 10.21037/jgo.2018.07.02.

Kim, Youn H.; Bagot, Martine; Pinter-Brown, Lauren; Rook, Alain H.; Porcu, Pierluigi; Horwitz, Steven M. et al. (2018): Mogamulizumab versus vorinostat in previously treated cutaneous T-cell lymphoma (MAVORIC): an international, open-label, randomised, controlled phase 3 trial. In *The Lancet Oncology* 19 (9), pp. 1192–1204. DOI: 10.1016/S1470-2045(18)30379-6.

Kleinman, Hynda K.; Martin, George R. (2005): Matrigel: basement membrane matrix with biological activity. In *Seminars in cancer biology* 15 (5), pp. 378–386. DOI: 10.1016/j.semcancer.2005.05.004.

Klieser, Eckhard; Swierczynski, Stefan; Mayr, Christian; Schmidt, Johanna; Neureiter, Daniel; Kiesslich, Tobias; Illig, Romana (2015): Role of histone deacetylases in pancreas: Implications for pathogenesis and therapy. In *World journal of gastrointestinal oncology* 7 (12), pp. 473–483. DOI: 10.4251/wjgo.v7.i12.473.

Knies, Christine; Hammerbacher, Katharina; Bonaterra, Gabriel A.; Kinscherf, Ralf; Rosemeyer, Helmut (2016): Nucleolipids of Canonical Purine ß-d-Ribo-Nucleosides: Synthesis and Cytostatic/Cytotoxic Activities Toward Human and Rat Glioblastoma Cells. In *ChemistryOpen* 5 (2), pp. 129–141. DOI: 10.1002/open.201500197.

Kobayashi, Hiroki; Enomoto, Atsushi; Woods, Susan L.; Burt, Alastair D.; Takahashi, Masahide; Worthley, Daniel L. (2019): Cancer-associated fibroblasts in gastrointestinal cancer. In *Nature reviews. Gastroenterology & hepatology* 16 (5), pp. 282–295. DOI: 10.1038/s41575-019-0115-0.

Kolbeinsson, Hordur Mar; Chandana, Sreenivasa; Wright, G. Paul; Chung, Mathew (2023): Pancreatic Cancer: A Review of Current Treatment and Novel Therapies. In *Journal of investigative surgery : the*

official journal of the Academy of Surgical Research 36 (1), p. 2129884. DOI: 10.1080/08941939.2022.2129884.

Koutsounas, Ioannis; Giaginis, Constantinos; Patsouris, Efstratios; Theocharis, Stamatios (2013): Current evidence for histone deacetylase inhibitors in pancreatic cancer. In *World journal of gastroenterology* 19 (6), pp. 813–828. DOI: 10.3748/wjg.v19.i6.813.

Kuen, Janina; Darowski, Diana; Kluge, Tobias; Majety, Meher (2017): Pancreatic cancer cell/fibroblast co-culture induces M2 like macrophages that influence therapeutic response in a 3D model. In *PLoS ONE* 12 (7), e0182039. DOI: 10.1371/journal.pone.0182039.

Kumagai, Takashi; Wakimoto, Naoki; Yin, Dong; Gery, Sigal; Kawamata, Norihiko; Takai, Noriyuki et al. (2007): Histone deacetylase inhibitor, suberoylanilide hydroxamic acid (Vorinostat, SAHA) profoundly inhibits the growth of human pancreatic cancer cells. In *Int. J. Cancer* 121 (3), pp. 656–665. DOI: 10.1002/ijc.22558.

Kumar, Vijay L.; Verma, Sneh; Das, Prasenjit (2019): Artesunate suppresses inflammation and oxidative stress in a rat model of colorectal cancer. In *Drug development research* 80 (8), pp. 1089–1097. DOI: 10.1002/ddr.21590.

Kyriazis, A. P.; Kyriazis, A. A.; Scarpelli, D. G.; Fogh, J.; Rao, M. S.; Lepera, R. (1982): Human pancreatic adenocarcinoma line Capan-1 in tissue culture and the nude mouse: morphologic, biologic, and biochemical characteristics. In *The American journal of pathology* 106 (2), pp. 250–260.

Lamouille, Samy; Xu, Jian; Derynck, Rik (2014): Molecular mechanisms of epithelial–mesenchymal transition. In *Nature reviews. Molecular cell biology* 15 (3), pp. 178–196. DOI: 10.1038/nrm3758.

Lancaster, Madeline A.; Knoblich, Juergen A. (2014): Generation of cerebral organoids from human pluripotent stem cells. In *Nature protocols* 9 (10), pp. 2329–2340. DOI: 10.1038/nprot.2014.158.

Laplane, Lucie; Duluc, Dorothée; Bikfalvi, Andreas; Larmonier, Nicolas; Pradeu, Thomas (2019): Beyond the tumour microenvironment. In *International journal of cancer* 145 (10), pp. 2611–2618. DOI: 10.1002/ijc.32343.

Larson, Sara A.; Dolivo, David M.; Dominko, Tanja (2019): Artesunate inhibits myofibroblast formation via induction of apoptosis and antagonism of pro-fibrotic gene expression in human dermal fibroblasts. In *Cell biology international* 43 (11), pp. 1317–1322. DOI: 10.1002/cbin.11220.

Latt, S. A.; Stetten, G.; Juergens, L. A.; Willard, H. F.; Scher, C. D. (1975): Recent developments in the detection of deoxyribonucleic acid synthesis by 33258 Hoechst fluorescence. In *The journal of histochemistry and cytochemistry : official journal of the Histochemistry Society* 23 (7), pp. 493–505. DOI: 10.1177/23.7.1095650.

Laubach, Jacob P.; Moreau, Philippe; San-Miguel, Jesús F.; Richardson, Paul G. (2015): Panobinostat for the Treatment of Multiple Myeloma. In *Clinical cancer research : an official journal of the American Association for Cancer Research* 21 (21), pp. 4767–4773. DOI: 10.1158/1078-0432.CCR-15-0530.

LeBleu, Valerie S.; Kalluri, Raghu (2018): A peek into cancer-associated fibroblasts: origins, functions and translational impact. In *Disease models & mechanisms* 11 (4). DOI: 10.1242/dmm.029447.

Lee, Alexandra T. K.; Xu, Zhihong; Pothula, Srinivasa P.; Patel, Mishaal B.; Pirola, Romano C.; Wilson, Jeremy S.; Apte, Minoti V. (2015): Alcohol and cigarette smoke components activate human pancreatic stellate cells: implications for the progression of chronic pancreatitis. In *Alcoholism, clinical and experimental research* 39 (11), pp. 2123–2133. DOI: 10.1111/acer.12882.

Lee, Dong Hoon; Won, Hye-Rim; Ryu, Hyun-Wook; Han, Jung Min; Kwon, So Hee (2018a): The HDAC6 inhibitor ACY-1215 enhances the anticancer activity of oxaliplatin in colorectal cancer cells. In *International journal of oncology* 53 (2), pp. 844–854. DOI: 10.3892/ijo.2018.4405.

Lee, Hae-Ahm; Park, So-Min; Chu, Ki-Back; Quan, Fu-Shi; Kurz, Thomas; Pflieger, Marc; Moon, Eun-Kyung (2020): Application of Histone Deacetylase Inhibitors MPK472 and KSK64 as a Potential Treatment Option for Acanthamoeba Keratitis. In *Antimicrobial agents and chemotherapy* 64 (12). DOI: 10.1128/AAC.01506-20.

Lee, Ji-Hyun; Kim, Seul-Ki; Khawar, Iftikhar Ali; Jeong, Su-Yeong; Chung, Seok; Kuh, Hyo-Jeong (2018b): Microfluidic co-culture of pancreatic tumor spheroids with stellate cells as a novel 3D model for investigation of stroma-mediated cell motility and drug resistance. In *Journal of experimental & clinical cancer research : CR* 37 (1), p. 4. DOI: 10.1186/s13046-017-0654-6.

Lee, Jiyoon; Koehler, Karl R. (2021): Skin organoids: A new human model for developmental and translational research. In *Experimental dermatology* 30 (4), pp. 613–620. DOI: 10.1111/exd.14292.

Li, Hao; Xu, Kanghe; Pian, Guangzhe; Sun, Shu (2019a): Artesunate and sorafenib: Combinatorial inhibition of liver cancer cell growth. In *Oncology letters* 18 (5), pp. 4735–4743. DOI: 10.3892/ol.2019.10810.

Li, He; Dai, Weixing; Xia, Xi; Wang, Renjie; Zhao, Jing; Han, Lingyu et al. (2020a): Modeling tumor development and metastasis using paired organoids derived from patients with colorectal cancer liver metastases. In *Journal of hematology & oncology* 13 (1), p. 119. DOI: 10.1186/s13045-020-00957-4.

Li, He; Li, Xiaocheng; Lin, Huapeng; Gong, Jianping (2020b): High HDAC9 is associated with poor prognosis and promotes malignant progression in pancreatic ductal adenocarcinoma. In *Molecular medicine reports* 21 (2), pp. 822–832. DOI: 10.3892/mmr.2019.10869.

Li, Jian; Zhou, Bing (2010): Biological actions of artemisinin: insights from medicinal chemistry studies. In *Molecules (Basel, Switzerland)* 15 (3), pp. 1378–1397. DOI: 10.3390/molecules15031378.

Li, Yilong; Wang, Yongwei; Kong, Rui; Xue, Dongbo; Pan, Shangha; Chen, Hua; Sun, Bei (2016): Dihydroartemisinin suppresses pancreatic cancer cells via a microRNA-mRNA regulatory network. In *Oncotarget* 7 (38), pp. 62460–62473. DOI: 10.18632/oncotarget.11517.

Li, Yixuan; Seto, Edward (2016): HDACs and HDAC Inhibitors in Cancer Development and Therapy. In *Cold Spring Harbor perspectives in medicine* 6 (10). DOI: 10.1101/cshperspect.a026831.

Li, Yujie; Lu, Jing; Chen, Qin; Han, Shengnan; Shao, Hua; Chen, Pingyi et al. (2019b): Artemisinin suppresses hepatocellular carcinoma cell growth, migration and invasion by targeting cellular bioenergetics and Hippo-YAP signaling. In *Archives of toxicology* 93 (11), pp. 3367–3383. DOI: 10.1007/s00204-019-02579-3.

Li, Zoe; Salik, Irim (2021): A Dangerous Mimic: Chronic Pancreatitis Masquerading As Pancreatic Adenocarcinoma. In *Cureus* 13 (11). DOI: 10.7759/cureus.19795.

Lieber, M.; Mazzetta, J.; Nelson-Rees, W.; Kaplan, M.; Todaro, G. (1975): Establishment of a continuous tumor-cell line (panc-1) from a human carcinoma of the exocrine pancreas. In *Int. J. Cancer* 15 (5), pp. 741–747. DOI: 10.1002/ijc.2910150505.

Lim, Jungeun; Ching, Hanna; Yoon, Jeong-Kee; Jeon, Noo Li; Kim, YongTae (2021): Microvascularized tumor organoids-on-chips: advancing preclinical drug screening with pathophysiological relevance. In *Nano convergence* 8 (1), p. 12. DOI: 10.1186/s40580-021-00261-y.

Lin, George H.Y.; Brusick, David J. (1986): Mutagenicity studies on FD&C Red No.3. In *Mutagenesis* 1 (4), pp. 253–259.

Lin, Jau-Chen; Yang, Shuenn-Chen; Hong, Tse-Ming; Yu, Sung-Liang; Shi, Qian; Wei, Linyi et al. (2009): Phenanthrene-based tylophorine-1 (PBT-1) inhibits lung cancer cell growth through the Akt and NF-kappaB pathways. In *Journal of medicinal chemistry* 52 (7), pp. 1903–1911. DOI: 10.1021/jm801344j.

Lin, Jiunn-Chang; Liu, Tsang-Pai; Yang, Pei-Ming (2020): CDKN2A-Inactivated Pancreatic Ductal Adenocarcinoma Exhibits Therapeutic Sensitivity to Paclitaxel: A Bioinformatics Study. In *Journal of Clinical Medicine* 9 (12). DOI: 10.3390/jcm9124019.

Liou, Geou-Yarh; Döppler, Heike; Necela, Brian; Krishna, Murli; Crawford, Howard C.; Raimondo, Massimo; Storz, Peter (2013): Macrophage-secreted cytokines drive pancreatic acinar-to-ductal metaplasia through NF-κB and MMPs. In *The Journal of cell biology* 202 (3), pp. 563–577. DOI: 10.1083/jcb.201301001.

Liu, Yanmei; Gao, Shujun; Zhu, Jie; Zheng, Ya; Zhang, Haiyan; Sun, Hong (2018): Dihydroartemisinin induces apoptosis and inhibits proliferation, migration, and invasion in epithelial ovarian cancer via inhibition of the hedgehog signaling pathway. In *Cancer medicine* 7 (11), pp. 5704–5715. DOI: 10.1002/cam4.1827.

Liu, Yuxiu; Qing, Lihua; Meng, Chuisong; Shi, Jiajie; Yang, Yan; Wang, Ziwen et al. (2017): 6-OH-Phenanthroquinolizidine Alkaloid and Its Derivatives Exert Potent Anticancer Activity by Delaying S Phase Progression. In *Journal of medicinal chemistry* 60 (7), pp. 2764–2779. DOI: 10.1021/acs.jmedchem.6b01502.

Loh, Chin-Yap; Chai, Jian Yi; Tang, Ting Fang; Wong, Won Fen; Sethi, Gautam; Shanmugam, Muthu Kumaraswamy et al. (2019): The E-Cadherin and N-Cadherin Switch in Epithelial-to-Mesenchymal Transition: Signaling, Therapeutic Implications, and Challenges. In *Cells* 8 (10). DOI: 10.3390/cells8101118.

Longati, Paola; Jia, Xiaohui; Eimer, Johannes; Wagman, Annika; Witt, Michael-Robin; Rehnmark, Stefan et al. (2013): 3D pancreatic carcinoma spheroids induce a matrix-rich, chemoresistant phenotype offering a better model for drug testing. In *BMC cancer* 13, p. 95. DOI: 10.1186/1471-2407-13-95.

Looi, Chin-King; Gan, Li-Lian; Sim, Wynne; Hii, Ling-Wei; Chung, Felicia Fei-Lei; Leong, Chee-Onn et al. (2022): Histone Deacetylase Inhibitors Restore Cancer Cell Sensitivity towards T Lymphocytes Mediated Cytotoxicity in Pancreatic Cancer. In *Cancers* 14 (15). DOI: 10.3390/cancers14153709.

Ma, Ling; Fei, Honghua (2020): Antimalarial drug artesunate is effective against chemoresistant anaplastic thyroid carcinoma via targeting mitochondrial metabolism. In *Journal of bioenergetics and biomembranes* 52 (2), pp. 123–130. DOI: 10.1007/s10863-020-09824-w.

Maddalena, Martino; Mallel, Giuseppe; Nataraj, Nishanth Belugali; Shreberk-Shaked, Michal; Hassin, Ori; Mukherjee, Saptaparna et al. (2021): TP53 missense mutations in PDAC are associated with enhanced fibrosis and an immunosuppressive microenvironment. In *Proceedings of the National Academy of Sciences of the United States of America* 118 (23). DOI: 10.1073/pnas.2025631118.

Maehira, Hiromitsu; Miyake, Toru; Iida, Hiroya; Tokuda, Aya; Mori, Haruki; Yasukawa, Daiki et al. (2019): Vimentin Expression in Tumor Microenvironment Predicts Survival in Pancreatic Ductal Adenocarcinoma: Heterogeneity in Fibroblast Population. In *Annals of surgical oncology* 26 (13), pp. 4791–4804. DOI: 10.1245/s10434-019-07891-x.

Mahmood, Tahrin; Yang, Ping-Chang (2012): Western blot: technique, theory, and trouble shooting. In *North American journal of medical sciences* 4 (9), pp. 429–434. DOI: 10.4103/1947-2714.100998.

Malla, Rama Rao; Pandrangi, Santhi; Kumari, Seema; Gavara, Murali Mohan; Badana, Anil Kumar (2018): Exosomal tetraspanins as regulators of cancer progression and metastasis and novel diagnostic markers. In *Asia-Pacific journal of clinical oncology* 14 (6), pp. 383–391. DOI: 10.1111/ajco.12869.

Mandal, Anasuya; Boopathy, Archana V.; Lam, Lionel K. W.; Moynihan, Kelly D.; Welch, Mary E.; Bennett, Nitasha R. et al. (2018): Cell and fluid sampling microneedle patches for monitoring skin-resident immunity. In *Science translational medicine* 10 (467), eaar2227. DOI: 10.1126/scitranslmed.aar2227.

Mann, Bhupinder S.; Johnson, John R.; He, Kun; Sridhara, Rajeshwari; Abraham, Sophia; Booth, Brian P. et al. (2007): Vorinostat for treatment of cutaneous manifestations of advanced primary cutaneous T-cell lymphoma. In *Clinical cancer research : an official journal of the American Association for Cancer Research* 13 (8), pp. 2318–2322. DOI: 10.1158/1078-0432.CCR-06-2672.

Mikamori, Manabu; Yamada, Daisaku; Eguchi, Hidetoshi; Hasegawa, Shinichiro; Kishimoto, Tomoya; Tomimaru, Yoshito et al. (2017): MicroRNA-155 Controls Exosome Synthesis and Promotes Gemcitabine Resistance in Pancreatic Ductal Adenocarcinoma. In *Scientific reports* 7, p. 42339. DOI: 10.1038/srep42339.

Mini, E.; Nobili, S.; Caciagli, B.; Landini, I.; Mazzei, T. (2006): Cellular pharmacology of gemcitabine. In *Annals of oncology : official journal of the European Society for Medical Oncology* 17 Suppl 5, v7-12. DOI: 10.1093/annonc/mdj941.

Mishra, Vivek Kumar; Wegwitz, Florian; Kosinsky, Robyn Laura; Sen, Madhobi; Baumgartner, Roland; Wulff, Tanja et al. (2017): Histone deacetylase class-I inhibition promotes epithelial gene expression in

pancreatic cancer cells in a BRD4- and MYC-dependent manner. In *Nucl. Acids Res.* 45 (11), pp. 6334–6349. DOI: 10.1093/nar/gkx212.

Mizrahi, Jonathan D.; Surana, Rishi; Valle, Juan W.; Shroff, Rachna T. (2020): Pancreatic cancer. In *The Lancet* 395 (10242), pp. 2008–2020. DOI: 10.1016/S0140-6736(20)30974-0.

Moreira, Leticia; Bakir, Basil; Chatterji, Priya; Dantes, Zahra; Reichert, Maximilian; Rustgi, Anil K. (2018): Pancreas 3D Organoids: Current and Future Aspects as a Research Platform for Personalized Medicine in Pancreatic Cancer. In *Cellular and molecular gastroenterology and hepatology* 5 (3), pp. 289–298. DOI: 10.1016/j.jcmgh.2017.12.004.

Mundorf, Vanessa (2018): Cancer cell-fibroblast context-dependent actions of plant natural products in 2D and 3D models of human pancreatic adenocarcinoma. Technische Hochschule Köln, Köln. Fakultät für Angewandte Naturwissenschaften.

Murciano-Goroff, Yonina R.; Warner, Allison Betof; Wolchok, Jedd D. (2020): The future of cancer immunotherapy: microenvironment-targeting combinations. In *Cell Res*. DOI: 10.1038/s41422-020-0337-2.

Myasnikova, Dina; Osaki, Tatsuya; Onishi, Kisaki; Kageyama, Tatsuto; Zhang Molino, Binbin; Fukuda, Junji (2019): Synergic effects of oxygen supply and antioxidants on pancreatic β-cell spheroids. In *Scientific reports* 9 (1), p. 1802. DOI: 10.1038/s41598-018-38011-6.

Naito, Yutaka; Yoshioka, Yusuke; Yamamoto, Yusuke; Ochiya, Takahiro (2017): How cancer cells dictate their microenvironment: present roles of extracellular vesicles. In *Cellular and molecular life sciences : CMLS* 74 (4), pp. 697–713. DOI: 10.1007/s00018-016-2346-3.

Nam, Woong; Tak, Jungae; Ryu, Ju-Kyoung; Jung, Mankil; Yook, Jong-In; Kim, Hyung-Jun; Cha, In-Ho (2007): Effects of artemisinin and its derivatives on growth inhibition and apoptosis of oral cancer cells. In *Head & Neck* 29 (4), pp. 335–340. DOI: 10.1002/hed.20524.

Nguyen, Chan D. K.; Yi, Chunling (2019): YAP/TAZ Signaling and Resistance to Cancer Therapy. In *Trends in cancer* 5 (5), pp. 283–296. DOI: 10.1016/j.trecan.2019.02.010.

Nichols, Jennifer; Silva, Jose; Roode, Mila; Smith, Austin (2009): Suppression of Erk signalling promotes ground state pluripotency in the mouse embryo. In *Development (Cambridge, England)* 136 (19), pp. 3215–3222. DOI: 10.1242/dev.038893.

Novo, David; Heath, Nikki; Mitchell, Louise; Caligiuri, Giuseppina; MacFarlane, Amanda; Reijmer, Dide et al.: Mutant p53s generate pro-invasive niches by influencing exosome podocalyxin levels. In *Nature communications* 9 (1), p. 5069. DOI: 10.1038/s41467-018-07339-y.

Nyga, Agata; Cheema, Umber; Loizidou, Marilena (2011): 3D tumour models: Novel in vitro approaches to cancer studies. In *Journal of Cell Communication and Signaling* 5 (3), p. 239. DOI: 10.1007/s12079-011-0132-4.

Obaid, Girgis; Bano, Shazia; Mallidi, Srivalleesha; Broekgaarden, Mans; Kuriakose, Jerrin; Silber, Zachary et al. (2019): Impacting Pancreatic Cancer Therapy in Heterotypic in Vitro Organoids and in

Vivo Tumors with Specificity-Tuned, NIR-Activable Photoimmunonanoconjugates: Towards Conquering Desmoplasia? In *Nano letters*. DOI: 10.1021/acs.nanolett.9b00859.

Omura, S.; Iwai, Y.; Hirano, A.; Nakagawa, A.; Awaya, J.; Tsuchya, H. et al. (1977): A new alkaloid AM-2282 OF Streptomyces origin. Taxonomy, fermentation, isolation and preliminary characterization. In *J. Antibiot.* 30 (4), pp. 275–282. DOI: 10.7164/antibiotics.30.275.

Omura, Satoshi; Sasaki, Yasuharu; Iwai, Yuzuru; Takeshima, Hideo (1995): Staurosporine, a Potentially Important Gift from a Microorganism. In *J. Antibiot.* 48 (7), pp. 535–548. DOI: 10.7164/antibiotics.48.535.

Orth, Michael; Metzger, Philipp; Gerum, Sabine; Mayerle, Julia; Schneider, Günter; Belka, Claus et al. (2019): Pancreatic ductal adenocarcinoma: biological hallmarks, current status, and future perspectives of combined modality treatment approaches. In *Radiation oncology (London, England)* 14 (1), p. 141. DOI: 10.1186/s13014-019-1345-6.

Pausch, Thomas M.; Aue, Elisa; Wirsik, Naita M.; Freire Valls, Aida; Shen, Ying; Radhakrishnan, Praveen et al. (2020): Metastasis-associated fibroblasts promote angiogenesis in metastasized pancreatic cancer via the CXCL8 and the CCL2 axes. In *Scientific reports* 10 (1), p. 5420. DOI: 10.1038/s41598-020-62416-x.

Pelosi, Elvira; Castelli, Germana; Testa, Ugo (2017): Pancreatic Cancer: Molecular Characterization, Clonal Evolution and Cancer Stem Cells. In *Biomedicines* 5 (4). DOI: 10.3390/biomedicines5040065.

Pereira, Marina Ayres; Chio, Iok In Christine (2019): Metastasis in Pancreatic Ductal Adenocarcinoma: Current Standing and Methodologies. In *Genes* 11 (1). DOI: 10.3390/genes11010006.

Pflieger, Marc (2020): Synthesis and biological evaluation of HDAC class I/IIb and HDAC6 selective inhibitors. Dissertation. Heinrich-Heine-Universität, Düsseldorf. Institute of Pharmaceutical and Medicinal Chemistry.

Pflieger, Marc; Sönnichsen, Melf; Horstick-Muche, Nadine; Yang, Jing; Schliehe-Diecks, Julian; Schöler, Andrea et al. (2021): Oxa Analogues of Nexturastat A Demonstrate Improved HDAC6 Selectivity and Superior Antileukaemia Activity. In *ChemMedChem*. DOI: 10.1002/cmdc.202001011.

Polireddy, Kishore; Dong, Ruochen; McDonald, Peter R.; Wang, Tao; Luke, Brendan; Chen, Ping et al. (2016): Targeting Epithelial-Mesenchymal Transition for Identification of Inhibitors for Pancreatic Cancer Cell Invasion and Tumor Spheres Formation. In *PLoS ONE* 11 (10), e0164811. DOI: 10.1371/journal.pone.0164811.

Pratama, Nofran Putra; Wulandari, Septi; Nugroho, Agung Endro; Fakhrudin, Nanang; Astuti, Puji; Sudarsono (2018): Tylophorine Abrogates G2/M Arrest Induced by Doxorubicine and Promotes Increased Apoptosis in T47D Breast Cancer Cells. In *Asian Pacific journal of cancer prevention : APJCP* 19 (11), pp. 3065–3069. DOI: 10.31557/APJCP.2018.19.11.3065.

Puche, Juan E.; Saiman, Yedidya; Friedman, Scott L. (2013): Hepatic stellate cells and liver fibrosis. In *Comprehensive Physiology* 3 (4), pp. 1473–1492. DOI: 10.1002/cphy.c120035.

Qiao, Peter; Lu, Zheng-Rong (2020): Fibronectin in the Tumor Microenvironment. In *Advances in experimental medicine and biology* 1245, pp. 85–96. DOI: 10.1007/978-3-030-40146-7_4.

Qin, Tao; Cheng, Liang; Xiao, Ying; Qian, Weikun; Li, Jie; Wu, Zheng et al. (2020): NAF-1 Inhibition by Resveratrol Suppresses Cancer Stem Cell-Like Properties and the Invasion of Pancreatic Cancer. In *Frontiers in oncology* 10, p. 1038. DOI: 10.3389/fonc.2020.01038.

Quail, Daniela F.; Joyce, Johanna A. (2013): Microenvironmental regulation of tumor progression and metastasis. In *Nature medicine* 19 (11), pp. 1423–1437. DOI: 10.1038/nm.3394.

Raasch, Martin; Fritsche, Enrico; Kurtz, Andreas; Bauer, Michael; Mosig, Alexander S. (2019): Microphysiological systems meet hiPSC technology - New tools for disease modeling of liver infections in basic research and drug development. In *Advanced drug delivery reviews* 140, pp. 51–67. DOI: 10.1016/j.addr.2018.06.008.

Raasch, Martin; Rennert, Knut; Jahn, Tobias; Gärtner, Claudia; Schönfelder, Gilbert; Huber, Otmar et al. (2016): An integrative microfluidically supported in vitro model of an endothelial barrier combined with cortical spheroids simulates effects of neuroinflammation in neocortex development. In *Biomicrofluidics* 10 (4), p. 44102. DOI: 10.1063/1.4955184.

Rahn, Sascha; Barbosa, Philippe Dänzer; Möller, Julia Luisa; Ammar, Nourhane; Demetrowitsch, Tobias; Helm, Ole et al. (2019): Inflammation Associated Pancreatic Tumorigenesis: Upregulation of Succinate Dehydrogenase (Subunit B) Reduces Cell Growth of Pancreatic Ductal Epithelial Cells. In *Cancers* 12 (1). DOI: 10.3390/cancers12010042.

Ramamoorthy, Prabhu; Thomas, Sufi Mary; Kaushik, Gaurav; Subramaniam, Dharmalingam; Chastain, Katherine M.; Dhar, Animesh et al. (2019): Metastatic Tumor-in-a-Dish, a Novel Multicellular Organoid to Study Lung Colonization and Predict Therapeutic Response. In *Cancer research* 79 (7), pp. 1681–1695. DOI: 10.1158/0008-5472.CAN-18-2602.

Randriamanantsoa, S.; Papargyriou, A.; Maurer, H. C.; Peschke, K.; Schuster, M.; Zecchin, G. et al. (2022): Spatiotemporal dynamics of self-organized branching in pancreas-derived organoids. In *Nature communications* 13 (1), p. 5219. DOI: 10.1038/s41467-022-32806-y.

Rao, K. N.; Venkatachalam, S. R. (2000): Inhibition of dihydrofolate reductase and cell growth activity by the phenanthroindolizidine alkaloids pergularinine and tylophorinidine: the in vitro cytotoxicity of these plant alkaloids and their potential as antimicrobial and anticancer agents. In *Toxicology in vitro : an international journal published in association with BIBRA* 14 (1), pp. 53–59.

Rao, K.Narasimha; Bhattacharya, R. K.; Venkatachalam, S. R. (1997): Inhibition of thymidylate synthase and cell growth by the phenanthroindolizidine alkaloids pergularinine and tylophorinidine. In *Chemico-Biological Interactions* 106 (3), pp. 201–212. DOI: 10.1016/S0009-2797(97)00065-3.

Rawla, Prashanth; Sunkara, Tagore; Gaduputi, Vinaya (2019): Epidemiology of Pancreatic Cancer: Global Trends, Etiology and Risk Factors. In *World Journal of Oncology* 10 (1), pp. 10–27. DOI: 10.14740/wjon1166.

Reimche, Irene; Yu, Haiqian; Ariantari, Ni Putu; Liu, Zhen; Merkens, Kay; Rotfuß, Stella et al. (2022): Phenanthroindolizidine Alkaloids Isolated from Tylophora ovata as Potent Inhibitors of Inflammation, Spheroid Growth, and Invasion of Triple-Negative Breast Cancer. In *International journal of molecular sciences* 23 (18). DOI: 10.3390/ijms231810319.

Ren, Bo; Cui, Ming; Yang, Gang; Wang, Huanyu; Feng, Mengyu; You, Lei; Zhao, Yupei (2018): Tumor microenvironment participates in metastasis of pancreatic cancer. In *Molecular cancer* 17 (1), p. 108. DOI: 10.1186/s12943-018-0858-1.

Ricciardiello, Francesca; Gang, Yang; Palorini, Roberta; Li, Quanxiao; Giampà, Marco; Zhao, Fangyu et al. (2020): Hexosamine pathway inhibition overcomes pancreatic cancer resistance to gemcitabine through unfolded protein response and EGFR-Akt pathway modulation. In *Oncogene* 39 (20), pp. 4103–4117. DOI: 10.1038/s41388-020-1260-1.

Rice, A. J.; Cortes, E.; Lachowski, D.; Cheung, B. C. H.; Karim, S. A.; Morton, J. P.; Del Río Hernández, A. (2017): Matrix stiffness induces epithelial-mesenchymal transition and promotes chemoresistance in pancreatic cancer cells. In *Oncogenesis* 6 (7), e352. DOI: 10.1038/oncsis.2017.54.

Rode, Agata; Maass, Kendra Korinna; Willmund, Karolin Viktoria; Lichter, Peter; Ernst, Aurélie (2016): Chromothripsis in cancer cells: An update. In *International journal of cancer* 138 (10), pp. 2322–2333. DOI: 10.1002/ijc.29888.

Röder, Pia V.; Wu, Bingbing; Liu, Yixian; Han, Weiping (2016): Pancreatic regulation of glucose homeostasis. In *Experimental & molecular medicine* 48 (3), e219. DOI: 10.1038/emm.2016.6.

Ropero, Santiago; Esteller, Manel (2007): The role of histone deacetylases (HDACs) in human cancer. In *Molecular Oncology* 1 (1), pp. 19–25. DOI: 10.1016/j.molonc.2007.01.001.

Rosemeyer, Helmut; Knies, Christine; Hammerbacher, Katharina; Bender, Eugenia; Bonaterra, Gabriel A.; Hannen, Ricarda et al. (2019): Nucleolipids of the Nucleoside Antibiotics Formycins A and B: Synthesis and Biomedical Characterization Particularly Using Glioblastoma Cells. In *Chemistry & biodiversity* 16 (4), e1900012. DOI: 10.1002/cbdv.201900012.

Sanaei, Masumeh; Kavoosi, Fraidoon (2021): Effect of vorinostat on INK4 family and HDACs 1, 2, and 3 in pancreatic cancer and hepatocellular carcinoma. In *Research in pharmaceutical sciences* 16 (3), pp. 260–268. DOI: 10.4103/1735-5362.314824.

Sandoval, Juan; Esteller, Manel (2012): Cancer epigenomics: beyond genomics. In *Current opinion in genetics & development* 22 (1), pp. 50–55. DOI: 10.1016/j.gde.2012.02.008.

Schaefer, Eric W.; Loaiza-Bonilla, Arturo; Juckett, Mark; DiPersio, John F.; Roy, Vivek; Slack, James et al. (2009): A phase 2 study of vorinostat in acute myeloid leukemia. In *Haematologica* 94 (10), pp. 1375–1382. DOI: 10.3324/haematol.2009.009217.

Schmitz, Alexander; Fischer, Sabine C.; Mattheyer, Christian; Pampaloni, Francesco; Stelzer, Ernst H. K. (2017): Multiscale image analysis reveals structural heterogeneity of the cell microenvironment in homotypic spheroids. In *Scientific reports* 7, p. 43693. DOI: 10.1038/srep43693.

Schneider, Günter; Krämer, Oliver H.; Fritsche, Petra; Schüler, Susanne; Schmid, Roland M.; Saur, Dieter (2010): Targeting histone deacetylases in pancreatic ductal adenocarcinoma. In *Journal of cellular and molecular medicine* 14 (6A), pp. 1255–1263. DOI: 10.1111/j.1582-4934.2009.00974.x.

Schüler, Susanne; Fritsche, Petra; Diersch, Sandra; Arlt, Alexander; Schmid, Roland M.; Saur, D.; Schneider, Günter (2010): HDAC2 attenuates TRAIL-induced apoptosis of pancreatic cancer cells. In *Molecular cancer* 9 (80).

Shandilya, Ashutosh; Chacko, Sajeev; Jayaram, B.; Ghosh, Indira (2013): A plausible mechanism for the antimalarial activity of artemisinin: A computational approach. In *Scientific reports* 3, p. 2513. DOI: 10.1038/srep02513.

Shankar, Sharmila; Nall, Dara; Tang, Su-Ni; Meeker, Daniel; Passarini, Jenna; Sharma, Jay; Srivastava, Rakesh K. (2011): Resveratrol inhibits pancreatic cancer stem cell characteristics in human and KrasG12D transgenic mice by inhibiting pluripotency maintaining factors and epithelial-mesenchymal transition. In *PLoS ONE* 6 (1), e16530. DOI: 10.1371/journal.pone.0016530.

Shelkey, Ethan; Oommen, David; Stirling, Elizabeth R.; Soto-Pantoja, David R.; Cook, Katherine L.; Lu, Yong et al. (2022): Immuno-reactive cancer organoid model to assess effects of the microbiome on cancer immunotherapy. In *Scientific reports* 12 (1), p. 9983. DOI: 10.1038/s41598-022-13930-7.

Shen, Sida; Svoboda, Michal; Zhang, Guangming; Cavasin, Maria A.; Motlova, Lucia; McKinsey, Timothy A. et al. (2020): Structural and in Vivo Characterization of Tubastatin A, a Widely Used Histone Deacetylase 6 Inhibitor. In *ACS medicinal chemistry letters* 11 (5), pp. 706–712. DOI: 10.1021/acsmedchemlett.9b00560.

Shi, Min; Yu, Dang-Hui; Chen, Ying; Zhao, Chen-Yan; Zhang, Jing; Liu, Qing-Hua et al. (2012): Expression of fibroblast activation protein in human pancreatic adenocarcinoma and its clinicopathological significance. In *World journal of gastroenterology* 18 (8), pp. 840–846. DOI: 10.3748/wjg.v18.i8.840.

Shichi, Yuuki; Sasaki, Norihiko; Michishita, Masaki; Hasegawa, Fumio; Matsuda, Yoko; Arai, Tomio et al. (2019): Enhanced morphological and functional differences of pancreatic cancer with epithelial or mesenchymal characteristics in 3D culture. In *Scientific reports* 9 (1), p. 10871. DOI: 10.1038/s41598-019-47416-w.

Shields, Mario A.; Dangi-Garimella, Surabhi; Redig, Amanda J.; Munshi, Hidayatullah G. (2012): Biochemical role of the collagen-rich tumour microenvironment in pancreatic cancer progression. In *Biochemical Journal* 441 (2), pp. 541–552. DOI: 10.1042/BJ20111240.

Shin, Jung U.; Abaci, Hasan E.; Herron, Lauren; Guo, Zongyou; Sallee, Brigitte; Pappalardo, Alberto et al. (2020): Recapitulating T cell infiltration in 3D psoriatic skin models for patient-specific drug testing. In *Scientific reports* 10 (1), p. 4123. DOI: 10.1038/s41598-020-60275-0.

Shinke, Go; Yamada, Daisaku; Eguchi, Hidetoshi; Iwagami, Yoshifumi; Asaoka, Tadafumi; Noda, Takehiro et al. (2018): Role of histone deacetylase 1 in distant metastasis of pancreatic ductal cancer. In *Cancer science* 109 (8), pp. 2520–2531. DOI: 10.1111/cas.13700.

Shukla, Surendra K.; Purohit, Vinee; Mehla, Kamiya; Gunda, Venugopal; Chaika, Nina V.; Vernucci, Enza et al. (2017): MUC1 and HIF-1alpha Signaling Crosstalk Induces Anabolic Glucose Metabolism to Impart Gemcitabine Resistance to Pancreatic Cancer. In *Cancer cell* 32 (1), 71-87.e7. DOI: 10.1016/j.ccell.2017.06.004.

Siegel, Rebecca L.; Miller, Kimberly D.; Fuchs, Hannah E.; Jemal, Ahmedin (2022): Cancer statistics, 2022. In *CA: a cancer journal for clinicians* 72 (1), pp. 7–33. DOI: 10.3322/caac.21708.

Silver, Nicholas; Best, Steve; Jiang, Jie; Thein, Swee Lay (2006): Selection of housekeeping genes for gene expression studies in human reticulocytes using real-time PCR. In *BMC molecular biology* 7, p. 33. DOI: 10.1186/1471-2199-7-33.

Singh, Narendra P.; Lai, Henry C. (2004): Artemisinin Induces Apoptosis in Human Cancer Cells. In *Anticancer Research* 24.

Singh, Ritu Raj; O'Reilly, Eileen M. (2020): New Treatment Strategies for Metastatic Pancreatic Ductal Adenocarcinoma. In *Drugs*. DOI: 10.1007/s40265-020-01304-0.

Sirenko, Oksana; Mitlo, Trisha; Hesley, Jayne; Luke, Steve; Owens, Windsor; Cromwell, Evan F. (2015): High-content assays for characterizing the viability and morphology of 3D cancer spheroid cultures. In *Assay and drug development technologies* 13 (7), pp. 402–414. DOI: 10.1089/adt.2015.655.

Skrypek, N.; Duchêne, B.; Hebbar, M.; Leteurtre, E.; van Seuningen, I.; Jonckheere, N. (2013): The MUC4 mucin mediates gemcitabine resistance of human pancreatic cancer cells via the Concentrative Nucleoside Transporter family. In *Oncogene* 32 (13), pp. 1714–1723. DOI: 10.1038/onc.2012.179.

Slezakova, Silvia; Ruda-Kucerova, Jana (2017): Anticancer Activity of Artemisinin and its Derivatives. In *Anticancer Research* 37 (11), pp. 5995–6003. DOI: 10.21873/anticanres.12046.

Smolina, Margarita; Goormaghtigh, Erik (2015): Infrared imaging of MDA-MB-231 breast cancer cell line phenotypes in 2D and 3D cultures. In *The Analyst* 140 (7), pp. 2336–2343. DOI: 10.1039/c4an01833h.

Song, Jayoung; Kwon, Yongseok; Kim, Sanghee; Lee, Sang Kook (2015): Antitumor activity of phenanthroindolizidine alkaloids is associated with negative regulation of Met endosomal signaling in renal cancer cells. In *Chemistry & Biology* 22 (4), pp. 504–515. DOI: 10.1016/j.chembiol.2015.03.011.

Song, Yan; Yang, Hu; Lin, Rui; Jiang, Kui; Wang, Bang-Mao (2019): The role of ferroptosis in digestive system cancer. In *Oncology letters* 18 (3), pp. 2159–2164. DOI: 10.3892/ol.2019.10568.

Sothyratnam, Shaliny (2020): Evaluation of novel Purine ß-D-ribo-nucleosides in in vitro models of Pancreatic Ductal Adenocarcinoma (PDAC) and Triple-negative Breast Cancer (TNBC. Bachelor-Thesis. Universität Osnabrück, Osnabrück. Institut für Gesundheitswissenschaft und Bildung.

Sperlich, Julia; Teusch, Nicole (2018): Pseudopterosin Inhibits Proliferation and 3D Invasion in Triple-Negative Breast Cancer by Agonizing Glucocorticoid Receptor Alpha. In *Molecules (Basel, Switzerland)* 23 (8). DOI: 10.3390/molecules23081992.

Stefanius, Karoliina; Servage, Kelly; Souza Santos, Marcela de; Gray, Hillery Fields; Toombs, Jason E.; Chimalapati, Suneeta et al. (2019): Human pancreatic cancer cell exosomes, but not human normal cell exosomes, act as an initiator in cell transformation. In *eLife* 8. DOI: 10.7554/eLife.40226.

Stojanovic, N.; Hassan, Z.; Wirth, M.; Wenzel, P.; Beyer, M.; Schäfer, C. et al. (2017): HDAC1 and HDAC2 integrate the expression of p53 mutants in pancreatic cancer. In *Oncogene* 36 (13), pp. 1804–1815. DOI: 10.1038/onc.2016.344.

Strober, W. (2001): Trypan blue exclusion test of cell viability. In *Current protocols in immunology* Appendix 3, Appendix 3B. DOI: 10.1002/0471142735.ima03bs21.

Su, Liangping; Chen, Yitian; Huang, Cheng; Wu, Sangqing; Wang, XiaoJuan; Zhao, Xinbao et al. (2023): Targeting Src reactivates pyroptosis to reverse chemoresistance in lung and pancreatic cancer models. In *Science translational medicine* 15 (678), eabl7895. DOI: 10.1126/scitranslmed.abl7895.

Suárez-Álvarez, Beatriz; Baragaño Raneros, Aroa; Ortega, Francisco; López-Larrea, Carlos (2013): Epigenetic modulation of the immune function: a potential target for tolerance. In *Epigenetics* 8 (7), pp. 694–702. DOI: 10.4161/epi.25201.

Sun, C.; Yamato, T.; Furukawa, T.; Ohnishi, Y.; Kijima, H.; Horii, A. (2001): Characterization of the mutations of the K-ras, p53, p16, and SMAD4 genes in 15 human pancreatic cancer cell lines. In *Oncology reports* 8 (1), pp. 89–92. DOI: 10.3892/or.8.1.89.

Sun, Liyun; Shang, Huoli; Wu, Yuzhen; Xin, Xiujuan (2022): Hypericin-mediated photodynamic therapy enhances gemcitabine induced Capan-2 cell apoptosis via inhibiting NADPH level. In *The Journal of pharmacy and pharmacology* 74 (4), pp. 596–604. DOI: 10.1093/jpp/rgab073.

Taipale, J.; Beachy, P. A. (2001): The Hedgehog and Wnt signalling pathways in cancer. In *Nature* 411 (6835), pp. 349–354. DOI: 10.1038/35077219.

Takeda, Tsuyoshi; Sasaki, Takashi; Suzumori, Chisaki; Mie, Takafumi; Furukawa, Takaaki; Yamada, Yuto et al. (2021): The impact of cachexia and sarcopenia in elderly pancreatic cancer patients receiving palliative chemotherapy. In *International journal of clinical oncology*. DOI: 10.1007/s10147-021-01912-0.

Tan, Zhen; Xu, Jin; Zhang, Bo; Shi, Si; Yu, Xianjun; Liang, Chen (2020): Hypoxia: a barricade to conquer the pancreatic cancer. In *Cellular and molecular life sciences : CMLS*. DOI: 10.1007/s00018-019-03444-3.

Thellin, O.; Zorzi, W.; Lakaye, B.; Borman, B. de; Coumans, B.; Hennen, G. et al. (1999): Housekeeping genes as internal standards. Use and limits. In *Journal of biotechnology* 75 (2-3), pp. 291–295. DOI: 10.1016/S0168-1656(99)00163-7.

Thibodeau, Stephane; Voutsadakis, Ioannis A. (2018): FOLFIRINOX Chemotherapy in Metastatic Pancreatic Cancer: A Systematic Review and Meta-Analysis of Retrospective and Phase II Studies. In *Journal of Clinical Medicine* 7 (1). DOI: 10.3390/jcm7010007.

Thornton, Renee S.; Kerr, Russell G. (2002): Induction of Pseudopterosin Biosynthesis in the Gorgonian Pseudopterogorgia elisabethae. In *Journal of Chemical Ecology* 28 (10), pp. 2083–2090. DOI: 10.1023/A:1020758113694.

Tibbitt, Mark W.; Anseth, Kristi S. (2009): Hydrogels as extracellular matrix mimics for 3D cell culture. In *Biotechnology and bioengineering* 103 (4), pp. 655–663. DOI: 10.1002/bit.22361.

Tiriac, Hervé; Plenker, Dennis; Baker, Lindsey A.; Tuveson, David A. (2019): Organoid models for translational pancreatic cancer research. In *Current opinion in genetics & development* 54, pp. 7–11. DOI: 10.1016/j.gde.2019.02.003.

Tolliday, Nicola (2010): High-throughput assessment of Mammalian cell viability by determination of adenosine triphosphate levels. In *Current protocols in chemical biology* 2 (3), pp. 153–161. DOI: 10.1002/9780470559277.ch100045.

Tomás-Bort, Elena; Kieler, Markus; Sharma, Shreya; Candido, Juliana B.; Loessner, Daniela (2020): 3D approaches to model the tumor microenvironment of pancreatic cancer. In *Theranostics* 10 (11), pp. 5074–5089. DOI: 10.7150/thno.42441.

Tsai, Susan; McOlash, Laura; Palen, Katie; Johnson, Bryon; Duris, Christine; Yang, Qiuhui et al. (2018): Development of primary human pancreatic cancer organoids, matched stromal and immune cells and 3D tumor microenvironment models. In *BMC cancer* 18 (1), p. 335. DOI: 10.1186/s12885-018-4238-4.

Tsuchiya, Benio; Sato, Yuichi; Kameya, Toru; Okayasu, Isao; Mukai, Kiyoshi (2006): Differential expression of N-cadherin and E-cadherin in normal human tissues. In *Archives of histology and cytology* 69 (2), pp. 135–145. DOI: 10.1679/aohc.69.135.

Tu, Bo; Yao, Jun; Ferri-Borgogno, Sammy; Zhao, Jun; Chen, Shujuan; Wang, Qiuyun et al. (2019): YAP1 oncogene is a context-specific driver for pancreatic ductal adenocarcinoma. In *JCI insight* 4 (21). DOI: 10.1172/jci.insight.130811.

Turpin, Anthony; Neuzillet, Cindy; Colle, Elise; Dusetti, Nelson; Nicolle, Rémy; Cros, Jérôme et al. (2022): Therapeutic advances in metastatic pancreatic cancer: a focus on targeted therapies. In *Therapeutic advances in medical oncology* 14, 17588359221118019. DOI: 10.1177/17588359221118019.

Valcz, Gábor; Buzás, Edit I.; Sebestyén, Anna; Krenács, Tibor; Szállási, Zoltán; Igaz, Péter; Molnár, Béla (2020): Extracellular Vesicle-Based Communication May Contribute to the Co-Evolution of Cancer Stem Cells and Cancer-Associated Fibroblasts in Anti-Cancer Therapy. In *Cancers* 12 (8). DOI: 10.3390/cancers12082324.

Valenzuela-Fernandez, Agustin; Cabrero, J. Roman; Serrador, Juan M.; Sanchez-Madrid, Francisco (2008): HDAC6: a key regulator of cytoskeleton, cell migration and cell-cell interactions. In *Trends in Cell Biology* 18 (6), pp. 291–297. DOI: 10.1016/j.tcb.2008.04.003.

van Roy, F.; Berx, G. (2008): The cell-cell adhesion molecule E-cadherin. In *Cell. Mol. Life Sci.* 65 (23), pp. 3756–3788. DOI: 10.1007/s00018-008-8281-1.

Vaz, Arokia Priyanka; Deb, Shonali; Rachagani, Satyanarayana; Dey, Parama; Muniyan, Sakthivel; Lakshmanan, Imayavaramban et al. (2016): Overexpression of PD2 leads to increased tumorigenicity and metastasis in pancreatic ductal adenocarcinoma. In *Oncotarget* 7 (3), pp. 3317–3331. DOI: 10.18632/oncotarget.6580.

Ververis, Katherine; Hiong, Alison; Karagiannis, Tom C.; Licciardi, Paul V. (2013): Histone deacetylase inhibitors (HDACIs): multitargeted anticancer agents. In *Biologics : targets & therapy* 7, pp. 47–60. DOI: 10.2147/BTT.S29965.

Vietri, Maria Teresa; D'Elia, Giovanna; Caliendo, Gemma; Albanese, Luisa; Signoriello, Giuseppe; Napoli, Claudio; Molinari, Anna Maria (2022): Pancreatic Cancer with Mutation in BRCA1/2, MLH1, and APC Genes: Phenotype Correlation and Detection of a Novel Germline BRCA2 Mutation. In *Genes* 13 (2), p. 321. DOI: 10.3390/genes13020321.

Vishwakarma, Santosh; Iyer, Lakshmi R.; Muley, Milind; Singh, Pankaj Kumar; Shastry, Arun; Saxena, Ambrish et al. (2013): Tubastatin, a selective histone deacetylase 6 inhibitor shows anti-inflammatory and anti-rheumatic effects. In *International immunopharmacology* 16 (1), pp. 72–78. DOI: 10.1016/j.intimp.2013.03.016.

Vita, Ferdinando de; Ventriglia, Jole; Febbraro, Antonio; Laterza, Maria Maddalena; Fabozzi, Alessio; Savastano, Beatrice et al. (2016): NAB-paclitaxel and gemcitabine in metastatic pancreatic ductal adenocarcinoma (PDAC): from clinical trials to clinical practice. In *BMC cancer* 16 (1), p. 709. DOI: 10.1186/s12885-016-2671-9.

Wang, Kang; Zhang, Zhengyang; Wang, Ming; Cao, Xiongfeng; Qi, Jianchen; Wang, Dongqing et al. (2019): Role of GRP78 inhibiting artesunate-induced ferroptosis in KRAS mutant pancreatic cancer cells. In *Drug design, development and therapy* 13, pp. 2135–2144. DOI: 10.2147/DDDT.S199459.

Wang, Shuang-Jia; Gao, Yue; Chen, Hua; Kong, Rui; Jiang, Hong-Chi; Pan, Shang-Ha et al. (2010): Dihydroartemisinin inactivates NF-kappaB and potentiates the anti-tumor effect of gemcitabine on pancreatic cancer both in vitro and in vivo. In *Cancer letters* 293 (1), pp. 99–108. DOI: 10.1016/j.canlet.2010.01.001.

Wang, Wei; Gao, Jun; Man, Xiao-Hua; Li, Zhao-Shen; Gong, Yan-Fang (2009): Significance of DNA methyltransferase-1 and histone deacetylase-1 in pancreatic cancer. In *Oncology reports* 21 (6), pp. 1439–1447. DOI: 10.3892/or_00000372.

Wang, Weibin; Dong, Liangbo; Zhao, Bangbo; Lu, Jun; Zhao, Yupei (2018): E-cadherin is downregulated by microenvironmental changes in pancreatic cancer and induces EMT. In *Oncology reports* 40 (3), pp. 1641–1649. DOI: 10.3892/or.2018.6528.

Wang, Xin-Xing; Yin, Guo-Qing; Zhang, Zhen-Hai; Rong, Zhong-Hou; Wang, Zhi-Yi; Du, Dong-Dong et al. (2020): TWIST1 transcriptionally regulates glycolytic genes to promote the Warburg metabolism in pancreatic cancer. In *Experimental cell research* 386 (1), p. 111713. DOI: 10.1016/j.yexcr.2019.111713.

Wang, Ying; Lam, Wing; Chen, Shao-Ru; Guan, Fu-Lan; Dutchman, Ginger E.; Francis, Samson et al. (2016): Tylophorine Analog DCB-3503 Inhibited Cyclin D1 Translation through Allosteric Regulation of Heat Shock Cognate Protein 70. In *Scientific reports* 6, p. 32832. DOI: 10.1038/srep32832.

Wang, Ying; Lee, Sangwon; Ha, Ya; Lam, Wing; Chen, Shao-Ru; Dutschman, Ginger E. et al. (2017): Tylophorine Analogs Allosterically Regulates Heat Shock Cognate Protein 70 And Inhibits Hepatitis C Virus Replication. In *Scientific reports* 7 (1), p. 10037. DOI: 10.1038/s41598-017-08815-z.

Wang, Zimu; Liu, Jiaxin; Huang, Hairong; Ye, Mingxiang; Li, Xinying; Wu, Ranpu et al. (2021): Metastasis-associated fibroblasts: an emerging target for metastatic cancer. In *Biomarker research* 9 (1), p. 47. DOI: 10.1186/s40364-021-00305-9.

Wang, Ziwen; Wu, Meng; Wang, Yi; Li, Zheng; Wang, Lei; Han, Guifang et al. (2012): Synthesis and SAR studies of phenanthroindolizidine and phenanthroquinolizidine alkaloids as potent anti-tumor agents. In *European journal of medicinal chemistry* 51, pp. 250–258. DOI: 10.1016/j.ejmech.2012.02.048.

Ware, Matthew J.; Colbert, Kevin; Keshishian, Vazrik; Ho, Jason; Corr, Stuart J.; Curley, Steven A.; Godin, Biana (2016): Generation of Homogenous Three-Dimensional Pancreatic Cancer Cell Spheroids Using an Improved Hanging Drop Technique. In *Tissue engineering. Part C, Methods* 22 (4), pp. 312–321. DOI: 10.1089/ten.TEC.2015.0280.

Wei, Lusheng; Ye, Huilin; Li, Guolin; Lu, Yuanting; Zhou, Quanbo; Zheng, Shangyou et al. (2018): Cancer-associated fibroblasts promote progression and gemcitabine resistance via the SDF-1/SATB-1 pathway in pancreatic cancer. In *Cell death & disease* 9 (11), p. 1065. DOI: 10.1038/s41419-018-1104-x.

Wei, Shupei; Liu, Lili; Chen, Zhiyu; Yin, Wenli; Liu, Yingzi; Ouyang, Qianying et al. (2020): Artesunate inhibits the mevalonate pathway and promotes glioma cell senescence. In *Journal of cellular and molecular medicine* 24 (1), pp. 276–284. DOI: 10.1111/jcmm.14717.

Werno, Christian; Menrad, Heidi; Weigert, Andreas; Dehne, Nathalie; Goerdt, Sergij; Schledzewski, Kai et al. (2010): Knockout of HIF-1α in tumor-associated macrophages enhances M2 polarization and attenuates their pro-angiogenic responses. In *Carcinogenesis* 31 (10), pp. 1863–1872. DOI: 10.1093/carcin/bgq088.

Wilson, Christina R.; Sauer, John-Michael; Hooser, Stephen B. (2001): Taxines: a review of the mechanism and toxicity of yew (Taxus spp.) alkaloids. In *Toxicon* 39 (2-3), pp. 175–185. DOI: 10.1016/S0041-0101(00)00146-X.

Wong, T.W; Heng, P.W.S; Yeo, T.N; Chan, L.W (2002): Influence of polyvinylpyrrolidone on aggregation propensity of coated spheroids. In *International Journal of Pharmaceutics* 242 (1-2), pp. 357–360. DOI: 10.1016/S0378-5173(02)00216-8.

Xiao, Hui; Verdier-Pinard, Pascal; Fernandez-Fuentes, Narcis; Burd, Berta; Angeletti, Ruth; Fiser, Andras et al. (2006): Insights into the mechanism of microtubule stabilization by Taxol. In *Proceedings of the National Academy of Sciences of the United States of America* 103 (27), pp. 10166–10173. DOI: 10.1073/pnas.0603704103.

Xie, Bailu (2018): Molecular mechanisms of YAP signalling in the context of cancer. Promotionsschrift. University of Bath, Bath. Department of Pharmacy and Pharmacology.

Xie, Bailu; Hänsel, Jan; Mundorf, Vanessa; Betz, Janina; Reimche, Irene; Erkan, Mert et al. (2020): Pseudopterosin and O-Methyltylophorinidine Suppress Cell Growth in a 3D Spheroid Co-Culture Model of Pancreatic Ductal Adenocarcinoma. In *Bioengineering (Basel, Switzerland)* 7 (2), p. 57. DOI: 10.3390/bioengineering7020057.

Xie, Ruiling; Chen, Rui (2020): Mechanisms of Hippo pathway in the pancreatic cancer. In *Journal of Pancreatology* 3 (1), pp. 21–28. DOI: 10.1097/JP9.0000000000000041.

Xu, Manlong; McCanna, David J.; Sivak, Jacob G. (2015): Use of the viability reagent PrestoBlue in comparison with alamarBlue and MTT to assess the viability of human corneal epithelial cells. In *Journal of pharmacological and toxicological methods* 71, pp. 1–7. DOI: 10.1016/j.vascn.2014.11.003.

Xu, Shuaishuai; Xu, Huaxiang; Wang, Wenquan; Li, Shuo; Li, Hao; Li, Tianjiao et al. (2019): The role of collagen in cancer: from bench to bedside. In *Journal of translational medicine* 17 (1), p. 309. DOI: 10.1186/s12967-019-2058-1.

Yang, Jiyong; Chheda, Chintan; Lim, Adrian; Hauptschein, Dina; Zayou, Latifa; Tang, Josiah et al. (2022): HDAC4 Mediates Smoking-Induced Pancreatic Cancer Metastasis. In *Pancreas* 51 (2), pp. 190–195. DOI: 10.1097/MPA.0000000000001998.

Yang, Kege; Li, Yaqing; Lian, Guoda; Lin, Haoming; Shang, Changzhen; Zeng, Linjuan et al. (2018): KRAS promotes tumor metastasis and chemoresistance by repressing RKIP via the MAPK-ERK pathway in pancreatic cancer. In *International journal of cancer* 142 (11), pp. 2323–2334. DOI: 10.1002/ijc.31248.

Yang, Shengcai; Zhang, Dawei; Shen, Na; Wang, Guanyi; Tang, Zhaohui; Chen, Xuesi (2019): Dihydroartemisinin increases gemcitabine therapeutic efficacy in ovarian cancer by inducing reactive oxygen species. In *J Cell Biochem* 120 (1), pp. 634–644. DOI: 10.1002/jcb.27421.

Yao, Yuyuan; Guo, Qinglong; Cao, Yue; Qiu, Yangmin; Tan, Renxiang; Yu, Zhou et al. (2018): Artemisinin derivatives inactivate cancer-associated fibroblasts through suppressing TGF-β signaling in breast cancer. In *Journal of experimental & clinical cancer research : CR* 37 (1), p. 282. DOI: 10.1186/s13046-018-0960-7.

Yin, Tao; Wei, Hongji; Gou, Shanmiao; Shi, Pengfei; Yang, Zhiyong; Zhao, Gang; Wang, Chunyou (2011): Cancer stem-like cells enriched in Panc-1 spheres possess increased migration ability and resistance to gemcitabine. In *IJMS* 12 (3), pp. 1595–1604. DOI: 10.3390/ijms12031595.

Yoon, Somy; Eom, Gwang Hyeon (2016): HDAC and HDAC Inhibitor: From Cancer to Cardiovascular Diseases. In *Chonnam medical journal* 52 (1), pp. 1–11. DOI: 10.4068/cmj.2016.52.1.1.

Yoshii, Yukie; Waki, Atsuo; Yoshida, Kaori; Kakezuka, Anna; Kobayashi, Maki; Namiki, Hideo et al. (2011): The use of nanoimprinted scaffolds as 3D culture models to facilitate spontaneous tumor cell migration and well-regulated spheroid formation. In *Biomaterials* 32 (26), pp. 6052–6058. DOI: 10.1016/j.biomaterials.2011.04.076.

Youn, Gi Soo; Cho, Hyundong; Kim, Donggyu; Choi, Soo Young; Park, Jinseu (2017): Crosstalk between HDAC6 and Nox2-based NADPH oxidase mediates HIV-1 Tat-induced pro-inflammatory responses in astrocytes. In *Redox biology* 12, pp. 978–986. DOI: 10.1016/j.redox.2017.05.001.

Zambirinis, Constantinos P.; Pushalkar, Smruti; Saxena, Deepak; Miller, George (2014): Pancreatic cancer, inflammation, and microbiome. In *Cancer journal (Sudbury, Mass.)* 20 (3), pp. 195–202. DOI: 10.1097/PPO.0000000000000045.

Zhang, Ge; Song, Xiaoping; Mei, Jie; Ye, Genlan; Wang, Leyu; Yu, Lei et al. (2017): A simple 3D cryogel co-culture system used to study the role of CAFs in EMT of MDA-MB-231 cells. In *RSC Adv.* 7 (28), pp. 17208–17216. DOI: 10.1039/C6RA28721B.

Zhang, Jin-Ying; Zhang, Fan; Hong, Chao-Qun; Giuliano, Armando E.; Cui, Xiao-Jiang; Zhou, Guang-Ji et al. (2015): Critical protein GAPDH and its regulatory mechanisms in cancer cells. In *Cancer biology & medicine* 12 (1), pp. 10–22. DOI: 10.7497/j.issn.2095-3941.2014.0019.

Zhang, Zhengle; Duan, Qingke; Zhao, Hengqiang; Liu, Tao; Wu, Heshui; Shen, Qiang et al. (2016): Gemcitabine treatment promotes pancreatic cancer stemness through the Nox/ROS/NF-κB/STAT3 signaling cascade. In *Cancer letters* 382 (1), pp. 53–63. DOI: 10.1016/j.canlet.2016.08.023.

Zhao, Ming; Mishra, Lopa; Deng, Chu-Xia (2018): The role of TGF-β/SMAD4 signaling in cancer. In *International journal of biological sciences* 14 (2), pp. 111–123. DOI: 10.7150/ijbs.23230.

Zhen, Yueying; Huang, Xueshi; Yu, Dequan; Yu, Shishan (2002): Antitumor alkaloids isolated from Tylophora ovata. In *Acta Botanica Sinica* 44 (3), pp. 349–353.

Zheng, Yawen; Yang, Xiaohui; Wang, Chunyan; Zhang, Shuo; Wang, Zhiling; Li, Meng et al. (2020): HDAC6, modulated by miR-206, promotes endometrial cancer progression through the PTEN/AKT/mTOR pathway. In *Scientific reports* 10 (1), p. 3576. DOI: 10.1038/s41598-020-60271-4.

Zhou, He-Ming; Zhang, Ji-Gang; Zhang, Xue; Li, Qin (2021): Targeting cancer stem cells for reversing therapy resistance: mechanism, signaling, and prospective agents. In *Signal Transduction and Targeted Therapy* 6 (1), p. 62. DOI: 10.1038/s41392-020-00430-1.

10 Acknowledgements

Foremost, I'd like to thank Professor Nicole Teusch for her supervision and mentoring these past four years of my PhD. Changing universities twice during this time was quite an experience, and together with all that has transpired, I am thankful and grateful for it.

A great many people have helped, supported and encouraged me and contributed to this work: Johanna Hölken and Irene Reimche, my fellow colleagues, whose help and input was always appreciated; Daria Janßen, who wrote her master's thesis in our group; Karin Peter, who was of invaluable help for this work, and our projects in general, with her technical experience and knowledge, aiding in the establishment of the miniaturised organoids, the application of the pipetting robot and many more experiments; Bailu Xie and Professor Randall Mrsny from the University of Bath, where I learned the handling and cultivation of the organoids; Professor Thomas Kurz, who agreed to mentor this thesis, and his research team at the Heinrich Heine University: Leandro Alves-Avelar, Mark Pflieger and Fabian Fischer; Professor Axel Griesbeck and Christina Bold from the University of Cologne; Professor Peter Proksch and Haiqian Yu, both from the Heinrich Heine University as well; Gabriele Baron-Ruppert, Meike Siedenkersting, Professor Helmut Rosemeyer, Mona Lünswilken and Rainer Kurre from the University of Osnabrück; Martin Raasch, Knut Rennert, Daniela Schulz and Philipp Albrecht from Dynamic42; Julia Sperlich, Alessandra Grossert and Vanessa Mundorf from the Cologne University of Applied Sciences; and Michael Schell from CENiBRA.

I'd also like to thank Kate Gridley, Katja Schiedlauske, Rizwan Rehimi, Russel G. Kerr, Katja Friedrich, Simone Miljanovic, Dina Hassouna El-Kashef, Arta Kuci, Shaliny Sothyrathnam, Claudia Eckelskemper, Nan Qin, Ni Putu Ariantari, the DAAD for the Erasmus+ financing, the SFB 944, and my family, who always supported me during all these years of studying.

Affidavit

I hereby declare that I have written and authored this thesis on my own, according to the Guidelines for the Safeguarding of Good Research Practice as defined and stated by the Heinrich Heine University Düsseldorf and the German Research Foundation. All sources and research data have been cited correctly. This thesis has not been submitted to another university or faculty.

_____

Düsseldorf, the 12th of June 2023